

Appendix A.

Material Test Report

By

University of Dayton Research Institute (UDRI)

UDRI

UNIVERSITY
of DAYTON
RESEARCH
INSTITUTE

UDR-TR-2011-78

**INVESTIGATE OPPORTUNITIES
FOR LIGHTWEIGHTING
VEHICLES USING ADVANCED
PLASTICS AND COMPOSITES -
HIGHER RATE TESTING OF TWO
DIMENSION TRIAXIAL BRAID
CARBON COMPOSITE**

Prepared for:

Dr. Cing-Dao (Steve) Kan
Director of FHWA/NHTSA National Crash Analysis
Center
The George Washington University, Virginia Campus
20101 Academic Way
Ashburn, VA 20147

FINAL REPORT

Purchase Order Number 1000142132

Prepared by:

Susan I. Hill
Structural Integrity Division
University of Dayton Research Institute
300 College Park
Dayton, OH 45469-0123

JUNE 2011

INDUSTRY PROPRIETARY
Distribution limited to those
with Sponsor approval

TABLE OF CONTENTS

TABLE OF CONTENTS	A - 3
LIST OF FIGURES	A - 5
LIST OF TABLES	A - 7
1.0 INTRODUCTION	A - 8
2.0 INITIAL TEST MATRIX	A - 8
3.0 MATERIAL	A - 9
3.1 General Background	A - 9
3.2 Composite Architecture and Resin	A - 10
3.3 Final Material Selection	A - 11
3.4 2D3A Specifications	A - 11
3.5 Panel Fabrication and Properties	A - 12
3.6 Tube Fabrication and Properties	A - 14
3.7 Unit Cell Size and Orientation	A - 16
4.0 SPECIMEN DESIGN	A - 18
4.1 Standards	A - 18
4.2 General Background on High Rate Testing	A - 18
4.3 Gage Width for Testing the 2D3A	A - 20
4.4 Tensile Specimen Configuration for Quasi-static Tests per ASTM D 3039	A - 20
4.5 Bowtie Tensile for Higher Rates	A - 21
4.5.1 Background	A - 21
4.5.2 High Rate Tensile Specimen Configuration	A - 22
4.6 Compression Specimen for Higher Rates	A - 24
4.6.1 Background	A - 24
4.6.2 High Rate Compression Specimen Configuration	A - 24
4.7 Shear Specimen for Higher Rates	A - 25
4.7.1 Background	A - 25
4.7.2 High Rate Shear Specimen Configuration	A - 25
4.8 Braided Tubes	A - 26
5.0 FINAL TEST MATRICES	A - 26
6.0 TEST PROCEDURES – SME AT UDRI	A - 27
6.1 SME Servo-hydraulic Equipment	A - 27
6.2 Oak Ridge National Laboratory (ORNL) Equipment	A - 31
6.3 Strain Measurement with Digital Image Correlation System (DIC) with ISTRA Software	A - 32
6.3.1 General	A - 32
6.3.2 Specimen Preparation	A - 33

6.3.3 DIC Measured Region	A - 33
6.4 Strain Measurement with Strain Gages	A - 34
7.0 DATA ANALYSES	A - 35
7.1 General	A - 35
7.2 DIC Strain Analysis	A - 35
7.3 DIC Strain	A - 37
7.4 Tube Crush Analysis	A - 38
8.0 RESULTS AND DISCUSSION	A - 39
8.1 Fixture Design – General	A - 39
8.2 Rate Effect on 2D3A Strength	A - 39
8.3 Tensile	A - 41
8.3.1 Modified ASTM D 3039 Tensile	A - 41
8.3.2 Bowtie Axial Tensile	A - 44
8.3.3 Bowtie Transverse Tensile	A - 45
8.3.4 Comparison of Bowtie Axial and Transverse Tensile Mechanical Properties	A - 49
8.3.3 Comparison of Modified D 3039 and Bowtie Axial and Transverse	A - 49
8.4 Compression	A - 53
8.4.1 Axial Compression	A - 53
8.4.2 Transverse Compression	A - 57
8.4.3 Comparison of Axial and Transverse Compression	A - 61
8.5 Shear	A - 63
8.5.1 Comparison to Published Data	A - 63
8.5.2 Axial Shear (Shearing Across 0° Fiber Bundles)	A - 63
8.5.2 Transverse Shear (Shearing Along 0° Fiber bundles)	A - 68
8.5.3 Comparison of Axial and Transverse Shear	A - 71
8.6 Compression Tube Tests	A - 73
8.6.1 Tube Compression Strength	A - 76
8.6.2 Tube Compression Strain	A - 78
8.6.3 Tube Temperatures	A - 79
9.0 OVERALL SUMMARY	A - 80
9.1 Material Selection and High Rate Specimen Designs	A - 80
9.2 Comparison of Tensile Data Using the ASTM D 3039 and Bowtie Configuration	A - 80
9.3 High Rate Coupon Mechanical Properties	A - 81
9.3.1 Tensile	A - 81
9.3.2 Compression	A - 81
9.3.3 Shear	A - 81
9.4 Tube Compression	A - 82
10.0 RECOMMENDATIONS	A - 82
11.0 REFERENCES	A - 82

APPENDIX A. MATERIAL PRODUCT SHEETS	A - 86
APPENDIX B. LAMINATE AND TUBE PHYSICAL PROPERTIES	A - 91
APPENDIX C. SELECTED PANEL LAYOUTS	A - 110
APPENDIX D. SAMPLE PHOTOMICROGRAPHS OF PANEL CROSS-SECTIONS AT 50X PHOTOMICROGRAPHS OF TUBE CROSS-SECTIONS AT 25X	A - 117
APPENDIX E. UNIT CELL MEASUREMENTS AND LOCATIONS	A - 129
APPENDIX F. BOWTIE TENSILE SPECIMENS AND FIXTURE DRAWINGS	A - 138
APPENDIX G. COMPRESSION SPECIMEN AND FIXTURE DRAWINGS	A - 143
APPENDIX H. SHEAR SPECIMEN AND FIXTURE DRAWINGS	A - 146
APPENDIX I. SME EQUIPMENT LIST AND CALIBRATIONS	A - 152
APPENDIX J. MODIFIED ASTM D3039 TENSILE DATA PACKAGE	A - 161
APPENDIX K. BOWTIE AXIAL TENSILE DATA PACKAGE	A - 165
APPENDIX L. BOWTIE TRANSVERSE TENSILE DATA PACKAGE	A - 171
APPENDIX M. AXIAL COMPRESSION DATA PACKAGE	A - 179
APPENDIX N. TRANSVERSE COMPRESSION DATA PACKAGE	A - 189
APPENDIX O. AXIAL SHEAR DATA PACKAGE	A - 197
APPENDIX P. TRANSVERSE SHEAR DATA PACKAGE	A - 206
APPENDIX Q. TUBE COMPRESSION DATA PACKAGE	A - 215

LIST OF FIGURES

Figure 1. Axial Cross-Section of Panel 073010-1 at 25X	A - 14
Figure 2. Axial Cross-Section of Panel 080210-6 at 25X	A - 14
Figure 3. Transverse Cross-Section of Panel 073010-1 at 25X	A - 14
Figure 4. Transverse Cross-Section of Panel 080210-6 at 25X	A - 14
Figure 5. Axial Cross-Section of Tube STL103-1 at 25X	A - 15
Figure 6. Transverse Cross-Section of Tube STL103-1 at 25X	A - 15
Figure 7. Smallest Unit Cells for a 2-D Braid and 2-D Triaxial Braid	A - 16
Figure 8. Unit Cell Size	A - 16
Figure 9. Test Orientation for Panels	A - 17
Figure 10. Difference in the Measured Response for Test Systems with Different Natural Resonant Frequencies	A - 20
Figure 11. Modified ASTM D 3039 Axial Tensile	A - 21
Figure 12. Modified ASTM D 3039 Transverse Tensile	A - 21
Figure 13. NASA Bowtie Tensile Specimens [Reference 11]	A - 22
Figure 14. Relative Amounts of Bias and Axial Tows Gripped in Modified ASTM D 3039 and Bowtie Specimen Configurations	A - 22
Figure 15. Bowtie Tensile Nominal Specimen Dimensions	A - 23
Figure 16. Shear Specimen Nominal Dimensions	A - 26
Figure 17. Low Rate Setup for Axial Tensile Testing	A - 28
Figure 18. High Rate Setup for Axial Tensile Testing	A - 29
Figure 19. Transverse Tensile in Fixture	A - 29
Figure 20. Edge View of Compression Setup showing Unsupported Region	A - 30
Figure 21. Front View of Compression Setup Used with Strain Measurement	A - 30
Figure 22. Axial Shear Setup	A - 31
Figure 23. Transverse Shear Setup	A - 31
Figure 24. TMAC Equipment at ORNL	A - 32
Figure 25. DIC Pattern on Axial Shear Specimen	A - 33
Figure 26. Grid Mesh and Measured Regions for a Slow Rate Axial Tension Test	A - 34
Figure 27. Possible Features for DIC Analysis	A - 34
Figure 28. Grid Mesh (a) and Measured Regions (b) for an Axial Compression Test	A - 34
Figure 29. DIC Strain Output for Different Regions (a) and DIC Image (b) for an Axial Shear Test [Specimen STL095-1]	A - 37
Figure 30. Stress Response at Low (a) and Fast Test Rate (b) for an Axial Shear Test	A - 37
Figure 31. Peak Axial Strength of 2D3A at All Rates – Normalized to 56% Fiber Content	A - 40
Figure 32. Peak Transverse Strength of 2D3A at All Rates Rates – Normalized to 56% Fiber Content	A - 41
Figure 33. Tensile Stress-strain Curves for Modified ASTM D 3039 2D3A	A - 42
Figure 34. Strain Gage Location for Axial Modified ASTM D 3039 2D3A	A - 43
Figure 35. Comparison of Stress-strain Curves using Strain Gage and DIC Data	A - 43
Figure 36. Typical Failure Locations for Axial (a) and Tensile (b) Modified D 3039 Specimens	A - 43

Figure 37. Representative Stress-strain Curves for 2D3A Bowtie Axial Specimens at All Rates	A - 45
Figure 38. Typical Failure of Axial Bowtie Tensile Specimen	A - 45
Figure 39. Representative Stress-strain Curves for 2D3A Bowtie Transverse Specimens at All Rates	A - 47
Figure 40. Schematic of Fiber Tow Location in Center Gage for Axial (a) and Transverse (b) Tensile Bowtie Specimen	A - 48
Figure 41. Measured Peak Tensile Stress of Axial and Transverse 2D3A Normalized to 56 vol% Fiber	A - 49
Figure 42. Measured Modulus of Axial and Transverse 2D3A	A - 50
Figure 43. Failure Strain of Axial and Transverse 2D3A	A - 50
Figure 44. Comparison of Axial Tensile Stress-strain Response at 1.27 mm/min	A - 51
Figure 45. Comparison of Transverse Tensile Stress-strain Response at 0.6 to 1.27 mm/min for Modified ASTM D 3039 and Bowtie Specimens	A - 52
Figure 46. Axial Compressive Stress-strain Response at All Rates Using Straight-sided Specimens	A - 55
Figure 47. Axial Compressive Stress-strain Response at All Rates Using Dogbone and Straight-sided Specimens	A - 55
Figure 48. 2D3A Axial Compressive Strength as a Function of Strain Rate	A - 56
Figure 49. 2D3A Axial Compressive Modulus as a Function of Strain Rate	A - 56
Figure 50. 2D3A Axial Compressive Failure Strain as a Function of Strain Rate	A - 57
Figure 51. Failure Location for Dogbone and Straight-sided Axial Compressive Specimens	A - 57
Figure 52. Transverse Compressive Stress-strain of 2D3A at All Rates	A - 59
Figure 53. 2D3A Transverse Compressive Strength as a Function of Strain Rate	A - 59
Figure 54. 2D3A Transverse Compressive Modulus as a Function of Strain Rate	A - 60
Figure 55. 2D3A Transverse Compressive Failure Strain as a Function of Strain Rate	A - 60
Figure 56. Typical Failure Location for Transverse Compressive Specimens	A - 61
Figure 57. 2D3A Compressive Strength as a Function of Strain Rate	A - 61
Figure 58. 2D3A Compressive Modulus as a Function of Strain Rate	A - 62
Figure 59. 2D3A Compressive Modulus as a Function of Strain Rate Using Straight-sided Specimens	A - 62
Figure 60. 2D3A Compressive Failure Strain as a Function of Strain Rate	A - 63
Figure 62. Axial Shear Stress-Strain Response of 2D3A Across Tested Rates	A - 65
Figure 62. Axial Shear Strength of 2D3A Across Tested Rates	A - 65
Figure 63. Axial Shear Modulus of 2D3A Across Tested Rates	A - 66
Figure 64. Axial Shear Failure Strain of 2D3A Across Tested Rates	A - 66
Figure 65. Typical Axial Shear Failure Locations	A - 67
Figure 66. Unsmoothed Axial Shear Stress-Strain Response at 0.25/s	A - 67
Figure 67. Transverse Shear Stress-Strain Response of 2D3A Across Tested Rates	A - 69
Figure 68. Transverse Shear Strength of 2D3A Across Tested Rates	A - 69
Figure 69. Transverse Shear Modulus of 2D3A Across Tested Rates	A - 70
Figure 70. Transverse Shear Failure Strain of 2D3A Across Tested Rates	A - 70
Figure 71. Typical Transverse Shear Failure Locations	A - 71
Figure 72. 2D3A Shear Strength as a Function of Strain Rate	A - 71
Figure 73. 2D3A Shear Modulus as a Function of Strain Rate	A - 72

Figure 74. 2D3A Shear Failure Strain as a Function of Strain Rate A - 72

Figure 75. Typical Tube Crush Load-Displacement Curves at a Slow and Fast Rate A - 73

Figure 76. Low Rate Tube Failure A - 74

Figure 77. High Rate Tube Failure A - 74

Figure 78. Polygon Regions Tracked by the DIC and Comparison of the Measured
Displacements to the Actuator Displacement A - 75

Figure 79. Load-Displacement Curves Across the Tested Rates A - 76

Figure 80. SEA Across Tested Rates A - 77

Figure 81. Tube Compressive Stress-Strain at 1.5 m/min A - 78

Figure 82. Comparison of Tube and Coupon Compressive Stress-Strain A - 78

Figure 83. Composite Tube Temperatures During Crush A - 79

LIST OF TABLES

Table 1. Initial Coupon-Level Test Matrix	A - 9
Table 2. Initial Tube Compression Matrix	A - 9
Table 3. Carbon and Glass Fiber Strength and Stiffness	A - 10
Table 4. 2D3A Tow Description	A - 12
Table 5. Laminate Physical Properties	A - 13
Table 6. Tube Physical Properties	A - 15
Table 7. Unit Cell Sizes for Panels	A - 17
Table 8. Final Coupon-Level Test Matrix	A - 27
Table 9. Final Tube Compression Matrix	A - 27
Table 10. Comparison of UDRI and Published Data for 2D3A with Epon 862W at Quasi-static Rates	A - 42
Table 11. Bowtie Axial Tensile Data Summary for 2D3A	A - 44
Table 12. Bowtie Transverse Tensile Data Summary for 2D3A	A - 46
Table 13. Comparison of Bowtie and Modified ASTM D 3039 Tensile Properties at 1.27 mm/min	A - 51
Table 14. Comparison of Axial Compression UDRI and Published Data [13]	A - 54
Table 15. Axial Compression Data Summary for 2D3A	A - 54
Table 16. Comparison of Transverse Compression UDRI and Published Data [13]	A - 58
Table 17. Transverse Compression Data Summary for 2D3A	A - 58
Table 18. Comparison of UDRI Shear Data and Published Data [13]	A - 64
Table 19. Axial Shear Data Summary for 2D3A	A - 64
Table 20. Transverse Shear Summary Table of 2D3A	A - 68
Table 21. Compression Tube Strength and Peak Temperatures	A - 77

1.0 INTRODUCTION

The Plastic and Composite Intensive Vehicle (PCIV) safety research programs, sponsored by the Department of Energy, are focused on increasing fuel efficiency and reducing vehicle weight without compromising crash safety. Some of the materials currently under investigation are long fiber-filled polymers and composites. It is critical to understand the change in the material response and energy absorption of these materials under impact conditions if they are to be considered in the design of automotive components and structures.

The behavior and deformation of composites under impact conditions is different from the typical metals used in structural components. The failure modes (delamination, matrix debonding, fiber breakage, etc.) have to be modeled on both a micro and macroscopic scale to capture the correct response. Material property data at rates above quasi-static (typically above 0.0001/s) are needed to validate and optimize the models.

The small specimen length needed to achieve the high rates is usually in direct conflict with the size needed to represent bulk material properties, especially for composites. The gage length and cross-sectional area of current high rate specimens are relatively small (approximately 3 to 10 mm) and approach the magnitude of the unit "cell" of many fabric weaves, braids, or hybrid sandwich materials. Increasing the specimen width in order to test a larger volume of material often runs into the roadblock of equipment capacity.

Composite testing at quasi-static rates poses a unique set of concerns, such as specimen-to-specimen variability, failures within the gage section, and non-homogeneous regions. High rate testing introduces several others, such as specimen configuration, resonant ringing, strain measurement to failure, and actuator capacity. The goal of generating representative bulk material properties may be difficult to achieve over a wide strain rate regime depending on the type of composite and equipment capacities.

The goal of the effort at the Structures and Materials Evaluation (SME) Group of the University of Dayton Research Institute (UDRI) was to identify a composite that would be suitable to use for automotive structural components and to generate material property data on a coupon and component level at rates above quasi-static. The program involved material selection, specimen and fixture design, specimen and fixture fabrication, coupon testing (tensile, compression, and shear), and tube testing.

2.0 INITIAL TEST MATRIX

The original scope of the test program is outlined in Tables 1 and 2. The maximum test rates were not known at the start. The results from the lower rate tests and the final specimen designs were to dictate the upper rate for each test. However, some assumptions had to be made regarding the scope of the test program to serve as the basis for the composite panel requirements. The final test matrices are summarized in Section 4.0.

Table 1. Initial Coupon-Level Test Matrix

		Machine Rate [m/min]		
		0.0006	0.6	12-24
		Estimated Nominal Strain Rate [1/s]		
		0.0004	0.04-0.08	4-8
Tension-per ASTM D 3039	Axial	3	0	0
	Transverse	0	0	0
Higher Rate Tension	Axial	3	3	3
	Transverse	3	3	3
Compression	Axial	3	3	3
	Transverse	3	3	3
Higher Rate Shear	Axial	3	3	3
	Transverse	3	3	3
Total		21	18	18
Grand total		57		

Table 2. Initial Tube Compression Matrix

	Machine Rate [m/min]		
	1.5	~60	~480
Straight End	3	0	0
Single bevel	3	3	3
Total	6	3	3
Grand total	12		

3.0 MATERIAL

3.1 General Background

Composite materials are available in a large variety of fiber types, resin systems, and architectures. Current automotive applications are mainly non-structural, such as instrument panels, interior trim, leaf springs, fuel tanks, hoods, fenders and other exterior panels.

Composites are attractive because of the high strength to weight ratio, design versatility, corrosion resistance, and potential for parts consolidation. Some of the disadvantages are low ductility, recyclability, energy absorption, high material costs, and low production volume [1,2]. They are generally made with either glass or carbon fibers and a matrix of a thermoset or thermoplastic polymer. Composite recyclability has increased the interest in the use of natural fibers, such as bamboo, flax, jute, sisal, and banana, as a replacement for glass fiber. [3,4,5]

The focus of this study was to identify a composite architecture that would provide high strength, stiffness, and energy absorption. The potential application was for a F150 truck body rail, which was being modeled by George Washington University (GWU). The DOE specifically tasked UDRI and GWU

to not consider the overall cost of the material nor part production¹ in the material selection. The DOE wanted to identify what scale of improvement could be achieved using composites and to use this as a target benchmark. GWU and DOE were also interested in selecting a material for which there was some published quasi-static material properties for comparison to the high rate data. A secondary goal was to provide the general engineering community with a data set of material properties which would be used for model validation.

3.2 Composite Architecture and Resin

The high strength and stiffness of carbon fiber makes it an ideal candidate for an automotive structural application. As shown in Table 3, its strength and stiffness is two to three times that of the typical E-glass. Its modulus is also at least twice that of either E or S-glass. Since the carbon fiber density is also low, the overall performance to weight ratio of a carbon composite is higher than a glass composite. This is an advantage in the design of integrated parts for lightweighting vehicles.

Table 3. Carbon and Glass Fiber Strength and Stiffness

Material	Tensile Strength [MPa]	Elastic Modulus [GPa]	Density [gm/ml]
Carbon Fiber T700S ⁽⁶⁾	4900	230	2.0
E Glass ⁽⁷⁾	1900-2600	73	2.5
S-glass ⁽²⁾	4380-4590	88-91	2.48
Natural fibers ⁽⁸⁾	400-1500		

Thermoset polymers are preferred for high performance applications since the polymer matrix will not soften at the expected maximum service temperatures (e.g. 80°C). Epoxy resins are often used with carbon fibers since epoxies offer high strength, low shrinkage, electrical insulation, and chemical and solvent resistance with low cost [2]. They wet the material easily and the composite can be processed using a variety of methods. Phenolic resins are slightly more expensive and tend to be used for those applications which have stringent fire and smoke requirements.

The polymeric resin serves to bind the fiber architecture and to transfer the applied loads. The composite mechanical properties are mainly defined by the fiber architecture. The optimum design for maximum strength and stiffness is a unidirectional layup of carbon fibers which are located parallel to the loading axis [2] A single directional fiber lay-up is only practical if the loading direction is well-defined.

Multi-directional loading requires a series of layers or plies of unidirectional fibers which can be oriented at various angles to coincide with the expected loading directions. The composite can also be designed to represent an isotropic material, usually by using alternating layers of +/-45° and 0° unidirectional plies. The mechanical properties are dependent on the angles of the layers and the symmetry. The properties will approach, but not equal, those of a unidirectional laminate along a given axis [8].

Some alternative methods use chopped fibers, fabric weaves, or fiber braid as a way to handle the issue of off-axis or multi-directional loads. Chopped fibers can be incorporated in several ways. Two common methods are to use a mat which consists of randomly oriented fibers of a given length or to

¹ Kick-off meeting at the National Crash Analysis Center GWU 19 November 2009

injection mold the precut fibers along with the resin into the final part. The mechanical attrition of the fiber varies with the processing parameters. Injection molding tends to cause the most damage to the fiber, often reducing the starting length by a factor of 10 or more [9,10].

Fabric weaves provide bundles of fibers in the 0° and 90° directions. The mechanical properties are affected by the number of fiber bundles, or tows, the number of fibers per tow, and the weave pattern. A loose weave, such as an 8 harness satin, allows the fabric to drape and match mold contours. However, the looser weave pattern is a result of fewer bundles per inch of fabric, and the mechanical properties are less than for a tighter weave.

Triaxial braided composites can offer an isotropic design by utilizing axial and angled fiber bundles in a single plane. These are called two-dimensional triaxial braid (2D braid). Typical angles are 0° axial tows with $\pm 60^\circ$ or $\pm 45^\circ$ tows. Through-the-thickness fibers result in a three-dimensional triaxial braid (3D braid). Braided composites also offer better damage resistance, torsional stability, and bearing strength compared to unidirectional or weaved composites [1,2]

Triaxial braid has been used in the commercial aerospace and automotive industry for over 20 years. It has been the focus of the Automotive Composites Consortium (ACC) of US Car and NASA for several years and many articles have been published. [11-14]. It is well-suited for components which are of simple geometry, such as a vehicle shaft, and can provide off-axis as well as unidirectional strength.

3.3 Final Material Selection

Input was solicited from technical members in the aerospace and automotive community regarding the best suited composite material and architecture for the proposed application. Some of the technical points of contact were: Dr. Khaled Shahwan (Chair-ACC100, Energy Management Committee Automotive Composites Consortium, Chrysler Group), Dr. Gary Roberts (Material Engineer, National Aeronautics and Space Administration Glenn Research Center [NASA]), Dr. Ming Xie (Senior Engineer, GE Aviation), Mike Schneider (Chief Consulting Engineer, Composite Applications, GE Aviation), Todd Bullions (Staff Engineer, Composite Material Behavior, GE Aviation), Dan Houston (Chair ACC Materials Committee, Technical Specialist, Manufacturing and Processes Department, Ford Motor Co.), Dr. Steve Mitchell (Group Leader, Composites Manufacturing and Technology Transition, UDRI), Alan Fatz (Director, National Composites Center), Dr. Anthony Waas (Professor, Aerospace Engineering, University of Michigan) and Dr. Mike Braley (Vice-President Application Engineering, A&P Technology).

The overall consensus from the technical experts was to use a braided carbon-thermoset composite since both mechanical and impact properties were important in the potential application of a shaft. Various studies by NASA had published articles using $0^\circ/\pm 60^\circ$ 2D triaxial braid and quasi-static tensile, compression, and shear data were available [11-14]. The literature and survey results were discussed with GWU and it was decided to proceed using a $0^\circ/\pm 60^\circ$ 2D triaxial braid, hereafter referred to as 2D3A. Although the 60° braid angle may not be the one selected for a final shaft component, results from the program could be used to validate finite element models.

3.4 2D3A Specifications

The carbon fiber was Torayca® T700S C 12000, manufactured by Toray Carbon Fibers America, Inc. The braid architecture is given in Table 4. The axial fiber tows contained 24K fibers. The bias tows contained 12K fibers. The spacing of the axial and bias tows were such to provide the same volume of fiber bundles in all directions so that the properties were in-plane isotropic. The resin was Epon 862 epoxy with Epikure W curing agent, both manufactured by Momentive. The resin and agent were selected

because it was the same combination used in the published literature for the 2D3A [11-14]. The material properties are in Appendix A.

Table 4. 2D3A Tow Description

Triaxial Broadgood Design Form (Double Slit)					
Product Code:		AP6699			
INPUTS	Fiber orientation	Bias	Axial	Total	
	Fiber type	T700SC 12K	T700SC 12K		
	Total Sleeve Perimeter (in)	47.89			
	Slit Broadgood Width (in)	23.94			
	Diameter (in)	15.243	15.243		
	Angle °	60.0	0.0		
	Number of Carriers	272	136		
	Ends/Carrier	1	2		
	Raw Fiber Yield (yd/lb)	621	621		
	Fiber Density (lb/in ³)	0.064	0.064		
	Yarn Bulk Factor	1.10	1.10		
	Yarn Aspect Ratio	0.056	0.056		
	Part Fiber Volume	57%	57%		
	OUTPUTS	Layer Thickness (in)	0.0139	0.0070	0.0209
		Material Content (% by volume)	66.7%	33.3%	100.0%
Material Content (% by weight)		66.7%	33.3%	100.0%	
Percent Coverage		100.0%	57.9%		
Areal Weight (oz/yd ²)		10.5	5.3	15.8	
Areal Weight (gsm)		357.3	178.6	535.9	
Yield of full Sleeve (ft/lb)		3.42	6.85	2.28	
Yield of double slit B/G (ft/lb)				4.57	
PPI		4.9		4.9	
EPI		5.7	2.8		
Bundle Width		0.175	0.247		
Bias Yarn CL Spacing (in)		0.176			
Bias Yarn Edge Spacing (in)		0.001			

3.5 Panel Fabrication and Properties

The required number of panels was selected based on initial specimen configuration concepts, discussed in detail in Section 4. A large panel was used to accommodate the expected specimen lengths and to minimize the scrap. The panel thickness was dictated by expected tensile coupon size and UDRI equipment capacity. A maximum of three layers could be accommodated, based on published quasi-static mechanical properties [11-14].

The 2D3A was received as a braided sock. The sock was split along the longitudinal axis and cut to length. Three layers were used for each panel to minimize out-of-plane strains and warpage². The appropriate amount of resin film was added to achieve the desired thickness and target fiber content of 56%. Each panel was assembled, bagged for the autoclave, and then cured by the following cycle: The temperature was ramped up at 1.7°C/min (3°F/min) to 121°C (250°F). The pressure was held at 0.68 MPa (100 psi) for two hours. The temperature was ramped up to 176°C (350°F) at 1.7°C/min and held for two hours. The autoclave was then cooled to room temperature and the pressure released.

Six panels were cured in each cycle. The final panel dimensions were 610 mm x 610 mm x 1.7 mm (24"x24"x0.68"). A total of 18 panels were fabricated. There was some settling of each fiber layer during processing and the 0° axial fiber tows did not necessarily align through the thickness. Regions in a panel where it did occur had wide variations in thickness with noticeable peaks and valleys on the free surface, i.e. the surface not against the tooling. For example, the thickness variation of a relatively flat panel was 0.12 mm compared to 0.47 mm for a panel with noticeable peaks and valleys. The specimen measurement sheets, located on the program CD, illustrate the overall range in thickness.

² Warpage has been noted using single and double layers, as discussed in phone conversations with Mike Braley on 10 April 2010 (A&P Technology) and Todd Bullions (GE Aviation).

At least two samples were selected for fiber content analysis. The specific gravity and fiber content of the tested panels are summarized in Table 5. The average specific gravity was 1.522 ± 0.028 and the average fiber content was $57.16\% \pm 5.86\%$. Four of the panels (073010-3, 073010-4, 073010-5, and 080210-6) had standard deviations in the fiber content in excess of 4 percentage points. The rest had standard deviations less than 2 percentage points. The data in Table 5 reflect the input from all of the samples for each panel. The detailed panel physical properties are in Appendix B.

Axial and transverse cross-sections were taken from two regions to check on the fiber distribution. Appendix C contains photographs of select panels and shows the sample locations used for fiber content analyses and the cross-sections. It also shows the specimen locations.

Figures 1 and 2 show the typical axial cross-sections for two panels. The grey regions are the 0° fibers. The two panels vary by 0.24 mm in peak thickness, illustrating the variation mentioned earlier. The 0° fibers are the lighter regions in the transverse cross-section of Figures 3 and 4. A higher amount of resin is noticeable in the tow cross-over regions in both orientations. Sample photomicrographs taken at 50X are in Appendix D. Additional photomicrographs are on the program CD.

Table 5. Laminate Physical Properties

Panel Identification	Specific Gravity (standard deviation)	Fiber content % (standard deviation)
072910-1	1.528 (0.005)	56.75 (0.91)
072910-2	1.538 (0.006)	59.45 (0.44)
073010-1	1.505	54.11
073010-2	1.516 (0.028)	56.99 (1.90)
073010-3	1.524 (0.006)	59.45 (5.18)
073010-4	1.536 (0.003)	51.71 (6.69)
073010-5	1.529 (0.14)	61.35 (10.8)
073010-6	1.527 (0.007)	57.35 (0.17)
080210-6	1.481 (0.076)	55.30 (3.96)
Overall	1.522 (0.028)	57.16 (5.86)

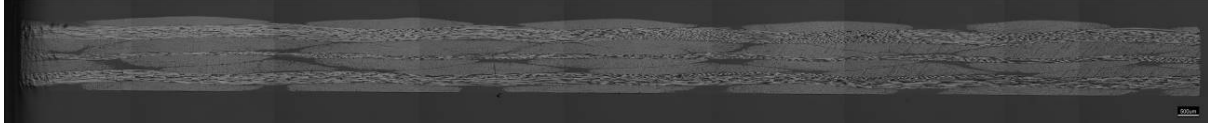


Figure 1. Axial Cross-Section of Panel 073010-1 at 25X

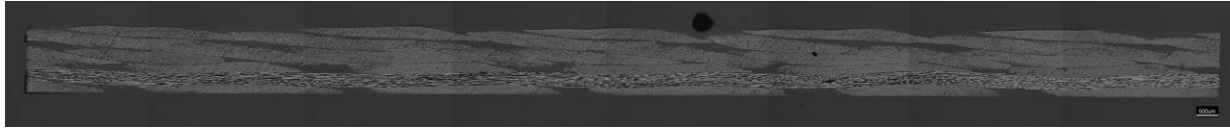


Figure 2. Axial Cross-Section of Panel 080210-6 at 25X

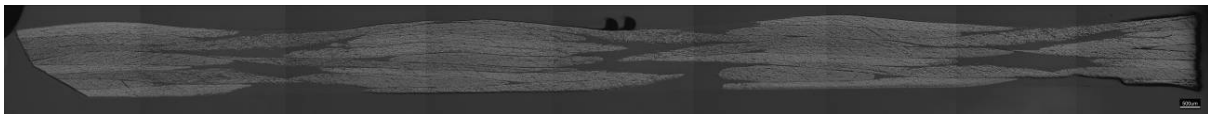


Figure 3. Transverse Cross-Section of Panel 073010-1 at 25X

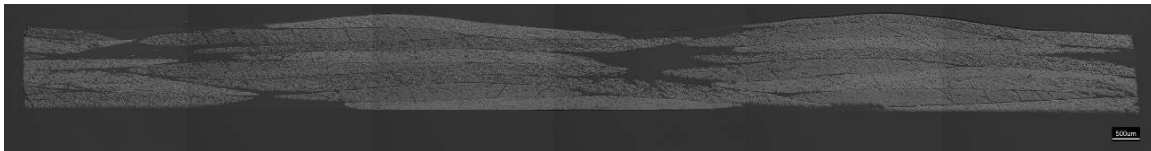


Figure 4. Transverse Cross-Section of Panel 080210-6 at 25X

3.6 Tube Fabrication and Properties

Part of the test program included testing of a structure, such as a box or tube. Several papers are available detailing the results of crush tests of rectangular boxes, open sided boxes, and tubes [15-17]. A cylindrical tube was chosen because of its simplicity for modeling and ease of fabrication.

The bulk fiber volume of a braided tube is different from a flat panel. The initial layer goes over a mandrel that has been machined to the desired diameter. The first layer will have the tightest braid. Each subsequent layer is a little looser in comparison as the carbon is braided over an increasingly larger diameter. The tows have more freedom to move and settle compared to a flat plaque. Wrinkling can also occur as the number of layers increases. Differences in tube fiber content can be adjusted by normalizing to a given fiber level, given the assumption that the resin contribution is negligible. While this is sufficient for uni-axial compression, it is not accurate for off-axis crush tests.

The bulk volume can be increased by adding a tackifier to the resin. The overbraided mandrel is debulked between layers to remove entrapped air. This method was not chosen for two reasons: 1) the flat panels did not contain a tackifier, and 2) the additional cost was not within the program budget.

Ten mandrels were machined by the composite molder, AAR Precision, to the desired diameter of 101 mm (4.0"). The mandrels were shipped to A&P Technologies for overbraiding with three layers of $0^\circ/\pm 60^\circ$ T700 carbon fiber. The braided tubes were then shipped back to AAR for molding using Epon 862W resin. One of the tube preforms was damaged during fabrication and was not molded.

The final tube length was 610 mm with a wall thickness of approximately 1.9 mm. Each tube was cut into two pieces, approximately 266 mm long. Samples were taken for fiber content analysis from each end of the original tube and the center. The tube physical properties are in Table 6. The average specific gravity was 1.448 ± 0.019 and the average fiber content was $44.44\% \pm 2.77$. Appendix B contains the detailed physical properties. Both the specific gravity and fiber content was lower than the flat panels. The fiber content was lower by 17 percentage points.

The axial and transverse cross-sections of a tube are shown Figures 5 and 6. The grey areas in Figure 5 are the 0° fibers. The vertical alignment has not been maintained through the thickness. The pockets of resin at the tow intersections are higher than that seen in the panels (Figures 1 to 4). Additional photomicrographs are in Appendix D.

Table 6. Tube Physical Properties

Tube Identification	Specific Gravity (standard deviation)	Fiber content % (standard deviation)
103-1	1.470 (0.022)	46.58 (4.14)
103-2	1.446 (0.014)	43.17 (1.64)
103-3	1.446 (0.005)	42.59 (1.03)
103-4	1.446 (0.012)	42.90 (1.91)
103-5	1.470 (0.020)	46.89 (3.31)
103-6	1.441 (0.010)	43.89 (2.97)
103-7	1.425 (0.026)	42.55 (4.11)
103-8	1.442 (0.005)	45.27 (0.34)
103-9	1.441 (0.008)	44.78 (1.84)
Overall	1.448 (0.019)	44.44 (2.77)

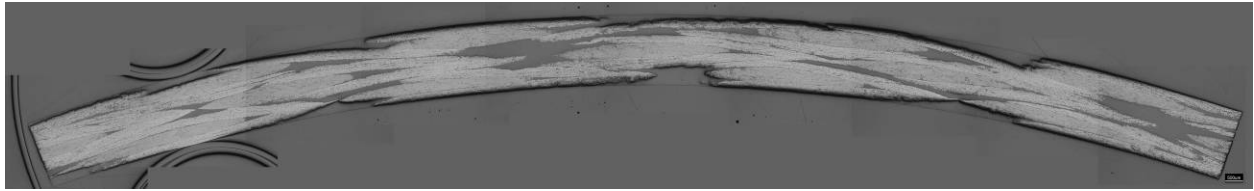


Figure 5. Axial Cross-Section of Tube STL103-1 at 25X

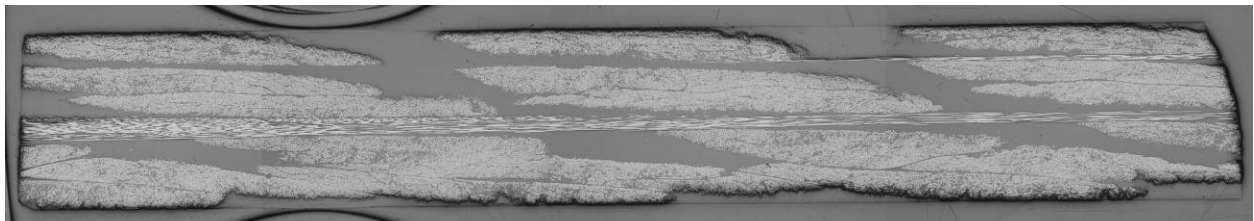


Figure 6. Transverse Cross-Section of Tube STL103-1 at 25X

3.7 Unit Cell Size and Orientation

ASTM D 6856-03 Standard Guide for Testing Fabric-Reinforced “Textile” Composite Materials [18] defines the smallest repeating geometric pattern as the unit cell. Figure 7 illustrates the features defining the unit cell for 2D braid. The unit cell of a 2x2, 2D triaxial braid contains two full axial braids and three full widths of both bias tows. This is the definition used for a unit cell in this program.

Figure 8 shows the outline of a unit cell for one of the laminates. The unit cell size varied with each panel and location within the panel. The variations are probably from the relative amount of settling and compaction of the braid layers during processing.

Table 7 summarizes the average unit cell sizes for each panel. The individual cell size measurements and their locations are in Appendix E. The average unit cell size was 17.9 mm ± 0.53 mm x 5.2 mm ± 0.22mm (0.71” x 0.20”).

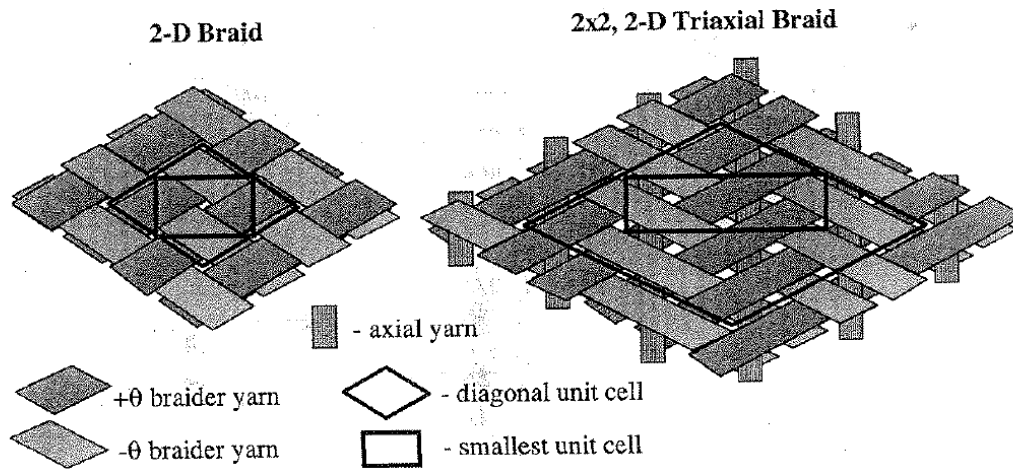


Figure 7. Smallest Unit Cells for a 2-D Braid and 2-D Triaxial Braid
(Reference Figure 2 of ASTM D 6856)

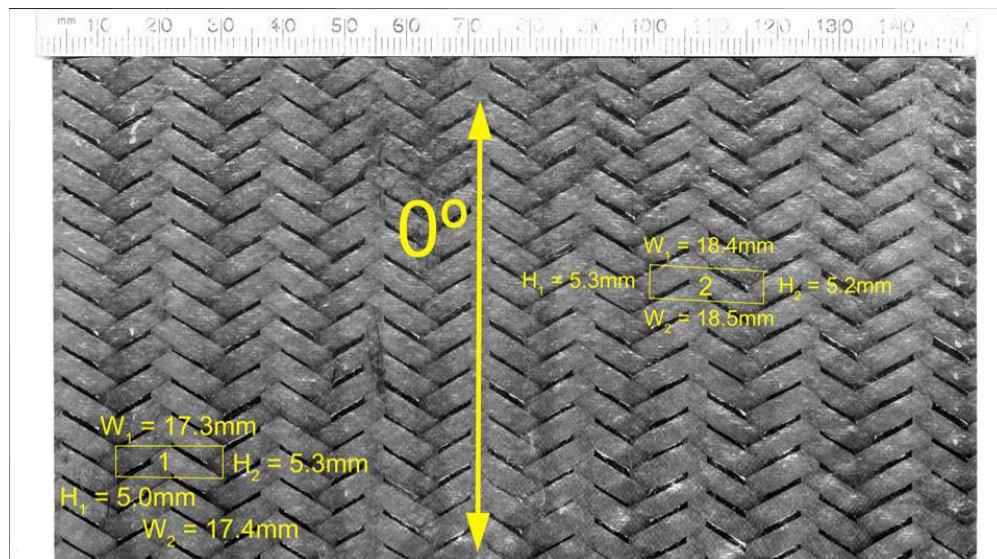


Figure 8. Unit Cell Size

Table 7. Unit Cell Sizes for Panels

Panel		Cell width [mm]	Cell height [mm]
072910-1	Average	18.3	5.3
	Std Dev	0.3	0.2
073010-1	Average	17.6	5.2
	Std Dev	0.7	0.2
073010-2	Average	17.9	5.2
	Std Dev	0.5	0.3
073010-3	Average	18.0	5.4
	Std Dev	0.4	0.3
073010-4	Average	17.8	5.2
	Std Dev	0.4	0.2
073010-5	Average	18.2	5.2
	Std Dev	0.5	0.2
073010-6	Average	17.8	5.4
	Std Dev	0.6	0.1
080210-6	Average	18.1	5.1
	Std Dev	0.3	0.2
OVERALL	Average	17.9	5.2
	Std Dev	0.53	0.22

The testing orientation is shown in Figure 9. The 0° fiber tows are parallel to the short side of the unit cell. This was designated as the axial direction for the tensile and compression specimens as the fibers were parallel to the loading direction. The “axial” shear specimens had the loading parallel to the long side of the unit cell, i.e., it was shearing across the 0° fibers. The transverse shear specimens were 90° from the axial orientation.

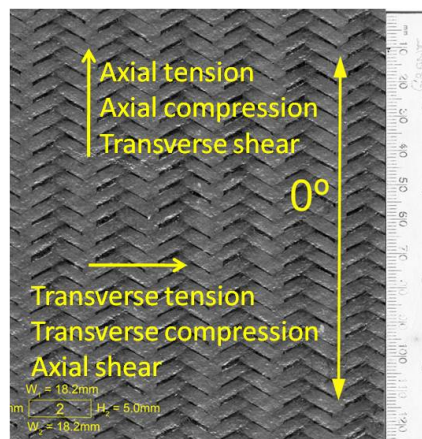


Figure 9. Test Orientation for Panels

4.0 SPECIMEN DESIGN

4.1 Standards

There are several standards referenced by ASTM D 6856 regarding tensile, compression, and shear testing of textile composites, specifically ASTM D 3039 *Test Method for Tensile Properties of Polymer Matrix Composite Materials*, ASTM D 3410 *Test Method for Compressive Properties of Polymer Matrix Composite Materials with Unsupported Gage Section by Shear Loading*, ASTM D 6641 *Test Method for Determining the Compressive Properties of Polymer Matrix Composite Laminates Using a Combined Loading Compression Test Fixture*, ASTM D 4255, *Test Method for In-Plane Shear Properties of Polymer Matrix Composite Materials by the Rail Shear Method*, ASTM D 5379 *Test Method for Shear Properties of Composite Materials by the V-Notched Beam Method*, and ASTM³ D 7078 *Standard Test Method for Shear Properties of Composite Materials by V-Notched Rail Shear Method*.

All of these standards refer to test procedures under quasi-static conditions, i.e., test speeds below 51 mm/min (2 in/min). These standards have been refined over time through the collaborative efforts of a consortium of members which include academia, research laboratories, industry, and government representatives.

Standardized test procedures are mostly lacking for high rate tests. Several guidelines or recommended procedures have been issued related to tensile testing of polymers and steels, such as SAE J2749 *High Strain Rate Tensile Testing of Polymers* [19] and SEP 1230 *The Determination of the Mechanical Properties of Sheet Metal at High Strain Rates in High-Speed Tensile Tests* [20]. No high rate standards are available for compression or shear testing.

High rate test equipment and procedures tend to be specific to a given laboratory, type of equipment, and material. As a result, high rate data are being generated using a variety of test procedures and specimen sizes. While quasi-static procedures serve as a guideline and basis for many of the high rate methods, the high rate methods will be different.

SAE J2749 provides some additional details regarding the generation of useable data at upper rates. Recommendations related to using a small specimen, minimizing the length of the load train, and raising the natural resonant frequency of the test system were important considerations in the design of the specimen geometries of the 2A3D.

4.2 General Background on High Rate Testing

The main purpose or goal of quasi-static test methods is to create a relatively large homogeneous stress and strain field. This is usually accomplished by having as large a specimen gage section as possible. Four implicit assumptions are made when reducing the data from these tests: 1) the load is equal in any cross section of the load train, 2) the strain is equal in the gage section of the specimen, 3) the strain and stress fields are in equilibrium, and, 4) the inertial forces are negligible.

The above assumptions must be scrutinized when measuring material properties at high strain rates. Normally, a constitutive equation is thought of as a function relating stresses to the strains at a point (i.e., an infinitesimal volume of material). A quasi-static test assumes that the stress and strain fields are

³ All ASTM standards are available through ASTM International, 100 Bar Harbor Drive, West Conshohocken, PA

homogeneous in the gage section. The constitutive equation is simply derived from the average response of the tested volume of material.

The wave propagation speed must be considered in a high rate test. The stress wave propagates along the specimen and is reflected and transmitted at each interface along the line of travel. These interfaces include the transition from grip to specimen, specimen to grip, grip to load washer, etc. As a result, stress waves of varying amplitudes are present in the gage section and a homogeneous stress state does not exist.

The goal in high strain rate tests becomes one of “shocking up” the gage area; i.e., introducing enough stress waves in the gage area so that one can assume that an average stress is present. At best, there is an approximate equilibrium. Since the interest is to find any strain rate dependency in the material properties, it is not necessary to determine the “true” material behavior. Instead, a comparison can be made between the behavior at static rate conditions and the material behavior at higher rates.

High rate tests dictate the use of a small specimen in order to maximize the number of reflected stress waves along the gage length. If one assumes that specimen geometry will bias the results equally over the range of strain rates used, then one can determine information on the strain rate dependency of the material.

An example of the importance of the natural test frequency is described below. SAE J2749 states that at least 10 to 15 reflected stress waves should be present in the elastic region to generate acceptable yield data. A general equation relating the speed of a stress wave through the test system is given by Eq. A 13 of SAE J2749 as:

$$t_{\text{wave}} = 2 * \left[\frac{L_{\text{fixt}}}{v_{\text{fixt}}} + \frac{L_{\text{dbg}}}{v_m} \right] \quad (1)$$

where, t_{wave} is the travel time for one stress wave, L_{fixt} is the length of the fixturing, L_{dbg} is the distance between the grips, v_{fixt} is the wave propagation speed through the fixturing and v_m is the wave propagation speed through the material.

The goal is to minimize t_{wave} so that a high number of waves can propagate through the material and fixturing. At some test speed the time scale for t_{wave} will approach that of the time required to achieve the 10 to 15 waves in the elastic region. Discrete stress waves will be observed on the material response.

The v_m is fixed for a given test. The v_{fixt} is dependent on the fixturing material. Test fixtures for composites are made of metal since most composites are high strength materials. The wave propagation speed of most metals is 4000 to 5000 m/s and altering the fixture metal offers relatively little improvement. The terms which can be easily modified thorough fixture and specimen design are L_{fixt} and L_{dbg} . Minimizing the specimen length, and hence the fixture length and weight, is a key component for a successful high rate test system. Figure 10 illustrates the difference in output one can expect by simply from changing the fixture length and weight and, thus, the natural resonant frequency.

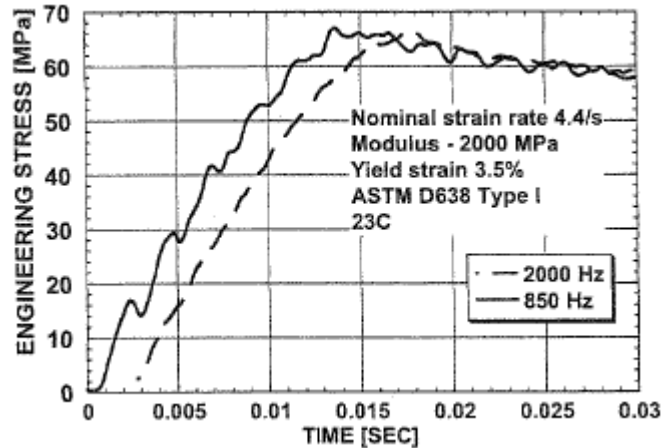


Figure 10. Difference in the Measured Response for Test Systems with Different Natural Resonant Frequencies

Curves shifted along the time axis for ease of comparison. Reference Figure A3 of SAE J2749

4.3 Gage Width for Testing the 2D3A

The ASTM D 6856 recommendation of using at least two unit cells in the gage section was followed for all tests. The final selected widths used at least 2.5 times the unit cell to ensure that at least two full unit cells were located in the gage section. In addition, technical experts who had used this configuration indicated that cracks initiated at the edges were usually blunted within half of one unit cell⁴ from the notch. A gage width of 2.5 unit cells would allow for at least a full unit cell remaining if edge cracking was initiated.

4.4 Tensile Specimen Configuration for Quasi-static Tests per ASTM D 3039

A gage width of 2.5 unit cells was selected for the quasi-static tensile specimens based on the ASTM D 3039 and ASTM D 6825. The specimen length was based on the minimum recommended length using the sum of the gripping, two times the width, and a gage length. The final size for the modified D 3039 axial tensile was 286 mm (l) x 44.2 mm (w) [11.265" x 1.74"], with 185 mm (7.265") between the tabs. The modified D 3039 transverse tensile specimen was 203 mm (l) x 19 mm (w) [8.0" x 0.75"], with 102 mm (4.0") between the tabs. The specimens are shown in Figures 11 and 12.

Several trial runs with tabbed specimens and bolt-loaded specimens were also run in order to determine the load-carrying capability of the 2D3A. The bearing strength data were used to calculate the size and number of bolt holes for the bowtie specimen fixturing.

⁴ Conversations with Dr. Lee Coleman and Dr. Gary Roberts (NASA) on 24 April 2010, Dr. Mike Braley (A&P Technologies) on 10 April 2010, Todd Bullions (GE Aviation)

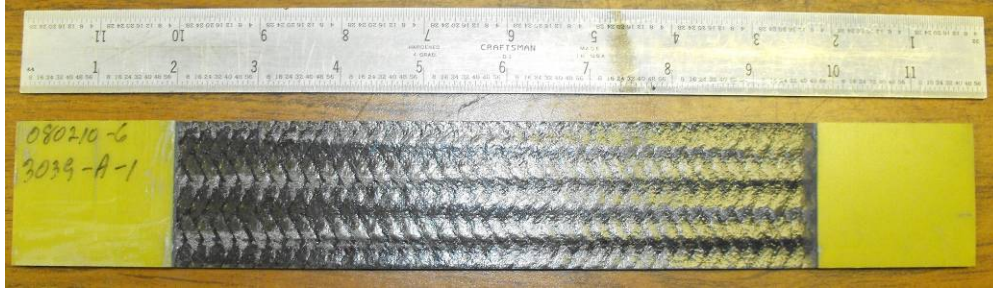


Figure 11. Modified ASTM D 3039 Axial Tensile



Figure 12. Modified ASTM D 3039 Transverse Tensile

4.5 Bowtie Tensile for Higher Rates

4.5.1 Background

A new high rate tensile specimen was designed based on the need for a short specimen length, lightweight grips, low fixture weight, and a shorter load train. All of these factors combined would serve to shorten the load train length, reduce inertial effects, and raise the natural resonant frequency of the test system. This would enable the generation of useable data with minimal resonant stress waves at the higher test speeds.

A review of published literature did not locate any specimen configuration which would have been suitable for high rate testing of the 2A3D. The reported widths ranged from 3 mm to 15 mm [21-26], which were smaller than one unit cell.

A bowtie-shaped specimen had been used by A&P Technologies, a carbon braid supplier, for their aerospace customers. The axial unit cell defined by A&P is half the size of the unit cell used in this program. The A&P transverse unit cell is equivalent. Data from this type of specimen had also been reported by NASA[11]. The NASA configuration was slightly different, as shown in Figure 13. Both of the bowtie configurations modified the angle of the notch to

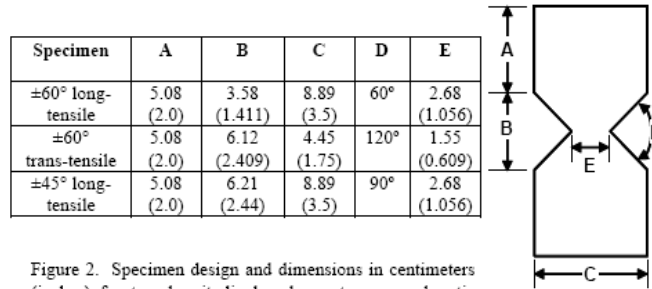


Figure 2. Specimen design and dimensions in centimeters (inches) for two longitudinal and one transverse bowtie configurations.

Figure 13. NASA Bowtie Tensile Specimens [Reference 11]

account for the bias tow angle in a given orientation, e.g. 60° for the axial and 120° for the transverse.

The bowtie configuration has the advantage of a shorter length for the axial orientation than the modified ASTM D 3039. This shape has 100% of the axial and bias fibers in the gage section gripped and fully loaded and should be a better measure of the tensile strength of the 2D3A.

The straight-sided ASTM D 3039 specimen has most of the bias fibers in the gage section cut and not gripped, thus minimizing their contribution to the measured strength. In addition, the cut bias fibers can act as crack initiation sites and cause early failure. In contrast to the bowtie configuration, the modified ASTM D 3039 axial specimen grips 100% of the axial and approximately 28% of the bias tows. The transverse tensile grips a few of the axial tows, and only about 70% of the bias tows. The schematic in Figure 14 illustrates the point using the axial tensile specimen configurations.

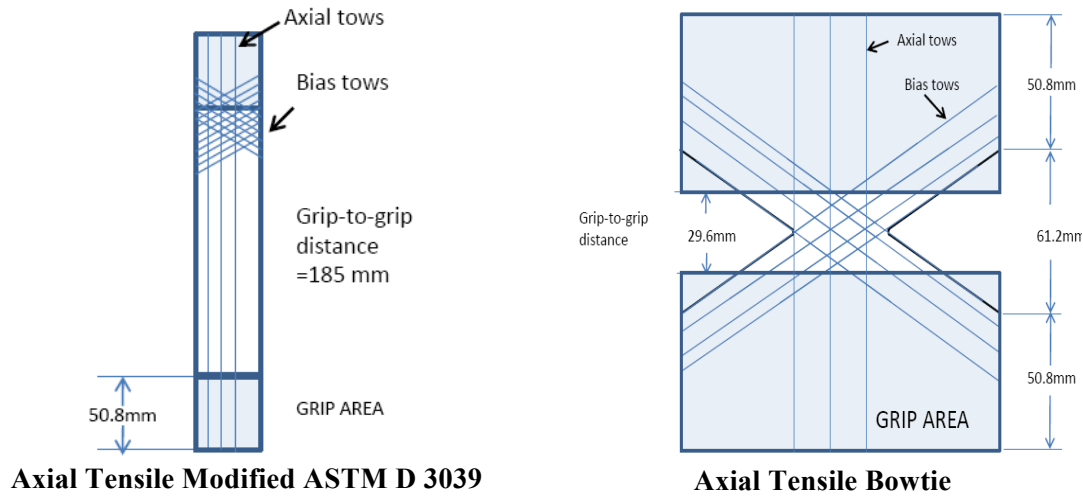


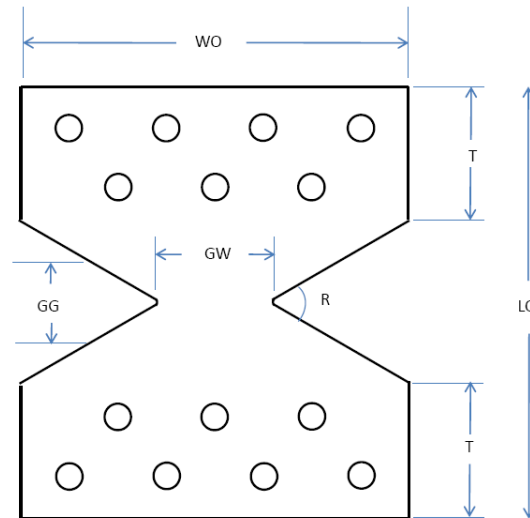
Figure 14. Relative Amounts of Bias and Axial Tows Gripped in Modified ASTM D 3039 and Bowtie Specimen Configurations

4.5.2 High Rate Tensile Specimen Configuration

The final axial and transverse bowtie specimens were designed using the A&P Technologies and NASA configurations as a guideline. The final specimens had 2.5 unit cells in the gage section. The grips

were serrated and extended down past the end of tab (as shown in Figure 14) to ensure full engagement of the bias tows. Figure 15 summarizes the tensile specimen dimensions. The specimens were shear and bolt loaded. Appendix F contains the specimen and fixture drawings for both orientations.

Preliminary tensile tests were performed at 1.27 mm/min using tabbed and bolt-loaded specimens to determine the load-carrying capability of the 2D3A for the final specimen design. The final size and number of bolt holes were a result of these tests.



Specimen Orientation	LO Length overall [mm]	WO Width Overall [mm]	GW Gage Width [mm]	GG Grip-to-grip Distance [mm]	R Notch Radius [degrees]	T Tab length [mm]	Fixture Weight [kg]
0°/+60°/-60° Axial	162.8	147.8	45.7	29.6	60	50.8	3.81
0°/+60°/-60° Transverse	172.7	58.42	17.8	46.8	120	50.8	1.48

Figure 15. Bowtie Tensile Nominal Specimen Dimensions

4.6 Compression Specimen for Higher Rates

4.6.1 Background

ASTM D 6856 recommends ASTM D 3410 (shear loading) or ASTM D 6641 (shear and end loading) for quasi-static compression testing of textile composites. The goal is to force failure into an unsupported section. The preferred failure modes include angled, brooming, though the thickness cracking, and longitudinal splitting. Unacceptable modes include delamination and cracking in the tab region [Reference D 6641]. Strain measurement is usually with strain gages, when applicable.

The high rate specimen configuration had to consider the added width due to multiple unit cells and a region for strain measurement. The standard sizes for ASTM D 3410 (140 mm x 25 mm) [5.5" x 1.0"] and ASTM D 6641 (140 mm x 12 mm) [5.5" x 0.5"] are smaller than the desired 2.5 unit cell width of 44.5 mm (1.75"). Mike Booker, Laboratory Manager of Cincinnati Testing Laboratories, has tested various braided composites and uses a modified version of ASTM D 6641. The specimen has a 25 mm (1.0") width with a proportionally longer straight section. The grips are also heavier because of the additional loading from the wider specimen. While the larger specimen accommodated at least one unit cell, the heavy grip weight and long length of the specimen and fixturing were at odds with the requirements for higher rate testing mentioned in Sections 3.1 and 3.2. For these reasons, a simple modification of the standard quasi-static specimen was not considered for the higher rate tests.

Edge compression of a sandwich construction was investigated because of the potentially small specimen size and minimal fixture length and weight. Kim and Crasto [27,28] developed a specimen similar to that used in ASTM D 3410 using a sandwich of composite with a core of the neat resin used in the composite. The panels were cured as a unit and the specimen tabbed and machined to size. The reported compression strength was much higher than using conventional specimens because buckling was avoided. This method was not considered because of the issues mentioned in the previous paragraph and the added specimen fabrication cost.

A combination of the NASA short block method [29] was also considered. It would have used a composite sandwich with foam or honeycomb as the core and clamped ends. However, the NASA report indicated issues with end-loading of sandwich columns because of core:face separation. The reported strengths were significantly lower than those from other compression techniques. This specimen configuration type was also abandoned.

4.6.2 High Rate Compression Specimen Configuration

The initial high rate compression configuration used a tapered dogbone style, using the ASTM D 695 *Standard Test Method for Compressive Properties of Rigid Plastics* specimen as a guideline. The specimen gage section was designed to be at least 3.5 unit cells wide by at least 3 unit cells tall. However, cracking was initiated at the radius/tab transition of the dogbone during the trial runs. The specimen was modified to a straight-sided rectangle. The widths ranged from 66.7 mm [2.62"] to 71.1 mm [2.80"] wide and 92.2 mm [3.63"] long. This allowed for at least 3.75 and 13 unit cells along the loading direction for the axial and transverse orientations, respectively. The unsupported section was 3 mm (0.125") long.

Anti-buckling support was provided with a backing plate that covered the entire back surface. The front plate covered most of the surface and included a window for strain measurement. The window size for the axial orientation was 2.75 unit cells x 3.75 unit cells (high) for the axial and 3.75 unit cells x 2.5 unit cells (high) for the transverse. Appendix G contains the specimen and fixture drawings.

4.7 Shear Specimen for Higher Rates

4.7.1 Background

The shear standards referenced by ASTM D 6856 for textile composites are ASTM D 4255, ASTM D 5379, ASTM D 7079. ASTM D 4255 uses an un-notched specimen that is bolt and tab loaded. The D 5379 specimen is a V-notched specimen loaded on the edges. The ASTM D 7079 specimen is a V-notched specimen that is loaded through the tabs.

ASTM D 7079 is suitable for braid composites; ASTM 4255 and D 5379 are suitable for uni-directional fiber layups or fabric. Technical experts in braid composite testing⁵ and recent literature [11-14] have tried variations on ASTM D 7079 in order to try to drive the crack through the center. Some variations included tabbing, an extended tab length to add stiffness and limit twisting during loading, fixture modifications to limit the spread of the fixturing during loading, increased notched depths, and various notch angles ranging from 45° to 110° [30].

The literature mentioned failures in the center and towards the edges. Cracks would initiate at the notch tip, propagate down along the center, and then often travel along the braid bias angle and into the grip region. In an email dated 5 October 2010, Dr. Dan Adams wrote regarding determining a “good” failure:

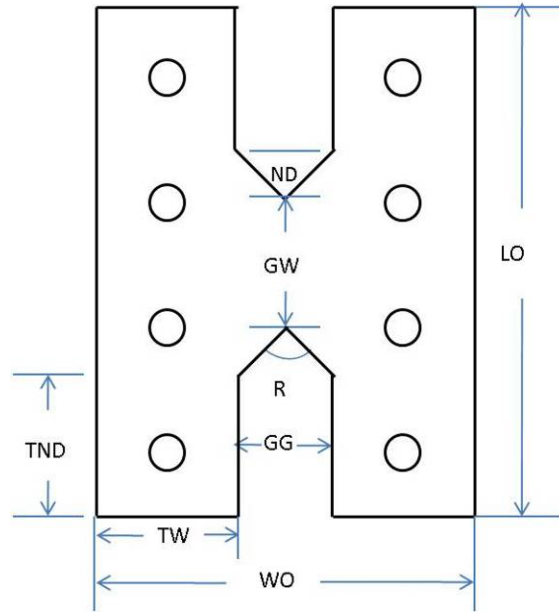
From what I can tell from your emails, you prefer the deeper notch and “sharper” 60 degree notch angle because you can get a crack to form between the notches. I can see why you’d like this to happen... However I feel it’s important to keep in mind that you are testing a 0/+60 laminate(braid) under shear loading, and who’s to say how the “laminate” will fail in shear? That is, a Tau-xy shear stress applied to such a laminate will, in general, produce multiaxial stresses in the plies (in their material coordinate system), and thus at the ply level, the failure may not be through shear... but might be transverse tensile. When we test 0/+45/90 quasi laminates as well as +-45 laminates, the failure is not a crack occurring between the notches, and yet I believe that is how these laminates fail under shear loading.

Dr. Adams’ comments reiterated that there was no clear consensus regarding the specimen configuration or acceptable modes of failure for braid composites. Research programs are currently ongoing at NASA and the University of Utah trying variations on the D 7078 test specimen. The results were not available in time for this program. The experts’ opinions and comments were incorporated as much as possible into a modified specimen that would be suitable for high rate testing.

4.7.2 High Rate Shear Specimen Configuration

The modified high rate specimen included bolt loading in the tab and an extended tab length in order to maximize load transfer and minimize twisting of the specimen during loading. The ASTM D 7078 notch angle was followed. The specimen details are in Figure 16. The “axial” shear specimen had the 0° fibers located perpendicular to the loading direction; i. e. shearing was across the 0° fibers. Conversely, the transverse specimen had the 0° fibers parallel to the loading direction and shearing was across the bias fibers. Appendix H contains the specimen and fixture drawings.

⁵ Conversations and email correspondence with Mike Booker (Cincinnati Testing Laboratories), Dr. Mike Braley (A&P Technologies), and Todd Bullions (GE Aviation), Dr. Dan Adams (Professor, Mechanical Engineering, University of Utah), .Dr. Suresh (Raju) Keshavanarayana (Assoc Professor, Aerospace Engineering, Wichita State University)



Specimen Orientation	LO Length overall [mm]	WO Width Overall [mm]	GW Gage Width [mm]	GG Grip-to-grip Distance [mm]	R Notch Radius [degrees]	TND Tab Notch Depth [mm]	Tab Width [mm]	Notch Depth [mm]	Fixture Weight [kg]
0°/+60°/-60° Axial	162.8	137.2	47.9	35.8	90	50.8	50.8	17.9	1.44
0°/+60°/-60° Transverse	104	86.4	12.7	10.2	90	39.9	50.8	5.1	0.582

Figure 16. Shear Specimen Nominal Dimensions

4.8 Braided Tubes

The 610 mm long tubes were cut into two specimens for a total of 18 specimens. Each specimen was 254 mm long [10.0"] and had a nominal inner diameter of 102 mm [4.0"] and a wall thickness of 3.8 mm [0.15"]. The length to diameter ratio was 2.5. A single 45° bevel was machined into one end of a select number of tubes to act as a crack initiator.

5.0 FINAL TEST MATRICES

The original test matrices in Tables 1 and 2 were modified, based on test results at the lower levels. The revised test matrices are in Tables 8 and 9. The numbers in the table indicate the minimum number of tests at each rate.

Quasi-static transverse tensile tests were added for comparison to published literature. Higher test rates were achieved with the new high rate coupon configurations than originally planned; however, discrete stress waves were noticed in some of the responses at the upper rate.

The straight-ended tube exceeded the actuator capacity and so this part of the tube test matrix was dropped. The balance of the tests used tubes which had a single bevel on the end for crack initiation. The tests above 1.5 m/min were performed at Oak Ridge National Laboratories (ORNL) Test Machine for Automotive Crashworthiness facility (TMAC).

Table 8. Final Coupon-Level Test Matrix

		Machine Rate [m/min]			
		0.00127	0.5	4.5-5.0	38-49
Tension-per ASTM D 3039	Axial	3	-	-	-
	Transverse	3	-	-	-
Higher Rate Tension	Axial	3	3	3	3
	Transverse	3	3	3	3
Compression	Axial	3	3	3	-
	Transverse	3	3	3	-
Higher Rate Shear	Axial	3	3	3	3
	Transverse	3	3	3	3
Total		24	18	18	12
Grand total		72			

Table 9. Final Tube Compression Matrix

	Machine Rate [m/min]		
	1.5	140	440
Straight End	1	-	-
Single bevel	3	7	6
Total	4	7	6
Grand total	17		

6.0 TEST PROCEDURES – SME AT UDRI

The test procedures and guidelines of SAE J2749 and SEP1230 were followed, where applicable. The SME equipment list and calibration records are in Appendix I.

6.1 SME Servo-hydraulic Equipment

Tests were performed at room temperature ambient conditions on MTS servo-hydraulic stations equipped with a 97.8 kN (22,000 lb_f) actuator. Actuator displacement was measured with a linear variable differential transformer (LVDT). The tensile and shear tests used a slack adapter to allow the actuator to attain test speed before applying load to the specimen. While this was not necessarily needed at rates below 500 mm/min, it was included for consistency in the load train across the tested rates.

Load at 1.27 mm/min and 500 mm/min was measured using a load cell calibrated up to 90 kN (20,000 lb_f). The LVDT full scale was 1270 mm. Load at rates above 500 mm/min were measured using a

piezoelectric load washer dynamically calibrated at 5Hz up to 90 kN (20,000 lb_f). The data acquisition computer used a high speed National Instruments PCI 6110E data acquisition card.

The axial tensile test setups are in Figures 17, 18 and 19. The compression setups are shown in Figures 20 and 21. The shear setups are in Figures 22 and 23.

The composite tubes were compressed between two flat platens. A thin film of petroleum jelly was placed on the platens to minimize friction. The load washer was located behind the fixed platen. The tube was placed on the moving platen. The 45° crack initiator was located on the end of the tube towards the fixed end. The angle of the cut was such that the lower edge of the cut was located on the outside diameter of the tube, i.e., the high point was on the inside edge of the tube.

Tube tests at 1.5 m/min were performed at SME. Tests were filmed using the two high speed Phantom cameras (described in the following section) and displacement and strain data were captured. The filming rate was 250 frames per second (fps). A thin film of petroleum jelly was placed on the platen

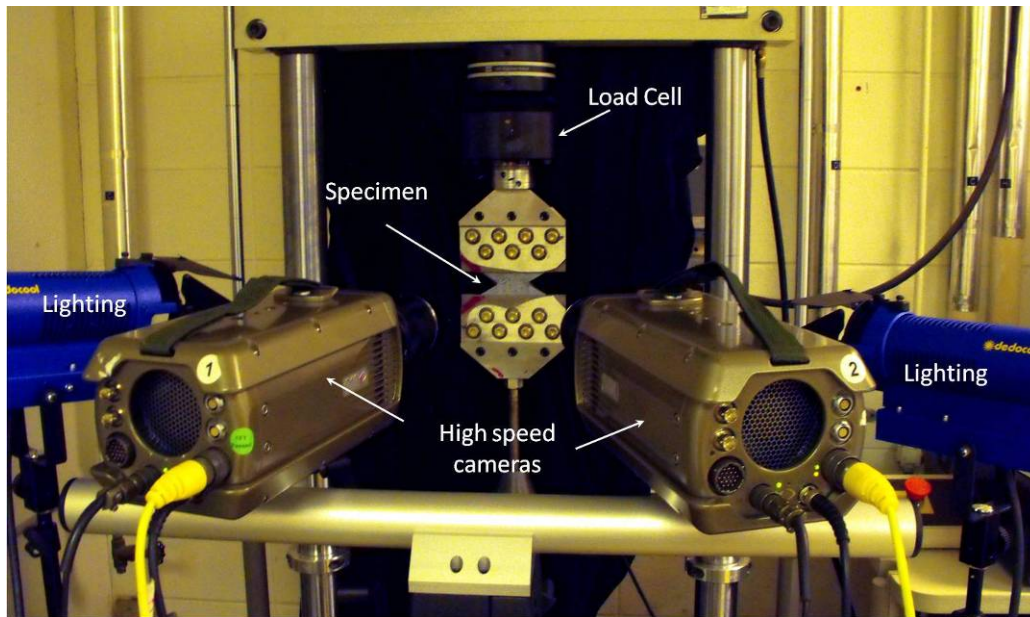


Figure 17. Low Rate Setup for Axial Tensile Testing

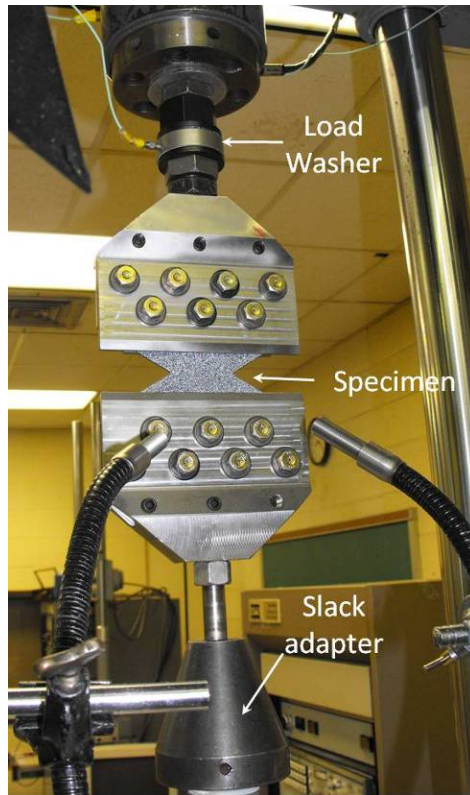


Figure 18. High Rate Setup for Axial Tensile Testing

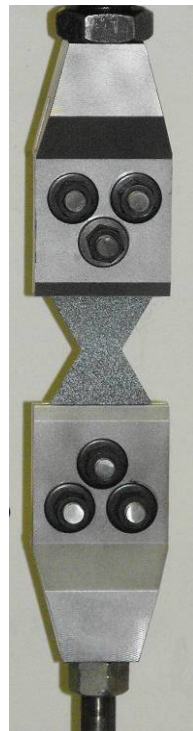


Figure 19. Transverse Tensile in Fixture

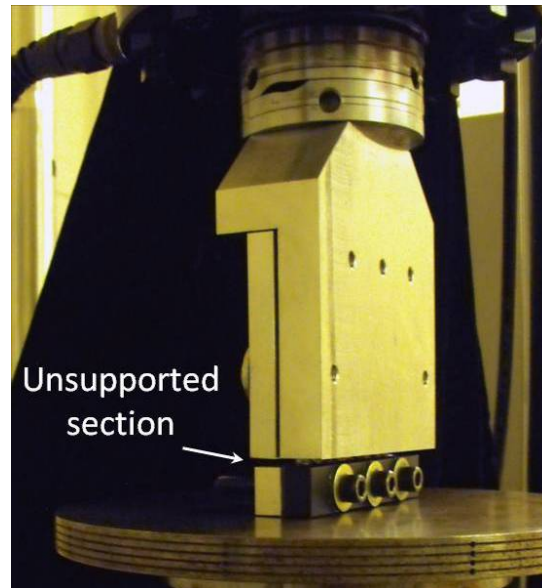


Figure 20. Edge View of Compression Setup showing Unsupported Region

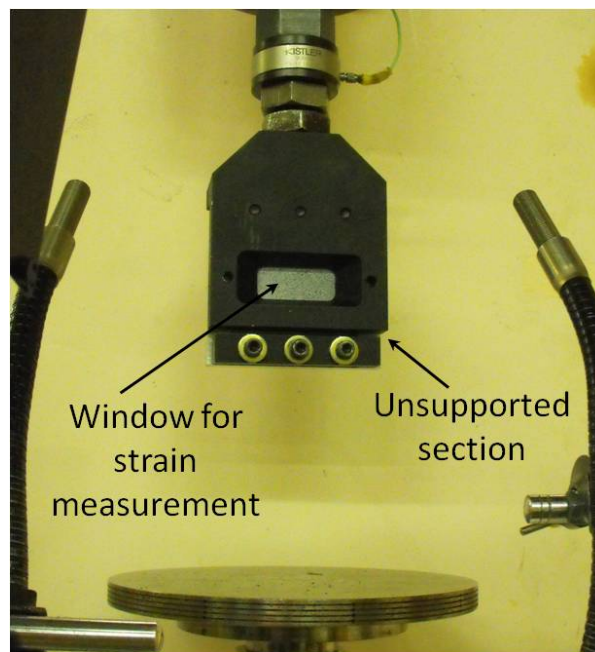


Figure 21. Front View of Compression Setup Used with Strain Measurement

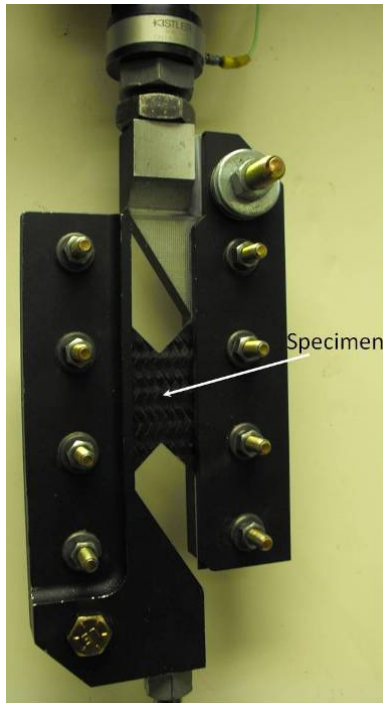


Figure 22. Axial Shear Setup



Figure 23. Transverse Shear Setup

6.2 Oak Ridge National Laboratory (ORNL) Equipment

Tests at 140 m/min and 440 m/min were performed at the TMAC (Test machine for Automotive Crashworthiness) facility of ORNL. The technical point of contact was Dr. Don Erdman. The MTS test station was equipped 1600 gallon per minute servo-valve system and had a load capacity of up to 250 kN at 480 m/min⁶. Load was measured with a piezoelectric load washer. The tubes were compressed between two flat platens. The tube was located on the fixed end. No lubrication was used. The tests were filmed with a single Photron high speed camera. The filming rate was 10K fps. Correlated Solutions Vic 2-D image analysis software was used to estimate displacements. The resolution was too coarse to yield strain data.

The thermal response during the crush was captured with an infrared camera [Phoenix Mid-Wave IR Camera, 320 x 256 pixels, 3-5 micron spectral response). Its capture rate was 800 fps. One of the composite tubes was used to generate a correlation curve relating the IR image to temperature. The TMAC is shown in Figure 24.

⁶ <http://www.volpe.dot.gov/safety/pciv/docs/warren.pdf>

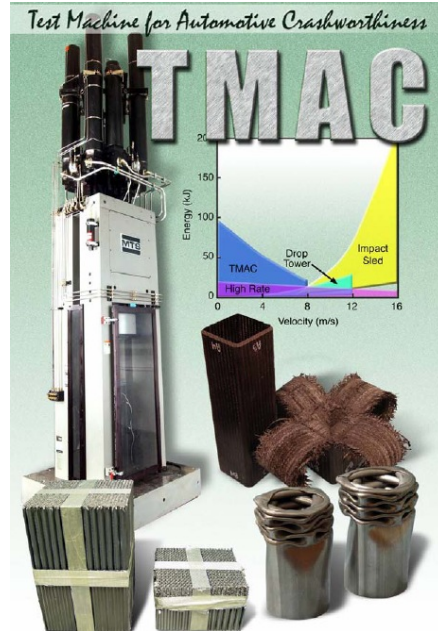


Figure 24. TMAC Equipment at ORNL

6.3 Strain Measurement with Digital Image Correlation System (DIC) with ISTR A Software

6.3.1 General

Full-field 3D deformation was measured using either two high resolution, low-speed Q400 cameras or two Phantom V710 high speed cameras and Dantec Dynamic ISTR A digital image correlation (DIC) software. The general setup is shown in Figure 17.

The ISTR A software tracked the motion of a random pattern on the specimen through the test. Three-dimensional analysis of the pattern movement was used to calculate the net displacements and strains of the features of the pattern. The DIC allowed the user to review the strain response throughout the entire test and then extract strain data for various regions of interest, such as the global strain across the entire straight section or at failure. Several sources are available for additional information regarding DIC measurements [31-34].

The user can select the mesh size for the DIC calculations. A typical grid size is 12 pixels and the facet size is 17 pixels. The grid point is located at the center point of each facet. A facet size larger than the grid size allows for some overlap between calculation points. The deformation data are referenced back to the areas defined by the facets.

High speed DIC measurement is limited by the resolution of the images, not the software. The Phantom high speed cameras are capable of framing rates above 600k frames per sec (fps). However, the available region of interest (ROI) is limited to 256x16 pixels at this speed. This in turn limits the number of data points that can be used in the DIC calculations.

The image size varied with the camera type, filming rate, and the specimen size. Typical framing rates were 25 fps at a test rate of 1.27 mm/min and 50k fps at 46 m/min. The corresponding ROI was

approximately 1280 x 456 pixels down to 336 x 332 pixels, respectively. The actual number of pixels across the specimen was less. The test run sheets, located on the program CD, indicate the number of pixels for the ROI for the various runs.

6.3.2 Specimen Preparation

The measured regions were spray painted with black paint to remove any surface reflections. They were then oversprayed with white to generate the random pattern. The size of the paint drops varied depending on the camera parameters. An example is shown in Figure 25.

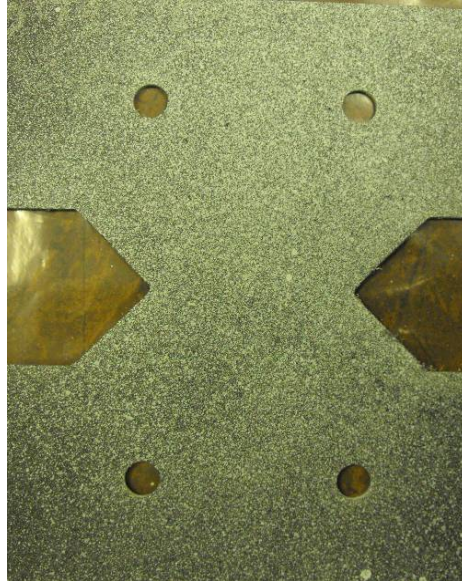


Figure 25. DIC Pattern on Axial Shear Specimen

6.3.3 DIC Measured Region

As mentioned in Section 6.3.1, The DIC software creates a grid over the measured surface. The user can define a point, line or shape over which the displacement and strain data can be extracted. An example is shown in Figure 26, illustrating the grid mesh and the measured regions. The red regions in the V-notch in Figure 26a indicate areas of higher strain and cracking. One can also see differences in the strain carried along the bias tows by the differences in the color (the lighter color blue representing higher strain).

Strain was taken from local regions showing a high or low strain during the test for a select number of specimens. An example is shown in Figure 27. The image shows a high strain point, a low strain point, a line at the center of the V-notch, a small polygon, and a large polygon. The polygon strain data represent a global strain value since the data are averaged across a larger number of grid points than the line and point. The point strain data represented a local strain.

The regions selected for the DIC data extraction varied depending on the specimen shape. In the case of the shear and tensile tests, strain was measured along a line and/or polygon located at the center of the V-notch, as shown in Figures 26 and 27. A larger polygon was used for the compression tests (Figure 28). In contrast to what was seen in the tension and shear tests (Figure 26b), the uniform shading of the center section of the compression tests indicated a relatively uniform strain state.

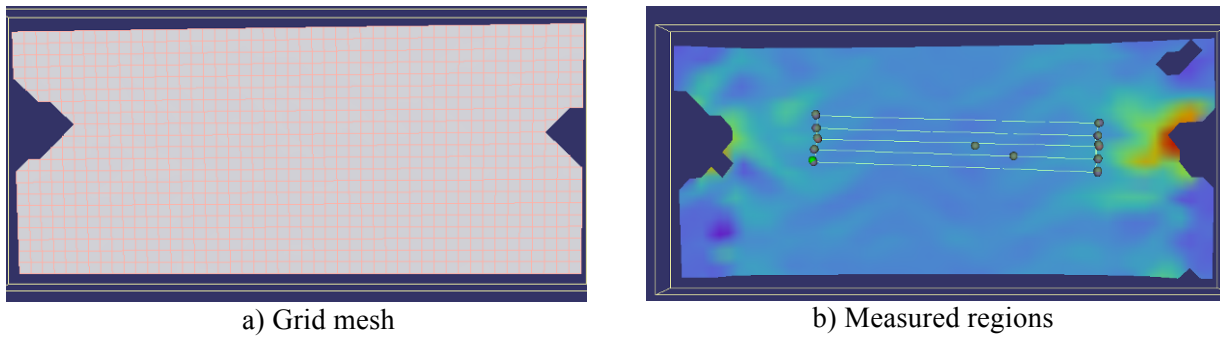


Figure 26. Grid Mesh and Measured Regions for a Slow Rate Axial Tension Test

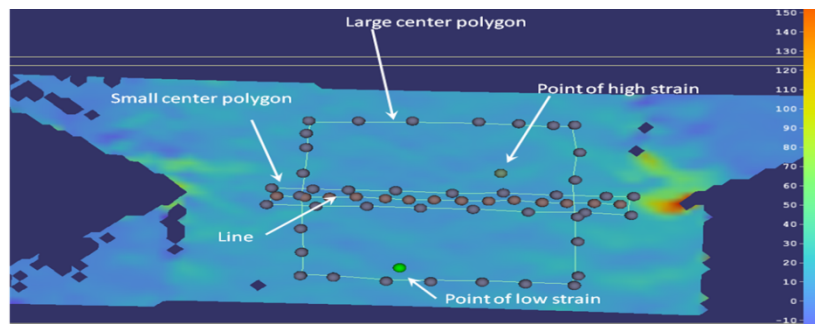


Figure 27. Possible Features for DIC Analysis

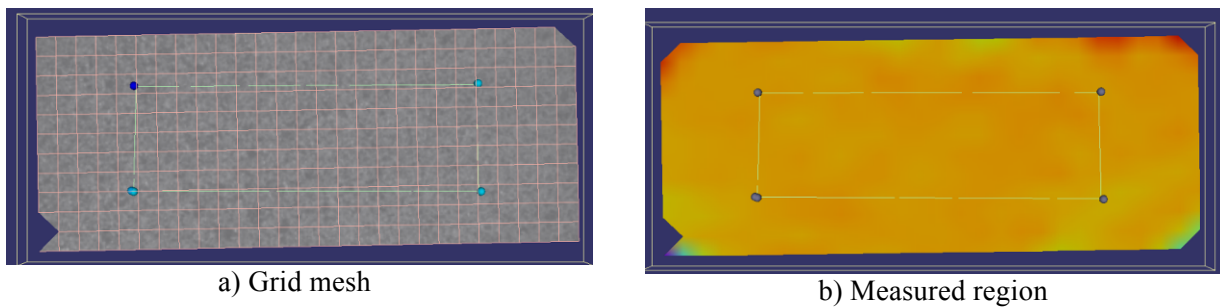


Figure 28. Grid Mesh (a) and Measured Regions (b) for an Axial Compression Test

6.4 Strain Measurement with Strain Gages

Stock strain gages with the grid size needed to cover an entire unit cell were not found. One of the modified ASTM D 3039 axial tensile specimens was strain gaged with a single axis general purpose Vishay Micro Measurements CEA-06-500UW-350 gage. The grid size was 4.57 mm wide (0.19”) x 12.7 mm long (0.50”). It was aligned with the long axis parallel to the 0° fibers. The gage grid covered one-third of a unit cell (horizontally) and 2.5 unit cells (longitudinally).

7.0 DATA ANALYSES

7.1 General

The panel thickness varied depending on whether one measured the “peak” or valley of the surface. The maximum peak was noted where the three layers aligned through the thickness. Two measurements were taken at a peak and two at a valley and averaged for the stress calculations. The specimens measurement sheets, located on the program CD, contain the individual specimen information.

The peak stress was taken as the maximum value before a sudden drop in strength, typically over 25%. Some of the specimens exhibited tearing before failure. The summary tables indicate both peak and failure stress, if applicable. The failure strain was taken at a point of a large drop in load or minimal increase in strain upon continued loading.

The data summary tables include stress data normalized to a fiber content of 56 volume %. This allowed for comparison amongst panels and between the coupon and tube data.

The modulus was determined from the initial slope of the linear best-fit equation to the stress strain curve. The moduli are for informational purposes only and may not represent the bulk material properties. The test procedures did not meet all of the requirements for modulus measurements per ASTM E 111 , such as: a longer specimen (and, hence, a larger volume), a Class B-1 or better extensometer, precise alignment, and a slow test speed in order to avoid adiabatic heating.

The strain rate was determined from the slope of the strain versus time curve over a region before failure. This was generally over a strain range of 0.4 to 1.0% strain. The specific range is listed in the data summary tables.

The physical set-up of the test system results in a time lag between the collection of load and the strain data. The load is measured at one end of the specimen while the strain is measured at the middle of the gage section. It is necessary to transform the load data to the same point in time as that of the strain data via a translation of the strain data in the time domain. The validity of this practice relies on a constant wave propagation velocity in the tested material.

The test speed at which the synchronization is required depends on the data collection frequency and the propagation speed of the stress wave through the fixture and specimen. The time shift was in the order of 40 microseconds for most of the tests in this program.

7.2 DIC Strain Analysis

The Dantec Dynamics ISTR software allows one to select a region of interest for analysis. One can choose to track a point, a line, or a shape (*e.g.*, a polygon). The data can be exported as maximum, minimum, and average values for the chosen shape. The polygon data can also be exported as data for the values around the border or across the surface. The data for this program used the average strain for a line and the average strain across the polygon surface.

The default setting of the software is for unfiltered data. Several levels of filtering are available in order to smooth out the calculations between each displacement. The majority of the program data were filtered using the internal local regression program with a 5x5 level of smoothing.

Some oscillations are present in the strain output. The oscillations have several contributing factors:

1. Strain variations in the braid upon loading
2. Artifact of the DIC analysis technique.
3. Resonant ringing in the system.

Strain variations along the fiber were noted, as seen in Figures 26 and 27. Data were extracted from regions which showed a high and low amount of strain for a select number of specimens. The summary tables list a local strain value for those specimens which had a large difference between the local and global strain.

The magnitude of the oscillations is also affected by the resolution of the grid mesh and the number of grids over which the strain data are calculated. Displacement data for each grid point are used for the strain calculations. Strain data for a point are interpolated from the four grid points closest to it. Strain data for a line uses data interpolated using the four grid points defining each grid block intersected by the line. Strain data for a polygon uses data from each grid point defining the grid blocks intersected by the outline of the polygon. Therefore, the localized fluctuations are reflected in point and line data to a greater extent than a polygon. Local fluctuations are minimized further if a finer grid mesh is used as long as sufficient tracked features remain in the measurement facet.

Figure 29a shows the type of data variations one can have depending on the relative size of the measured area (Figure 29b). The curves are shifted in time to allow for comparison. Note the large oscillations in the data for individual points of high and low strain. The large polygon data are relatively smooth, reflecting the global strain response.

Not all of the oscillations were an artifact of the DIC software. Most of the larger amplitude oscillations occurred after the specimen was loaded. Therefore, a part of the fluctuations are from the transfer of load along the carbon tows.

The strain fluctuations were translated into the stress-strain curve. The stress-strain curve was smoothed using a piecewise polynomial fit of varying orders. The data set for each specimen included both the original and best-fit data for the stress-strain curve. The summary graphs for each data set includes both the as-is and best-fit summary curves. The plots included in the body of the report use the best-fit curves for ease of comparison.

DIC image for the specimen (Figure 29b) shows the strain before failure. The holes in the DIC image are regions where the surface was reflective or the paint was missing. Cracking or flaking of the paint occurred as the specimen started to fail either on or below the surface.

Resonant ringing was not an issue until the top test rate. Figure 30 shows the stress response at the slowest and fastest test rates. The curve at 0.00127 m/min exhibits no resonant waves. A best-fit to the stress curve is the simplest method to filter the response of the small amplitude waves at the 50 m/min rate.

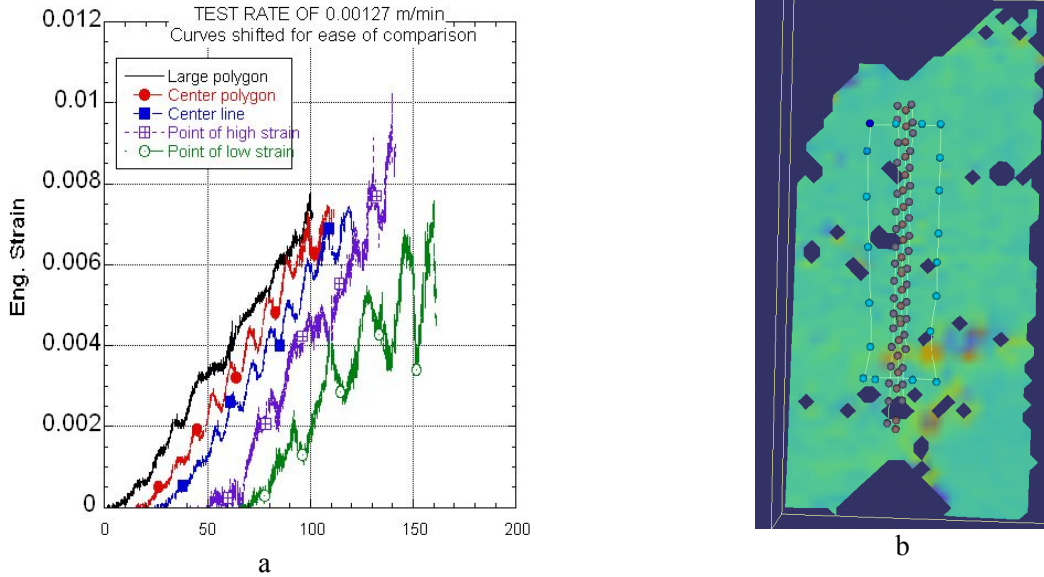


Figure 29. DIC Strain Output for Different Regions (a) and DIC Image (b) for an Axial Shear Test [Specimen STL095-1]

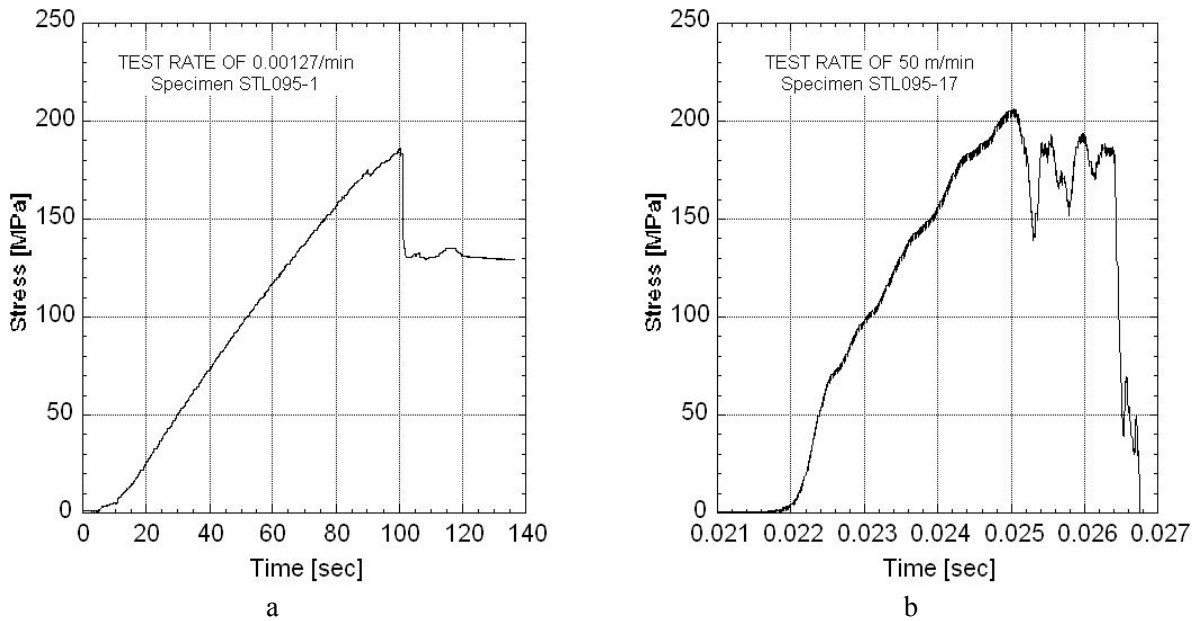


Figure 30. Stress Response at Low (a) and Fast Test Rate (b) for an Axial Shear Test

7.3 DIC Strain

The DIC strain data are given as Lagrangian strain (LS). A MATLAB script was used to compute engineering strain (ES) and true strain, via Eqs. (2) and (3):

$$\begin{vmatrix} T_{11} & T_{12} \\ T_{12} & T_{22} \end{vmatrix} = \frac{1}{2} * \ln \left(2 * \begin{vmatrix} L_{11} & L_{12} \\ L_{12} & L_{22} \end{vmatrix} + \begin{vmatrix} 1 & 0 \\ 0 & 1 \end{vmatrix} \right) \quad (2)$$

$$\begin{vmatrix} E_{11} & E_{12} \\ E_{12} & E_{22} \end{vmatrix} = \sqrt{\left(2 * \begin{vmatrix} L_{11} & L_{12} \\ L_{12} & L_{22} \end{vmatrix} + \begin{vmatrix} 1 & 0 \\ 0 & 1 \end{vmatrix} \right) - \begin{vmatrix} 1 & 0 \\ 0 & 1 \end{vmatrix}} \quad (3)$$

where,

L = Lagrangian Strain 11 = Transverse Strain
 T = True Strain 22 = Longitudinal Strain
 E = Engineering Strain 12 = Shear Strain

7.4 Tube Crush Analysis

Various methods can be used for the data analysis [35], such as the energy absorption (EA), the specific energy absorption (SEA), the specific sustained crushing stress (SSCS), and the crush compression ratio (CCR). The various equations are:

$$\text{EA} \quad W = \int_0^{\delta} p dx \quad (4)$$

$$\text{SEA} \quad E_s = \frac{W}{A\rho\delta} \quad (5a)$$

$$\text{Fold failure} \quad \text{SEA} \quad E_s = \frac{W}{A\rho(\delta + d)} \quad (5b)$$

$$\text{For design purposes} \quad \text{SEA} \quad E_s = \frac{W(\delta_2 - \delta_1)}{m\delta_2} \quad (5c)$$

$$\text{SSCS} \quad \overline{\sigma}_s = \frac{\overline{\sigma}}{\rho} \quad (6)$$

$$\text{CCR} \quad CCR = \frac{\overline{\sigma}}{\sigma_{ult}} \quad (7)$$

P = load, δ = crushed length of tube/displacement, ρ = density, $\overline{\sigma}$ = average crush stress, σ_{ult} = ultimate compressive stress of the braid, d= crush/fan fold length, and m= mass of the entire tube. The value for δ is used for the total crush length if the value for d is small in comparison to the total crush length.

The data for this program were compared using the SEA, the SSCS, and the CCR. The W was calculated using an embedded macro within Kalediagraph® graphing software⁷.out to a zeroed displacement of 115 mm. The specific starting and endpoints used for δ_1 and δ_2 were selected after analysis of the crush behavior across all rates. Further details are given in Section 8.6.

⁷ The area is found by calculating the sum of the trapezoids formed by the data points selected.

8.0 RESULTS AND DISCUSSION

The program CD contains electronic copies of the individual specimen data files, specimen measurements, test data, summary graphs in JPEG and Kalediagraph[®] format, test setup photographs, calibration records, panel information, photomicrographs of the cross-section, photographs of the failed specimens, and other relevant documents.

8.1 Fixture Design – General

The fiber architecture of the braid was the primary concern in the fixture design for the various tests. Incorporation of at least 2.5 unit cells in the test section defined the specimen length, failure loads, fixture length, and fixture mass.

The various fixture designs were able to transfer the load into the specimens. Grip marks were evident in the tab region which was indicative of load transfer through shear. The specific amount of load transferred through the bolts was not determined. No deformation was noted in the bolt holes.

A maximum test rate of 12 to 24 m/min was thought to be a practical limit for the various tests. Clean, useable tension and shear data were generated at rates of 5 m/min. Data at 49 m/min had system resonant waves superimposed onto the material response. Approximately five to 10 waves of varying amplitudes were present before specimen failure, depending on the exact test type and fixture. The compression curves showed resonant waves at a lower test rate (~5 m/min).

The waves are a result of the excitation of the natural resonant frequency of the test system. The limited number of resonant waves indicated that a dynamic equilibrium may not have been present before specimen failure. The resonant waves were not of high amplitude and useable data could be generated with curve fitting. However, this is not the optimum solution.

A specimen and/or fixture redesign would be needed to generate higher quality data at the upper rates. Some modifications of the fixture design would include minimizing the number of bolt holes, and reducing the fixture weight by removing material and/or changing material.

These changes would help improve the data quality at rates from 5 to 50 m/s. Generating useable data at even faster rates would require a specimen redesign. The major contributor to the current specimen design was the decision to include 2.5 unit cells within the test section. This choice dictated the overall specimen and fixture length.

As shown in Eq. 1 of Section 4.2, the specimen length affects both the distance between the grips and the fixture length. These factors directly affect the time for the stress wave to propagate in the system. Minimizing the specimen gage section would reduce the specimen failure loads, reduce the specimen length, reduce the fixture length, and reduce the resulting fixture weight. All of the factors would contribute to reducing the stress wave propagation speed and increasing the natural resonant frequency of the system. Increasing the natural frequency will result in minimizing the resonant wave amplitudes and maintaining a dynamic equilibrium at faster rates.

8.2 Rate Effect on 2D3A Strength

The 2D3A braid is designed to be in-plane quasi-isotropic. Additional layers introduce variations that are dependent on the braid stack-up, nesting of braid tows, mechanical bonding between layers, and resin content, amongst others. A fiber-dominated mechanical property should show little sensitivity to test rate since

carbon fiber is relatively insensitive to strain rate over the tested rate regime [36]. A matrix-dominated property should exhibit some rate effect [37].

The peak tensile, compressive, and shear strengths of the 2D3A for the axial and transverse orientations are shown in Figures 31 and 32, respectively. The axial mechanical properties remain relatively unchanged through the tested rate regime. The slight decrease in the axial tensile strength at the fastest rate is not statistically significant⁸. Five to seven resonant waves were present in the specimens before failure at the fastest rate and the specimens were probably not in dynamic equilibrium.

The transverse tensile strength does not change across the tested rates. There is a slight increase in the compression and shear strengths with increasing rate. Note the large difference between the transverse strength using the modified ASTM D 3039 and the bowtie configuration (Figure 32).

The following sections discuss each test type (tension, compression, shear, tube) in detail.

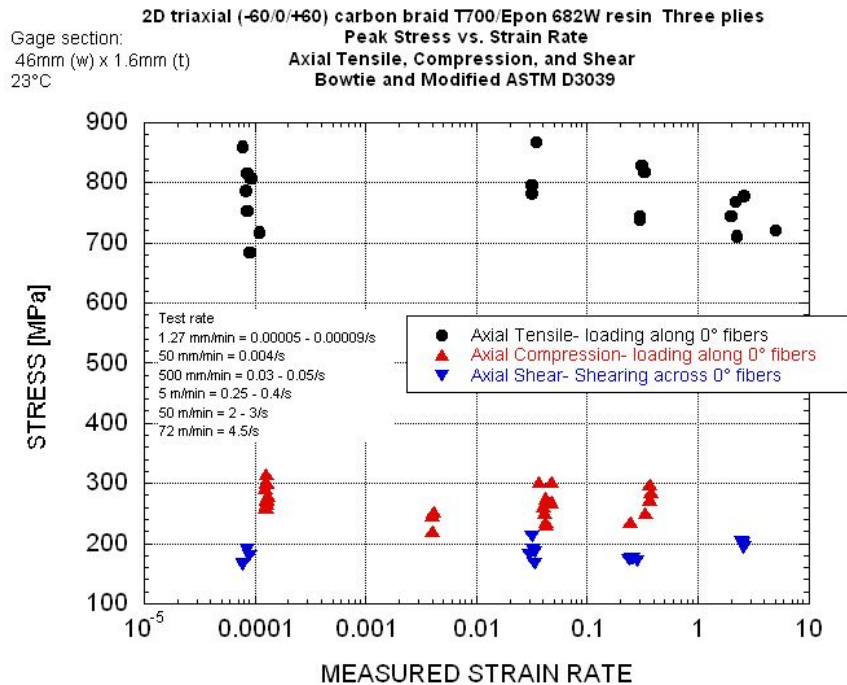


Figure 31. Peak Axial Strength of 2D3A at All Rates – Normalized to 56% Fiber Content

⁸ Two-tail Student’s t-test assuming unequal variances and an alpha=0.05. All comments regarding statistical significance are based on this hypothesis.

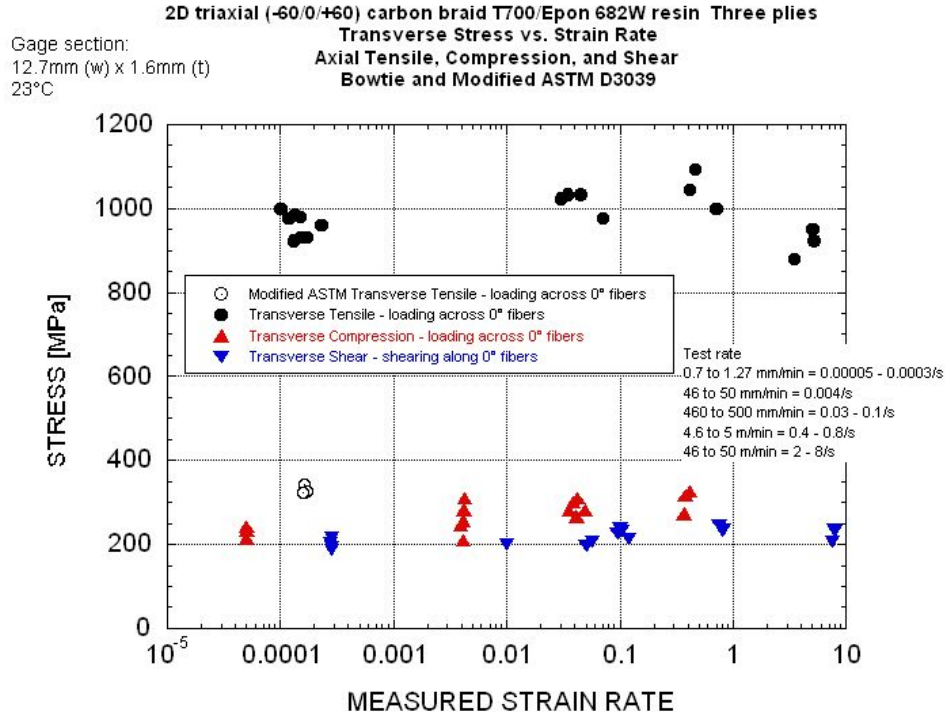


Figure 32. Peak Transverse Strength of 2D3A at All Rates Rates – Normalized to 56% Fiber Content

8.3. Tensile

8.3.1 Modified ASTM D 3039 Tensile

The tensile stress-strain curves for both the axial and transverse modified ASTM D 3039 are in Figure 33. The mechanical properties are summarized in Table 10 along with published results using a 6-layer laminate. Detailed summary tables and graphs are in Appendix J.

The UDRI results are similar to those of published data [11-14], except for the transverse tensile strength. The lower strength of the UDRI specimens was probably due to their smaller width (19.5 mm versus 35.8 mm) and greater sensitivity to edge cracks and early failure. The similarity in the other data indicated that the UDRI measured properties could be used for comparison to the published literature.

One of the axial specimens was strain gaged and the strain data were compared to DIC strain data taken over a similar region. Figure 34 shows the location of the strain gage and its relative size to the gage section. DIC data were in good agreement with the strain-gage data, as seen in Figure 35.

Axial failures were at both ends of the specimen and located close to the tab, as seen in Figure 36a. These failures were at the transition of the gripped and ungripped bias tows. One specimen (STL064-7) failed in the center gage. Its tensile strength was not significantly different from the ones that failed closer to the tab.

Half of the transverse specimens failed in the middle of the gage section (Figure 36b) and half towards the tab. The average strength of the two groups was significantly different. The average strength for the ones breaking in the center was 340 MPa versus 326 MPa for those that broke near to the tab.

The distinct variations in the surface contour can be seen in Figure 37a. The depth of the “ripple” increased with increasing alignment of the 0° tows through the thickness.

Table 10. Comparison of UDRI and Published Data for 2D3A with Epon 862W at Quasi-static Rates
Normalized to 56% Fiber Volume

		UDRI Modified ASTM D 3039 Test Rate of 1.27 mm/min Measured rate of 0.00007/s to 0.00016/s				Modified ASTM D 3039 from Littell PhD Thesis Test Rate of 0.635 mm/min			
		Engineering Breaking Stress [MPa]	Engineering Breaking Strain [%]	Elastic Modulus [GPa]	Poisson's Ratio	Engineering Breaking Stress [MPa]	Engineering Breaking Strain [%]	Elastic Modulus [GPa]	Poisson's Ratio
Axial	Average [DIC data]	857	1.95	43.3	0.31	800	1.78	46.9	0.30
	Std.Dev.	48.4	0.09	1.72	0.01	6	0.08	1.6	0.03
	Coeff. of Var. [%]	5.65	4.81	3.98	4.38	0.75	4.49	3.41	10.00
Transverse	Average [DIC data]	337	1.44	34.7	0.32	462	1.44	41.6	0.29
	Std.Dev.	8.08				36	0.09	1.3	0.02
	Coeff. of Var. [%]	2.40				7.79	6.25	3.13	6.90

Six layer laminate used by Littell versus 3-layer for UDRI

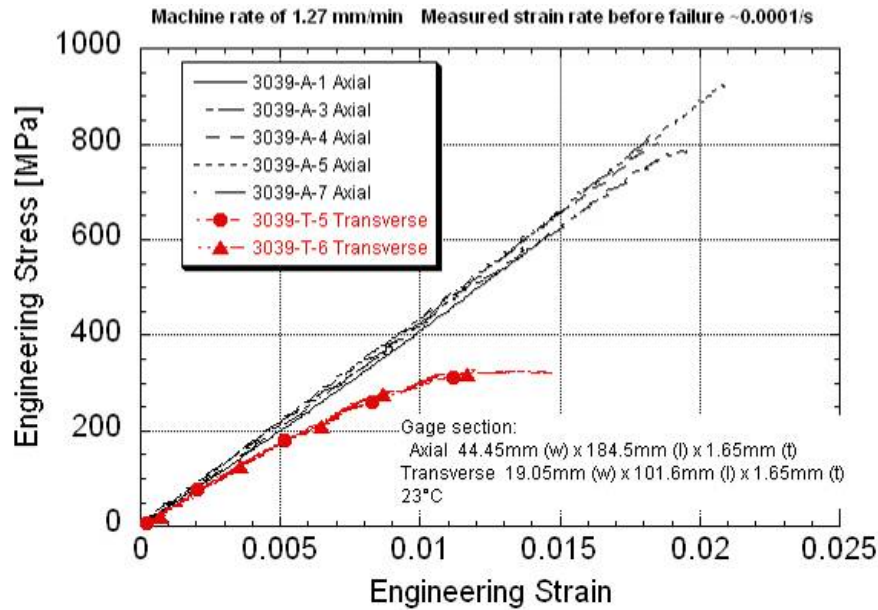


Figure 33. Tensile Stress-strain Curves for Modified ASTM D 3039 2D3A

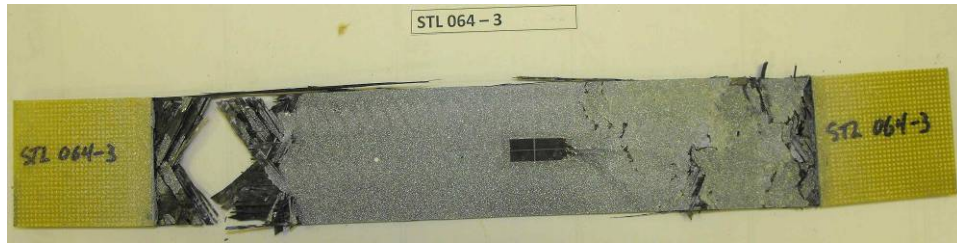


Figure 34. Strain Gage Location for Axial Modified ASTM D 3039 2D3A

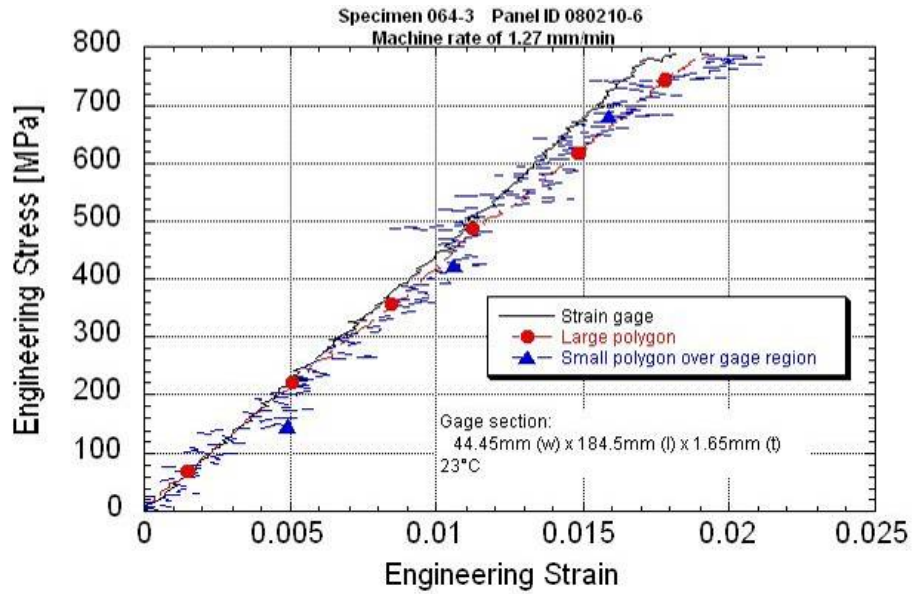


Figure 35. Comparison of Stress-strain Curves using Strain Gage and DIC Data

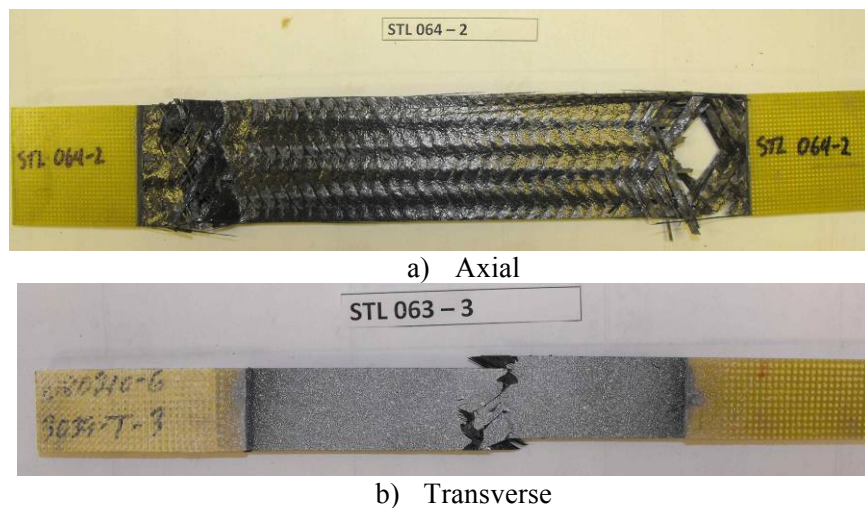


Figure 36. Typical Failure Locations for Axial (a) and Tensile (b) Modified D 3039 Specimens

8.3.2 Bowtie Axial Tensile

Table 11 summarizes the axial mechanical property data. A summary stress-strain graph of the bowtie axial tests across all rates is given in Figure 37. Detailed data and summary graphs are in Appendix K.

Specimens which exhibited vertical cracking by the notch and towards the grip before final failure had a peak strength 30 to 50 MPa lower than those that did not. This contributed to the large standard deviation at certain rates.

The material response was similar within and amongst all rates. The strength and failure strain were insensitive to increasing strain rate. The stiffness at the two lower rates was equivalent. The modulus at the two upper rates was 25% higher. All specimens failed in the center section. A typical failure is shown in Figure 38.

Table 11. Bowtie Axial Tensile Data Summary for 2D3A

		Engineering Breaking Stress [MPa]	Normalized Peak Stress to 56 vol % Fiber [MPa]	Engineering Breaking Strain [%]	Elastic Modulus [GPa]	Poisson's Ratio
0.0001-0.0002/s 1.27 mm/min	Average	798	775	1.31	67.0	0.25
	Std.Dev.	56.7	60.1	0.06	2.47	
	Coeff. of Var. [%]	7.11	7.76	4.81	3.69	
0.03/s 0.5 m/min	Average	865	815	1.44	66.4	0.36
	Std.Dev.	48.9	46.1	0.07	4.18	
	Coeff. of Var. [%]	5.65	5.65	5.13	6.30	
0.3-0.45/s 5 m/min	Average	803	782	1.27	80.6	0.38
	Std.Dev.	60.4	47.7	0.21	5.36	0.01
	Coeff. of Var. [%]	7.53	6.09	16.2	6.66	2.33
2 to 5/s 36 to 45 m/min	Average	783	744	1.33	85.4	0.40
	Std.Dev.	19.2	29.4	0.13	6.62	0.06
	Coeff. of Var. [%]	2.46	3.96	10.0	7.76	15.2

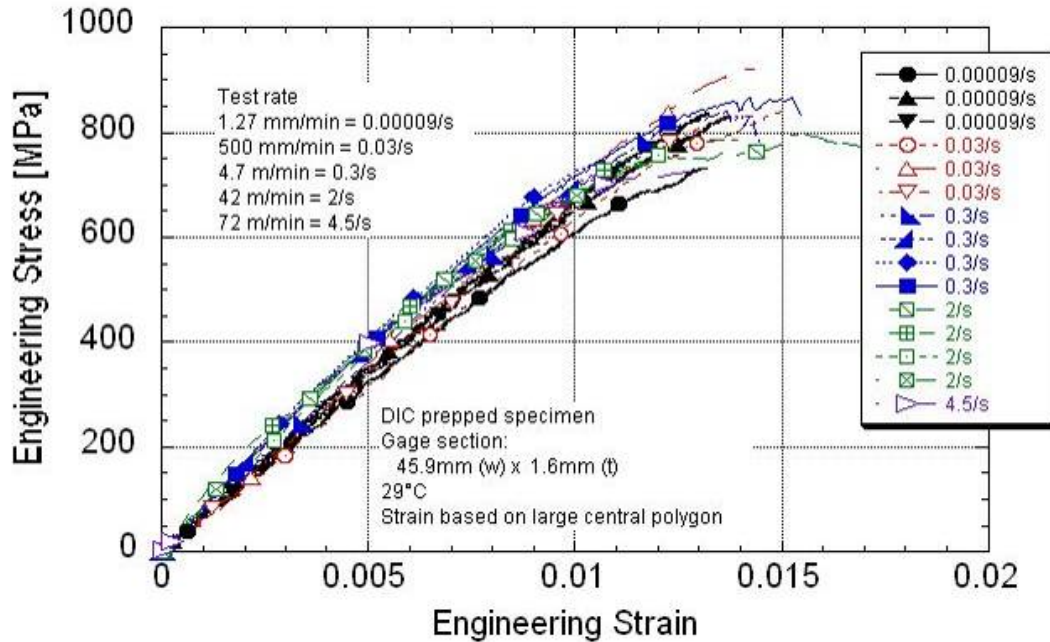


Figure 37. Representative Stress-strain Curves for 2D3A Bowtie Axial Specimens at All Rates

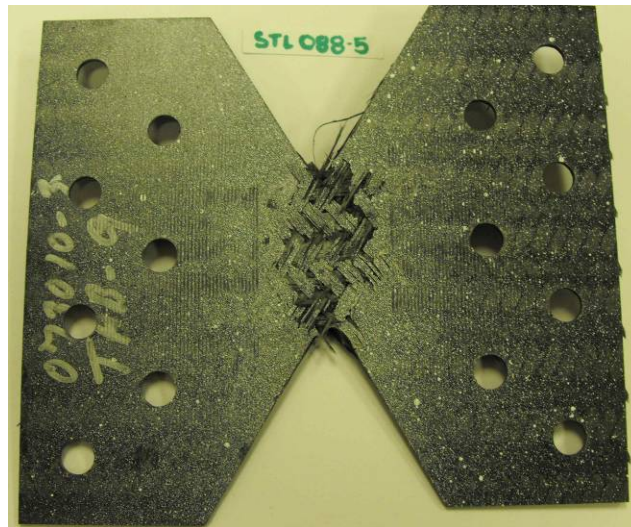


Figure 38. Typical Failure of Axial Bowtie Tensile Specimen

8.3.3 Bowtie Transverse Tensile

The initial bowtie specimens run at 1.27 mm/min showed extended tearing and cracking into the grip before final failure. Shortening the grip-to-grip distance by ~6mm increased the specimen area in the grip and resulted in less tearing before failure. All further tests were done with the shorter grip-to-grip distance.

Table 12 summarizes the transverse mechanical property data. A summary stress-strain graph of the transverse tensile stress-strain curves all rates is given in Figure 39. Detailed data and summary graphs are in Appendix L.

The peak strengths were rate insensitive and the coefficient of variability (COV) was low (3 to 4%). This suggests that all of the fiber tows were engaged and gripped in the fixture and the overall strength is a direct function of the contribution of both the axial and bias tows.

There was a wide disparity in the stress-strain response (Figure 39) compared to the axial tension (Figure 37). The stiffness and breaking strain had a very high COV (14 to 54%) and the material response appeared to fall into two groups.

Table 12. Bowtie Transverse Tensile Data Summary for 2D3A

		Egr Breaking Stress [MPa]	Normalized Peak Stress to 56 vol% Fiber [MPa]	Egr Breaking Strain [%]	Elastic Modulus [GPa]	Poisson's Ratio
0.00015/s 1.27 mm/min	Average	965	942	2.07	66.4	0.01-0.36
	Std.Dev.	30.1	29	0.50	9.6	
	Coeff. of Var. [%]	3.12	3.12	24.3	14.5	
0.045/s 0.5 m/min	Average	1017	992	1.72	116	0.25-0.6
	Std.Dev.	26.9	26	0.31	17.2	
	Coeff. of Var. [%]	2.65	2.65	18.1	14.8	
0.45/s 5 m/min	Average	1046	1026	2.02	81.9	0.03-0.47
	Std.Dev.	45.5	45	0.38	42.8	
	Coeff. of Var. [%]	4.35	4.40	18.6	52.2	
5/s 45 m/min	Average	918	950	2.34	57.9	.03-0.06
	Std.Dev.	34.6	36	0.74	7.1	
	Coeff. of Var. [%]	3.77	3.77	31.7	12.2	

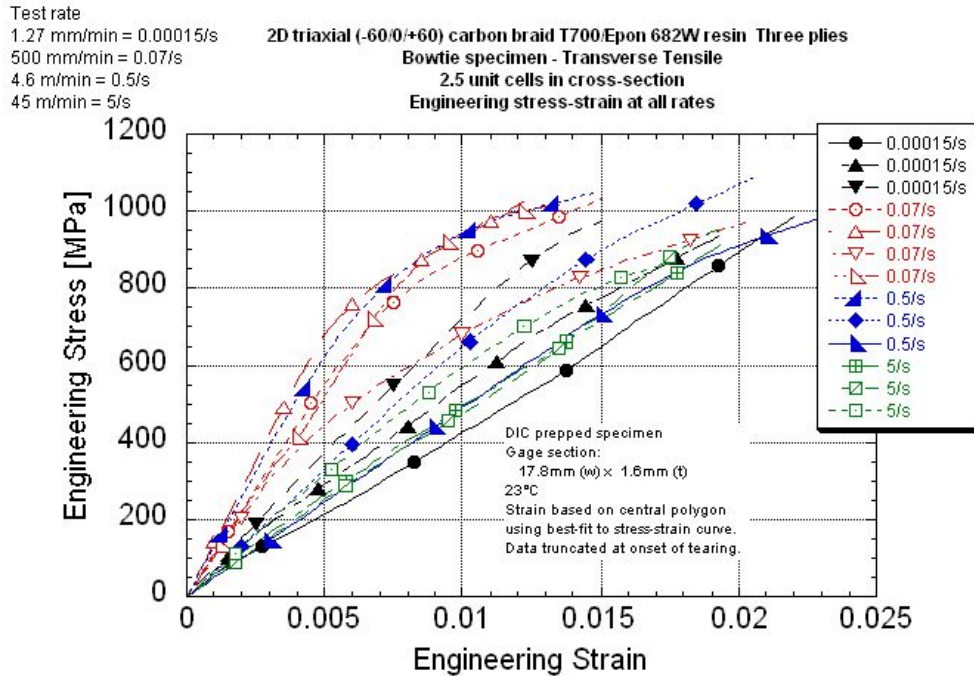


Figure 39. Representative Stress-strain Curves for 2D3A Bowtie Transverse Specimens at All Rates

The stiffness and failure strain reflects the ability of the fiber bundles in the center gage section to move in response to the applied load. The lower COV of the axial tension stiffness and strain (1 to 16%) compared to the transverse suggests that the material response is affected by the relative amount of axial and bias tows in the center gage.

The 2D3A panels consisted of three layers which were free to move and shift during processing. This resulted in panels with varying levels of alignment of the fibers through the thickness. Those with a high amount of alignment had higher variations in thickness in the center gage section. Each center gage width was equivalent to 2.5 unit cells in the corresponding direction. The beginning and end of a unit cell, as defined by the top layer, did not necessarily track through the thickness. Therefore, the amount of axial and bias tows in the tested center gage section could vary depending on the amount of alignment of the tows through the thickness.

Figure 40 illustrates the idealized locations of the 0° and bias tows for the axial and transverse cross-sections in a single layer. The ideal axial notch section (Figure 40a) should have five full tows of 0° fibers with the sixth tow just outside the notch (lightly shaded in Figure 40a). There are five full bias tows in both directions plus one partial tow in each direction. Small misalignment of the fiber bundles through the thickness would add some additional bias fibers. Larger misalignments would increase the number of axial fibers, which should raise the measured stiffness and modulus.

The similar behavior of the axial stiffness within a given rate suggests that the axial mechanical properties were dominated by the 0° fiber tows. Variations due to fiber misalignment through the thickness or along the 0° direction had minimal affects.

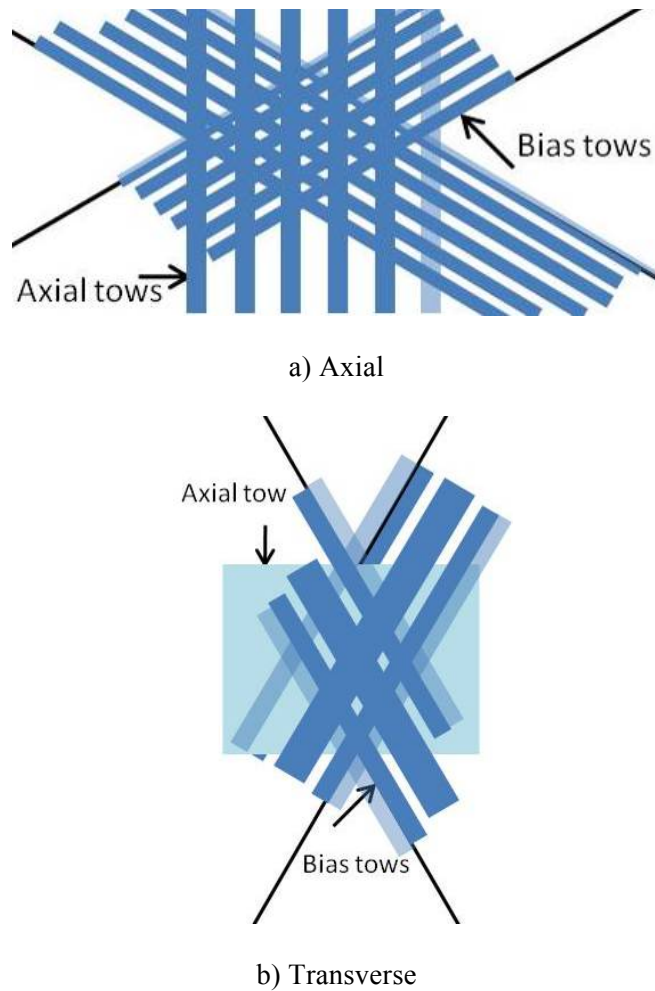


Figure 40. Schematic of Fiber Tow Location in Center Gage for Axial (a) and Transverse (b) Tensile Bowtie Specimen

The notch area of an idealized transverse gage (Figure 40b) will have one full bias tow in both directions and two partial tows (as represented by the lighter shaded rectangles). The axial tow width in the unmolded braid is over 6 mm with sections of bias tows ~ 4 mm wide in-between. The axial fiber tow width is of the same scale as the notch length. Therefore, the amount of axial fibers present in the center can vary depending on whether the notch is mainly in-between two axial tows or intersecting an axial tow; i.e., the center gage can contain anywhere from ~30% up to 100% of the axial fibers in a bundle. This assumes perfect alignment through the thickness. Misalignment of the bundles through the thickness would increase the likelihood of a larger percentage of axial fibers in the gage.

The variability in the transverse material stress-strain curves suggests that the stiffness (and corresponding failure strain) is highly sensitive to the fiber bundle distribution within the center gage. The amount of axial fibers in the notch is the probable cause for the range of values for the stiffness and strain.

8.3.4 Comparison of Bowtie Axial and Transverse Tensile Mechanical Properties

The 2D3A braid is designed to be in-plane quasi-isotropic. As such, one would expect similar properties testing in the axial or transverse direction. The tensile behavior across the rates is similar, as shown in Figure 41. The transverse strength is significantly higher than the axial.

The graph of the measured modulus and failure strain, Figures 42 and 43, reflect the variability in the transverse direction. It is difficult to identify a clear difference in the modulus between the axial and transverse. They are of similar magnitude. The transverse failure strain trends higher than the axial by 0.5 to 1.0 percentage points.

8.3.3 Comparison of Modified D 3039 and Bowtie Axial and Transverse

As mentioned in Section 4.5.1, the bowtie fixture grips 100% of the 0° and bias tows in the gage section under ideal conditions. A small number of fibers may not be gripped depending on the alignment of the tows through the thickness. Cracks initiated at the notch will be blunted by tows extending into the grips.

In contrast, the ASTM D 3039 straight-sided gage section allows for crack initiation along both sides of the straight edge. Only those bias tows close to the tab region are gripped. The axial and bias tows will also blunt the cracks, but the available surface for crack initiation and propagation is much higher than for the bowtie specimen.

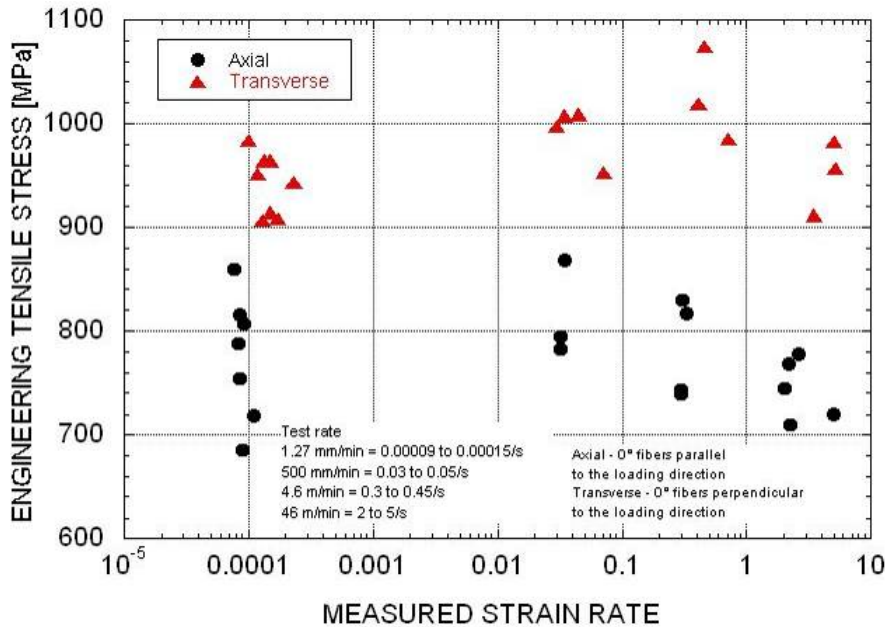


Figure 41. Measured Peak Tensile Stress of Axial and Transverse 2D3A Normalized to 56 vol% Fiber

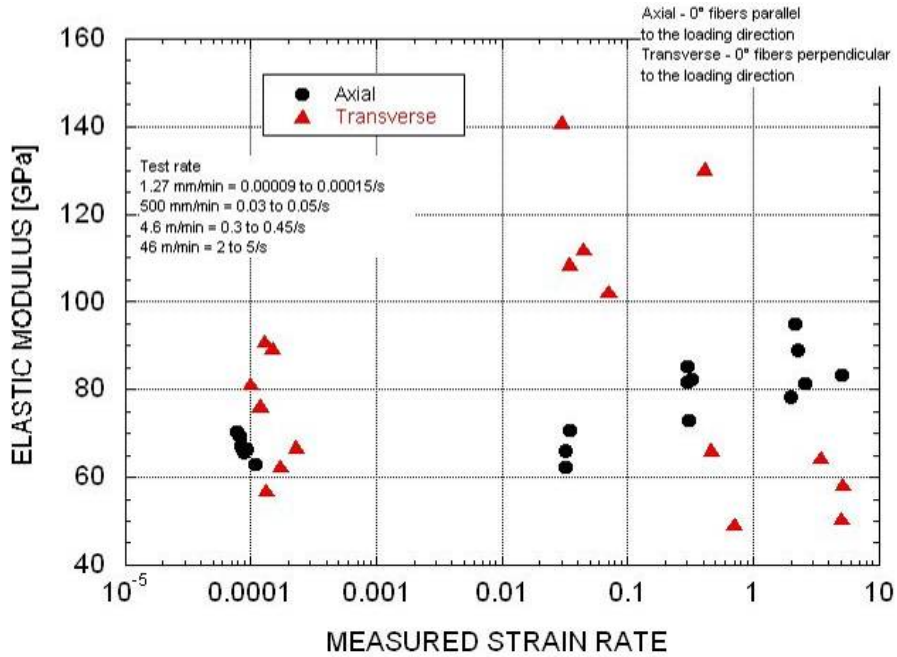


Figure 42. Measured Modulus of Axial and Transverse 2D3A

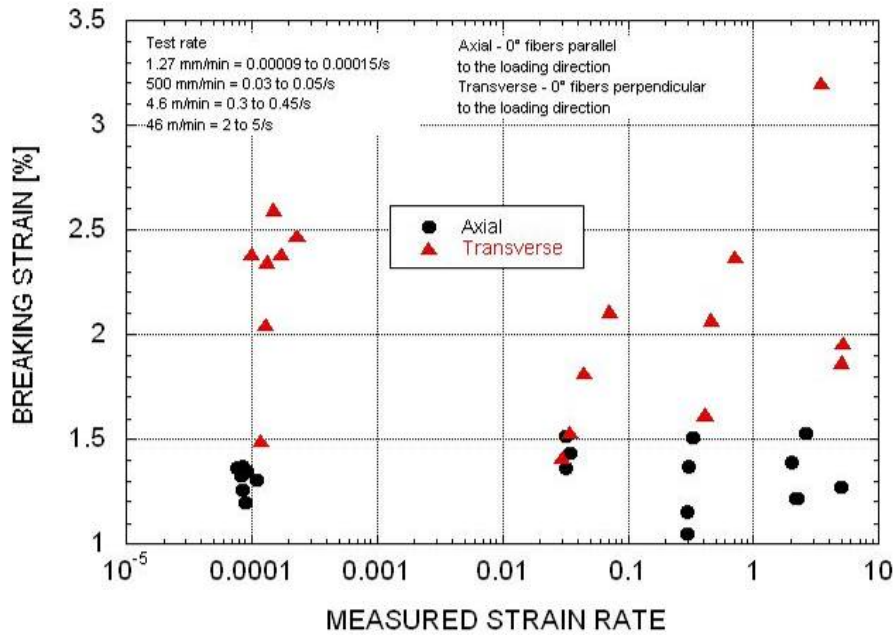


Figure 43. Failure Strain of Axial and Transverse 2D3A

Table 13 summarizes the tensile data for the bowtie and D 3039 configurations at an equivalent test rate. Additional details are given below.

Table 13. Comparison of Bowtie and Modified ASTM D 3039 Tensile Properties at 1.27 mm/min

		BOWTIE					MODIFIED ASTM D 3039				
		Egr Breaking Stress [MPa]	Normalized Peak Stress to 56 vol % Fiber [MPa]	Egr Breaking Strain [%]	Elastic Modulus [GPa]	Poisson's Ratio	Egr Breaking Stress [MPa]	Normalized Peak Stress to 56 vol % Fiber [MPa]	Egr Breaking Strain [%]	Elastic Modulus [GPa]	Poisson's Ratio
Axial	Average	841	817	1.35	68.4	0.25	846	857	1.95	43.3	0.31
	Std.Dev.	23.7	30.6	0.02	1.84		47.8	48.4	0.09	1.7	0.01
	Coeff. of Var. [%]	2.82	3.75	1.38	2.69		5.65	5.65	4.8	4.0	4.38
Transverse	Average	965	942	2.07	66.4	0.01-0.36	333	337	1.44	34.7	0.32
	Std.Dev.	30.1	29	0.50	9.6		8.0	8.1			
	Coeff. of Var. [%]	3.12	3.12	24.3	14.5		2.40	2.40			

8.3.3.1 Axial Tensile

The bowtie axial tensile strength at 1.27 mm/min was 40 MPa lower than the results using the modified ASTM D 3039 specimen. This was still within one standard deviation of the average. The equivalent axial tensile strength suggests that the contribution of the bias tows to the overall strength is minimal. However, the axial failure strain and stiffness were quite different, as seen in Figure 44. The bowtie failure strain was lower by a factor of 0.7 and the stiffness was 58% higher.

The difference in stiffness and failure strain is thought to be due to the restricted available movement of the fiber tows in the center gage section. The restriction is from both the specimen design, with a single region for the stress concentration and failure, and the engagement of all of the tows in the grip. Cracks initiated in the longer length of the straight-sided D 3039 specimen allows for more movement of the tows to accommodate the increasing load. The resultant stiffness is lower and the total strain before failure is greater.

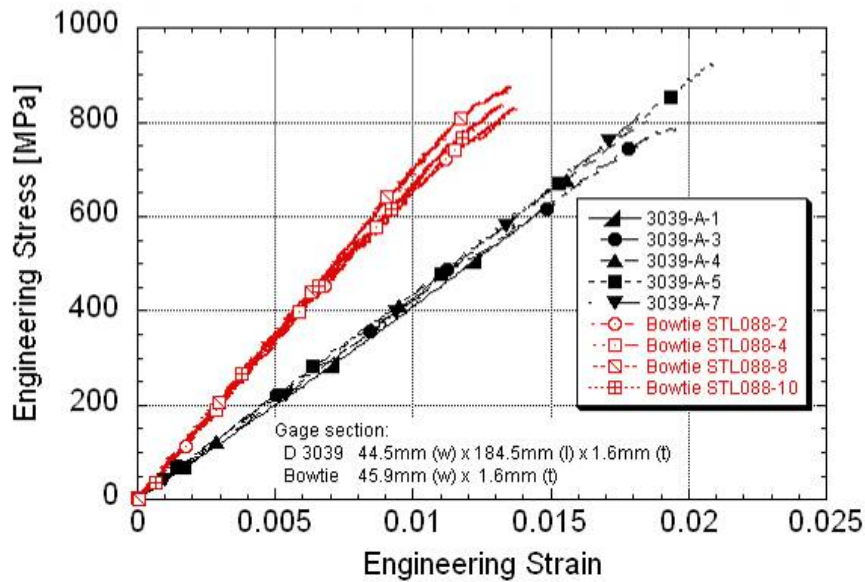


Figure 44. Comparison of Axial Tensile Stress-strain Response at 1.27 mm/min

8.3.3.2 Transverse Tensile

The bowtie transverse tensile properties are quite different. The tensile strength is 280% higher than for the ASTM D 3039. The failure strain is higher, probably because of limited crack propagation in the bowtie versus D 3039 specimen. The bowtie stiffness is higher because of the restricted movement of the gripped fiber tows and the varying amounts of axial fibers in the gage section. Figure 45 shows the stress-strain response for the two configurations.

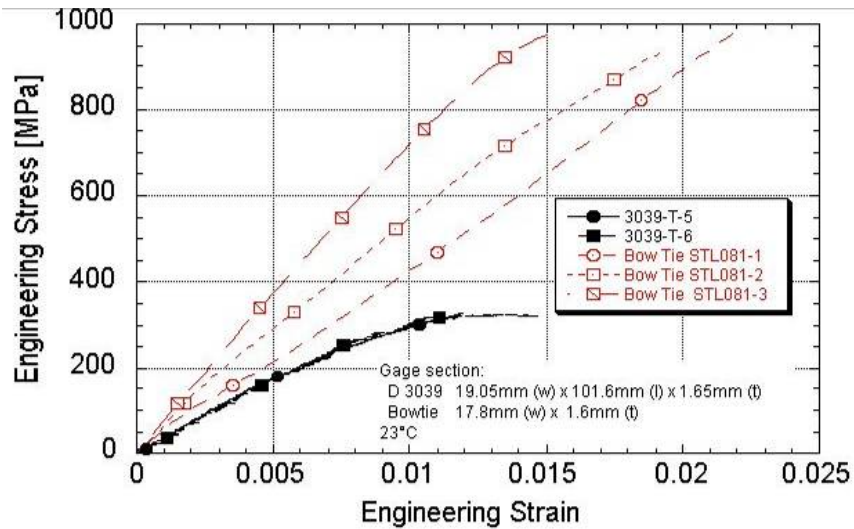


Figure 45. Comparison of Transverse Tensile Stress-strain Response at 0.6 to 1.27 mm/min for Modified ASTM D 3039 and Bowtie Specimens

8.4 Compression

As mentioned in Section 4.6.2, the tapered compression specimen had cracks initiating at the shoulder radius. Failure occurred at the shoulder radius and also in the unsupported section. Subsequent tests used a straight-sided specimen. The width of the specimen (66 to 71 mm) allowed for 4 unit cells in the axial direction and 14 unit cells in the transverse. The unsupported section was 3.2 mm long. The DIC window for the strain measurement covered at least 2.5 unit cells in the loading direction.

Specimens were tested at 1.27 mm/min using a solid backing plate and one with the DIC window to check to see whether the DIC window caused premature buckling or failure in the window. The results did not show a difference in the peak stress or failure location.

Detailed data and summary graphs are in Appendix M for the axial compression and Appendix N for the transverse compression.

8.4.1 Axial Compression

Table 14 summarizes the low rate data using the UDRI specimen configuration and results from Littell. The strength and modulus numbers are within one standard deviation. The failure strain is lower. However, variability data were not given by Littell and the difference may not be significant.

The mechanical properties for the test rates from 0.0004/s to 0.4/s are in Table 15. Figure 46 shows the axial compression stress-strain curves for the straight-sided specimens and Figure 47 includes the dogbone specimens. Figure 46 shows two individual specimens which appear to be outliers. However, two distinct groups are represented when the dogbone specimens are also plotted on the same curve (Figure 47).

The peak compressive strength of the dogbone specimen is not statistically different from the straight-sided specimen (Figure 48). They do have a higher measured modulus and lower failure strain (Figures 49 and 50). One would suspect that the differences are strictly due to the specimen shape. However, two of the straight-sided specimens had a similar response as the dogbone. The difference may be due to the onset of buckling of the axial tows. The modulus and failure strain were insensitive to the increasing strain rate.

The strength at 0.004/s is lower by 50 MPa than at the other rates. The strength data at the other rates are equivalent. There is no assignable cause for the lower strength at 0.004/s.

Figure 51 shows a typical failure for the dogbone and straight-sided axial specimen. Failure in the dogbone was initiated at the shoulder radius and propagated along the DIC window. The straight-sided specimen failed at the unsupported section.

Table 14. Comparison of Axial Compression UDRI and Published Data [13]

		Straight-sided UDRI Test Rate of 1.27 mm/min Measured rate of 0.00012/s			From Littell PhD Thesis [13] Test Rate of 0.635 mm/min		
		Engineering Breaking Stress [MPa]	Engineering Breaking Strain [%]	Elastic* Modulus [GPa]	Engineering Breaking Stress [MPa]	Engineering Breaking Strain [%]	Elastic Modulus [GPa]
Axial	Average [DIC data]	285	0.64	36.0/49.3	327	1.01	41.4
	Std.Dev.	20.6	0.04	2.96/4.27	47		6.0
	Coeff. of Var. [%]	7.22	6.84	8.22/8.66	14.5		14.5

*Two groupings in the stress strain response. Each group had a similar behavior across the rates. The two moduli represent the average for each grouping.

Six layer laminate used by Littell versus 3-layer for UDRI. Littell tested two specimens.

Table 15. Axial Compression Data Summary for 2D3A

		Engineering Breaking Stress [MPa]	Normalized Peak Stress to 56 vol % Fiber [MPa]	Engineering Breaking Strain [%]	Elastic Modulus [GPa]
0.00012/s 1.27 mm/min	Average	283	282	0.64	51.7
	Std.Dev.	13.1	18.0	0.04	4.12
	Coeff. of Var. [%]	4.63	6.37	6.84	7.97
0.004/s 0.48 m/min	Average	252	237	0.73	34.5
	Std.Dev.	16.1	15.1	0.06	2.57
	Coeff. of Var. [%]	6.37	6.37	8.80	7.46
0.45/s 0.48 m/min	Average	284	271	0.71	40.7
	Std.Dev.	26.6	24.7	0.05	5.68
	Coeff. of Var. [%]	9.39	9.12	7.2	13.96
0.4/s 4.5 m/min	Average	280	269	0.76	37.7
	Std.Dev.	30.8	25.1	0.15	4.50
	Coeff. of Var. [%]	10.99	9.32	19.4	11.94

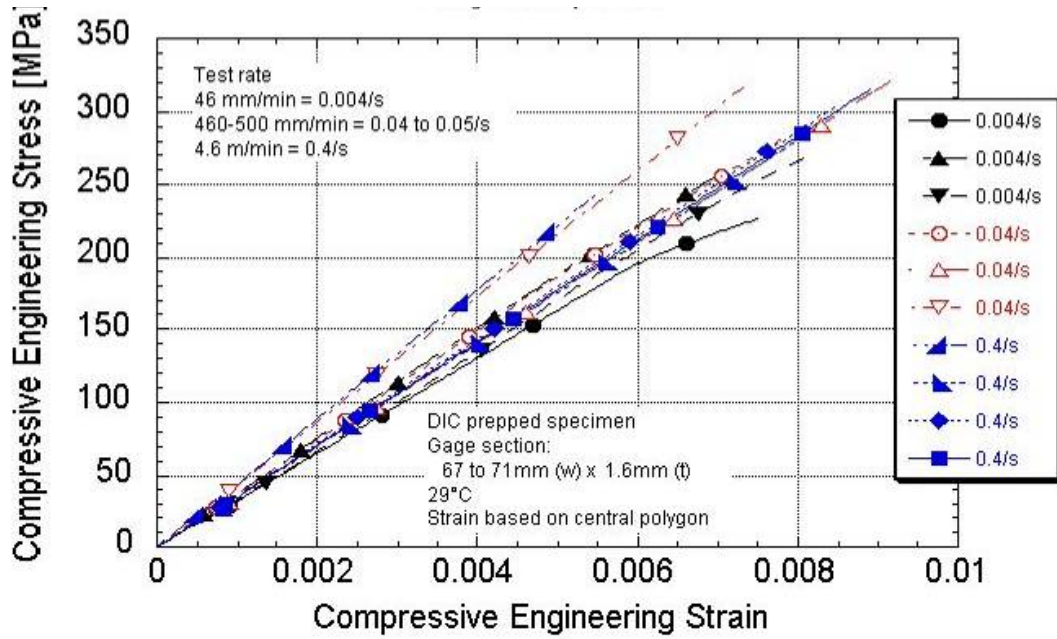


Figure 46. Axial Compressive Stress-strain Response at All Rates Using Straight-sided Specimens

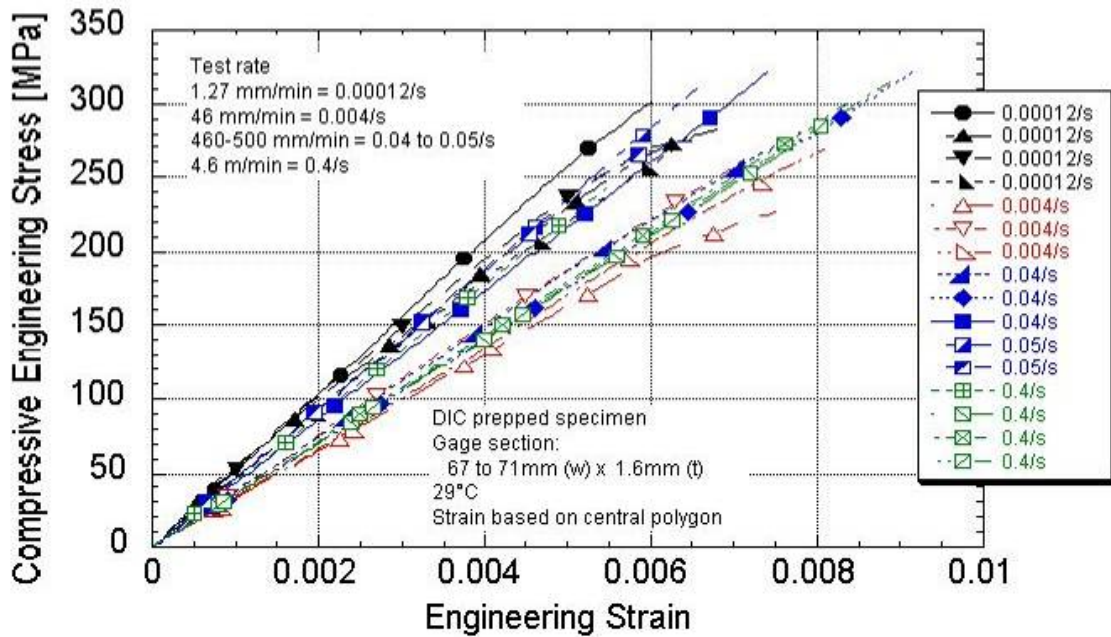


Figure 47. Axial Compressive Stress-strain Response at All Rates Using Dogbone and Straight-sided Specimens

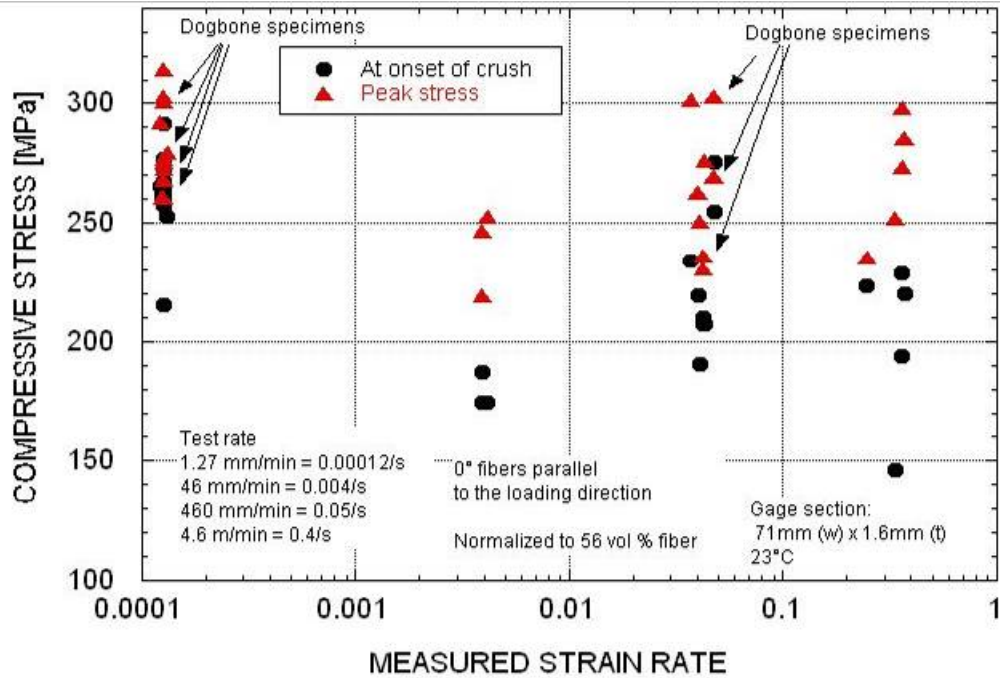


Figure 48. 2D3A Axial Compressive Strength as a Function of Strain Rate

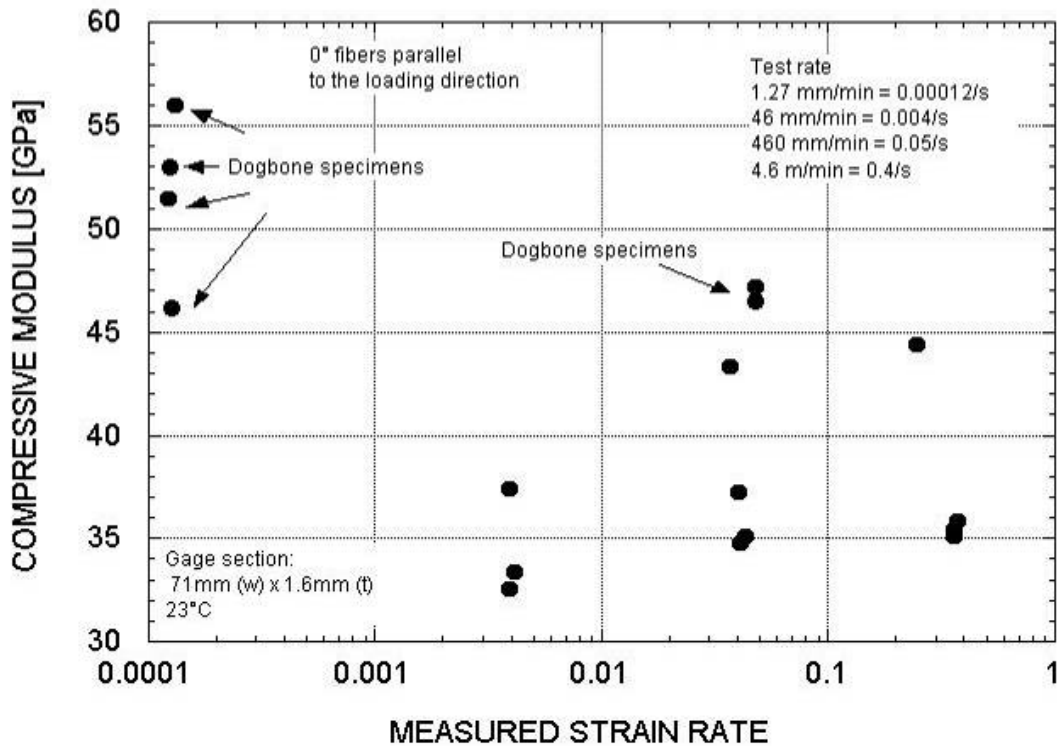


Figure 49. 2D3A Axial Compressive Modulus as a Function of Strain Rate

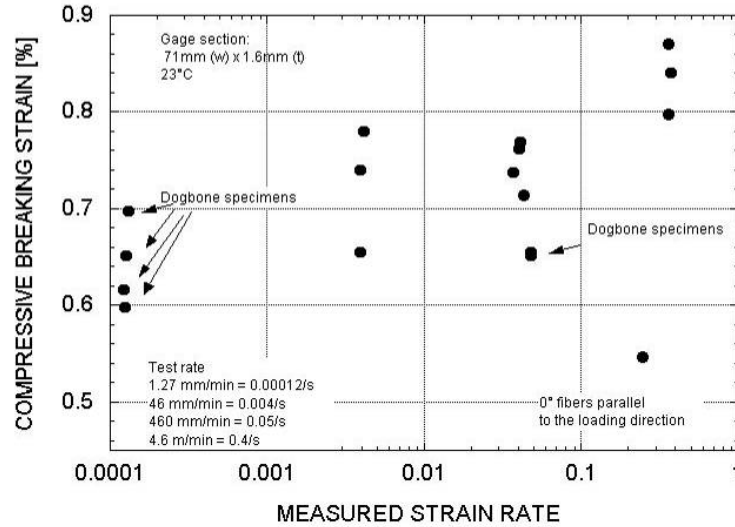


Figure 50. 2D3A Axial Compressive Failure Strain as a Function of Strain Rate

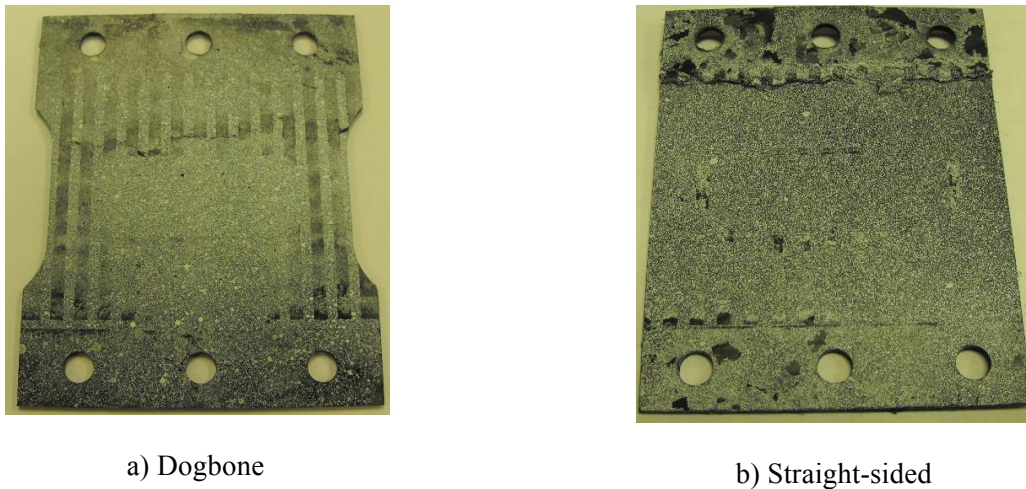


Figure 51. Failure Location for Dogbone and Straight-sided Axial Compressive Specimens

8.4.2 Transverse Compression

Table 16 summarizes the low rate data using the UDRI specimen configuration and results from Littell [13]. The strength data are within one standard deviation. The UDRI data using the high rate specimen are summarized in Table 17.

Figure 52 shows the transverse compression stress-strain curves. All of these specimens were straight-sided. There is an increase of 18% in strength between 0.0004/s and 0.004/s if one excludes an outlier at 0.004/s (Figure 53). The strength across 0.004/s to 0.04/s remains the same. The modulus does not change between 0.004/s and 0.4/s (Figure 54). The modulus increased 13% between 0.04/s and 0.4/s. The failure strain was insensitive to the increasing strain rate from 0.004/s to 0.4/s (Figure 55). Typical failures are shown in Figure 56.

Table 16. Comparison of Transverse Compression UDRI and Published Data [13]

		Straight-sided UDRI Test Rate of 1.27 mm/min Measured rate of 0.00012/s			From Littell PhD Thesis [13] Test Rate of 0.635 mm/min		
		Engineering Breaking Stress [MPa]	Engineering Breaking Strain [%]	Elastic Modulus [GPa]	Engineering Breaking Stress [MPa]	Engineering Breaking Strain [%]	Elastic Modulus [GPa]
Transverse	Average [DIC data]	255	-	-	304	0.87	42.7
	Std.Dev.	32.2	-	-	44		6.2
	Coeff. of Var. [%]	12.6	-	-	14.5		14.5

Six layer laminate used by Littell versus 3-layer for UDRI. Littell tested two specimens.

Table 17. Transverse Compression Data Summary for 2D3A

		Engineering Breaking Stress [MPa]	Normalized Peak Stress to 56 vol % Fiber [MPa]	Engineering Breaking Strain [%]	Elastic Modulus [GPa]
0.00005/s 0.6 mm/min	Average	226	221	-	-
	Std.Dev.	15.2	15	-	-
	Coeff. of Var. [%]	6.73	6.73	-	-
0.004/s 0.48 m/min	Average	265	249	0.72	39.3
	Std.Dev.	34.0	32	0.12	2.8
	Coeff. of Var. [%]	12.8	12.8	17.2	7.25
0.4/s 0.48 m/min	Average	288	271	0.75	40.1
	Std.Dev.	18.2	17	0.08	1.7
	Coeff. of Var. [%]	6.33	6.33	10.0	4.1
0.4/s 4.7 m/min	Average	305	288	0.74	45.0
	Std.Dev.	27.8	26	0.04	2.3
	Coeff. of Var. [%]	9.11	9.11	5.8	5.2

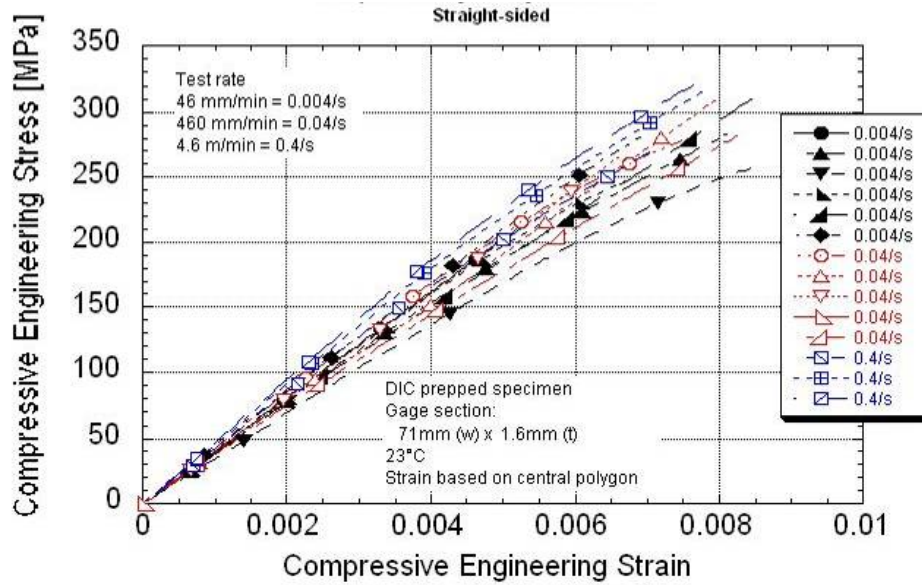


Figure 52. Transverse Compressive Stress-strain of 2D3A at All Rates

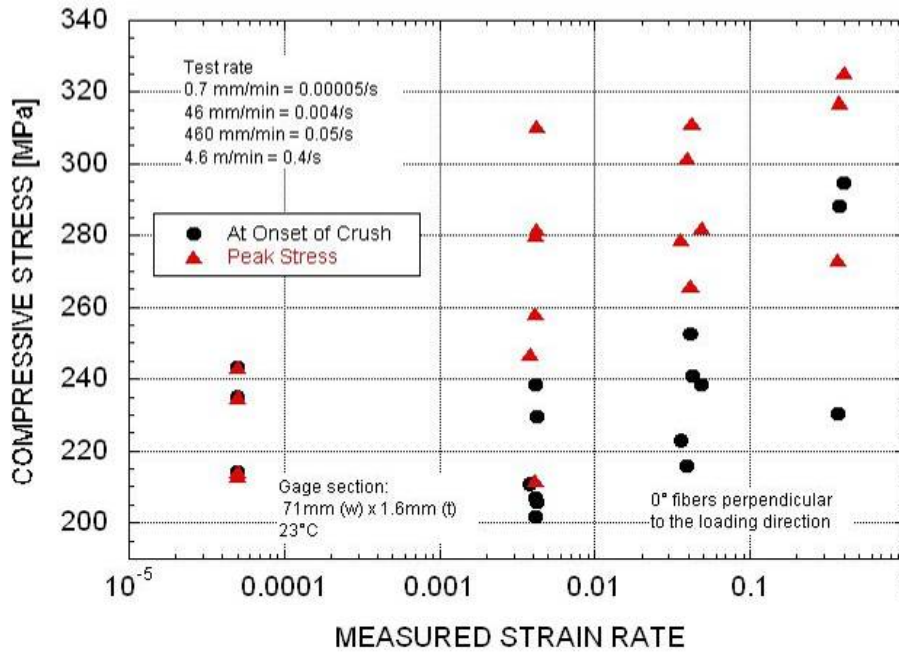


Figure 53. 2D3A Transverse Compressive Strength as a Function of Strain Rate

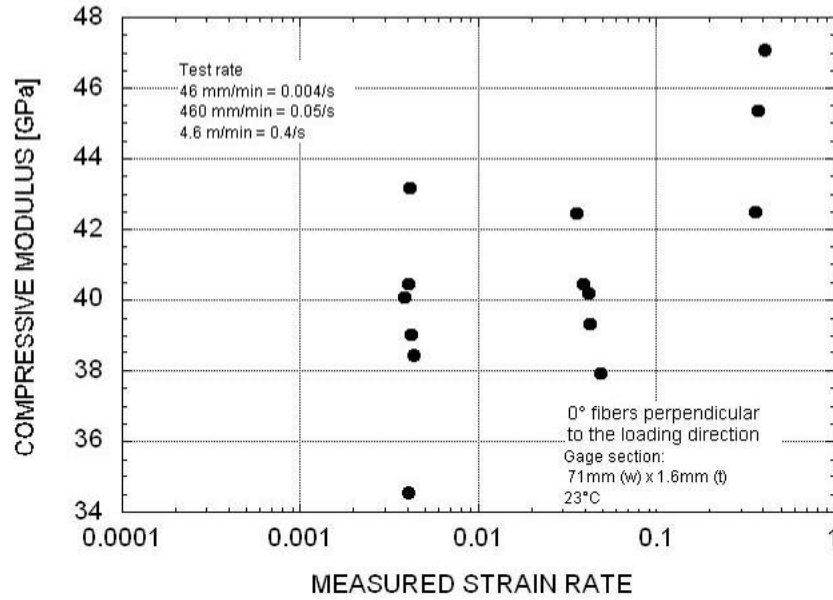


Figure 54. 2D3A Transverse Compressive Modulus as a Function of Strain Rate

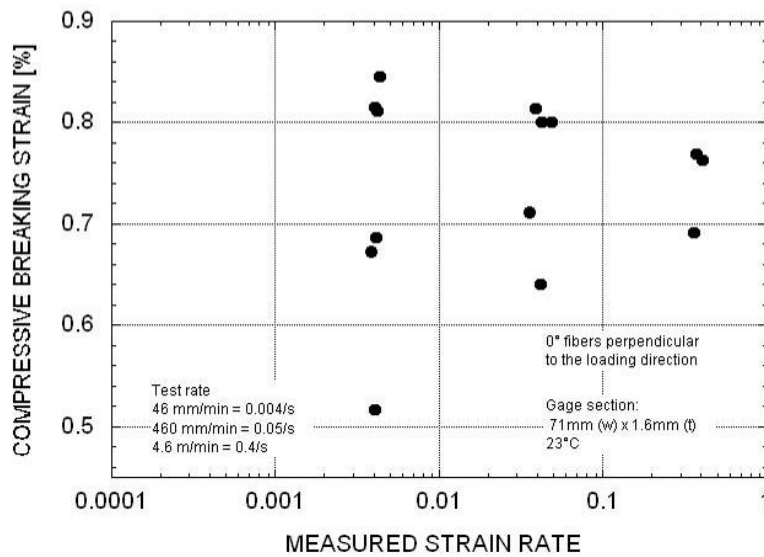


Figure 55. 2D3A Transverse Compressive Failure Strain as a Function of Strain Rate

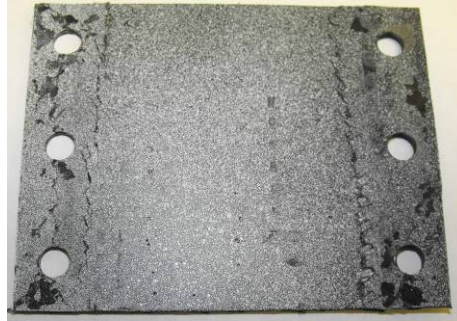


Figure 56. Typical Failure Location for Transverse Compressive Specimens

8.4.3 Comparison of Axial and Transverse Compression

The mechanical properties are shown in Figures 57 to 60. The axial and transverse peak strength data are equivalent across the tested rates. The exception is the transverse data at 0.00004/s, which had unusually low data as mentioned in Section 8.3.2. The data at this rate may not be an accurate representation of the strength, given the fact that both the axial and transverse strength data are equivalent and insensitive across the other tested rates.

The compressive modulus (Figure 58) is equivalent between the axial and transverse orientation. This is in part due to the two groupings of the axial stress-strain response. If one compares only the straight-sided specimens (Figure 59), then the transverse modulus appears to be slightly higher. However, the difference is not statistically significant because of the spread in the axial modulus data. The axial and transverse failure strains are equivalent (Figure 60).

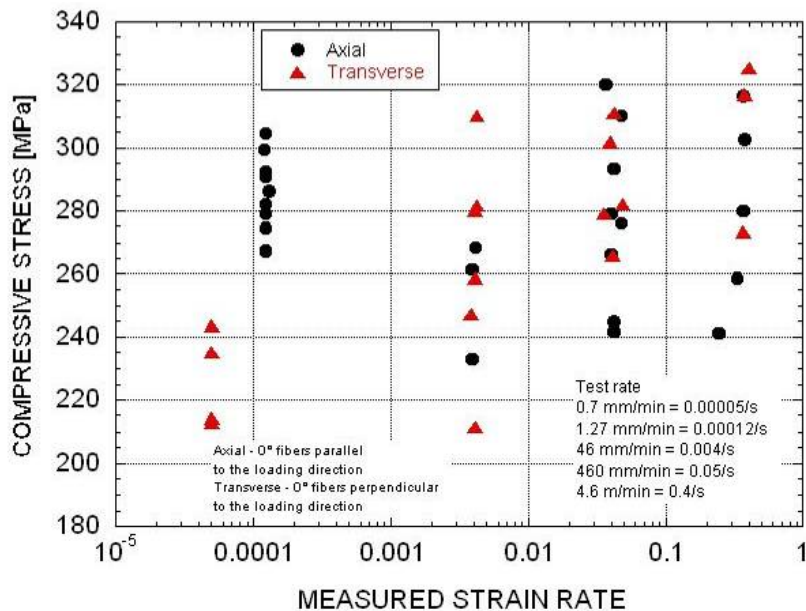


Figure 57. 2D3A Compressive Strength as a Function of Strain Rate

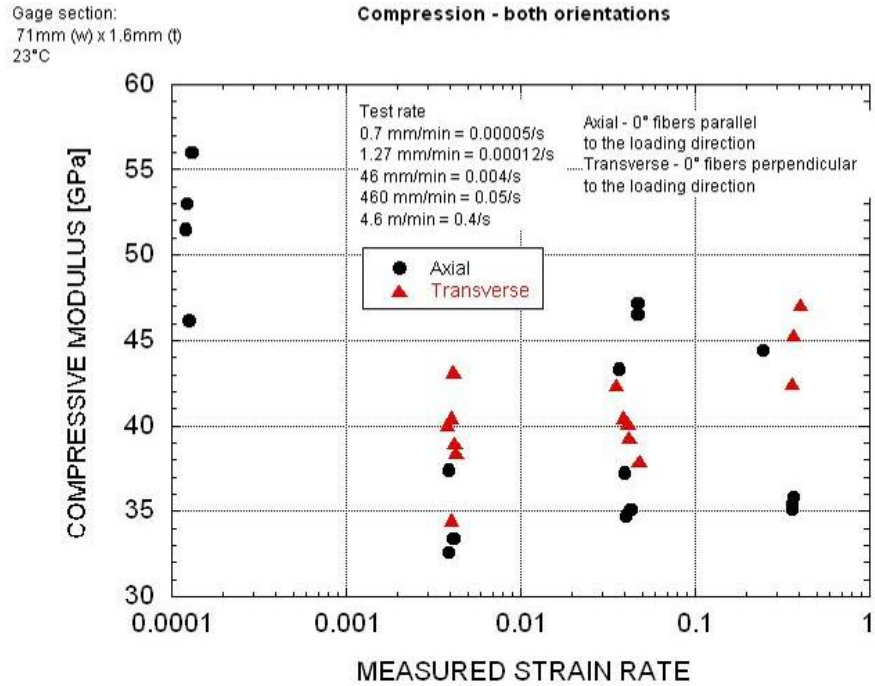


Figure 58. 2D3A Compressive Modulus as a Function of Strain Rate

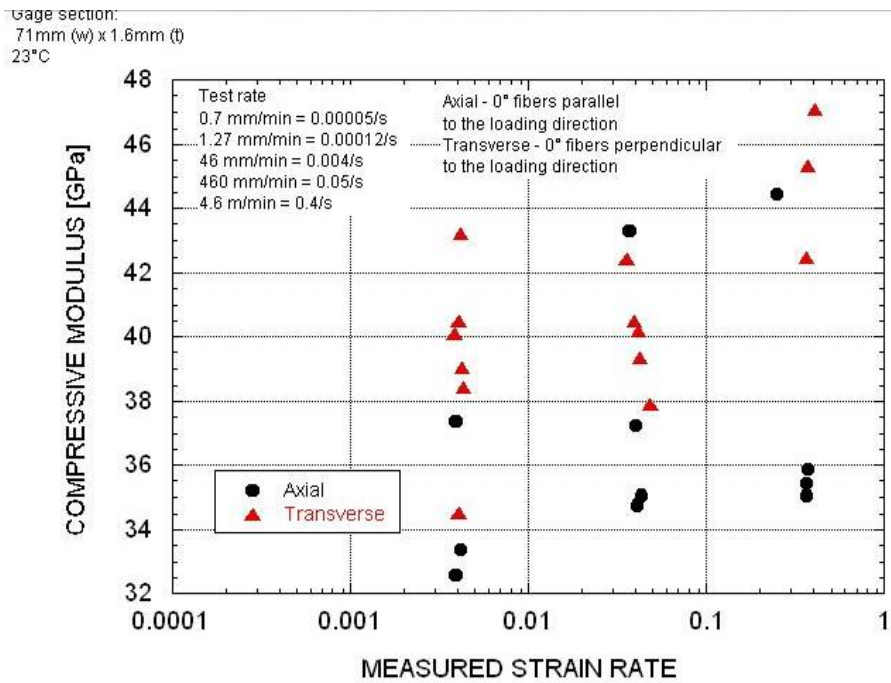


Figure 59. 2D3A Compressive Modulus as a Function of Strain Rate Using Straight-sided Specimens

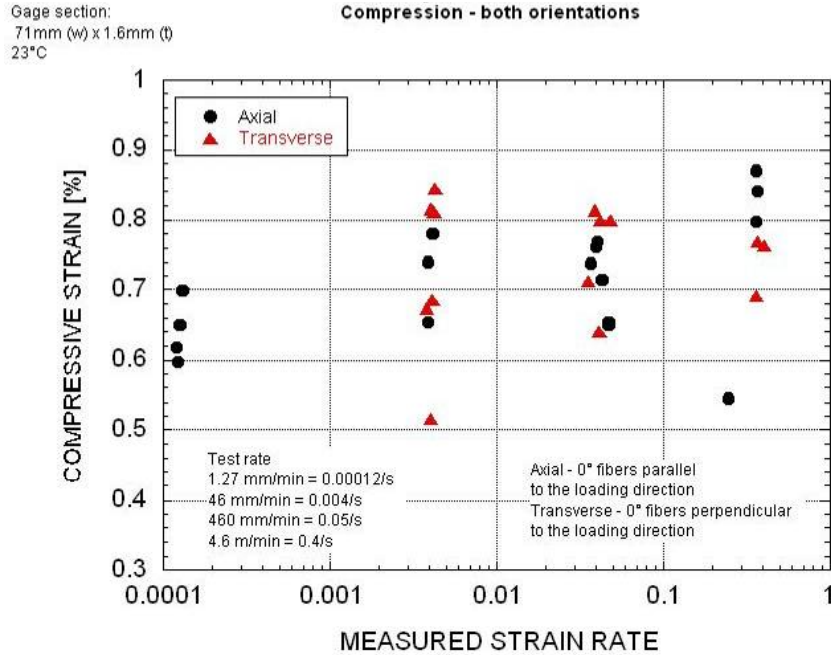


Figure 60. 2D3A Compressive Failure Strain as a Function of Strain Rate

8.5 Shear

The high rate fixture gripped the specimens out to the edge of the tab. Only the notch area was unsupported. About three to seven resonant waves were noticed at the maximum test rate of 45 m/s. The axial shear data package is in Appendix O and the transverse shear data are in Appendix P.

8.5.1 Comparison to Published Data

The data at the low rate are compared in Table 18. The UDRI shear data are lower by a factor of 0.72 than the data from Littell [13]. The shear modulus is equivalent.

8.5.2 Axial Shear (Shearing Across 0° Fiber Bundles)

The mechanical properties using the high rate shear specimen from 0.0008/s to 2.5/s are in Table 19. The axial stress-strain response across the tested rates is given in Figure 61. The peak strength, modulus, and strain as a function of the strain rate are graphed in Figures 62 to 64, respectively. Typical failures are shown in Figure 65.

About five to six low amplitude resonant waves were present before failure at the fastest rate of 49 m/min. This is below the desired 10 to 15 waves for dynamic equilibrium.

There is a positive trend in the strength as the rate increased. The average strength increased 10% between 0.0008/s and 2.5/s. However, there was no statistical significance in the data amongst the three lower rates because of the variability. Therefore, the increase per decade was hard to measure.

Table 18. Comparison of UDRI Shear Data and Published Data [13]

		UDRI V-Notch Test Rate of 1.27 mm/min Measured rate of 0.00012/s			Littell V-notch [13] Test Rate of 0.635 mm/min		
		Engineering Breaking Stress [MPa]	Engineering Breaking Strain [%]	Elastic* Modulus [GPa]	Engineering Breaking Stress [MPa]	Engineering Breaking Strain [%]	Elastic Modulus [GPa]
Axial Shearing across 0° fibers	Average [DIC data]	177	0.75	32.9	257	-	32.0
	Std.Dev.	12.4	0.10	1.45	10	-	1.1
	Coeff. of Var. [%]	7.01	13.2	4.4	3.9	-	3.4
Transverse Shearing along 0° fibers	Average [DIC data]	195	0.75	29.2	Similar results for both orientations		
	Std.Dev.	17.1	0.04	3.47			
	Coeff. of Var. [%]	8.8	4.82	11.89			

Six layer laminate used by Littell versus 3-layer for UDRI. Littell tested two specimens.

Table 19. Axial Shear Data Summary for 2D3A
Shearing Across 0° Fiber Tows

		Engineering Breaking Stress [MPa]	Normalized Peak Stress to 56 vol % Fiber [MPa]	Engineering Breaking Strain [%]	Elastic Modulus [GPa]
0.00008/s 1.27 mm/min	Average	180	177	0.75	32.9
	Std.Dev.	11.3	12.4	0.10	1.45
	Coeff. of Var. [%]	6.30	7.01	13.24	4.40
0.03/s 0.5 m/min	Average	190	188	0.83	28.5
	Std.Dev.	15.9	16.0	0.11	1.24
	Coeff. of Var. [%]	8.40	8.54	13.13	4.35
0.25/s 5 m/min	Average	177	174	0.72	25.5
	Std.Dev.	2.6	2.3	0.11	2.91
	Coeff. of Var. [%]	1.48	1.29	14.7	11.4
2.5/s 49 m/min	Average	201	199	0.84	26.0
	Std.Dev.	5.2	5.1	0.03	0.84
	Coeff. of Var. [%]	2.58	2.58	3.6	3.24

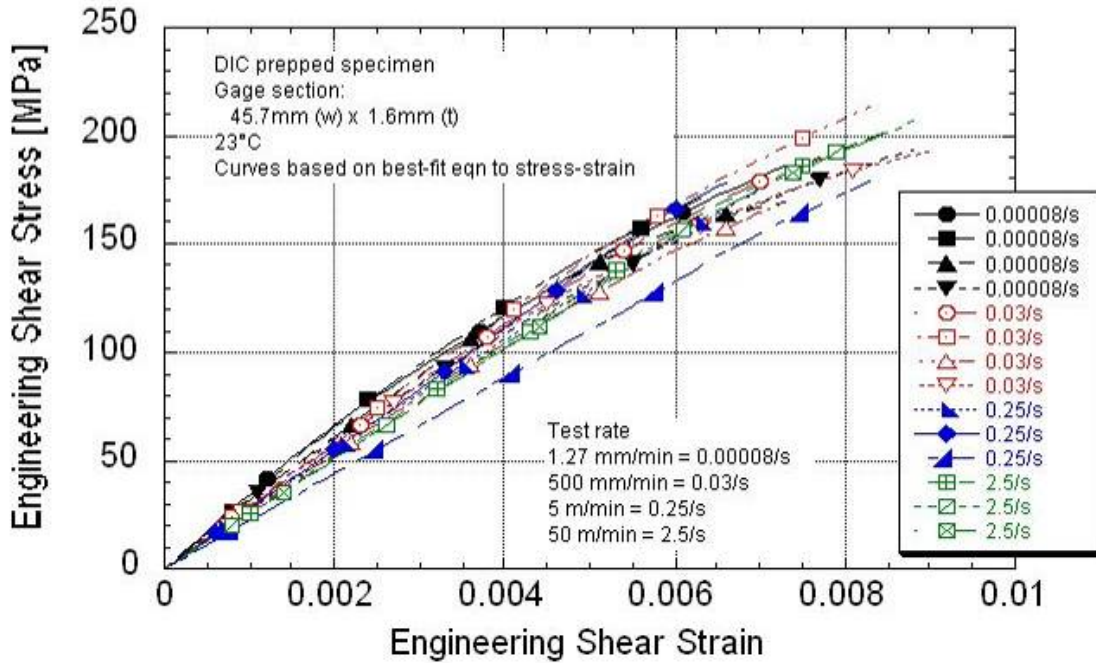


Figure 62. Axial Shear Stress-Strain Response of 2D3A Across Tested Rates

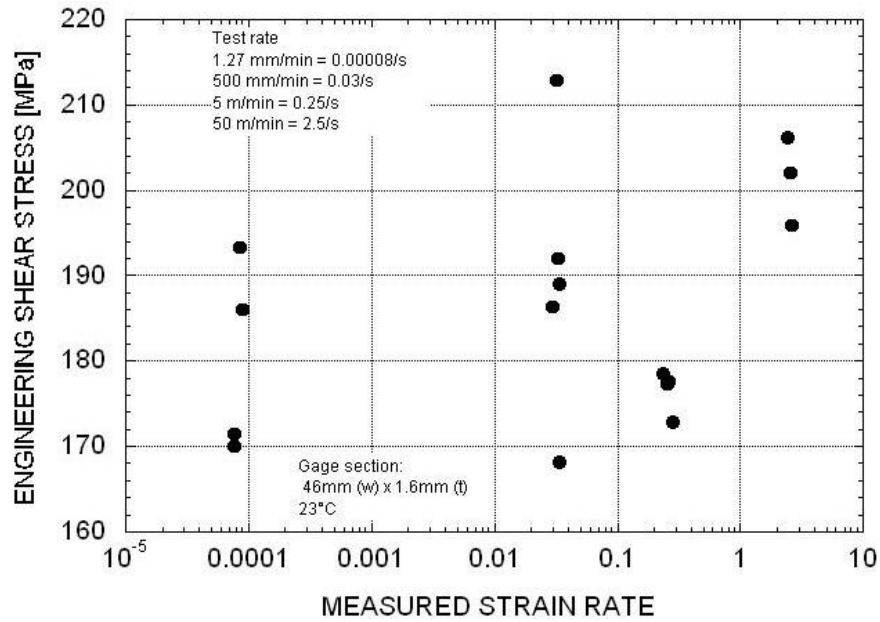


Figure 62. Axial Shear Strength of 2D3A Across Tested Rates

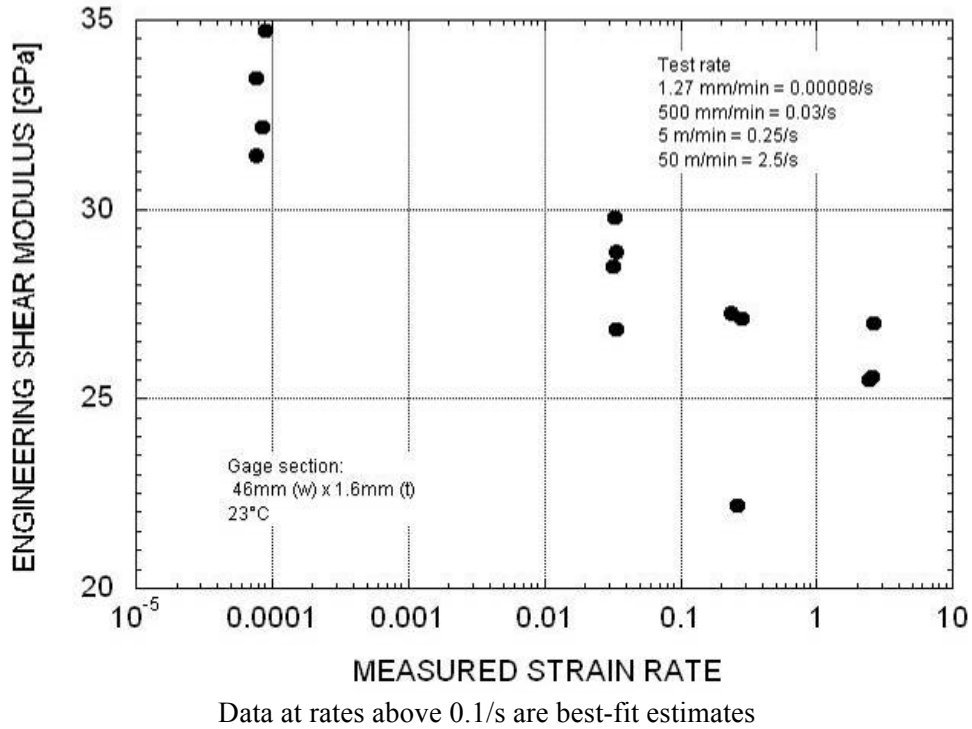


Figure 63. Axial Shear Modulus of 2D3A Across Tested Rates

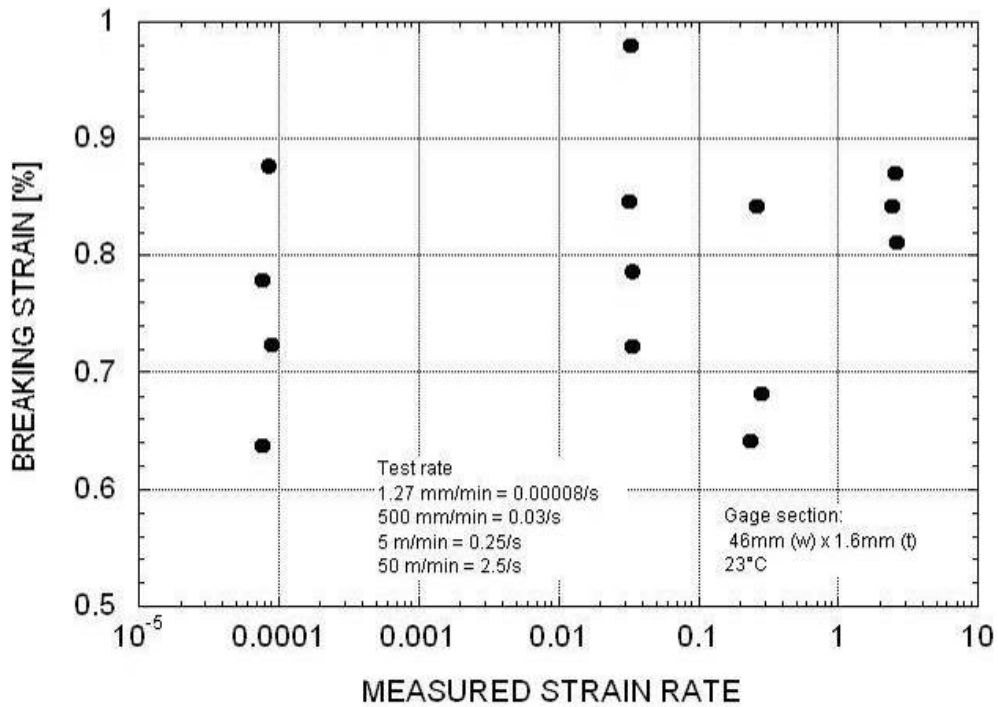
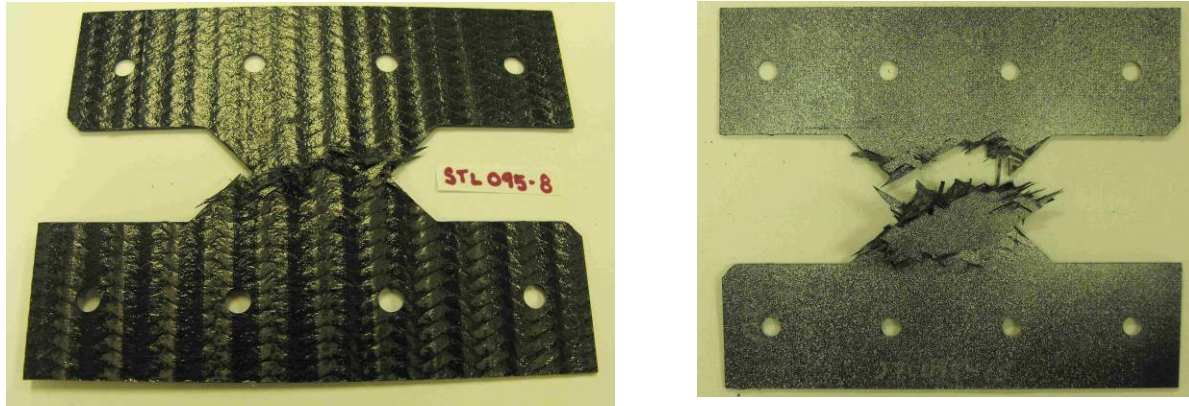


Figure 64. Axial Shear Failure Strain of 2D3A Across Tested Rates



a) Center

b) Center and into side

Figure 65. Typical Axial Shear Failure Locations

The stress-strain data were smoothed using a piecewise polynomial fit to the curve. The strain data at 0.25/s and 2.5/s [5 and 49 m/min] had a high amount of fluctuations, as seen in Figure 66. The elastic region for these curves was hard to define and the moduli for these rates are estimates. The apparent decrease in the modulus at rates above 0.025/s may be an artifact of the smoothing process.

The failure strain did not change across the tested rates.

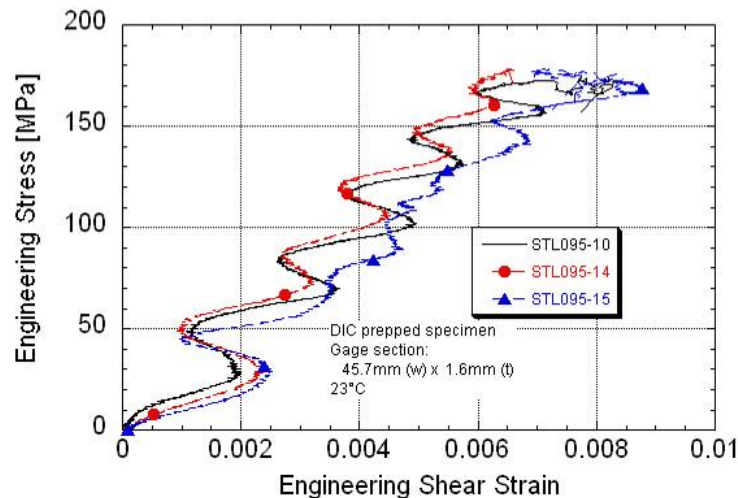


Figure 66. Unsmoothed Axial Shear Stress-Strain Response at 0.25/s

8.5.2 Transverse Shear (Shearing Along 0° Fiber bundles)

The mechanical properties using the high rate shear specimen from 0.0003/s to 8/s are in Table 20. The transverse shear stress-strain response across the tested rates is given in Figure 67. The peak strength, modulus, and strain as a function of the strain rate are graphed in Figures 68 to 70, respectively.

Typical failures are shown in Figure 71. Most of the specimen failed down the center or close to the center notch. It was noticed during testing that some of the initial failures occurred on the back face of the specimen, away from the DIC cameras (Figure 71b). The final surface crack was not necessarily indicative of where the crack initiated.

The strain oscillations were not as great as for the axial shear data and so it was easier to apply a polynomial fit to the data. The shear remained the same between 0.0003/s and 0.05/s. It increased about 10% with each decade up to 8/s. There was a large amount of variability at most rates. The modulus appears to increase slightly with rate, but the large spread in the data at 0.8/s makes it difficult to quantify the increase across each decade. The failure strain was insensitive to the increasing rate.

The transverse shear response was not sensitive to the number of unit cells in the center gage section. Increasing the specimen gage width by 250% did not change the stress-strain response.

The transverse shear fixture was slightly longer than the axial shear fixture and the natural resonance frequency was longer. Only three to five stress waves were present at the upper test rate of 49 m/min.

Table 20. Transverse Shear Summary Table of 2D3A
Shearing Along 0° Fibers

		Engineering Breaking Stress [MPa]	Normalized Peak Stress to 56 vol % Fiber [MPa]	Engineering Breaking Strain [%]	Elastic Modulus [GPa]
0.0003/s 1.27 mm/min	Average	200	195	0.75	29.2
	Std.Dev.	14.0	17.1	0.04	3.47
	Coeff. of Var. [%]	7.02	8.76	4.82	11.9
0.05/s to 0.1/s 0.5 m/min	Average	218	212	0.86	28.5
	Std.Dev.	17.1	18.8	0.12	2.08
	Coeff. of Var. [%]	7.86	8.87	13.5	7.28
0.8/s 5 m/min	Average	239	233	0.86	32.9
	Std.Dev.	6.4	6.1		
	Coeff. of Var. [%]	2.66	2.61		
8/s 49 m/min	Average	226	216	0.86	33.4
	Std.Dev.	15.9	10.9	0.09	1.59
	Coeff. of Var. [%]	7.02	5.08	10.9	4.76

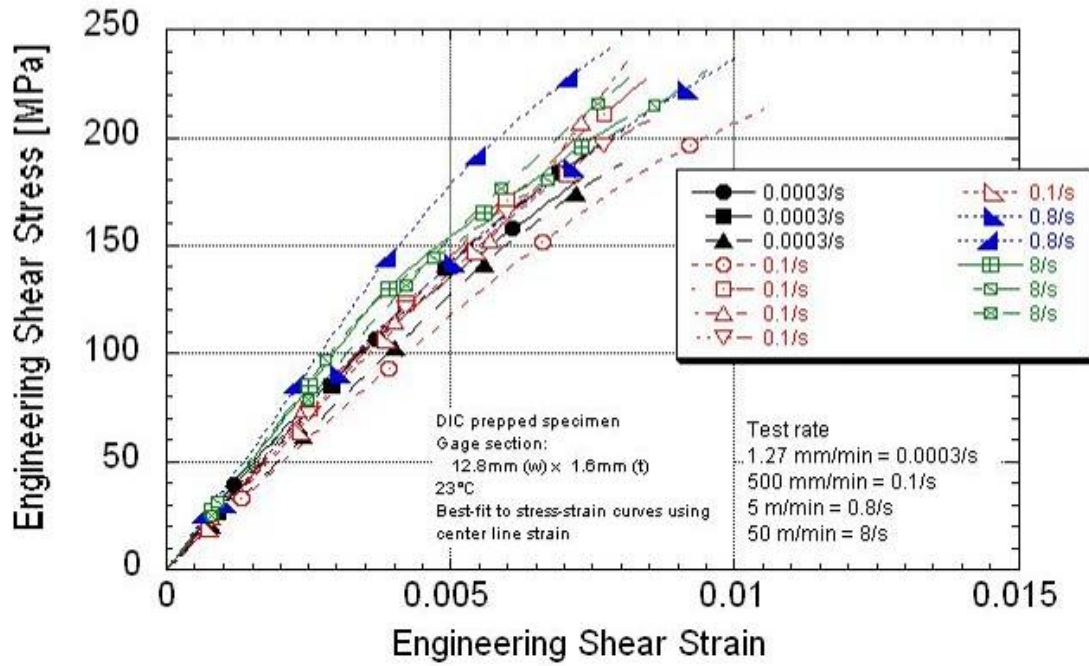


Figure 67. Transverse Shear Stress-Strain Response of 2D3A Across Tested Rates

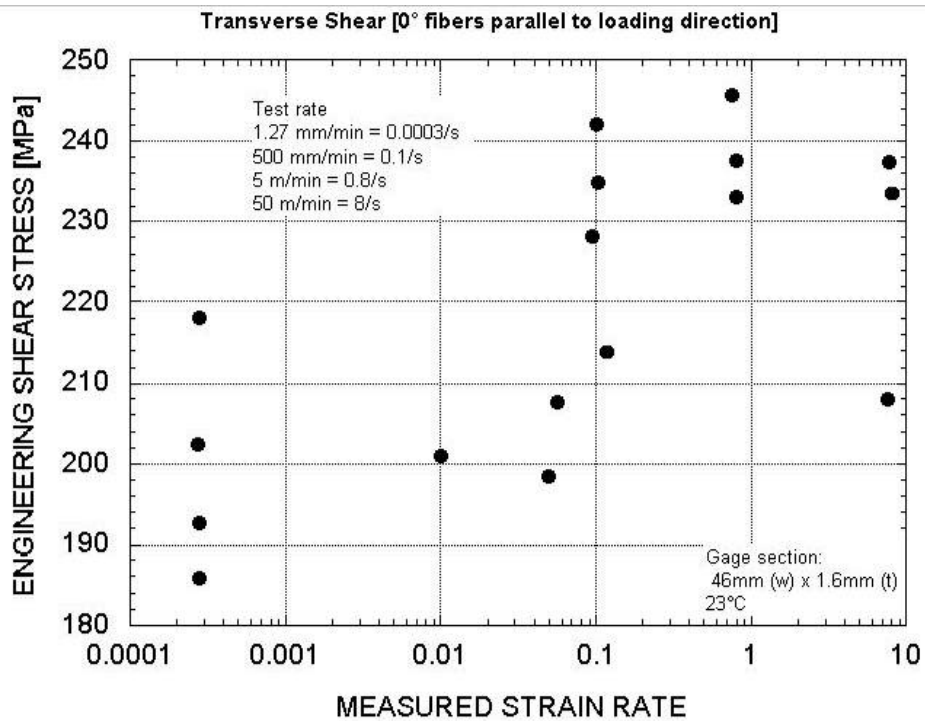


Figure 68. Transverse Shear Strength of 2D3A Across Tested Rates

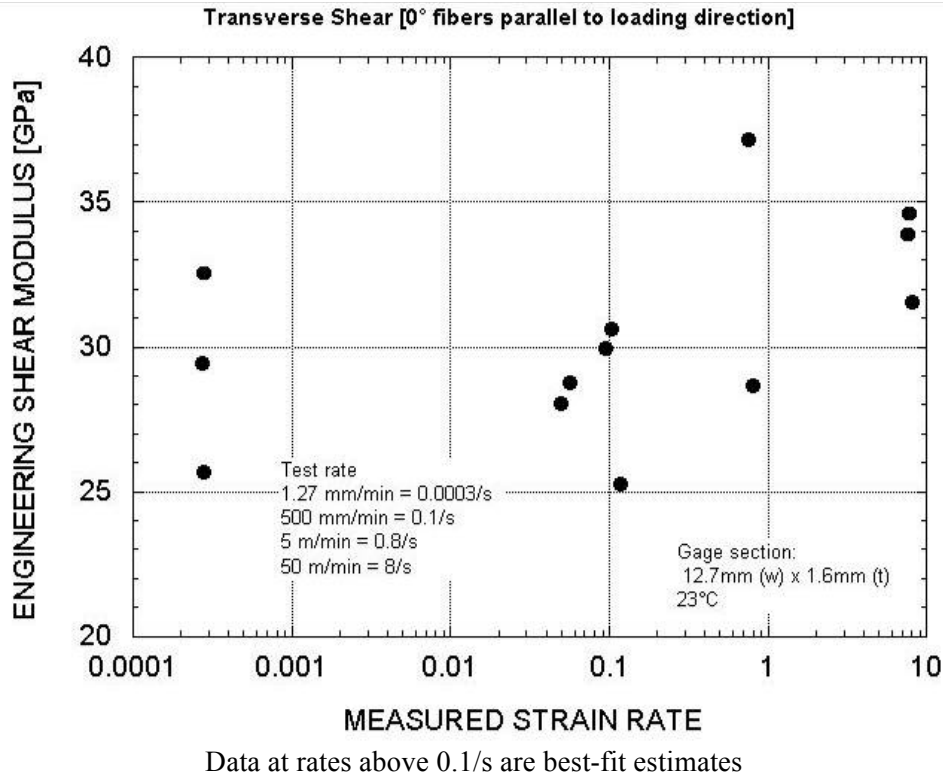


Figure 69. Transverse Shear Modulus of 2D3A Across Tested Rates

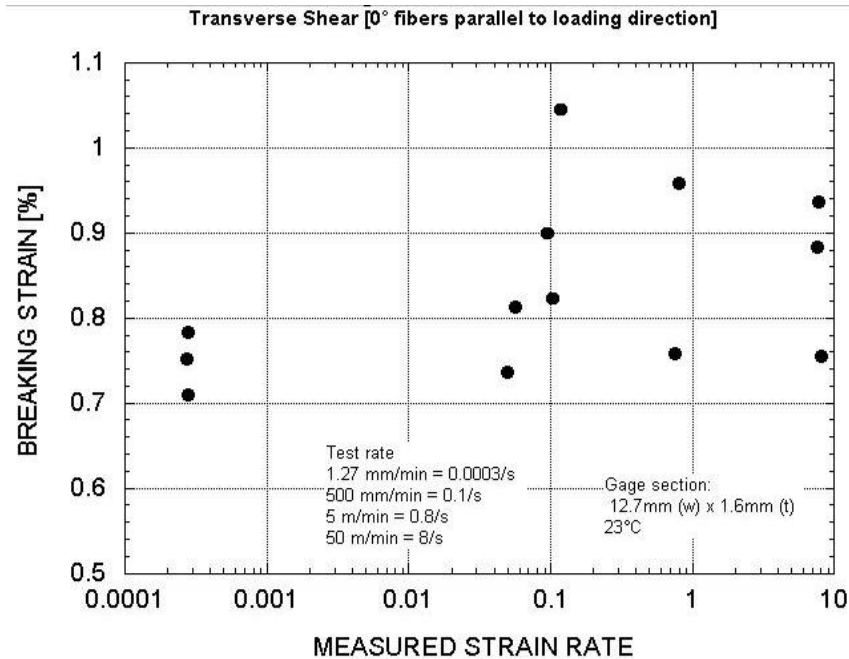


Figure 70. Transverse Shear Failure Strain of 2D3A Across Tested Rates

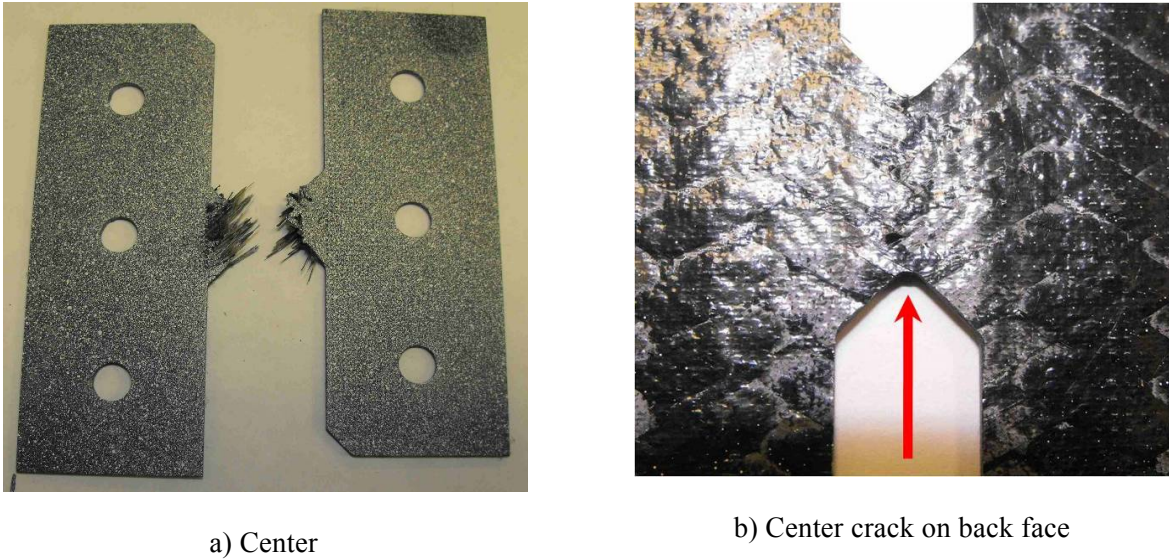


Figure 71. Typical Transverse Shear Failure Locations

8.5.3 Comparison of Axial and Transverse Shear

The mechanical properties are shown in Figures 72 to 74. The transverse shear strength is significantly higher than the axial shear strength (Figure 72). Differences in the modulus due to orientation are hard to identify (Figure 73). The axial and transverse failure strains are equivalent (Figure 74).

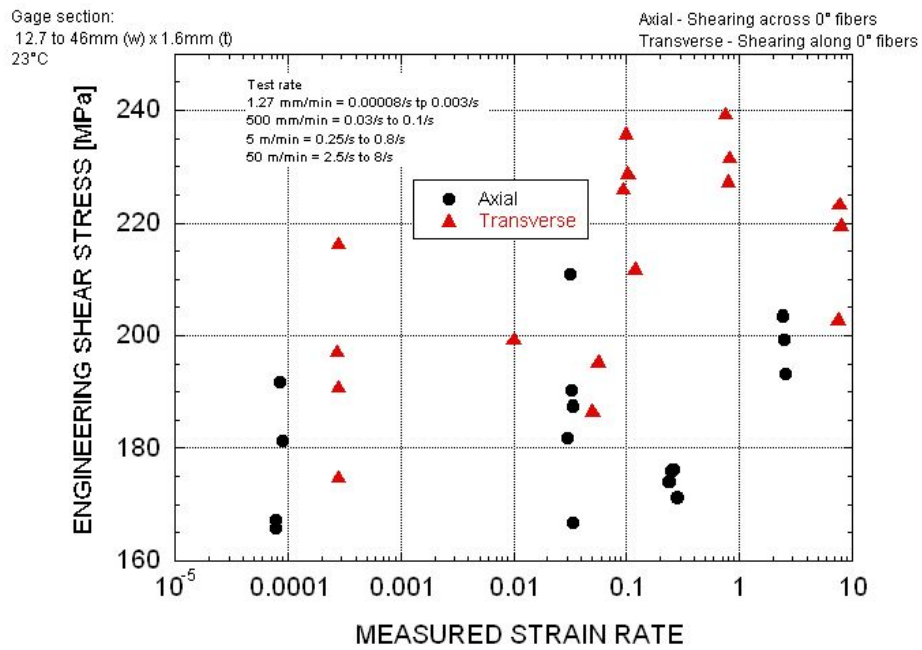


Figure 72. 2D3A Shear Strength as a Function of Strain Rate

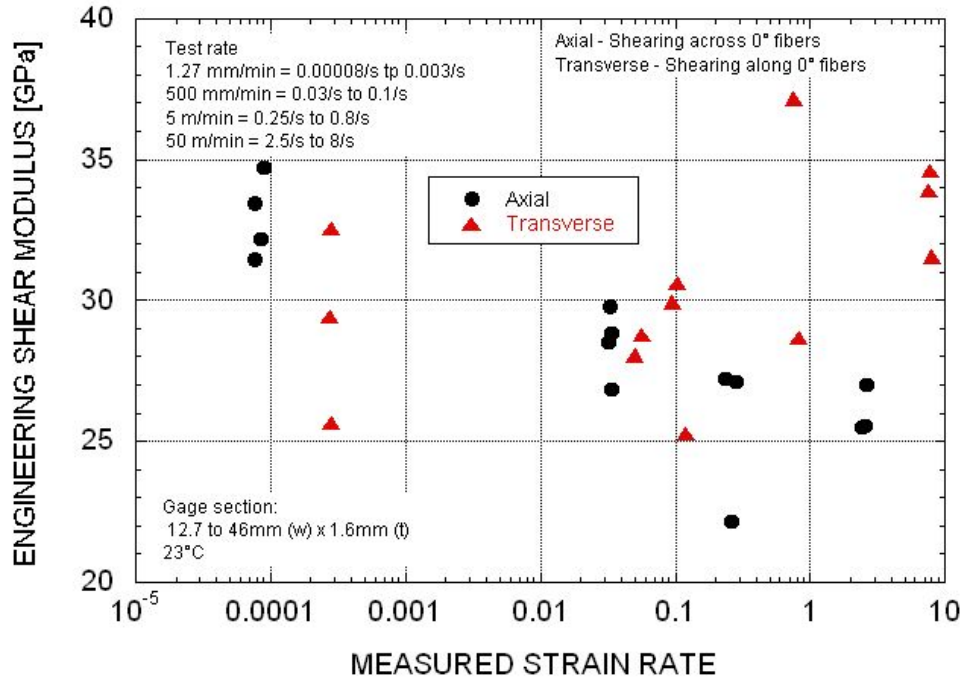


Figure 73. 2D3A Shear Modulus as a Function of Strain Rate

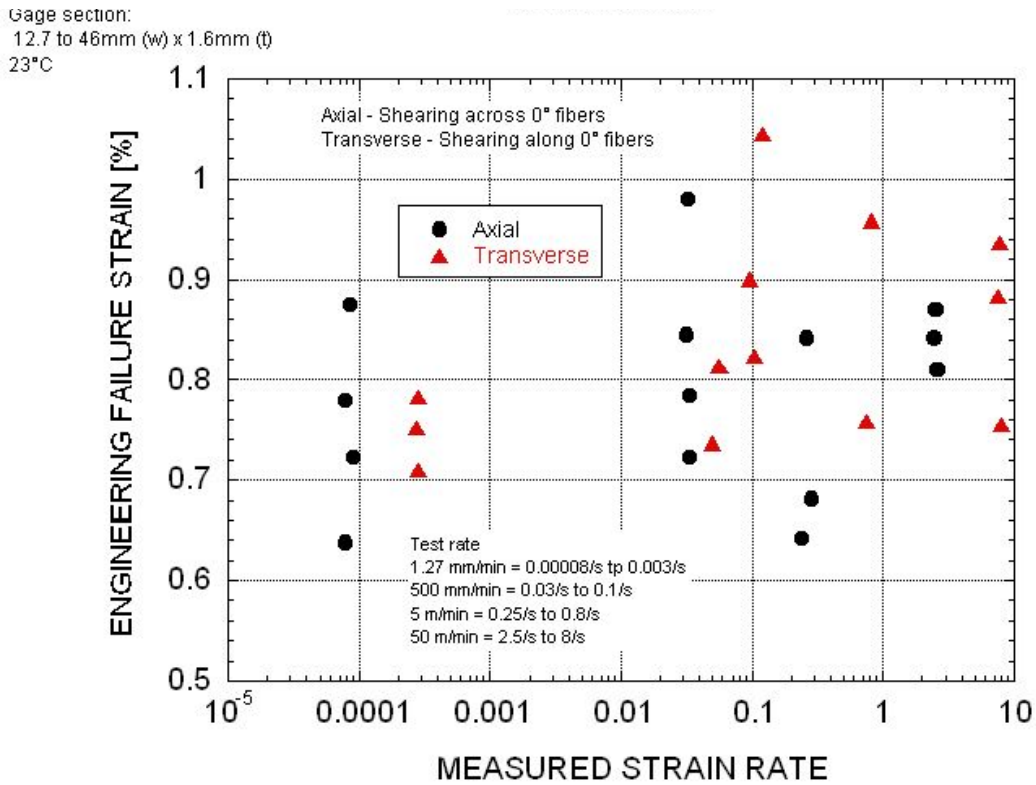


Figure 74. 2D3A Shear Failure Strain as a Function of Strain Rate

8.6 Compression Tube Tests

The flat ended tube exceeded the SME actuator capacity (98 kN). All subsequent tests were performed on tubes which had a single 45° angle cut on one end.

A typical low and high rate output curve is shown in Figure 75. The initial peak data can vary depending on the initial contact of the tube and the platen and the test speed. The slight variations can result in large differences in the measured peak. In addition, the initial load into the specimen is similar to an impulse load into the material and the first peak has a higher amplitude than all subsequent stress waves. The impulse load triggers resonant waves in the system and into the material. The high initial peaks are circled in Figure 75b. These waves cannot be avoided at the upper rates.

Figure 75b also shows the magnitude of the rebound of the platen at 440 m/min [7.4 m/s]. The load drops to zero after the initial impact. The platen is driven forward by the actuator and the platen continues to crush the tube.

All of the specimens exhibited a progressive crush. However, the failure modes varied. The low rate specimens failed in a combination of fan-folding and subsequent axial tearing of the sides with the torn sides (fronds) extending outward (Figure 76). The higher rate specimens had the outside layer folded over the outside of the tube. The next two layers were not able to fold over the first layer and tore along the axis in sections. The fronds either folded on the outside or into the middle of the tube (Figure 77).

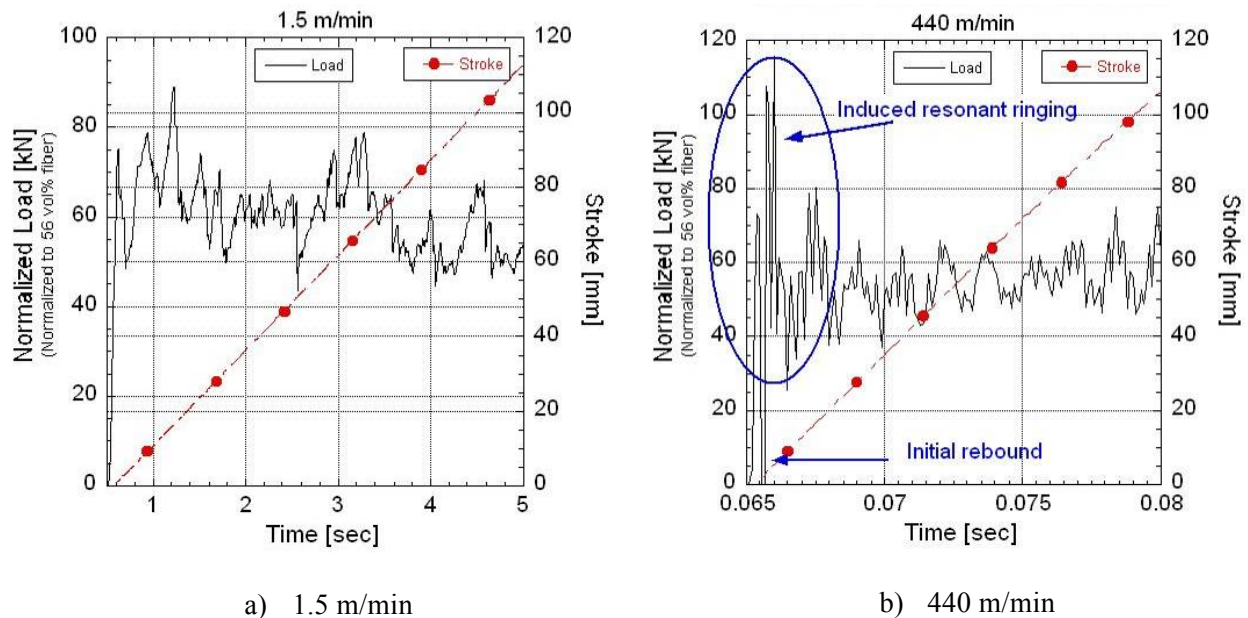


Figure 75. Typical Tube Crush Load-Displacement Curves at a Slow and Fast Rate



a) Fan folds



b) Fan folding and tearing

Figure 76. Low Rate Tube Failure



a) Side view with folded over braid



b) End view

Figure 77. High Rate Tube Failure

Comparison of the data across the test rates had to consider the differences in the initial part of the curve and the failure mode. The displacements were zeroed at a load level of 40 kN for ease of comparison across the rates and the test systems.

The displacement of various sections along the tube was measured at 1.5 m/min using the SEM DIC. Oftentimes the DIC data were not valid because of material debris in the film image or the compressed tube material covering up the DIC markers. Figure 78 shows an example of the points tracked by the DIC and the comparison to the actuator stroke. The measured point displacements were equivalent to the actuator stroke after the initial ~15 mm of crush. This portion of the displacement was over the region of initial impact and induced resonant ringing at the higher rates. Any comparison of average crush data across the tested rates would have to exclude this section of the curve. Therefore, the actuator displacement was considered to be representative of the tube displacement.

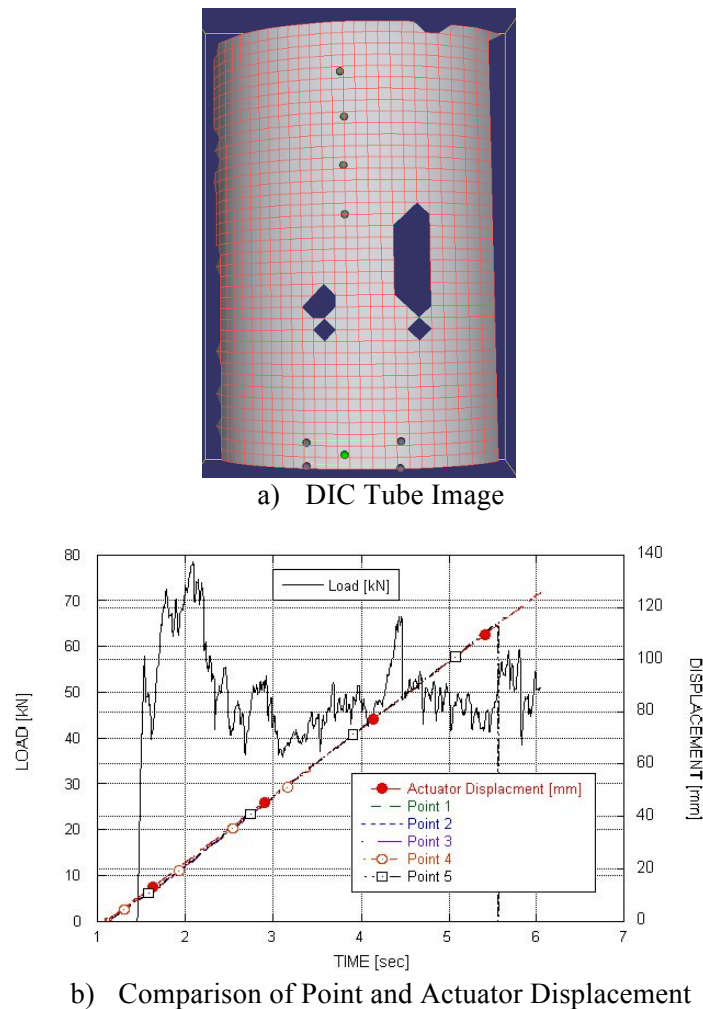


Figure 78. Polygon Regions Tracked by the DIC and Comparison of the Measured Displacements to the Actuator Displacement

8.6.1 Tube Compression Strength

As mentioned in Section 7.4, the characteristics of the tube crush can be analyzed using various equations. The data for this program were compared using the SEA (Eq. 5), the SSCS (Eq. 6), and the CCR (Eq. 7). The median stress response was used for SSCS and CCR to minimize the resonant wave contribution. The CCR equation used the median stress normalized to 56% fiber volume for direct comparison to the normalized coupon compressive stress.

The crush behavior was well established within the first 20 to 30 mm of zeroed displacement at all of the rates, as seen in Figure 79. An arbitrary level of 25 mm was used as the start point for the median crush strength. A common endpoint of 115 mm of zeroed displacement was used for δ_2 because this value was reached at all of the rates.

Table 21 summarizes the results for the tube crush. A detailed summary table is in Appendix Q along with plots for each rate.

The SSCS and CCR were equivalent at 1.5 m/min and 140 m/min. The SSCS and CCR decreased by a factor of 0.88 to 0.91 between 140 and 440 m/min.

The SEA used for design purposes was equivalent at 1.5 m/min and 140 m/min. It was lower by a factor of 0.91 at 440 m/min (Figure 80). The SEA calculated under the assumption that the crush zone was equivalent to the actuator displacement (Eq. 5a) had similar results; i.e. equivalency at 1.5 and 140 m/min with a reduction by a factor of 0.93 by 440 m/min. However, the SEA at 1.5 m/min calculated via Eq 5b (considering the total deformation with the folds) is much lower than via Eq. 5a. This indicates that the fold length must be incorporated into the SEA calculation.

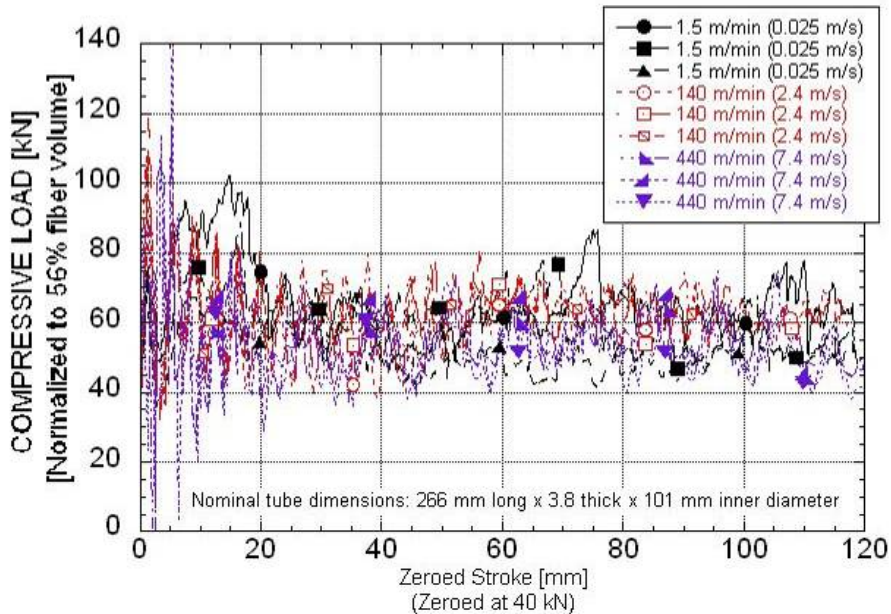


Figure 79. Load-Displacement Curves Across the Tested Rates

Table 21. Compression Tube Strength and Peak Temperatures

		Median Crush Load* [kN]	Median Crush Stress* [MPa]	Median Stress Normalized to 56% Fiber Volume [MPa]	Specific Sustained Crushing Stress [SSCS] [MPa]	Crush Compression Ratio**	Specific Energy Absorption ⁽¹⁾ with folding mode failure [SEA-FM] [kJ/kg]	Specific Energy Absorption ⁽²⁾ [SEA] [kJ/kg]	Specific Energy Absorption ⁽³⁾ [SEA] [kJ/kg ²]	Range of Peak Temperatures During Crush [°C]
1.5 m/min 0.0254 m/s	Average	47.0	74.9	95.8	51.5	0.35	43.3	53.3	19.9	-
	Std.Dev.	3.66	5.79	9.61	4.29	0.04	2.96	4.56	2.00	-
	Coeff. of Var. [%]	7.78	7.74	10.0	8.32	10.0	6.84	8.56	10.0	-
140 m/min 2.4 m/s	Average	47.8	77.1	97.4	53.2	0.36	-	52.5	20.9	173-362
	Std.Dev.	2.14	3.44	4.55	2.01	0.02	-	2.30	0.81	
	Coeff. of Var. [%]	4.48	4.46	4.67	3.77	4.67	-	4.37	3.89	
440 m/min 7.4 m/s	Average	43.3	69.2	85.8	47.8	0.32	-	48.9	19.0	254-308
	Std.Dev.	2.35	3.24	3.77	1.95	0.01	-	1.95	0.94	
	Coeff. of Var. [%]	5.43	4.69	4.39	4.08	4.39	-	3.98	4.96	

1) SEA calculated using $E_s = \text{Work}/(\text{area} \cdot \text{density}) \cdot [\text{actuator displacement} + \text{displacement of folded length}]$
 2) SEA calculated using $E_s = \text{Work}/(\text{area} \cdot \text{density}) \cdot \text{total actuator displacement}$
 3) SEA for design purposes $E_s = \text{Work}(\text{displacement at peak} - \text{displacement at end})/(\text{mass of tube} \cdot \text{displacement at end})$
 The peak temperatures exceeded the calibration curve maximum of 200°C for all but one of the specimens.

A comparison of the SEA values using both Eq 5b at 1.5 m/min and Eq 5a at the two upper rates does not show a clear trend (Figure 80). The SEA for design purposes incorporated the fold length into the calculations and the trend tracks the trends seen in the SSCS and CCR. There is no clear consensus regarding the rate effects on carbon braid composites [35], although many report rate insensitivity at lower rates and a slight decrease with increasing rate. These tube results fall into this category.

A single tube with a flat end was tested at 2.4 m/s. The data were similar to the data for tubes which had the bevel crack initiator.

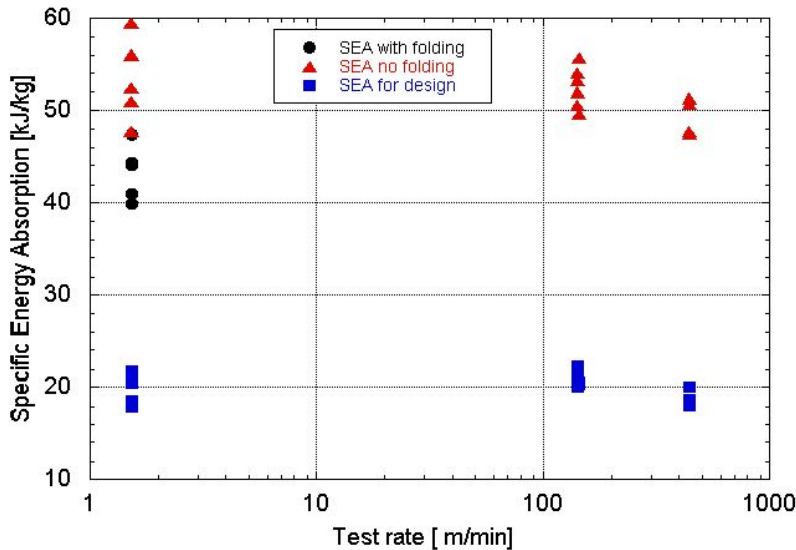


Figure 80. SEA Across Tested Rates

8.6.2 Tube Compression Strain

Strain data taken at discrete points along the length of the tube had a large amount of uncertainty. Strain data for a polygon taken ~130 mm from the top end of the tube is graphed in Figure 81. The peak of the stress-strain curve reflects the contribution of the high amplitude stress waves. The sustained crush strength was about one-quarter of that for the coupon data [~ 75 MPa vs 270 MPa] and the failure strain ranged from 0.4% to 0.8% compared to 0.9% for the coupons. The uncertainty level was fairly high (6 to 10%) but the shape of the tube compressive stress-strain curve was similar to the lower stiffness coupon data (Figure 82).

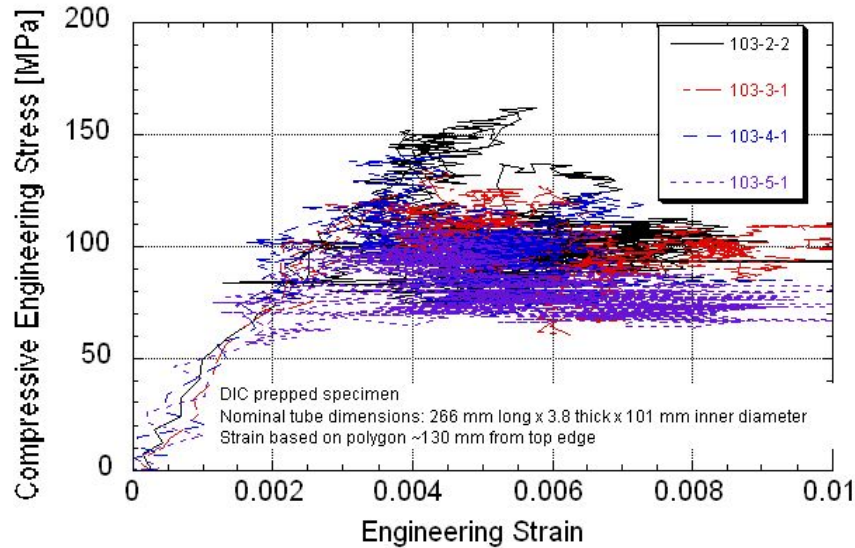


Figure 81. Tube Compressive Stress-Strain at 1.5 m/min

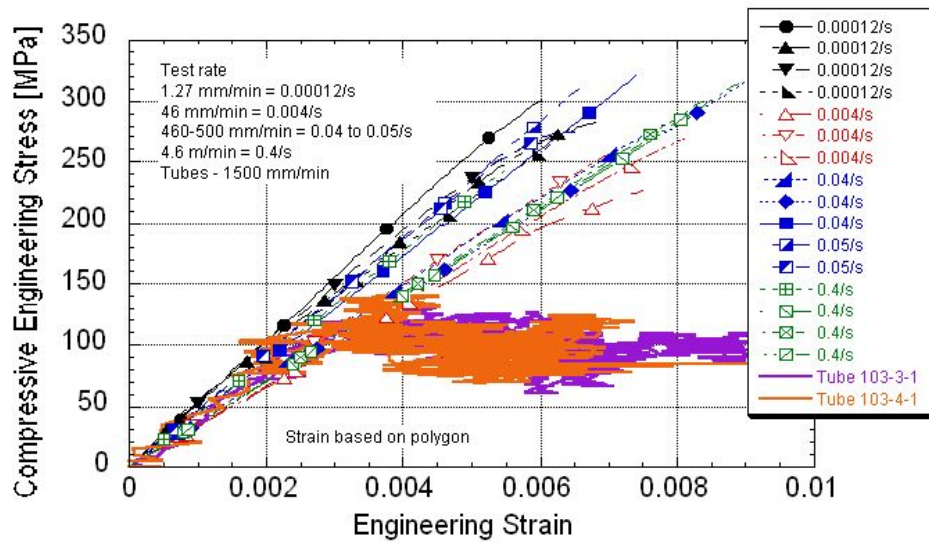


Figure 82. Comparison of Tube and Coupon Compressive Stress-Strain

8.6.3 Tube Temperatures

The peak temperatures exceeded the IR calibration curve maximum of 200°C for all but one of the specimens (STL103-7-2). Temperatures above 200°C were beyond the calibrated range. These data may be used for qualitative comparisons but should be used with extreme caution as absolute figures since they are extrapolated often well beyond the valid calibration range. The peak temperature given in Table 21 reflects the average peak temperature during the actual crush event.

Figure 83 shows the changing temperature as the test progressed in time over the region of the crush event. The actuator movement was complete within 0.05 seconds at 2.4 m/s and 0.02 seconds at 7.4 m/s, but the temperature continued to increase. The onset of the temperature rise was shifted to coincide with the load introduction as much as possible. The two data sets were not synchronized during the test.

The specimens run at 2.4 m/s showed a slower temperature rise than those at 7.4 m/s, as one would expect. The average peak temperature during the crush was ~270°C for both rates.

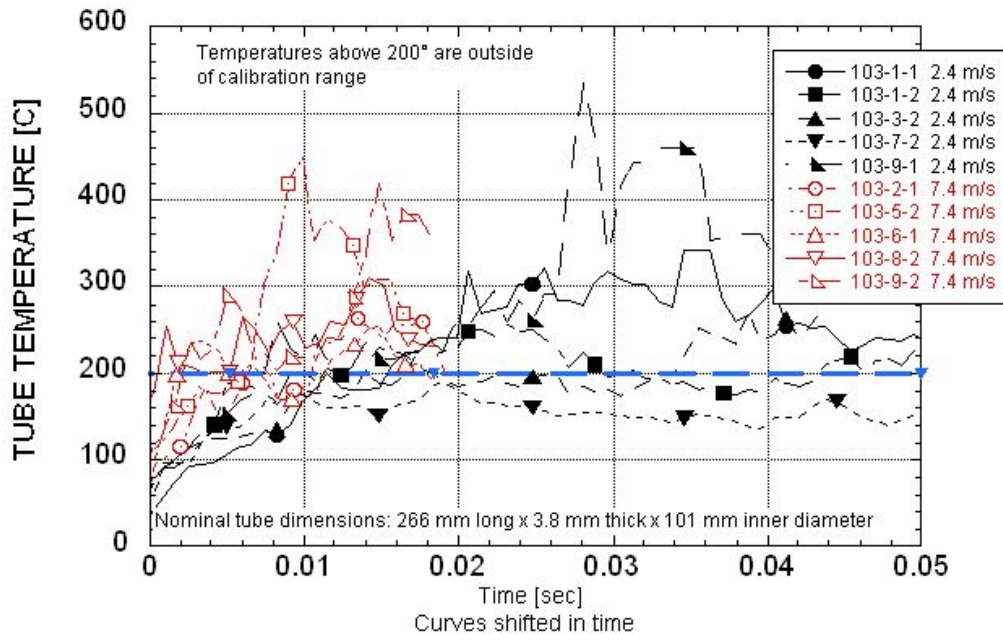


Figure 83. Composite Tube Temperatures During Crush

9.0 OVERALL SUMMARY

9.1 Material Selection and High Rate Specimen Designs

Two-dimensional triaxial carbon braid (2D3A) was selected for study after a review of the literature and consultation with technical experts. The $0^\circ/\pm 60^\circ$ braid was in-plane isotropic. The braid offered a method of providing off-axis strength and post-impact integrity in a form that would be suitable for an automotive structural component.

Composite panels and tubes were fabricated using Toray T700s C 12000 carbon fiber and Epon 862W epoxy resin. Each panel and tube contained three layers of the braid. The average fiber volume of the panels and braid were 57.2% and 44.4%, respectively.

Tension, compression, and shear mechanical properties were generated at test rates up to 50 m/min (0.8 m/sec). High rate specimens and fixtures were designed with the following requirements: a minimum of 2.5 unit cells in the test section, minimal specimen length, minimal fixture weight, and a failure load below 98 kN. The relevant quasi-static and high rate standards and recommended procedures were reviewed.

The final high rate specimens used the sizes in the standards as a guideline. The various fixture designs were able to transfer the loads into the specimens. Grip marks were evident in the tab region, which was indicative of shear loading through the tabs. The amount of load transferred through the bolts was not determined. No deformation was noted in the bolt holes.

Some resonant ringing was noted in the load response at the upper rates (~ 50 m/min). These data could be improved through fixture redesign, such as weight reduction and minimizing the number of bolts. Generating useable data at even faster rates would require a specimen redesign. The major contributor to the current specimen design was the decision to include 2.5 unit cells within the test section. Minimizing the test gage width would reduce the specimen length, failure loads, fixture length, and fixture weight. All of these factors combined would raise the natural system resonant frequency and improve the data quality at rates above 50 m/min.

The measured peak strengths had relatively low levels of variability (3 to 7%) compared to the modulus and failure strains (10% and higher). Future tests should include a minimum of five replicates per condition in order to identify statistically significant changes due to rate.

9.2 Comparison of Tensile Data Using the ASTM D 3039 and Bowtie Configuration

The high rate tensile specimen was a bowtie design. Data were generated at quasi-static rates for comparison to standard ASMT D 3039 tensile data. The bowtie axial tensile strength was similar to the data using the D 3039 specimen, but the stiffness was higher and the failure strain lower. The transverse tensile strength was almost three times higher than the D 3039 data. The D 3039 failure strain was lower, probably because of cracks initiated at the edge. The bowtie transverse stiffness varied, depending on the amount of axial fiber tows in the cross section.

The major difference between the specimen designs was the amount of fiber tows gripped in the fixture. The bowtie specimen gripped all of the axial and bias fiber tows which ran through the center gage section. The D 3039 gripped a limited number of bias and axial tows, especially in the transverse orientation. In addition, the D 3039 long gage section had many cut fiber tows along the edge which could

act as crack initiation sites. The bow tie configuration had a central notch. Cracks initiated at this location, but they were blunted within 0.5 unit cells from the notch.

9.3 High Rate Coupon Mechanical Properties

9.3.1 Tensile

The bowtie axial tensile strength was 778 ± 50 MPa and the failure strain was $1.33 \pm 0.13\%$. The strength was rate insensitive. The failure strain had a negative trend with increasing rate, but it was not statistically significant due to the high variability. The stiffness increased with rate and was 25% higher at 2/s compared to 0.00009/s (82 GPa versus 67 GPa).

The bowtie transverse tensile strength and failure strain were significantly higher than the axial (979 ± 45 MPa and $2.01 \pm 0.49\%$). Both were rate insensitive. The modulus had a high amount of variability thought to be due to the relative amount of axial fibers in the center gage section. The transverse modulus was of similar magnitude as the axial modulus, but it ranged from 58 to 116 GPa.

9.3.2 Compression

The axial compression strength was 270 ± 25 MPa. It was rate insensitive. The stress-strain response exhibited two distinct groups in the behavior. The dogbone-shaped specimens tended to have a higher modulus and shorter failure strain. However, some of the straight-sided specimens also fell within this grouping. The difference may be due to the onset of buckling of the axial tows. The stiffness and failure strain were insensitive to rate within a given group.

The transverse compression strength exhibited a trend of increasing strength with rate but it was not statistically significant. A positive trend is expected since the compressive loads are loading bias fibers and resin rather than the axial fibers. The rate sensitivity of the epoxy should be reflected in the transverse compressive response. The overall strength was 259 ± 30 MPa, which was equivalent to the axial strength.

The transverse compressive modulus increased 13% between 0.04/s and 0.4/s (39.6 to 45 GPa). The failure strain had a large amount of variability. It had a decreasing trend with increasing rate but the trend was not statistically significant. The overall failure strain was $0.74 \pm 0.09\%$. The transverse modulus and failure strain were similar to the axial.

9.3.3 Shear

A discrete number of resonant stress waves (4 to 7) were present at the upper test rate of 50 m/min. Specimen and fixture redesign would improve the dynamic equilibrium and data quality at this rate.

The axial shear strength increased 13% between 0.0008/s to 2.5/s from 176 MPa to 198 MPa. The shear modulus was rate insensitive. The apparent decrease in axial modulus is thought to be due to an artifact of the smoothing function used in the data analysis. The axial shear failure strain was $0.79 \pm 0.1\%$ and was rate insensitive.

The transverse shear strength increased 10% with each decade increase above 0.05/s. The shear modulus had a positive trend with rate. It increased 15% between the two bottom and two top rates, from 28.8 GPa at 0.0003/s to 33.1 GPa at 8/s. Once again, the variability within rates made it difficult to quantify the increase per decade. The transverse shear strain was $0.84 \pm 0.1\%$ and was rate insensitive.

The transverse shear strength was at least 13% higher than the axial shear strength at all rates. The failure strains were equivalent for both orientations.

9.4 Tube Compression

Carbon fiber 2D3A tubes were compressed at rates up to 440 m/min (7.4 m/s). The crush behavior was well established within 25 mm of the zeroed displacement. There was rate insensitivity between 1.5 m/min and 140 m/min. There was a slight decrease in the specific sustained crushing stress (SSCS), crush compression ratio (CCR), and the specific energy absorption (SEA) by a factor of 0.9 between 140 m/min and 440 m/min.

The sustained crush strength was about one-quarter of that for the coupon data [~75 MPa vs 270 MPa] and the failure strain ranged from 0.4% to 0.8% compared to 0.9% for the coupons. The uncertainty level was fairly high (6 to 10%) but the shape of the tube compressive stress-strain curve was similar to the lower stiffness coupon data. The average peak tube temperature during the crush was ~270°C at both rates.

10.0 RECOMMENDATIONS

The overall specimen size and thickness was dictated by the requirements for generating valid data at higher rates. The optimum gage width, determined through sensitivity studies, would help to optimize the fixture design. The combination of proper specimen size and fixture design will help to generate valid data at higher rates.

A minimum of five replicates per test condition is recommended to identify significant variations due to rate. In addition, the contribution of panel-to-panel variations and fiber tow alignment through the thickness were confounded in the data. A sensitivity study would be needed to establish these effects on the measured properties using the various specimen configurations.

The fiber tow locations through the thickness may have contributed to the variations in the measured material stiffness using the bowtie and V-notch design. Use of additional layers would help to homogenize the response. However, additional layers would increase the peak loads, which may limit the maximum test speeds. An optimized specimen width may reduce the peak loads. One could also use a different number of layers for the different orientations and tests. A&P Technologies has developed a tacking agent which helps to maintain fiber tow alignment during processing. This would help to identify the contribution of tow location to the measured material response using the bowtie or V-notched specimens.

11.0 REFERENCES

1. Handbook of Composites, Lubin, G., editor, Society of Plastics Engineers Technical Monograph, Van Nostrand Reinhold Co., Inc., New York, 1982.
2. ASM Handbook Volume 21 Composites, ASM International, Material Park, OH, 2001.
3. Ganster, J., Fink, H. and Pinnow, M., "High-Tenacity Man-made Cellulose Fibre Reinforced Thermoplastics – Injection Moulding Compounds with Polypropylene and Alternative Matrices," *Composites Part A*, **37**, 2006, 1796-1804.

4. Lee, B., Kim, H. and Yu, W., "Fabrication of Long and Discontinuous Natural Fiber Reinforced Polypropylene Biocomposites and their Mechanical Properties," *Fibers and Polymers*, **10**, 2009, 83-90.
5. Ashori, A. and Nourbakhsh, A., "Mechanical Behavior of Agro-Residue-Reinforced Polypropylene Composites," *J. of Applied Polymer Science*, **111**, 2009, 2616-2620.
6. Torayca® T700S Technical Data Sheet No. CFA-005, Toray Carbon Fibers America, Inc.
7. <http://www.matbase.com/material/fibres/glass/e-glass-fibre/properties>.
8. *Materials, Design and Manufacturing for Lightweight Vehicles*, Mallick, P. K., Editor, Woodhead Publishing in Materials Series, Woodhead Publishing Limited, 2010.
9. Thomason, J.L., "The Influence of Fibre Length and Concentration on the Properties of Glass Fibre Reinforced Polypropylene. 6. The Properties of Injection Moulded Long Fibre PP at High Fibre Content," *Composites Part A*, **36**, 2005, 995-1003.
10. Short, W. T. and E. J. Wenzel, "Effects of Molding Process on Residual Fiber Length of Long Fiber Polypropylene Composites," Paper 0082, Society of Plastics Engineers - 65th Annual Technical Conference of the Society of Plastics Engineers, Plastics Encounter at ANTEC 2007, Mar 6-11, 2007, Cincinnati, OH.
11. Bowman, C. L., Roberts, G. D., Braley, M. S., Xie, M., and Booker, M. J., "Mechanical Properties of Triaxial Braided Carbon/Epoxy Composites," *NASA TM—2002-211702*, June 2002.
12. Littell, J. D., Binienda, W. K., Roberts, G. D. and Goldberg, R., "Characterization of Damage in Triaxial Braided Composites Under Tensile Loading," *Journal of Aerospace Engineering*, **22**, 2009, 270-279.
13. Littell, J. D., "The Experimental and Analytical Characterization of the Macromechanical Response for Triaxial Braided Composite Materials," Ph.D Dissertation, U of Akron, 2008.
14. Roberts, G. D., et. al, "Characterization of Triaxial Braided Composite Material Properties for Impact Simulation" *NASA TM-2009-215660*, 2009.
15. Chiu, C. H., Tsai, K.-H., Huang, W. J., "Crush Failure Modes of 2D Triaxially Braided Hybrid Composite Tubes," *Composites Science and Technology*, **59**, 1999, 1713-1723.
16. Beard, S., and Chang, F-K., "Design of Braided Composites for Energy Absorption," *J. of Thermoplastic Composite Materials*, **15**, 2002, 3-10.
17. McGregor, C., Vaziri, R., and Xiao, X., "Finite Element Modeling of the Progressive Crushing of Braided Composite Tubes Under Axial Impact," *International Journal of Impact Engineering*, **37**, 2010, 662-672.
18. ASTM International, 100 Bar Harbor Drive, West Conshohocken, PA, www.astm.org.
19. SAE J2749, "Surface Vehicle Recommended Practice - High Strain Rate Tensile Testing of Polymers," SAE International, 400 Commonwealth Drive, Warrendale, PA 15096, www.sae.org.

20. SEP 1230, "The Determination of the Mechanical Properties of Sheet Metal at High Strain Rates in High-Speed Tensile Tests," STAHL-EISEN-Prüfblätter (SEP) des Stahlinstituts VDEh, Verlag Stahleisen GmbH, Postfach 10 51 64, 40042 Düsseldorf, Germany.
21. Pinnell, M., Hill, S. and Minch, A., "Special Concerns in High Strain Rate Tensile Testing of Polymers," SAE 2006 Transactions Journal of Materials and Manufacturing V115-5, April 3-6, 2006, Detroit, Michigan.
22. Eskandari, H., and J. A. Nemes, "Dynamic Testing of Composite Laminates with a Tensile Split Hopkinson Bar," *J. Composite Mater.*, **34**, 2000, 260-73.
23. Fitoussi, J., *et al.*, "Experimental Methodology for High Strain-Rates Tensile Behaviour Analysis of Polymer Matrix Composites," *Composites Science and Technology*, **65**, 2005, 2174-88.
24. Harding, J., and L. M. Welsh, "A Tensile Testing Technique for Fibre-Reinforced Composites at Impact Rates of Strain," *Journal of Materials Science*, **18**, 1983, 1810-26.
25. Rong, Jian, *et al.*, "Tensile Impact Behavior of Multiaxial Multilayer Warp Knitted (MMWK) Fabric Reinforced Composites," *Journal of Reinforced Plastics and Composites*, **25**, 2006, 1305-15.
26. Zaïri, F., *et al.*, "Micromechanical Modelling and Simulation of Chopped Random Fiber Reinforced Polymer Composites with Progressive Debonding Damage," *International Journal of Solids and Structures*, **45**, 2008, 5220-36.
27. Kim, R. Y., Crasto, A. S., "Longitudinal Compression Strength of Glass Fiber-Reinforced Composites," *J. of Reinforced Plastics and Composites*, **12**, 1994, 326-338.
28. Kim, R. Y., Crasto, A. S., "A Longitudinal Compression Test for Composites Using a Sandwich Specimen," *J. of Composite Materials*, **26**, 1915-1929.
29. Masters, J. E., "Compression Testing of Textile Composite Materials," NASA Contractor Report 198285, 1996.
30. Adams, D., O., Moriarty, J. M., Gallegos, A. M., and Adams, D. F., "Development and Evaluation of the V-Notched Rail Shear Test for Composite laminates," Report No. DOT/FAA/AR-03/62, U. S. Department of Transportation, Federal Aviation Administration, September 2003.
31. Wang, Y. H., Jiang, J. H., Wanintrudal, C., *et al.*, "Whole Field Sheet-metal Tensile Test Using Digital Image Correlation," *Experimental Techniques*, March/April 2000, 54-62.
32. Sutton, M., Orteu, J-J., Schreirr, H., *Image Correlation for Shape, Motion and Deformation Measurements*, Springer Publishing, 2009.
33. Sutton, M., *et al.*, "Advances in Two-dimensional and Three-Dimensional Computer Vision," *Photomechanics, Topics Applied Physics*, **77**, 2000, 323-372.
34. "Basics of 3D Digital Image Correlation," Dantec Dynamics Application Note – T-Q-400-Basics 3DCORR-002a-EN."

35. M. A. Courteau, Adams, D. O., "Composite Tube Testing for Crashworthiness Applications: A Review," *J. of Advanced Materials*, **43**, 2011, 13 – 34.
36. Zhou, Y., Wang, Y., Jeelani, S., and Xia, Y., "Tensile Behavior of Carbon Fiber Bundles at Different Strain Rates," *Materials Letters*, **64**, 2010, 246-248.
37. Chen, W. and Zhou, B., "Constitutive Behavior of Epon 828/T-403 at Various Strain Rates," *Mechanics of Time-Dependent Materials*, **2**, 1998, 103-111.

APPENDIX A.
MATERIAL PRODUCT SHEETS

CARBON FIBER

**TECHNICAL
DATA SHEET**
No. CFA-005

TORAYCA® T700S DATA SHEET

Highest strength, standard modulus fiber available with excellent processing characteristics for filament winding and prepreg. This never twisted fiber is used in high tensile applications like pressure vessels, recreational, and industrial.

FIBER PROPERTIES

		<i>English</i>	<i>Metric</i>	<i>Test Method</i>
Tensile Strength		711 ksi	4,900 MPa	TY-030B-01
Tensile Modulus		33.4 Msi	230 GPa	TY-030B-01
Strain		2.1 %	2.1 %	TY-030B-01
Density		0.065 lbs/in ³	1.80 g/cm ³	TY-030B-02
Filament Diameter		2.8E-04 in.	7 μm	
Yield	6K	3,724 ft/lbs	400 g/1000m	TY-030B-03
	12K	1,862 ft/lbs	800 g/1000m	TY-030B-03
	24K	903 ft/lbs	1,650 g/1000m	TY-030B-03
Sizing Type	50C		1.0 %	TY-030B-05
& Amount	60E		0.3 %	TY-030B-05
	FoE		0.7 %	TY-030B-05
	Twist	Never twisted		

FUNCTIONAL PROPERTIES

CTE		-0.38 $\alpha \cdot 10^{-6}/^{\circ}\text{C}$
Specific Heat		0.18 Cal/g $\cdot^{\circ}\text{C}$
Thermal Conductivity		0.0224 Cal/cm $\cdot\text{s}\cdot^{\circ}\text{C}$
Electric Resistivity		1.6 $\times 10^{-3} \Omega\cdot\text{cm}$
Chemical Composition: Carbon		93 %
Na + K		<50 ppm

COMPOSITE PROPERTIES*

Tensile Strength	370 ksi	2,550 MPa	ASTM D-3039
Tensile Modulus	20.0 Msi	135 GPa	ASTM D-3039
Tensile Strain	1.7 %	1.7 %	ASTM D-3039
Compressive Strength	215 ksi	1,470 MPa	ASTM D-695
Flexural Strength	245 ksi	1,670 MPa	ASTM D-790
Flexural Modulus	17.5 Msi	120 GPa	ASTM D-790
ILSS	13 ksi	9 kgf/mm ²	ASTM D-2344
90° Tensile Strength	10.0 ksi	69 MPa	ASTM D-3039

* Toray 250°F Epoxy Resin. Normalized to 60% fiber volume.

TORAY CARBON FIBERS AMERICA, INC.

T700S

COMPOSITE PROPERTIES**

Tensile Strength	355 ksi	2,450 MPa	ASTM D-3039
Tensile Modulus	18.0 Msi	125 GPa	ASTM D-3039
Tensile Strain	1.7 %	1.7 %	ASTM D-3039
Compressive Strength	230 ksi	1,570 MPa	ASTM D-695
Compressive Modulus	--- Msi	--- GPa	ASTM D-695
In-Plane Shear Strength	14 ksi	98 MPa	ASTM D-3518
ILSS	15.5 ksi	11 kgf/mm ²	ASTM D-2344
90° Tensile Strength	10.0 ksi	70 MPa	ASTM D-3039

** Toray Semi-Toughened 350°F Epoxy Resin. Normalized to 60% fiber volume.

See Section 4 for Safety & Handling information. The above properties do not constitute any warranty or guarantee of values.

These values are for material selection purposes only. For applications requiring guaranteed values, contact our sales and technical team to establish a material specification document.

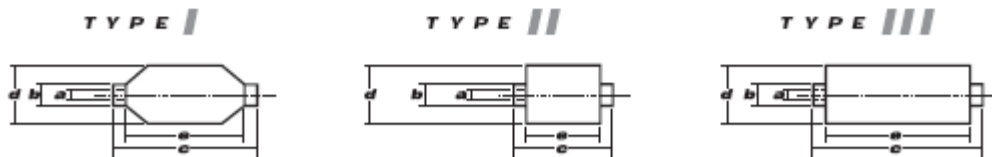
PACKAGING

The table below summarizes the tow sizes, twists, sizing types, and packaging available for standard material. Other bobbin sizes may be available on a limited basis.

Tow Sizes	Twist ¹	Sizing	Bobbin Net Weight (kg)	Bobbin Type ²	Bobbin Size (mm)					Spools per Case	Case Net Weight (kg)
					a	b	c	d	e		
6K	C	50C	2.0	III	76.5	82.5	280	140	252	12	24
	C	50C	6.0	III	76.5	82.5	280	200	252	4	24
12K	C	60E	6.0	III	76.5	82.5	280	200	252	4	24
	C	FoE	6.0	III	76.5	82.5	280	200	252	4	24
24K	C	50C	6.0	III	76.5	82.5	280	200	252	4	24
	C	60E	6.0	III	76.5	82.5	280	200	252	4	24
	C	FoE	6.0	III	76.5	82.5	280	200	252	4	24

¹ Twist A: Twisted yarn B: Untwisted yarn made from a twisted yarn through an untwisting process C: Never twisted yarn

² Bobbin Type See Diagram below



TORAY CARBON FIBERS AMERICA, INC.

6 Hutton Centre Drive, Suite #1270, Santa Ana, CA 92707 TEL: (714) 431-2320 FAX: (714) 424-0750
Sales@Toraycfa.com Technical@Toraycfa.com www.torayusa.com

RESIN EPON™ 862



Technical Data Sheet

Re-issued March 2005

EPON™ Resin 862

Product Description

EPON™ Resin 862 (Diglycidyl Ether of Bisphenol F) is a low viscosity, liquid epoxy resin manufactured from epichlorohydrin and Bisphenol-F. This resin contains no diluents or modifiers. EPON Resin 862 may be used as the sole epoxy resin or combined with other resins such as EPON Resin 828. When blended with EPON Resin 828, EPON Resin 862 provides a technique to reduce viscosity with no sacrifice in chemical and solvent resistance properties, and the blended resin will exhibit improved crystallization resistance properties when compared to the neat, liquid, Bisphenol-A or Bisphenol-F type resins. When EPON Resin 862 is cross-linked with appropriate curing agents, superior mechanical, adhesive, electrical and chemical resistance properties can be obtained.

Application Areas/Suggested Uses

- Solventless or high solids/low VOC maintenance and marine coatings
- Chemical resistant tank linings, floorings, and grouts
- Fiber reinforced pipes, tanks, and composites
- Tooling, casting, and molding compounds
- Construction, electrical, and aerospace adhesives

Benefits

- Low viscosity
- Low color
- Reacts with a full range of epoxy curatives
- Good balance of mechanical, adhesive, and electrical properties
- Good chemical resistance
- Superior physical properties vs. diluted (6 Poise) resins

Sales Specification

Property	Units	Value	Test Method/Standard
Weight per Epoxide	g/eq	165 – 173	ASTM D1862
Viscosity at 25°C	P	25 – 45	ASTM D445
Color	Pt-Co	200 max.	ASTM D1209

Typical Properties

Property	Units	Value	Test Method/Standard
Density at 25°C	lb/gal	9.8	ASTM D1475

RESIN CURING AGENT EPIKURE™ W

Table 9 / Typical Properties of EPIKURE™ – 9000 Series & Composites

Product	Chemical Type	Gel Time @ 25°C ¹ (hours)	Viscosity @ 25°C (cP)	Color ⁷	Density (lb/gal)	Eq. Wt ⁵	PHR ²	Comments
EPIKURE 9270	Polyamine	2.3 ⁵	500-1000	8	8.1	103	50 ⁴	For use in CIPP (Cured In Place Pipe) systems with EPOX 9215. Offers good wetting characteristics and maintains optimal physical properties.
EPIKURE 9551	Polyamine	6	30-70	2	8.0	57-67	33	Provides excellent toughness and elongation.
EPIKURE 9553	Polyamine	0.5	<10	<1	7.2	29	15	Aliphatic amine, low viscosity, room temperature curing agent. Provides increased toughness characteristics.
EPIKURE 9554	Polyamine	~4	15-24	5	7.9	35-41	20	Provides good balance of processing and performance. Designed for use in SCRIMP-type processes.
EPIKURE W	Non-MDA Aromatic Amine	1.5 ⁴	100-350	7	8.5	42-48	24	Non-MDA aromatic amine, provides low viscosity and very long working times, with high performance properties after an elevated temperature cure.

¹ 100 gram mass

² Parts by weight of curing agent per 100 parts of epoxy (EEW 180)

³ 200 gram mass

⁴ 3 gram mass @ 121°C

⁵ Pot-life of 1 gallon mass with EPOX 9215

⁶ Parts by weight of curing agent per 100 parts of EPOX 9215

⁷ Gardner Color Scale

⁸ Equivalent Weight Amount in grams required to react with one equivalent of epoxide

APPENDIX B.
LAMINATE AND TUBE PHYSICAL PROPERTIES

Investigation of Opportunities For Light-Weighting Vehicles Using Advanced Plastics And Composites

Panel 072910-1 Laminate Physical Properties								
Submitted By:	Susan Hill			Date Submitted:	1/21/2011			
Program:	George Washington University			IFAS No. :	4238020003			
Material:	2D carbon 0/+/-60 / Epon 862 W			Panel I.D.:	072910-1			
Job No:				PI Request No:				
Fiber Density (g/cc) =	1.77		Resin Density (g/cc) =	1.2		No. of Plies:		
<u>Specimen Thicknesses</u>								
Spec. Number	thickness (in)							
A								
B								
C								
Avg:	#DIV/0!							
<u>Specific Gravity Determination</u>								
Tested By:								
Spec. Number	Wc (wt. in air) (x.xxxx g)	W (wt. in water) (x.xxxx g)	Md Spec. Grav. (x.xxx)					
A	1.8014	0.6296	1.532					
B	1.4928	0.5193	1.529					
C	1.3754	0.4750	1.523					
		Avg:	1.528					
<u>Laminate Physical Properties Determinations</u>								
Tested By:								
Spec. Number	Wc (spec. wt.) (x.xxxx g)	Wf (Fiber wt.) (x.xxxx g)	F.C. (Fiber cont.) (x.xx Wt.%)	R.C. (Resin Cont.) (x.xx Wt.%)	Vf (Vol. of Fibers) (x.xxxx cm3)	Vc (Vol. of Comp.) (x.xxxx cm3)	Fiber Volume (x.xx Vol.%)	Void Volume (x.xx Vol.%)
A	1.8014	1.1978	66.4927	33.51	0.6767	1.1758	57.55	-0.33
B	1.4928	0.9840	65.9164	34.08	0.5559	0.9763	56.94	-0.37
C	1.3754	0.8912	64.7957	35.20	0.5035	0.9031	55.75	-0.43
			Avg. =	34.27		Avg. =	56.75	-0.38
Wf = (Crucible & Fiber wt.) - (Crucible wt.)				F.C. = (Wf / Wc) x 100				
R.C. = 100 - F.C.				Vf = Wf / Fiber Density				
Vc = Wc / Md				Fiber Volume = (Vf / Vc) x 100				
Void Volume = 100 - Md*[(R.C. / Resin Density) + (F.C. / Fiber Density)]								

Investigation of Opportunities For Light-Weighting Vehicles Using Advanced Plastics And Composites

Panel 072910-2 Laminate Physical Properties								
Submitted By:	Susan Hill			Date Submitted:	2/22/2011			
Program:	George Washington University			IFAS No. :	4238020003			
Material:	2D carbon 0/+/-60 / Epon 862 W			Panel I.D.:	072910-2			
Job No:				PI Request No:				
Fiber Density (g/cc) =	1.77		Resin Density (g/cc) =	1.2		No. of Plies:		
<u>Specimen Thicknesses</u>								
Spec. Number	thickness (in)							
A	0.0612							
B	0.0645							
C	0.0630							
Avg:	0.063							
<u>Specific Gravity Determination</u>								
Tested By:								
Spec. Number	Wc (wt. in air) (x.xxxx g)	W (wt. in water) (x.xxxx g)	Md Spec. Grav. (x.xxx)					
A	1.4292	0.0139	1.545					
B	1.4022	0.0114	1.534					
C	1.3979	0.0128	1.536					
		Avg:	1.538					
<u>Laminate Physical Properties Determinations</u>								
Tested By:								
Spec. Number	Wc (spec. wt.) (x.xxxx g)	Wf (Fiber wt.) (x.xxxx g)	F.C. (Fiber cont.) (x.xx Wt.%)	R.C. (Resin Cont.) (x.xx Wt.%)	Vf (Vol. of Fibers) (x.xxxx cm3)	Vc (Vol. of Comp.) (x.xxxx cm3)	Fiber Volume (x.xx Vol.%)	Void Volume (x.xx Vol.%)
A	1.4292	0.9816	68.6818	31.32	0.5546	0.9250	59.95	-0.27
B	1.4022	0.9572	68.2642	31.74	0.5408	0.9141	59.16	0.27
C	1.3979	0.9542	68.2595	31.74	0.5391	0.9101	59.24	0.14
			Avg. =	31.60		Avg. =	59.45	0.04
Wf = (Crucible & Fiber wt.) - (Crucible wt.)				F.C. = (Wf / Wc) x 100				
R.C. = 100 - F.C.				Vf = Wf / Fiber Density				
Vc = Wc / Md				Fiber Volume = (Vf / Vc) x 100				
Void Volume = 100 - Md*[(R.C. / Resin Density) + (F.C. / Fiber Density)]								

Investigation of Opportunities For Light-Weighting Vehicles Using Advanced Plastics And Composites

Panel 073010-1 Laminate Physical Properties								
Submitted By:	Susan Hill			Date Submitted:	1/10/2011			
Program:	George Washington University			IFAS No. :	4238020003			
Material:	2D carbon 0/+/-60 / Epon 862 W			Panel I.D.:	073010-1 Sample 1			
Job No:				PI Request No:				
Fiber Density (g/cc) =	1.77	Resin Density (g/cc) =	1.2	No. of Plies:				
<u>Specimen Thicknesses</u>								
Spec. Number	thickness (in)							
A	0.0622							
B	0.0660							
C								
Avg:	0.064							
<u>Specific Gravity Determination</u>								
Tested By:								
Spec. Number	Wc (wt. in air) (x.xxxx g)	W (wt. in water) (x.xxxx g)	Md (Spec. Grav.) (x.xxx)					
A (1)	1.3059	0.4410	1.505					
B (2)	2.0164	0.6801	1.504					
		Avg:	1.505					
<u>Laminate Physical Properties Determinations</u>								
Tested By:								
Spec. Number	Wc (spec. wt.) (x.xxxx g)	Wf (Fiber wt.) (x.xxxx g)	F.C. (Fiber cont.) (x.xx Wt.%)	R.C. (Resin Cont.) (x.xx Wt.%)	Vf (Vol. of Fibers) (x.xxxx cm3)	Vc (Vol. of Comp.) (x.xxxx cm3)	Fiber Volume (x.xx Vol.%)	Void Volume (x.xx Vol.%)
A (1)	1.3059	0.8359	64.0095	35.99	0.4723	0.8677	54.43	0.44
B (2)	2.0164	1.2765	63.3059	36.69	0.7212	1.3407	53.79	0.22
			Avg. =	36.34		Avg. =	54.11	0.33
Wf = (Crucible & Fiber wt.) - (Crucible wt.)				F.C. = (Wf / Wc) x 100				
R.C. = 100 - F.C.				Vf = Wf / Fiber Density				
Vc = Wc / Md				Fiber Volume = (Vf / Vc) x 100				
Void Volume = 100 - Md*[(R.C. / Resin Density) + (F.C. / Fiber Density)]								

Investigation of Opportunities For Light-Weighting Vehicles Using Advanced Plastics And Composites

Panel 073010-2 Laminate Physical Properties								
Submitted By:	Susan Hill			Date Submitted:	12/1/2010			
Program:	George Washington University			IFAS No. :	4238020003			
Material:	2D carbon 0/+/-60 / Epon 862 W			Panel I.D.:	073010-2			
Job No:				PI Request No:				
Fiber Density (g/cc) =		1.77		Resin Density (g/cc) =		1.2		No. of Plies:
<u>Specimen Thicknesses</u>								
Spec. Number	thickness (in)							
A	0.0590							
B	0.0669							
C	0.0668							
Avg:	0.064							
<u>Specific Gravity Determination</u>								
Tested By:								
Spec. Number	Wc (wt. in air) (x.xxxx g)	W (wt. in water) (x.xxxx g)	Md Spec. Grav. (x.xxx)					
A	1.8041	0.5853	1.484					
B	1.3503	0.4717	1.532					
C	1.4275	0.4987	1.532					
		Avg:	1.516					
<u>Laminate Physical Properties Determinations</u>								
Tested By:								
Spec. Number	Wc (spec. wt.) (x.xxxx g)	Wf (Fiber wt.) (x.xxxx g)	F.C. (Fiber cont.) (x.xx Wt.%)	R.C. (Resin Cont.) (x.xx Wt.%)	Vf (Vol. of Fibers) (x.xxxx cm3)	Vc (Vol. of Comp.) (x.xxxx cm3)	Fiber Volume (x.xx Vol.%)	Void Volume (x.xx Vol.%)
A	1.8041	1.1791	65.3567	34.64	0.6662	1.2157	54.80	2.36
B	1.3503	0.9043	66.9703	33.03	0.5109	0.8814	57.97	-0.13
C	1.4275	0.9598	67.2364	32.76	0.5423	0.9318	58.20	-0.02
			Avg. =	33.48		Avg. =	56.99	0.74
Wf = (Crucible & Fiber wt.) - (Crucible wt.)				F.C. = (Wf / Wc) x 100				
R.C. = 100 - F.C.				Vf = Wf / Fiber Density				
Vc = Wc / Md				Fiber Volume = (Vf / Vc) x 100				
Void Volume = 100 - Md*[(R.C. / Resin Density) + (F.C. / Fiber Density)]								

Investigation of Opportunities For Light-Weighting Vehicles Using Advanced Plastics And Composites

Panel 073010-3 Laminate Physical Properties								
Submitted By:	Susan Hill			Date Submitted:	10/27/2010			
Program:	George Washington University			IFAS No. :	4238020003			
Material:	2D carbon 0/+/-60 / Epon 862 W			Panel I.D.:	073010-3			
Job No:				PI Request No:				
Fiber Density (g/cc) =		1.77		Resin Density (g/cc) =		1.2		No. of Plies:
<u>Specific Gravity Determination</u>								
Tested By:								
Spec. Number	Wc (wt. in air) (x.xxxx g)	W (wt. in water) (x.xxxx g)	Md Spec. Grav. (x.xxx)					
A	1.2070	0.4184	1.526					
B	1.3279	0.4553	1.517					
C	1.5762	0.5481	1.528					
		Avg:	1.524					
<u>Laminate Physical Properties Determinations</u>								
Tested By:								
Spec. Number	Wc (spec. wt.) (x.xxxx g)	Wf (Fiber wt.) (x.xxxx g)	F.C. (Fiber cont.) (x.xx Wt.%)	R.C. (Resin Cont.) (x.xx Wt.%)	Vf (Vol. of Fibers) (x.xxxx cm3)	Vc (Vol. of Comp.) (x.xxxx cm3)	Fiber Volume (x.xx Vol.%)	Void Volume (x.xx Vol.%)
A	1.2070	0.9147	75.7829	24.22	0.5168	0.7910	65.34	3.87
B	1.3279	0.8613	64.8618	35.14	0.4866	0.8753	55.59	-0.01
C	1.5762	1.0482	66.5017	33.50	0.5922	1.0315	57.41	-0.06
			Avg. =	30.95			Avg. =	59.45
Wf = (Crucible & Fiber wt.) - (Crucible wt.)				F.C. = (Wf / Wc) x 100				
R.C. = 100 - F.C.				Vf = Wf / Fiber Density				
Vc = Wc / Md				Fiber Volume = (Vf / Vc) x 100				
Void Volume = 100 - Md*[(R.C. / Resin Density) + (F.C. / Fiber Density)]								

Investigation of Opportunities For Light-Weighting Vehicles Using Advanced Plastics And Composites

Panel 073010-4 Laminate Physical Properties								
Submitted By:	Susan Hill			Date Submitted:	10/27/2010			
Program:	George Washington University			IFAS No. :	4238020003			
Material:	2D carbon 0/+/-60 / Epon 862 W			Panel I.D.:	073010-4			
Job No:				PI Request No:				
Fiber Density (g/cc) =	1.77		Resin Density (g/cc) =	1.2		No. of Plies:		
Specimen Thicknesses								
Spec. Number	thickness (in)							
D (spec STL094-14)	0.0632							
Avg:	0.063							
Specific Gravity Determination								
Tested By:								
Spec. Number	Wc (wt. in air) (x.xxxx g)	W (wt. in water) (x.xxxx g)	Md (x.xxx)					
A	1.1371	0.3991	1.537					
B	1.5400	0.5418	1.538					
C	1.5755	0.5542	1.538					
D (spec STL094-14)	1.0639	0.3710	1.531					
		Avg:	1.536					
Laminate Physical Properties Determinations								
Tested By:								
Spec. Number	Wc (spec. wt.) (x.xxxx g)	Wf (Fiber wt.) (x.xxxx g)	F.C. (Fiber cont.) (x.xx Wt.%)	R.C. (Resin Cont.) (x.xx Wt.%)	Vf (Vol. of Fibers) (x.xxxx cm3)	Vc (Vol. of Comp.) (x.xxxx cm3)	Fiber Volume (x.xx Vol.%)	Void Volume (x.xx Vol.%)
A	1.1371	0.7604	66.8719	33.13	0.4296	0.7398	58.07	-0.50
B	1.5400	0.7966	51.7273	48.27	0.4501	1.0013	44.95	-6.82
C	1.5755	0.8524	54.1035	45.90	0.4816	1.0244	47.01	-5.84
D (spec STL094-14)	1.0639	0.6988	65.6829	34.32	0.3948	0.6949	56.81	-0.60
			Avg. =	40.40		Avg. =	51.71	-4.38
SG similar for all but fiber content is low. Disregard for calculating normalizing factor.								
Wf = (Crucible & Fiber wt.) - (Crucible wt.)			F.C. = (Wf / Wc) x 100					
R.C. = 100 - F.C.			Vf = Wf / Fiber Density					
Vc = Wc / Md			Fiber Volume = (Vf / Vc) x 100					
Void Volume = 100 - Md*[(R.C. / Resin Density) + (F.C. / Fiber Density)]								

Investigation of Opportunities For Light-Weighting Vehicles Using Advanced Plastics And Composites

Panel 073010-5 Laminate Physical Properties								
Submitted By:	Susan Hill			Date Submitted:	1/10/2011			
Program:	George Washington University			IFAS No. :	4238020003			
Material:	2D carbon 0/+/-60 / Epon 862 W			Panel I.D.:	073010-5			
Job No:				PI Request No:				
Fiber Density (g/cc) =		1.77		Resin Density (g/cc) =		1.2		No. of Plies:
<u>Specimen Thicknesses</u>								
Spec. Number	thickness (in)							
A	0.0579	SAB-6 STL095-11						
B								
C	0.0660	SAB-8 STL095-15						
Avg:	0.062							
<u>Specific Gravity Determination</u>								
Tested By:								
Spec. Number	Wc (wt. in air)	W (wt. in water)	Md (Spec. Grav.)					
	(x.xxxx g)	(x.xxxx g)	(x.xxx)					
A	1.1110	0.3820	1.520					
B								
C	1.1132	0.3795	1.512					
		Avg:	1.516					
<u>Laminate Physical Properties Determinations</u>								
Tested By:								
Spec. Number	Wc (spec. wt.)	Wf (Fiber wt.)	F.C. (Fiber cont.)	R.C. (Resin Cont.)	Vf (Vol. of Fibers)	Vc (Vol. of Comp.)	Fiber Volume	Void Volume
	(x.xxxx g)	(x.xxxx g)	(x.xx Wt.%)	(x.xx Wt.%)	(x.xxxx cm3)	(x.xxxx cm3)	(x.xx Vol.%)	(x.xx Vol.%)
A	1.1110	0.7448	67.0387	32.96	0.4208	0.7309	57.57	0.68
C	1.1132	0.7214	64.8042	35.20	0.4076	0.7362	55.36	0.30
			Avg. =	34.08		Avg. =	56.46	0.49
Wf = (Crucible & Fiber wt.) - (Crucible wt.)				F.C. = (Wf / Wc) x 100				
R.C. = 100 - F.C.				Vf = Wf / Fiber Density				
Vc = Wc / Md				Fiber Volume = (Vf / Vc) x 100				

Investigation of Opportunities For Light-Weighting Vehicles Using Advanced Plastics And Composites

Panel 073010-5 Laminate Physical Properties								
Submitted By:	Susan Hill			Date Submitted:	12/1/2010			
Program:	George Washington University			IFAS No. :	4238020003			
Material:	2D carbon 0/+/-60 / Epon 862 W			Panel I.D.:	073010-6			
Job No:				PI Request No:				
Fiber Density (g/cc) =		1.77	Resin Density (g/cc) =		1.2	No. of Plies:		
<u>Specimen Thicknesses</u>								
Spec. Number	thickness (in)							
A	0.0580							
B	0.0652							
C	0.0636							
Avg:	0.062							
<u>Specific Gravity Determination</u>								
Tested By:								
Spec. Number	Wc (wt. in air) (x.xxxx g)	W (wt. in water) (x.xxxx g)	Md (Spec. Grav.) (x.xxx)					
A	1.2645	0.4433	1.535					
B	1.5085	0.5207	1.522					
C	1.2674	0.4387	1.525					
		Avg:	1.527					
<u>Laminate Physical Properties Determinations</u>								
Tested By:								
Spec. Number	Wc (spec. wt.) (x.xxxx g)	Wf (Fiber wt.) (x.xxxx g)	F.C. (Fiber cont.) (x.xx Wt.%)	R.C. (Resin Cont.) (x.xx Wt.%)	Vf (Vol. of Fibers) (x.xxxx cm3)	Vc (Vol. of Comp.) (x.xxxx cm3)	Fiber Volume (x.xx Vol.%)	Void Volume (x.xx Vol.%)
A	1.2645	0.8356	66.0815	33.92	0.4721	0.8238	57.31	-0.70
B	1.5085	1.0094	66.9142	33.09	0.5703	0.9911	57.54	0.50
C	1.2674	0.8415	66.3958	33.60	0.4754	0.8311	57.21	0.09
			Avg. =	33.54		Avg. =	57.35	-0.04
Wf = (Crucible & Fiber wt.) - (Crucible wt.)				F.C. = (Wf / Wc) x 100				
R.C. = 100 - F.C.				Vf = Wf / Fiber Density				
Vc = Wc / Md				Fiber Volume = (Vf / Vc) x 100				
Void Volume = 100 - Md*[(R.C. / Resin Density) + (F.C. / Fiber Density)]								

Investigation of Opportunities For Light-Weighting Vehicles Using Advanced Plastics And Composites

Panel 080210-6 Laminate Physical Properties									
Submitted By:	Stonecash	Date Submitted:	9/2/2010						
Program:	GWU(Susan Hill)	IFAS No. :	4238020003						
Material:	2Dcarbon braid/862W	Panel I.D.:	080210-6						
Job No:	CKX	PI Request No:	CKX-JS-10-161						
Fiber Density (g/cc) =		1.77	Resin Density (g/cc) =			1.2	No. of Plies:		
<u>Specimen Thicknesses</u>									
Spec. Number	thickness (in)								
1	0.0635								
2	0.0641								
3	0.0618								
Avg:	0.0631								
<u>Specific Gravity Determination</u>									
Tested By:		Andrews							
Spec. Number	Wc (wt. in air) (x.xxxx g)	W (wt. in water) (x.xxxx g)	Md Spec. Grav. (x.xxx)						
1	0.6705	0.2348	1.534						
2	1.0695	0.3653	1.514						
3	1.1525	0.3357	1.394						
		Avg:	1.481						
<u>Laminate Physical Properties Determinations</u>									
Tested By:		Andrews							
Spec. Number	Wc (spec. wt.) (x.xxxx g)	Wf (Fiber wt.) (x.xxxx g)	F.C. (Fiber cont.) (x.xx Wt.%)	R.C. (Resin Cont.) (x.xx Wt.%)	Vf (Vol. of Fibers) (x.xxxx cm3)	Vc (Vol. of Comp.) (x.xxxx cm3)	Fiber Volume (x.xx Vol.%)	Void Volume (x.xx Vol.%)	
1	0.6705	0.4437	66.17	33.83	0.2507	0.4371	57.35	-0.59	
2	1.0695	0.7228	67.58	32.42	0.4084	0.7064	57.81	1.29	
3	1.1525	0.7424	64.42	35.58	0.4194	0.8268	50.73	7.93	
		Avg. =	66.06	33.94		Avg. =	55.30	2.88	
Wf = (Crucible & Fiber wt.) - (Crucible wt.)					F.C. = (Wf / Wc) x 100				
R.C. = 100 - F.C.					Vf = Wf / Fiber Density				
Vc = Wc / Md					Fiber Volume = (Vf / Vc) x 100				
Void Volume = 100 - Md*[(R.C. / Resin Density) + (F.C. / Fiber Density)]									

Investigation of Opportunities For Light-Weighting Vehicles Using Advanced Plastics And Composites

Tube Physical Properties								
Submitted By:	Susan Hill				Date Submitted:	3/28/2011		
Program:	George Washington University				IFAS No. :	4238020003		
Material:	2D carbon 0/+/-60 / Epon 862 W				Panel I.D.:	STL 103-1		
Job No:					PI Request No:			
Fiber Density (g/cc) = 1.77			Resin Density (g/cc) = 1.2			No. of Plies:		
Specimen Thicknesses								
Spec. Number	thickness (in)							
1	0.0785							
2	0.0789							
3	0.0790							
Avg:	0.0788							
Specific Gravity Determination								
Tested By:		Andrews						
Spec. Number	Wc	W	Md					
	(wt. in air)	(wt. in water)	Spec. Grav.					
	(x.xxxx g)	(x.xxxx g)	(x.xxx)					
1	0.8892	0.2819	1.460					
2	0.9653	0.3034	1.454					
3	0.7928	0.2641	1.495					
		Avg:	1.470					
Laminate Physical Properties Determinations								
Tested By:		Andrews						
Spec. Number	Wc	Wf	F.C.	R.C.	Vf	Vc	Fiber Volume	Void Volume
	(spec. wt.)	(Fiber wt.)	(Fiber cont.)	(Resin Cont.)	(Vol. of Fibers)	(Vol. of Comp.)	(x.xx Vol.%)	(x.xx Vol.%)
	(x.xxxx g)	(x.xxxx g)	(x.xx Wt.%)	(x.xx Wt.%)	(x.xxxx cm3)	(x.xxxx cm3)		
1	0.8892	0.4809	54.08	45.92	0.2717	0.6090	44.61	-0.48
2	0.9653	0.5147	53.32	46.68	0.2908	0.6639	43.80	-0.36
3	0.7928	0.4819	60.78	39.22	0.2723	0.5303	51.34	-0.20
			Avg. =	43.94		Avg. =	46.58	-0.35
Wf = (Crucible & Fiber wt.) - (Crucible wt.)				F.C. = (Wf / Wc) x 100				
R.C. = 100 - F.C.				Vf = Wf / Fiber Density				
Vc = Wc / Md				Fiber Volume = (Vf / Vc) x 100				
Void Volume = 100 - Md*[(R.C. / Resin Density) + (F.C. / Fiber Density)]								

Investigation of Opportunities For Light-Weighting Vehicles Using Advanced Plastics And Composites

Tube Physical Properties								
Submitted By:	Susan Hill			Date Submitted:	3/28/2011			
Program:	George Washington University			IFAS No. :	4238020003			
Material:	2D carbon 0/+/-60 / Epon 862 W			Panel I.D.:	STL 103-2			
Job No:				PI Request No:				
Fiber Density (g/cc) =		1.77		Resin Density (g/cc) =		1.2		No. of Plies:
Specimen Thicknesses								
Spec. Number	thickness (in)							
1	0.8040							
2	0.0765							
3	0.7920							
Avg:	0.5575							
Specific Gravity Determination								
Tested By:		Andrews						
Spec. Number	Wc	W	Md					
	(wt. in air)	(wt. in water)	Spec. Grav.					
	(x.xxxx g)	(x.xxxx g)	(x.xxx)					
1	0.8742	0.2647	1.430					
2	0.7638	0.2401	1.455					
3	1.0881	0.3414	1.453					
		Avg:	1.446					
Laminate Physical Properties Determinations								
Tested By:		Andrews						
Spec. Number	Wc	Wf	F.C.	R.C.	Vf	Vc	Fiber Volume	Void Volume
	(spec. wt.)	(Fiber wt.)	(Fiber cont.)	(Resin Cont.)	(Vol. of Fibers)	(Vol. of Comp.)		
	(x.xxxx g)	(x.xxxx g)	(x.xx Wt.%)	(x.xx Wt.%)	(x.xxxx cm3)	(x.xxxx cm3)	(x.xx Vol.%)	(x.xx Vol.%)
1	0.8742	0.4469	51.12	48.88	0.2525	0.6113	41.30	0.45
2	0.7638	0.4121	53.95	46.05	0.2328	0.5249	44.35	-0.18
3	1.0881	0.5815	53.44	46.56	0.3285	0.7489	43.87	-0.24
			Avg. =	47.16		Avg. =	43.17	0.01
Wf = (Crucible & Fiber wt.) - (Crucible wt.)				F.C. = (Wf / Wc) x 100				
R.C. = 100 - F.C.				Vf = Wf / Fiber Density				
Vc = Wc / Md				Fiber Volume = (Vf / Vc) x 100				
Void Volume = 100 - Md*[(R.C. / Resin Density) + (F.C. / Fiber Density)]								

Investigation of Opportunities For Light-Weighting Vehicles Using Advanced Plastics And Composites

<u>Tube Physical Properties</u>								
Submitted By:	Susan Hill			Date Submitted:	3/28/2011			
Program:	George Washington University			IFAS No. :	4238020003			
Material:	2D carbon 0/+/-60 / Epon 862 W			Panel I.D.:	STL 103-3			
Job No:				PI Request No:				
Fiber Density (g/cc) =		1.77		Resin Density (g/cc) =		1.2		No. of Plies:
<u>Specimen Thicknesses</u>								
Spec. Number	thickness (in)							
1	0.0813							
2	0.0791							
3	0.0821							
Avg:	0.081							
<u>Specific Gravity Determination</u>								
Tested By:	Andrews							
Spec. Number	Wc (wt. in air) (x.xxxx g)	W (wt. in water) (x.xxxx g)	Md Spec. Grav. (x.xxx)					
1	0.8869	0.2736	1.442					
2	0.9052	0.2839	1.452					
3	1.0175	0.3150	1.444					
		Avg:	1.446					
<u>Laminate Physical Properties Determinations</u>								
Tested By:	Andrews							
Spec. Number	Wc (spec. wt.) (x.xxxx g)	Wf (Fiber wt.) (x.xxxx g)	F.C. (Fiber cont.) (x.xx Wt.%)	R.C. (Resin Cont.) (x.xx Wt.%)	Vf (Vol. of Fibers) (x.xxxx cm3)	Vc (Vol. of Comp.) (x.xxxx cm3)	Fiber Volume (x.xx Vol.%)	Void Volume (x.xx Vol.%)
1	0.8869	0.4536	51.14	48.86	0.2563	0.6150	41.67	-0.37
2	0.9052	0.4822	53.27	46.73	0.2724	0.6234	43.70	-0.24
3	1.0175	0.5289	51.98	48.02	0.2988	0.7046	42.41	-0.19
			Avg. =	47.87		Avg. =	42.59	-0.27
Wf = (Crucible & Fiber wt.) - (Crucible wt.)				F.C. = (Wf / Wc) x 100				
R.C. = 100 - F.C.				Vf = Wf / Fiber Density				
Vc = Wc / Md				Fiber Volume = (Vf / Vc) x 100				
Void Volume = 100 - Md*[(R.C. / Resin Density) + (F.C. / Fiber Density)]								

Investigation of Opportunities For Light-Weighting Vehicles Using Advanced Plastics And Composites

<u>Tube Physical Properties</u>								
Submitted By:	Susan Hill			Date Submitted:	3/28/2011			
Program:	George Washington University			IFAS No. :	4238020003			
Material:	2D carbon 0/+/-60 / Epon 862 W			Panel I.D.:	STL 103-4			
Job No:				PI Request No:				
Fiber Density (g/cc) =		1.77		Resin Density (g/cc) =		1.2		No. of Plies:
<u>Specimen Thicknesses</u>								
Spec. Number	thickness (in)							
1	0.0790							
2	0.0803							
3	0.0850							
Avg:	0.0814							
<u>Specific Gravity Determination</u>								
Tested By:		Andrews						
Spec. Number	Wc (wt. in air) (x.xxxx g)	W (wt. in water) (x.xxxx g)	Md Spec. Grav. (x.xxx)					
1	0.8974	0.2532	1.456					
2	0.9443	0.2947	1.449					
3	1.3158	0.4001	1.433					
		Avg:	1.446					
<u>Laminate Physical Properties Determinations</u>								
Tested By:		Andrews						
Spec. Number	Wc (spec. wt.) (x.xxxx g)	Wf (Fiber wt.) (x.xxxx g)	F.C. (Fiber cont.) (x.xx Wt.%)	R.C. (Resin Cont.) (x.xx Wt.%)	Vf (Vol. of Fibers) (x.xxxx cm3)	Vc (Vol. of Comp.) (x.xxxx cm3)	Fiber Volume (x.xx Vol.%)	Void Volume (x.xx Vol.%)
1	0.8974	0.4840	53.93	46.07	0.2734	0.6163	44.37	-0.26
2	0.9443	0.5029	53.26	46.74	0.2841	0.6517	43.60	-0.04
3	1.3158	0.6620	50.31	49.69	0.3740	0.9182	40.73	-0.07
			Avg. =	47.50		Avg. =	42.90	-0.12
Wf = (Crucible & Fiber wt.) - (Crucible wt.)				F.C. = (Wf / Wc) x 100				
R.C. = 100 - F.C.				Vf = Wf / Fiber Density				
Vc = Wc / Md				Fiber Volume = (Vf / Vc) x 100				
Void Volume = 100 - Md*[(R.C. / Resin Density) + (F.C. / Fiber Density)]								

Investigation of Opportunities For Light-Weighting Vehicles Using Advanced Plastics And Composites

<u>Tube Physical Properties</u>								
Submitted By:	Susan Hill			Date Submitted:	3/28/2011			
Program:	George Washington University			IFAS No. :	4238020003			
Material:	2D carbon 0/+/-60 / Epon 862 W			Panel I.D.:	STL 103-5			
Job No:				PI Request No:				
Fiber Density (g/cc) =		1.77		Resin Density (g/cc) =		1.2		No. of Plies:
<u>Specimen Thicknesses</u>								
Spec. Number	thickness (in)							
1	0.0751							
2	0.0684							
3	0.0764							
Avg:	0.0733							
<u>Specific Gravity Determination</u>								
Tested By:		Andrews						
Spec. Number	Wc	W	Md					
	(wt. in air)	(wt. in water)	Spec. Grav.					
	(x.xxxx g)	(x.xxxx g)	(x.xxx)					
1	0.8513	0.2691	1.457					
2	0.6940	0.2307	1.493					
3	0.7724	0.2452	1.461					
		Avg:	1.470					
<u>Laminate Physical Properties Determinations</u>								
Tested By:		Andrews						
Spec. Number	Wc	Wf	F.C.	R.C.	Vf	Vc	Fiber Volume	Void Volume
	(spec. wt.)	(Fiber wt.)	(Fiber cont.)	(Resin Cont.)	(Vol. of Fibers)	(Vol. of Comp.)	(x.xx Vol.%)	(x.xx Vol.%)
	(x.xxxx g)	(x.xxxx g)	(x.xx Wt.%)	(x.xx Wt.%)	(x.xxxx cm3)	(x.xxxx cm3)		
1	0.8513	0.4639	54.49	45.51	0.2621	0.5843	44.86	-0.11
2	0.6940	0.4173	60.13	39.87	0.2358	0.4648	50.72	-0.32
3	0.7724	0.4221	54.65	45.35	0.2385	0.5287	45.11	-0.32
			Avg. =	43.58		Avg. =	46.89	-0.25
Wf = (Crucible & Fiber wt.) - (Crucible wt.)				F.C. = (Wf / Wc) x 100				
R.C. = 100 - F.C.				Vf = Wf / Fiber Density				
Vc = Wc / Md				Fiber Volume = (Vf / Vc) x 100				
Void Volume = 100 - Md*[(R.C. / Resin Density) + (F.C. / Fiber Density)]								

Investigation of Opportunities For Light-Weighting Vehicles Using Advanced Plastics And Composites

Tube Physical Properties								
Submitted By:	Susan Hill				Date Submitted:	4/19/2011		
Program:	George Washington University				IFAS No. :	4238020003		
Material:	2D carbon 0/+/-60 / Epon 862 W				Panel I.D.:	STL 103-6		
Job No:					PI Request No:			
Fiber Density (g/cc) = 1.77			Resin Density (g/cc) = 1.2			No. of Plies:		
Specimen Thicknesses								
Spec. Number	thickness (in)							
1	0.0825							
2	0.0782							
3	770.0000							
Avg:	256.7202							
Specific Gravity Determination								
Tested By:		Andrews						
Spec. Number	Wc	W	Md					
	(wt. in air)	(wt. in water)	Spec. Grav.					
	(x.xxxx g)	(x.xxxx g)	(x.xxx)					
1	1.3754	0.4232	1.440					
2	0.9175	0.2783	1.432					
3	1.0152	0.3182	1.452					
		Avg:	1.441					
Laminate Physical Properties Determinations								
Tested By:		Andrews						
Spec. Number	Wc	Wf	F.C.	R.C.	Vf	Vc	Fiber Volume	Void Volume
	(spec. wt.)	(Fiber wt.)	(Fiber cont.)	(Resin Cont.)	(Vol. of Fibers)	(Vol. of Comp.)	(x.xx Vol.%)	(x.xx Vol.%)
	(x.xxxx g)	(x.xxxx g)	(x.xx Wt.%)	(x.xx Wt.%)	(x.xxxx cm3)	(x.xxxx cm3)		
1	1.3754	0.7442	54.11	45.89	0.4205	0.9551	44.02	0.91
2	0.9175	0.4986	54.34	45.66	0.2817	0.6407	43.97	1.55
3	1.0152	0.6080	59.89	40.11	0.3435	0.6992	49.13	2.34
			Avg. =	43.89		Avg. =	45.71	1.60
Wf = (Crucible & Fiber wt.) - (Crucible wt.)				F.C. = (Wf / Wc) x 100				
R.C. = 100 - F.C.				Vf = Wf / Fiber Density				
Vc = Wc / Md				Fiber Volume = (Vf / Vc) x 100				
Void Volume = 100 - Md*[(R.C. / Resin Density) + (F.C. / Fiber Density)]								

Investigation of Opportunities For Light-Weighting Vehicles Using Advanced Plastics And Composites

Tube Physical Properties								
Submitted By:	Susan Hill				Date Submitted:	4/19/2011		
Program:	George Washington University				IFAS No. :	4238020003		
Material:	2D carbon 0/+/-60 / Epon 862 W				Panel I.D.:	STL 103-7		
Job No:					PI Request No:			
Fiber Density (g/cc) = 1.77			Resin Density (g/cc) = 1.2			No. of Plies:		
<u>Specimen Thicknesses</u>								
Spec. Number	thickness (in)							
1	0.0820							
2	0.0778							
3	0.0754							
Avg:	0.0784							
<u>Specific Gravity Determination</u>								
Tested By:		Andrews						
Spec. Number	Wc	W	Md					
	(wt. in air)	(wt. in water)	Spec. Grav.					
	(x.xxxx g)	(x.xxxx g)	(x.xxx)					
1	1.2711	0.3909	1.440					
2	1.0283	0.2935	1.395					
3	0.9334	0.2873	1.440					
		Avg:	1.425					
<u>Laminate Physical Properties Determinations</u>								
Tested By:		Andrews						
Spec. Number	Wc	Wf	F.C.	R.C.	Vf	Vc	Fiber Volume	Void Volume
	(spec. wt.)	(Fiber wt.)	(Fiber cont.)	(Resin Cont.)	(Vol. of Fibers)	(Vol. of Comp.)	(x.xx Vol.%)	(x.xx Vol.%)
	(x.xxxx g)	(x.xxxx g)	(x.xx Wt.%)	(x.xx Wt.%)	(x.xxxx cm3)	(x.xxxx cm3)		
1	1.2711	0.6914	54.39	45.61	0.3906	0.8827	44.25	1.02
2	1.0283	0.4940	48.04	51.96	0.2791	0.7371	37.86	1.73
3	0.9334	0.5225	55.98	44.02	0.2952	0.6482	45.54	1.63
			Avg. =	47.20		Avg. =	42.55	1.46
Wf = (Crucible & Fiber wt.) - (Crucible wt.)				F.C. = (Wf / Wc) x 100				
R.C. = 100 - F.C.				Vf = Wf / Fiber Density				
Vc = Wc / Md				Fiber Volume = (Vf / Vc) x 100				
Void Volume = 100 - Md*[(R.C. / Resin Density) + (F.C. / Fiber Density)]								

Investigation of Opportunities For Light-Weighting Vehicles Using Advanced Plastics And Composites

<u>Tube Physical Properties</u>								
Submitted By:	Susan Hill				Date Submitted:	4/19/2011		
Program:	George Washington University				IFAS No. :	4238020003		
Material:	2D carbon 0/+/-60 / Epon 862 W				Panel I.D.:	STL 103-8		
Job No:					PI Request No:			
Fiber Density (g/cc) = 1.77			Resin Density (g/cc) = 1.2			No. of Plies:		
<u>Specimen Thicknesses</u>								
Spec. Number	thickness (in)							
1	0.0810							
2	0.0802							
3	0.7790							
Avg:	0.3134							
<u>Specific Gravity Determination</u>								
Tested By:		Andrews						
Spec. Number	Wc	W	Md					
	(wt. in air)	(wt. in water)	Spec. Grav.					
	(x.xxxx g)	(x.xxxx g)	(x.xxx)					
1	1.4385	0.4406	1.437					
2	0.9300	0.2889	1.447					
3	1.0813	0.3335	1.442					
		0.3335	1.442					
<u>Laminate Physical Properties Determinations</u>								
Tested By:		Andrews						
Spec. Number	Wc	Wf	F.C.	R.C.	Vf	Vc	Fiber Volume	Void Volume
	(spec. wt.)	(Fiber wt.)	(Fiber cont.)	(Resin Cont.)	(Vol. of Fibers)	(Vol. of Comp.)		
	(x.xxxx g)	(x.xxxx g)	(x.xx Wt.%)	(x.xx Wt.%)	(x.xxxx cm3)	(x.xxxx cm3)	(x.xx Vol.%)	(x.xx Vol.%)
1	1.4385	0.7850	54.57	45.43	0.4435	1.0010	44.30	1.29
2	0.9300	0.5115	55.00	45.00	0.2890	0.6427	44.96	0.77
3	1.0813	0.5907	54.63	45.37	0.3337	0.7499	44.51	0.97
			Avg. =	45.27		Avg. =	44.59	1.01
Wf = (Crucible & Fiber wt.) - (Crucible wt.)				F.C. = (Wf / Wc) x 100				
R.C. = 100 - F.C.				Vf = Wf / Fiber Density				
Vc = Wc / Md				Fiber Volume = (Vf / Vc) x 100				
Void Volume = 100 - Md*[(R.C. / Resin Density) + (F.C. / Fiber Density)]								

Investigation of Opportunities For Light-Weighting Vehicles Using Advanced Plastics And Composites

<u>Tube Physical Properties</u>								
Submitted By:	Susan Hill				Date Submitted:	4/19/2011		
Program:	George Washington University				IFAS No. :	4238020003		
Material:	2D carbon 0/+/-60 / Epon 862 W				Panel I.D.:	STL 103-9		
Job No:					PI Request No:			
Fiber Density (g/cc) =			1.77		Resin Density (g/cc) =		1.2	
					No. of Plies:			
<u>Specimen Thicknesses</u>								
Spec. Number	thickness (in)							
1	0.0800							
2	0.0801							
3	0.0788							
Avg:	0.0796							
<u>Specific Gravity Determination</u>								
Tested By:		Andrews						
Spec. Number	Wc	W	Md					
	(wt. in air)	(wt. in water)	Spec. Grav.					
	(x.xxxx g)	(x.xxxx g)	(x.xxx)					
1	1.3359	0.4175	1.450					
2	0.9374	0.2871	1.437					
3	0.9454	0.2893	1.437					
		Avg:	1.441					
<u>Laminate Physical Properties Determinations</u>								
Tested By:		Andrews						
Spec. Number	Wc	Wf	F.C.	R.C.	Vf	Vc	Fiber Volume	Void Volume
	(spec. wt.)	(Fiber wt.)	(Fiber cont.)	(Resin Cont.)	(Vol. of Fibers)	(Vol. of Comp.)	(x.xx Vol.%)	(x.xx Vol.%)
	(x.xxxx g)	(x.xxxx g)	(x.xx Wt.%)	(x.xx Wt.%)	(x.xxxx cm3)	(x.xxxx cm3)		
1	1.3359	0.7676	57.46	42.54	0.4337	0.9213	47.07	1.53
2	0.9374	0.5105	54.46	45.54	0.2884	0.6523	44.21	1.25
3	0.9454	0.5082	53.76	46.24	0.2871	0.6579	43.64	0.98
			Avg. =	44.78		Avg. =	44.98	1.25
Wf = (Crucible & Fiber wt.) - (Crucible wt.)				F.C. = (Wf / Wc) x 100				
R.C. = 100 - F.C.				Vf = Wf / Fiber Density				
Vc = Wc / Md				Fiber Volume = (Vf / Vc) x 100				
Void Volume = 100 - Md*[(R.C. / Resin Density) + (F.C. / Fiber Density)]								

APPENDIX C.
SELECTED PANEL LAYOUTS

Sections used for fiber content analyses are labeled AD

**Sections for photomicrographs are identified with a number and a directional arrow indicating the
mount surface**

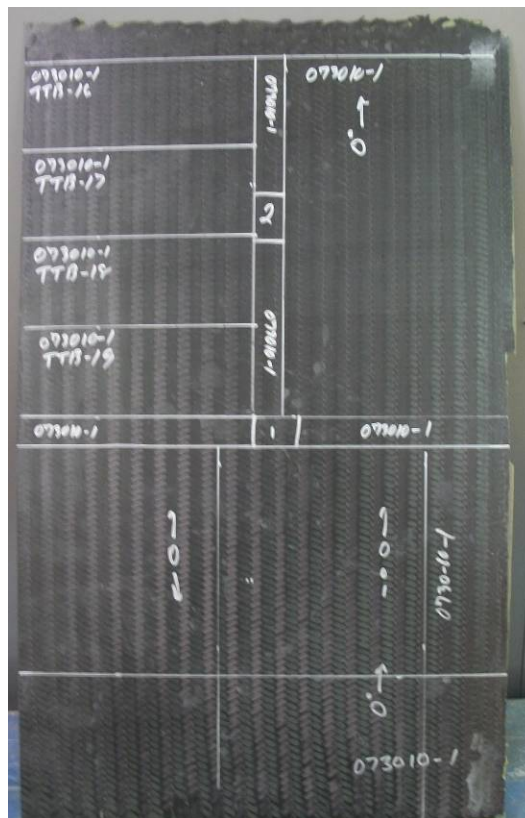
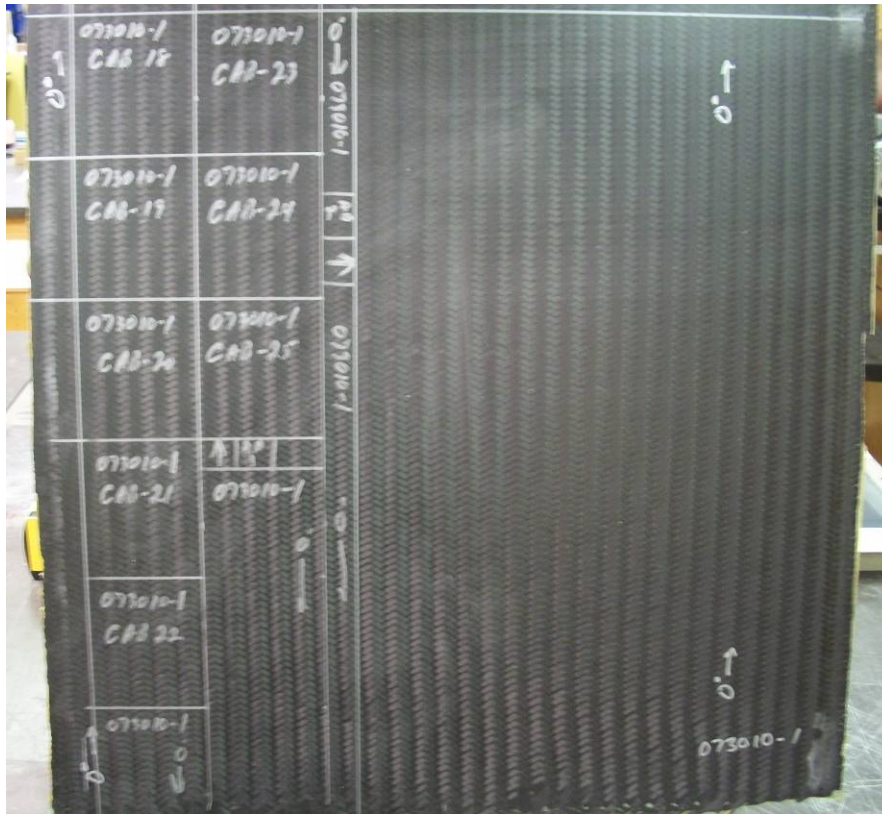
PANEL 072910-1



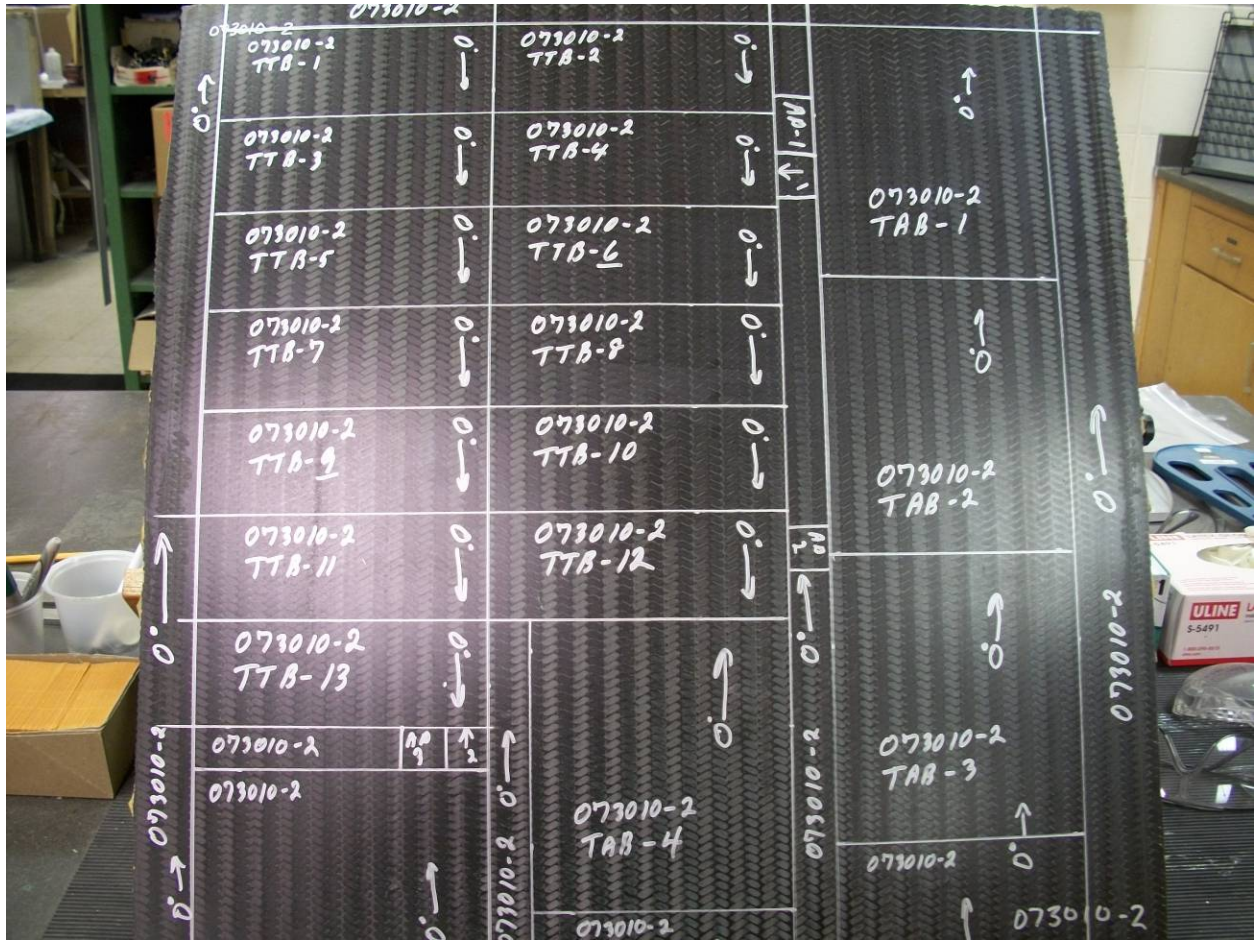
PANEL 072910-2



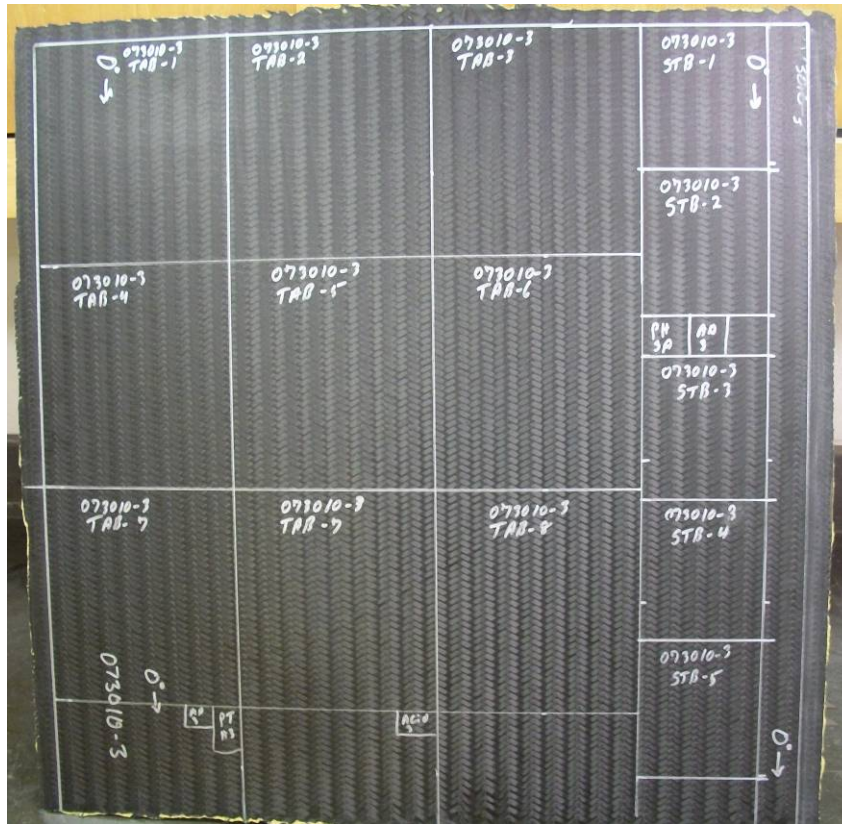
PANEL 073010-1



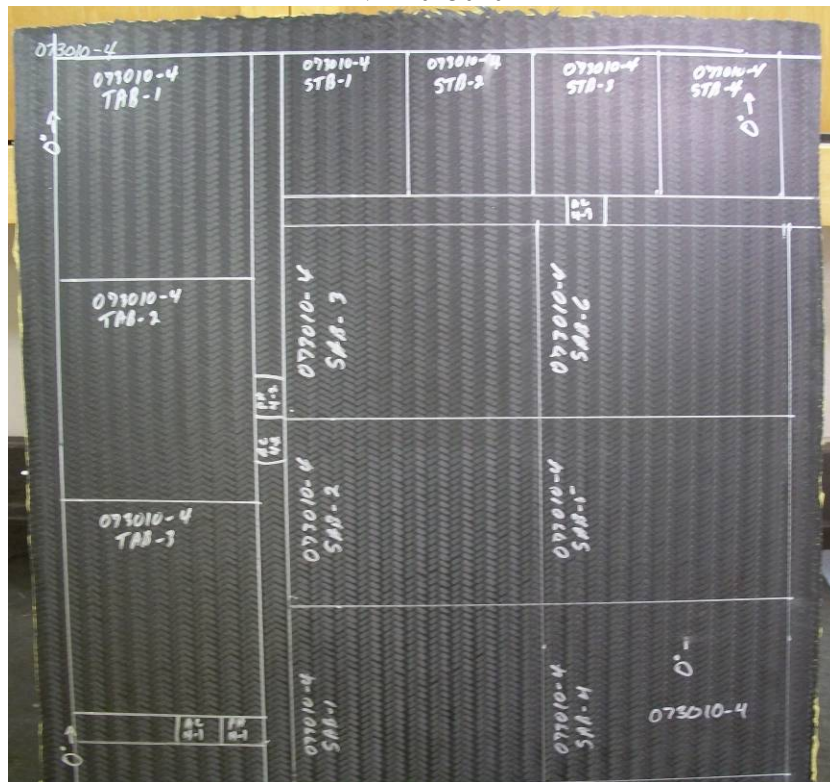
PANEL 073010-2



PANEL 073010-3



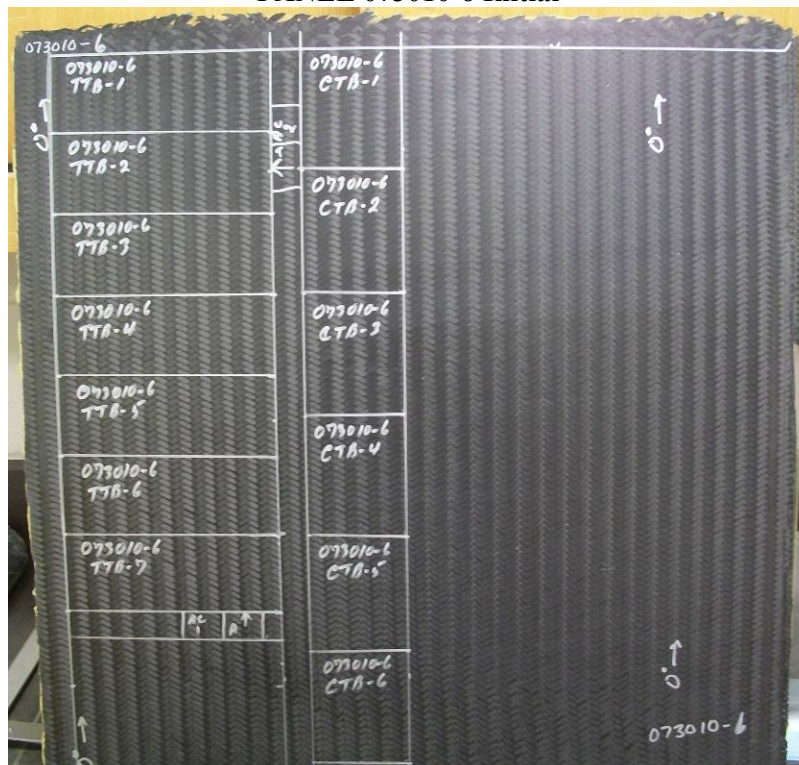
PANEL 073010-4



PANEL 073010-5



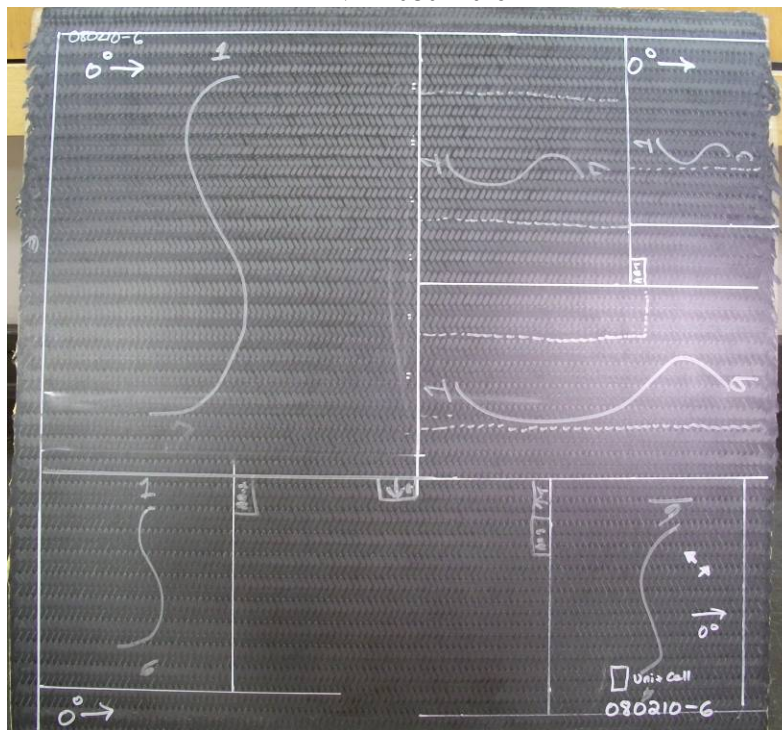
PANEL 073010-6 Initial



PANEL 073010-6 Balance



PANEL 080210-6

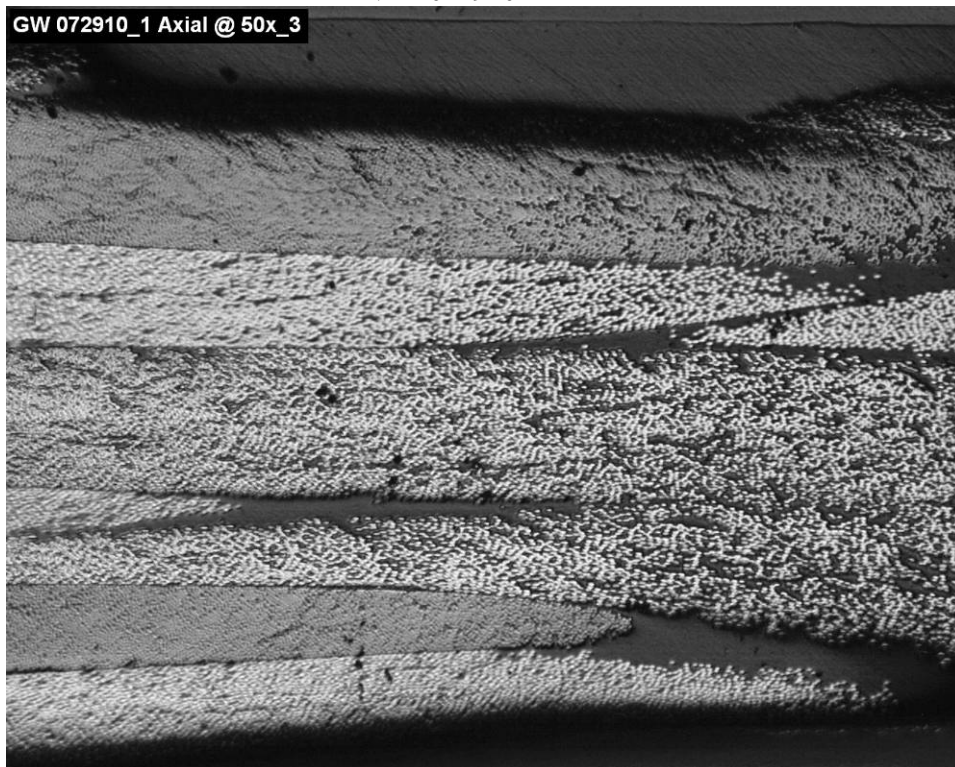


APPENDIX D.

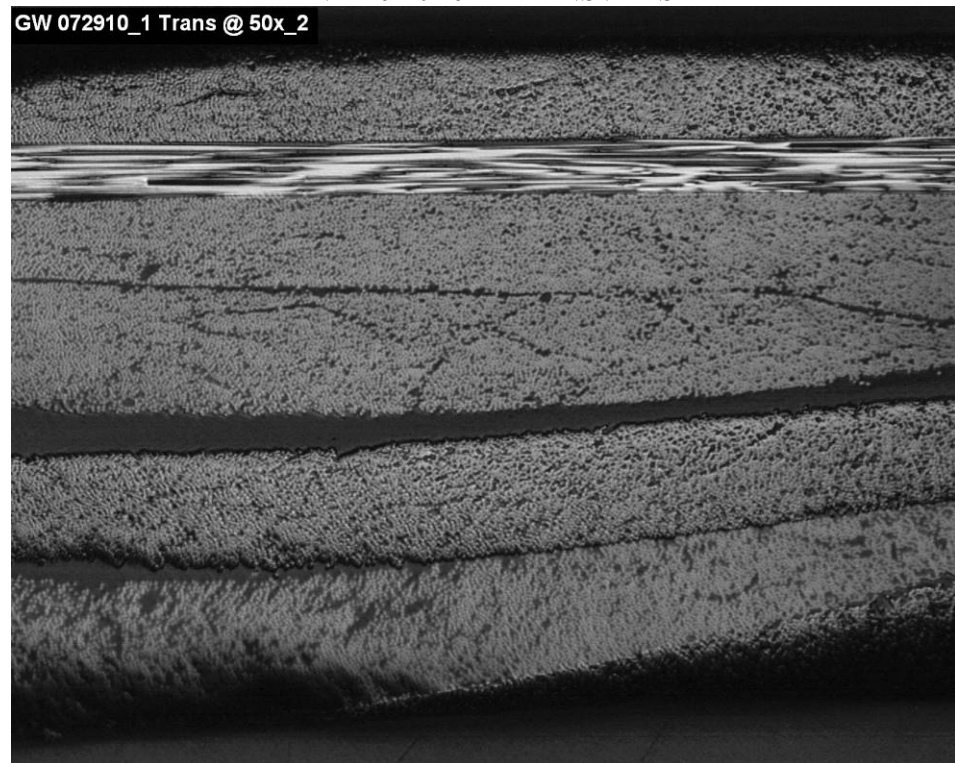
SAMPLE PHOTOMICROGRAPHS OF PANEL CROSS-SECTIONS AT 50X

PHOTOMICROGRAPHS OF TUBE CROSS-SECTIONS AT 25X

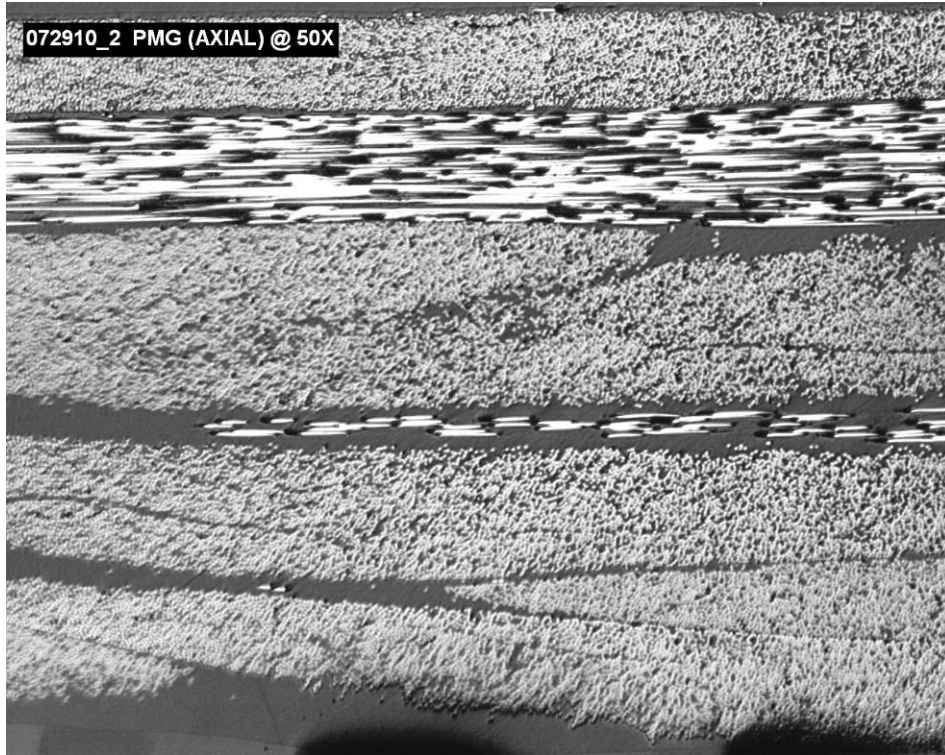
PANEL 072910-1 AXIAL



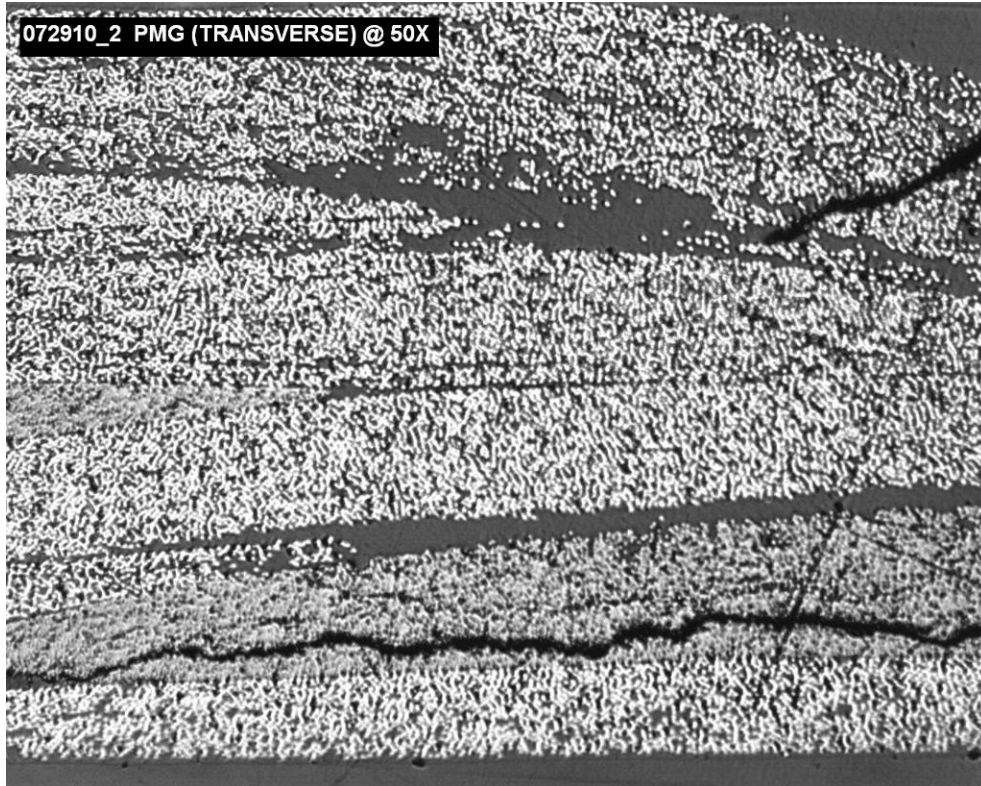
PANEL 072910-1 TRANSVERSE



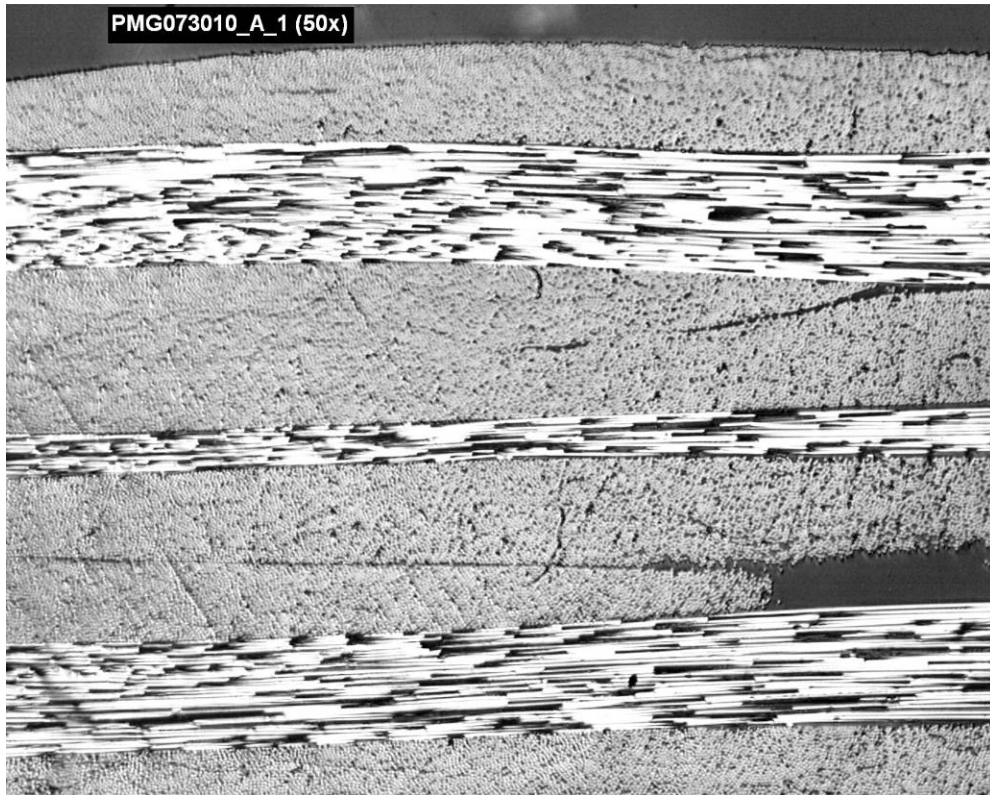
PANEL 072910-2 AXIAL



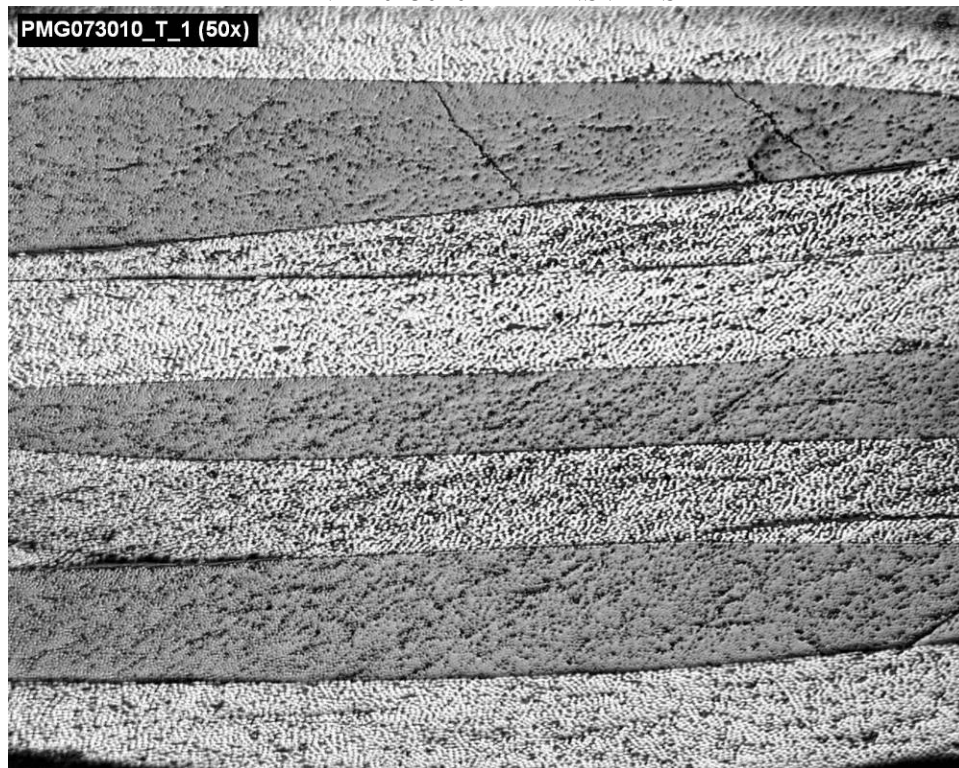
PANEL 072910-2 TRANSVERSE



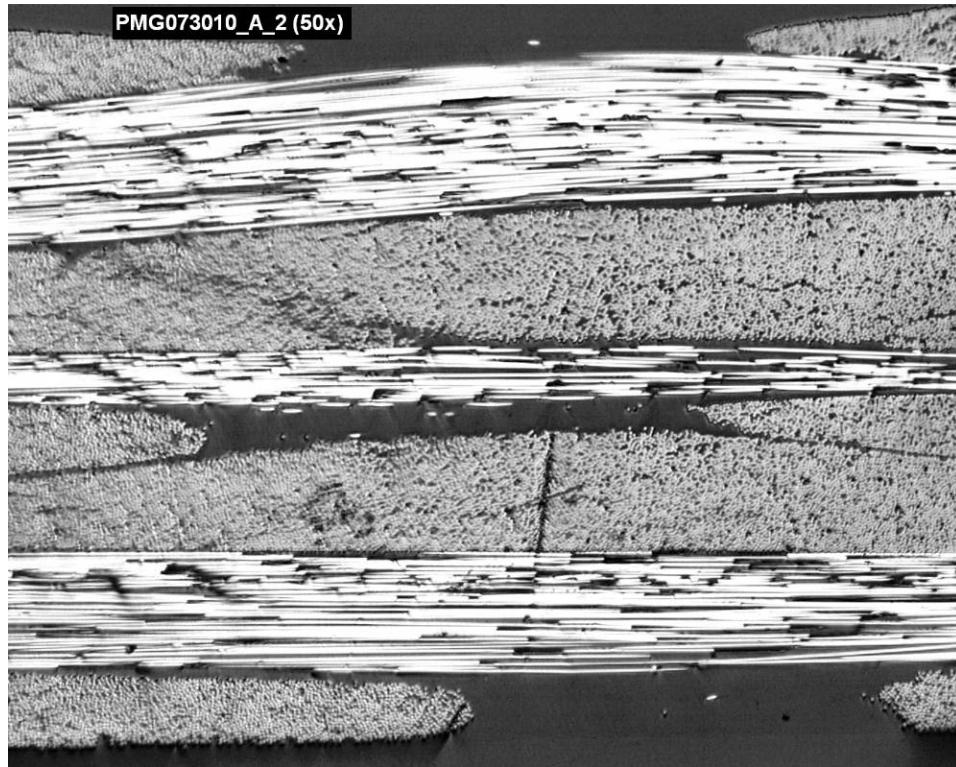
PANEL 073010-1 AXIAL



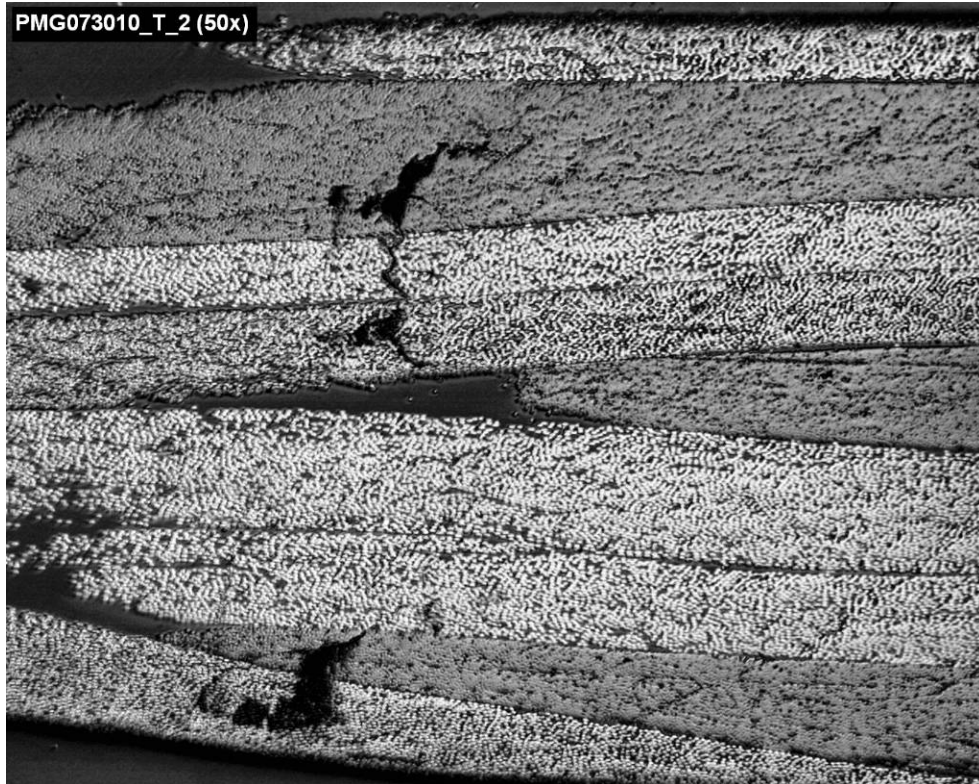
PANEL 073010-1 TRANSVERSE



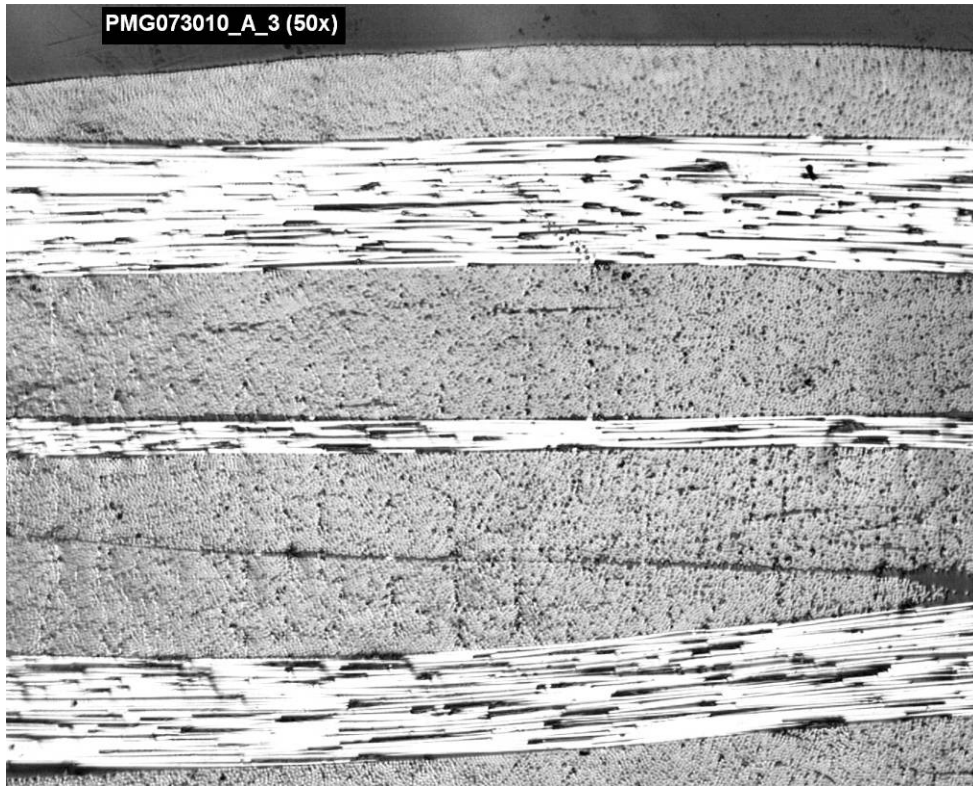
PANEL 073010-2 AXIAL



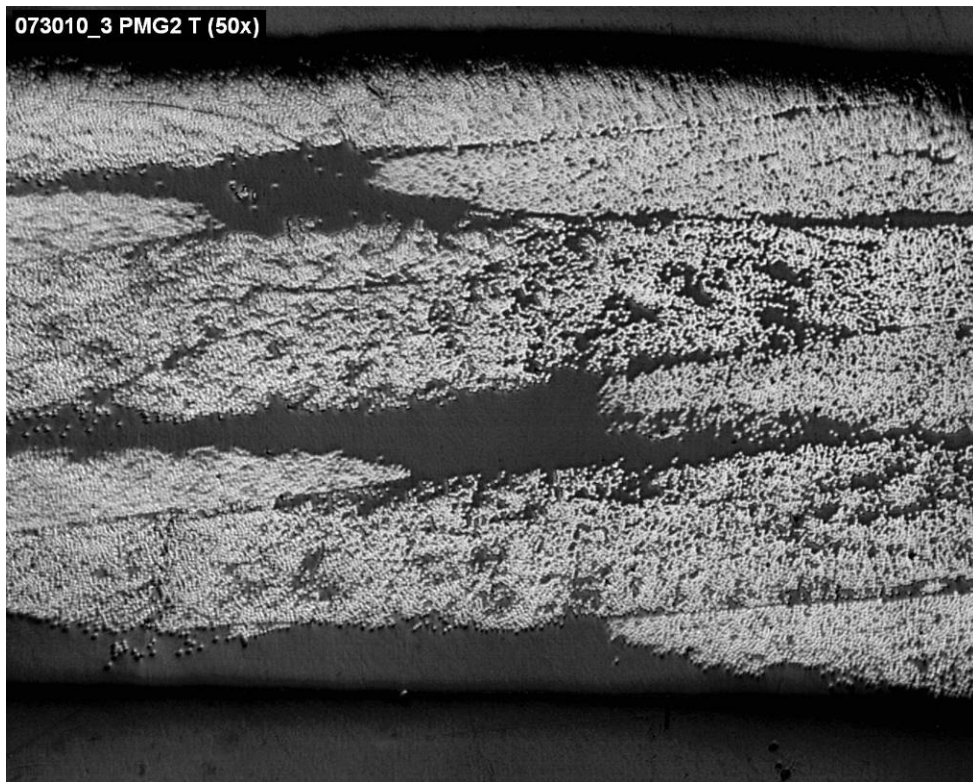
PANEL 073010-2 TRANSVERSE



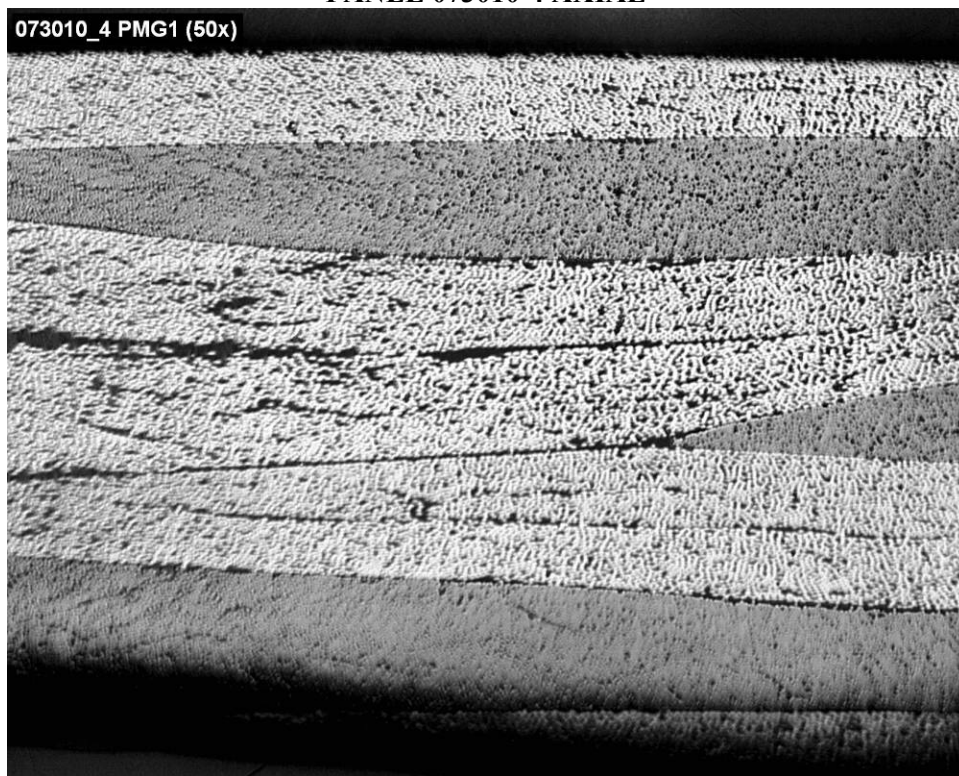
PANEL 073010-3 AXIAL



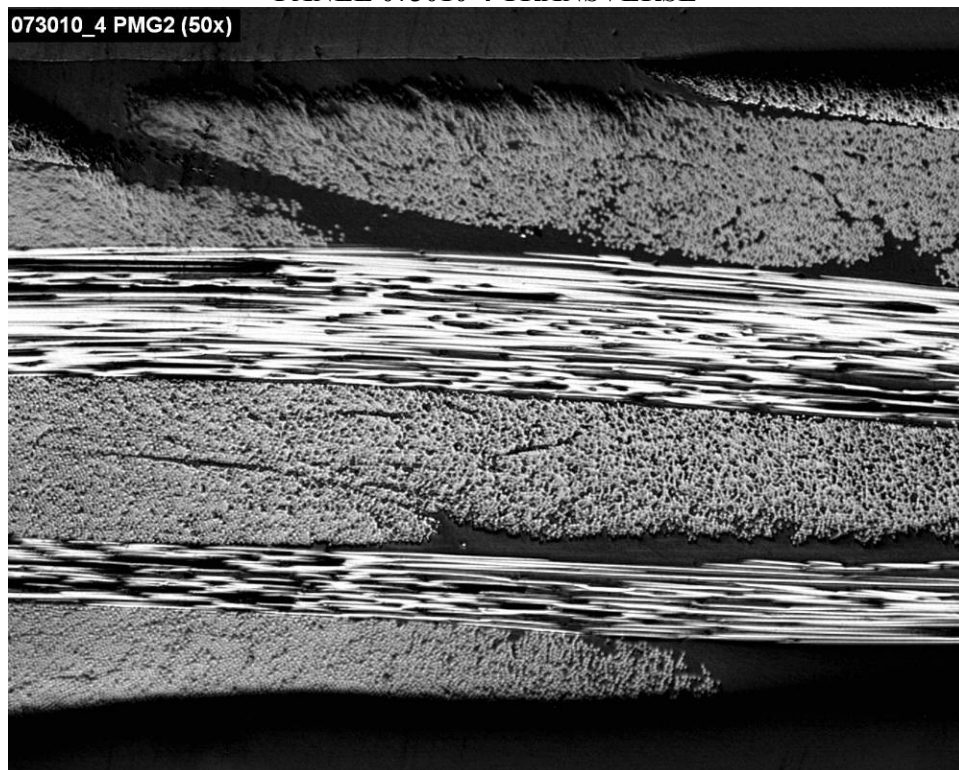
PANEL 073010-3 TRANSVERSE



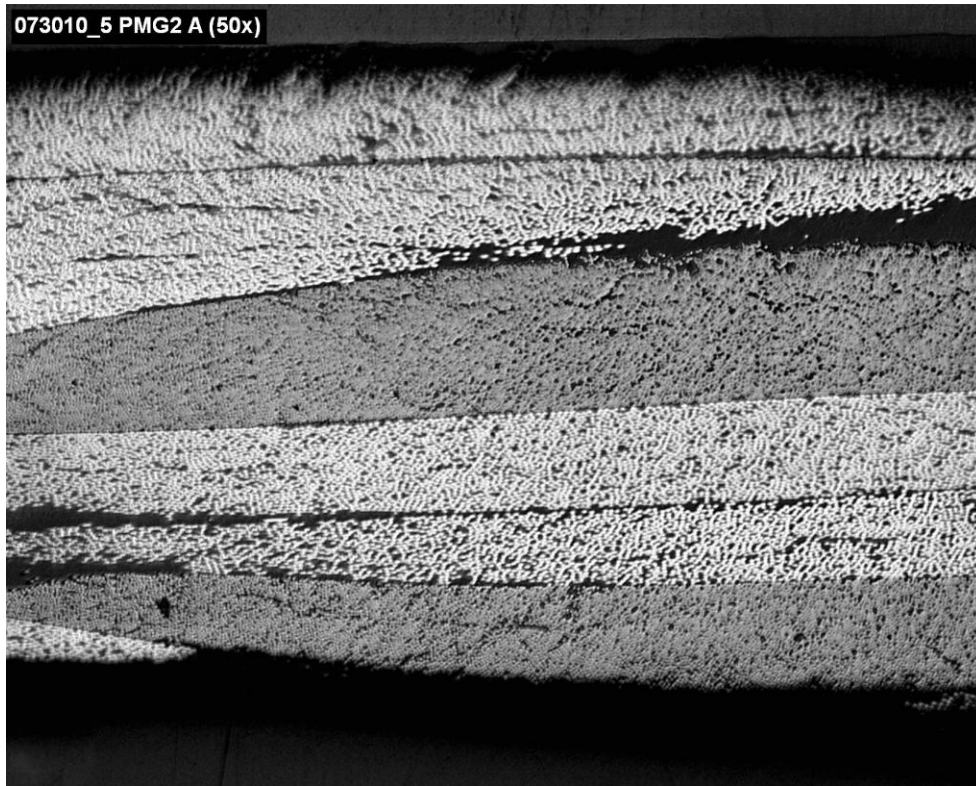
PANEL 073010-4 AXIAL



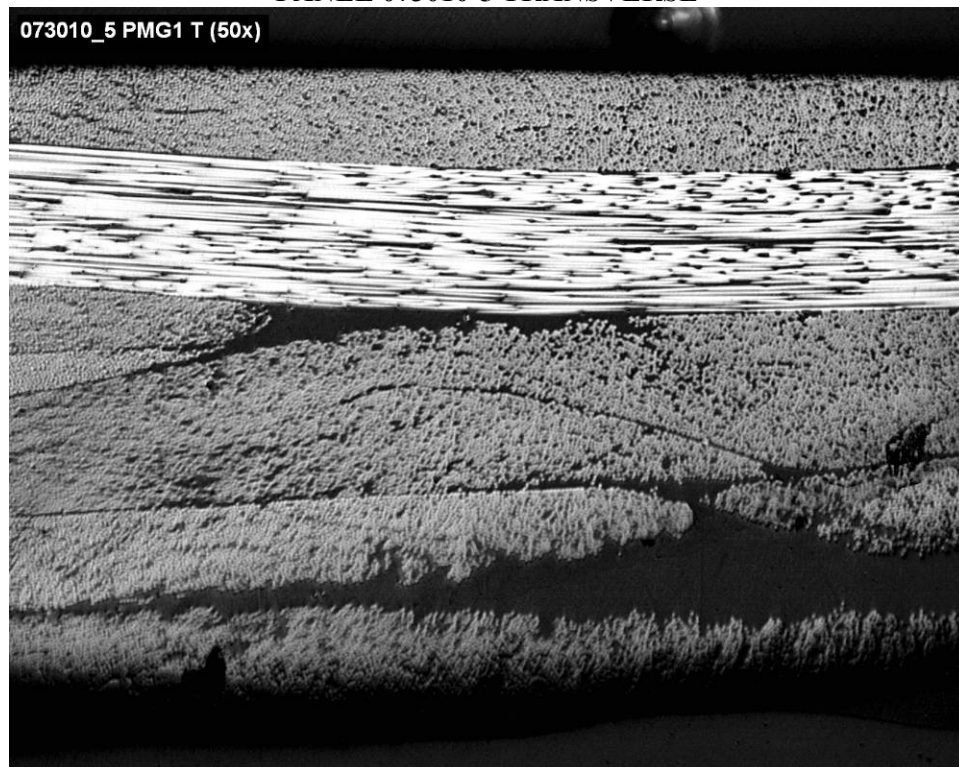
PANEL 073010-4 TRANSVERSE



PANEL 073010-5 AXIAL



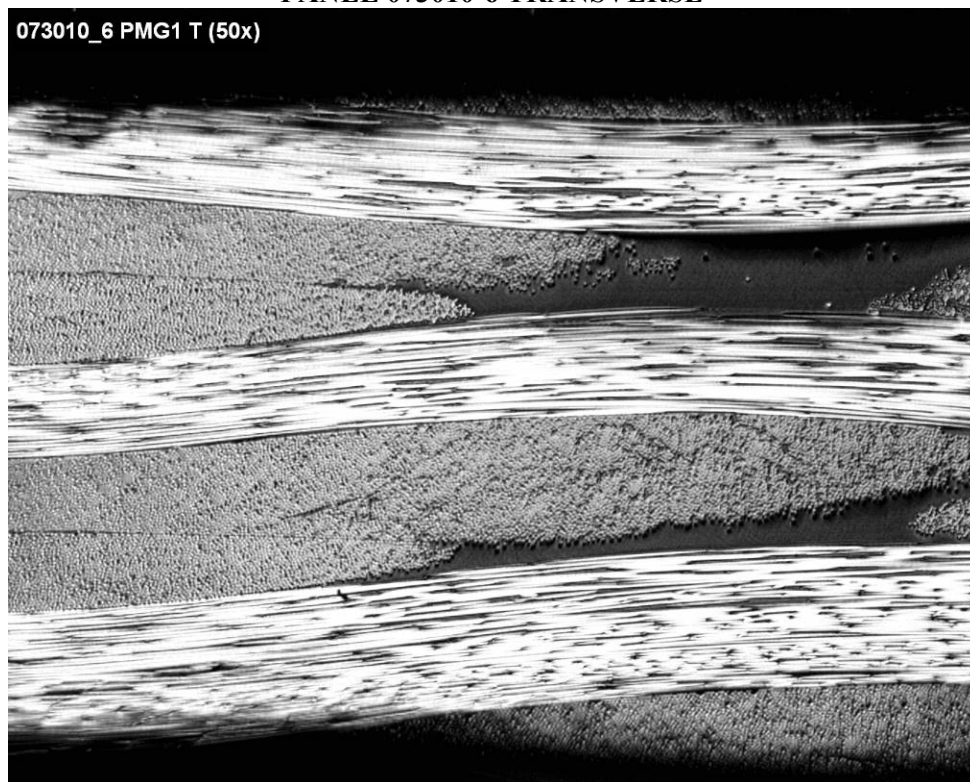
PANEL 073010-5 TRANSVERSE



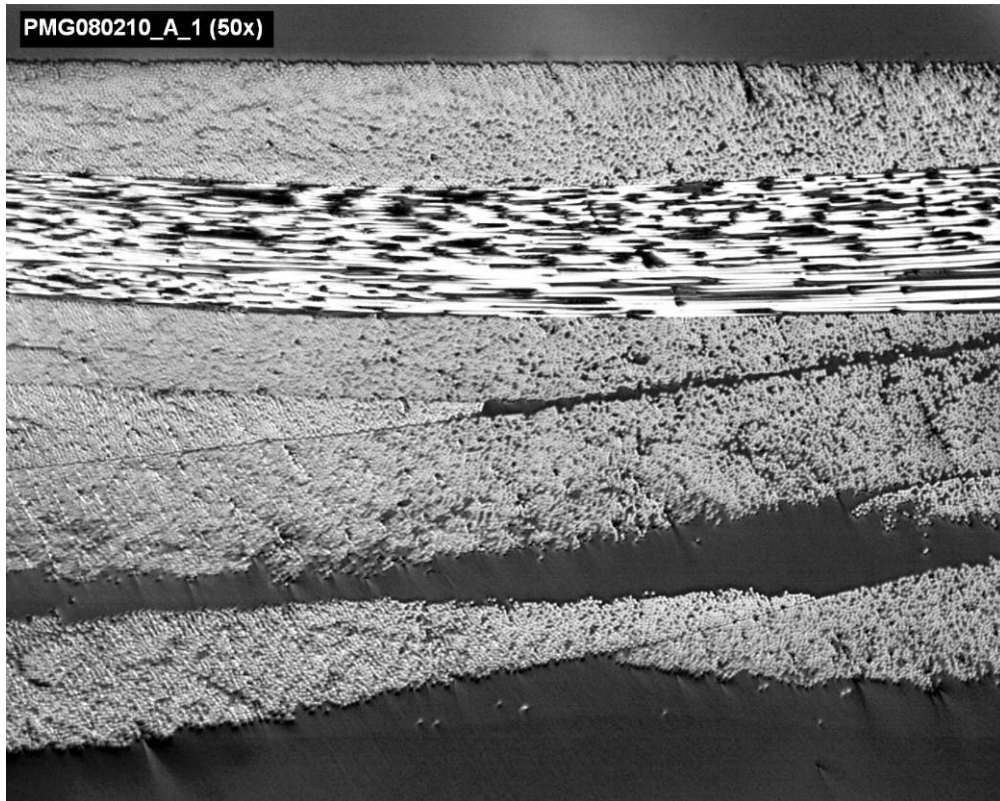
PANEL 073010-6 AXIAL



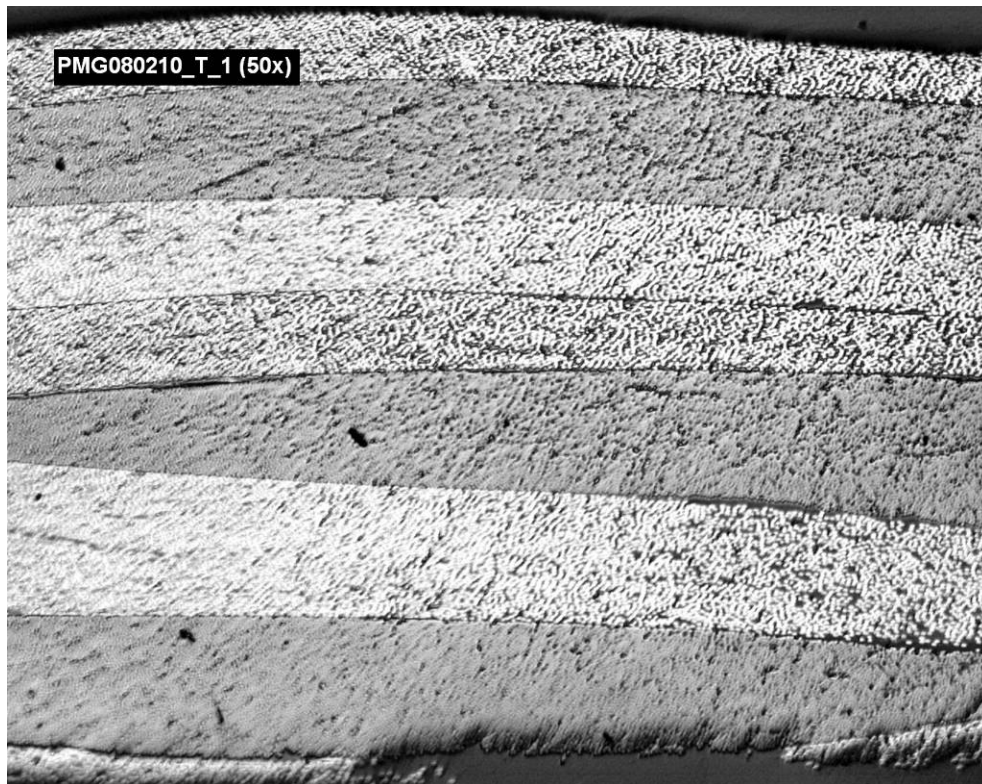
PANEL 073010-6 TRANSVERSE



PANEL 080210-6 AXIAL

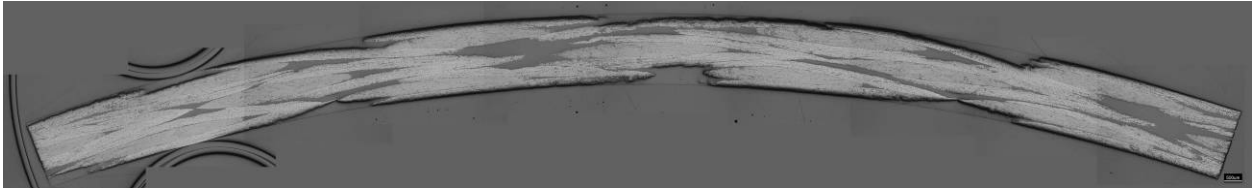


PANEL 080210-6 TRANSVERSE

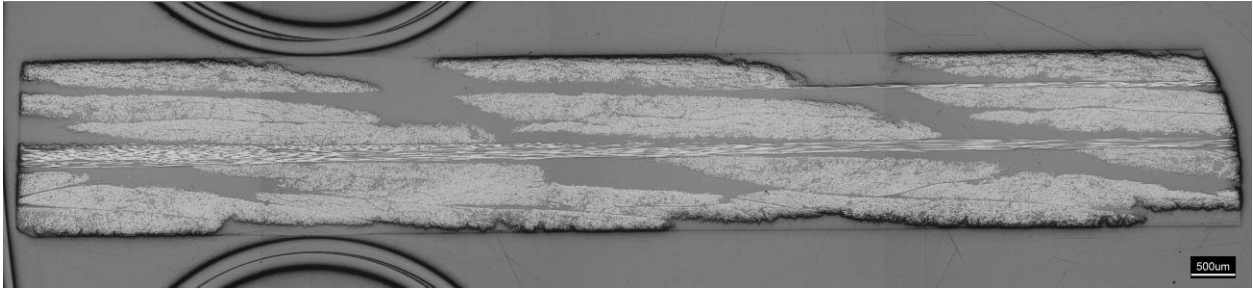


TUBE CROSS-SECTIONS AT 25X

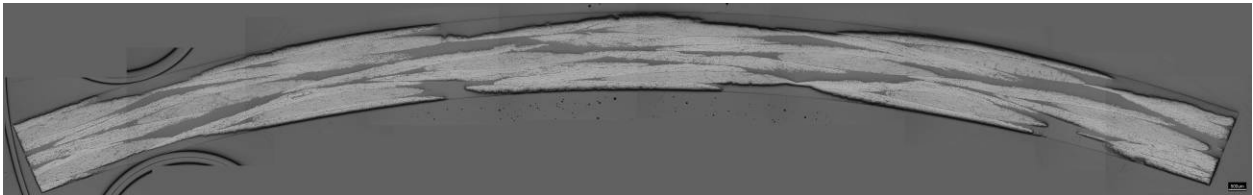
STL103-1 AXIAL



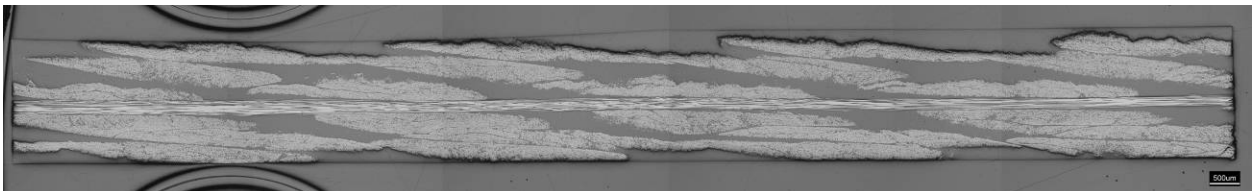
STL103-1 TRANSVERSE



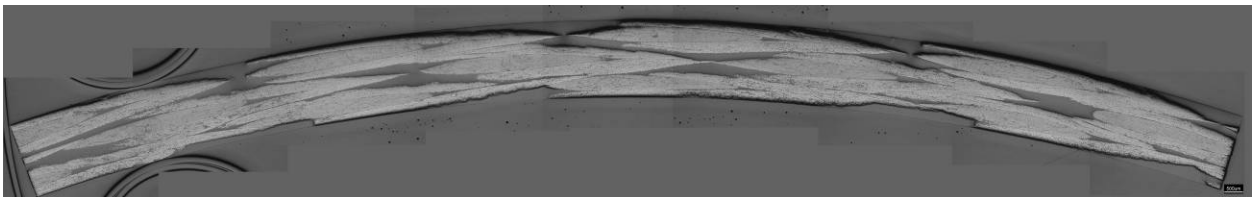
STL103-2 AXIAL



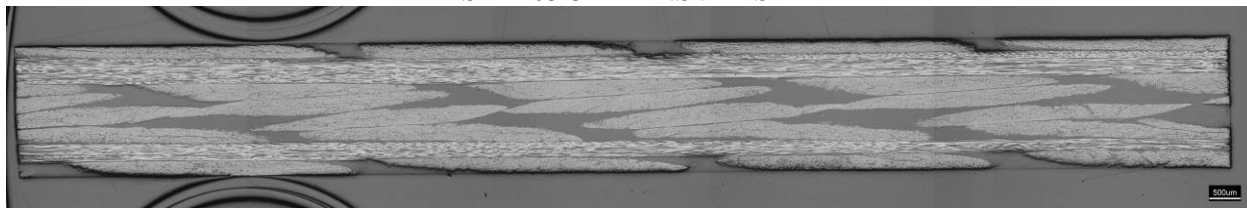
STL103-2 TRANSVERSE



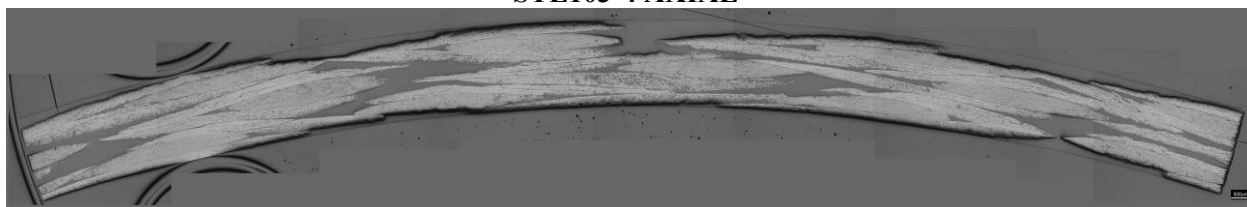
STL103-3 AXIAL



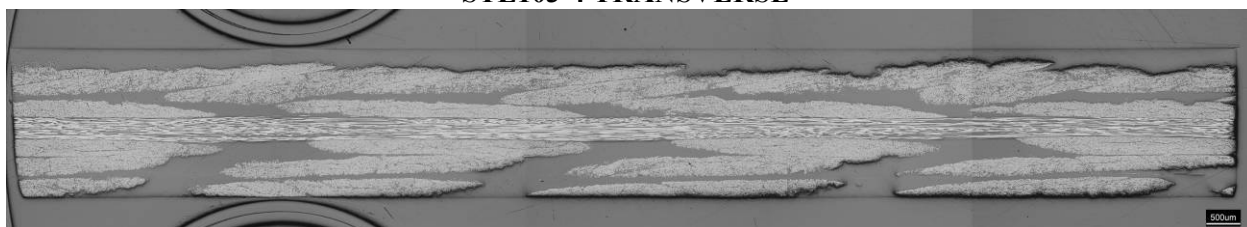
STL103-3 TRANSVERSE



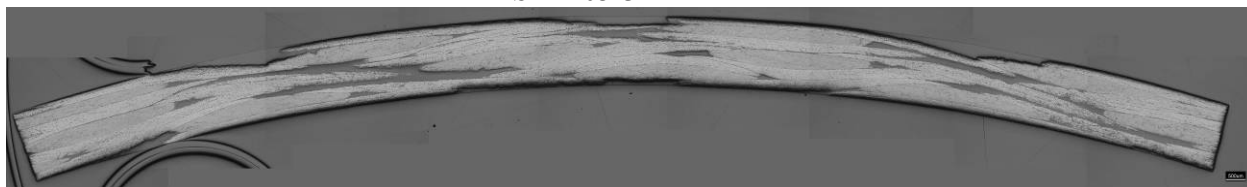
STL103-4 AXIAL



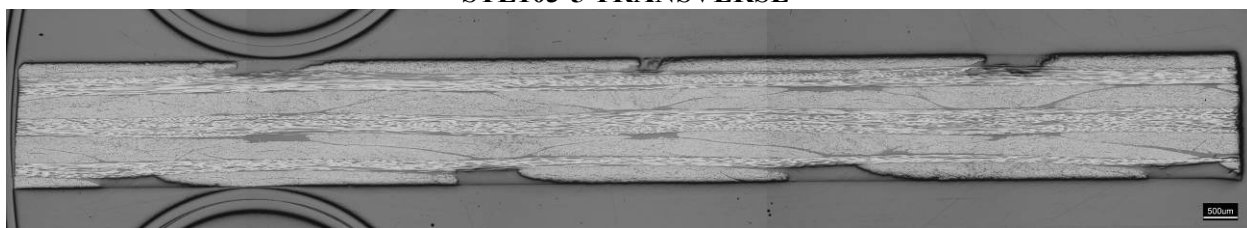
STL103-4 TRANSVERSE



STL103-5 AXIAL



STL103-5 TRANSVERSE



APPENDIX E.
UNIT CELL MEASUREMENTS AND LOCATIONS

Investigation of Opportunities For Light-Weighting Vehicles Using Advanced Plastics And Composites

Notes: All measurements in units of millimeters; sub 1 is left most or top most as image is oriented, sub 2 is right most or lowest measurement as image is oriented.

Sub panel # is completely arbitrary and relates to separate pieces from same panel ID; number corresponds to sequence in which it was imaged.

Panel ID

072910-1 Sub panel#

1				2				3			
H ₁	H ₂	W ₁	W ₂	H ₁	H ₂	W ₁	W ₂	H ₁	H ₂	W ₁	W ₂
5.4	5.1	18.1	18.2	5.1	5.2	17.9	18.4	5.4	5.5	18.3	18.7

073010-1 Sub panel#

1				2				3			
H ₁	H ₂	W ₁	W ₂	H ₁	H ₂	W ₁	W ₂	H ₁	H ₂	W ₁	W ₂
5.3	5.0	17.0	17.7	5.3	5.4	18.4	18.0	4.9	5.5	16.6	16.7

073010-1 Sub panel#

1				2			
H ₁	H ₂	W ₁	W ₂	H ₁	H ₂	W ₁	W ₂
5.3	5.3	17.1	17.5	5.4	5.3	18.4	18.5

073010-2 Sub panel#

1			
H ₁	H ₂	W ₁	W ₂
5.3	5.5	18.3	18.2

073010-2 Sub panel#

1			
H ₁	H ₂	W ₁	W ₂
5.0	5.1	18.0	18.2

073010-2 Sub panel#

1			
H ₁	H ₂	W ₁	W ₂
4.9	5.6	17.1	17.6

073010-3 Sub panel#

1				2			
H ₁	H ₂	W ₁	W ₂	H ₁	H ₂	W ₁	W ₂
5.0	5.3	17.3	17.4	5.3	5.2	18.4	18.5

073010-3 Sub panel#

1				2			
H ₁	H ₂	W ₁	W ₂	H ₁	H ₂	W ₁	W ₂
5.3	6.0	18.2	18.1	5.1	5.6	17.9	17.9

073010-4 Sub panel#

1				2			
H ₁	H ₂	W ₁	W ₂	H ₁	H ₂	W ₁	W ₂
5.3	5.0	18.3	18.3	5.2	5.4	17.5	17.6

073010-4 Sub panel#

1				2			
H ₁	H ₂	W ₁	W ₂	H ₁	H ₂	W ₁	W ₂
5.1	5.2	18.2	17.7	4.9	5.1	17.5	17.3

073010-5 Sub panel#

1				2			
H ₁	H ₂	W ₁	W ₂	H ₁	H ₂	W ₁	W ₂
4.8	5.3	17.7	18.3	5.4	5.1	18.2	18.8

073010-5 Sub panel#

3				4			
H ₁	H ₂	W ₁	W ₂	H ₁	H ₂	W ₁	W ₂
5.0	5.3	18.6	18.4	5.0	5.3	18.4	17.4

073010-6 Sub panel#

1				2				3			
H ₁	H ₂	W ₁	W ₂	H ₁	H ₂	W ₁	W ₂	H ₁	H ₂	W ₁	W ₂
5.5	5.4	16.9	17.5	5.5	5.4	18.4	18.7	5.4	5.5	18.5	17.9

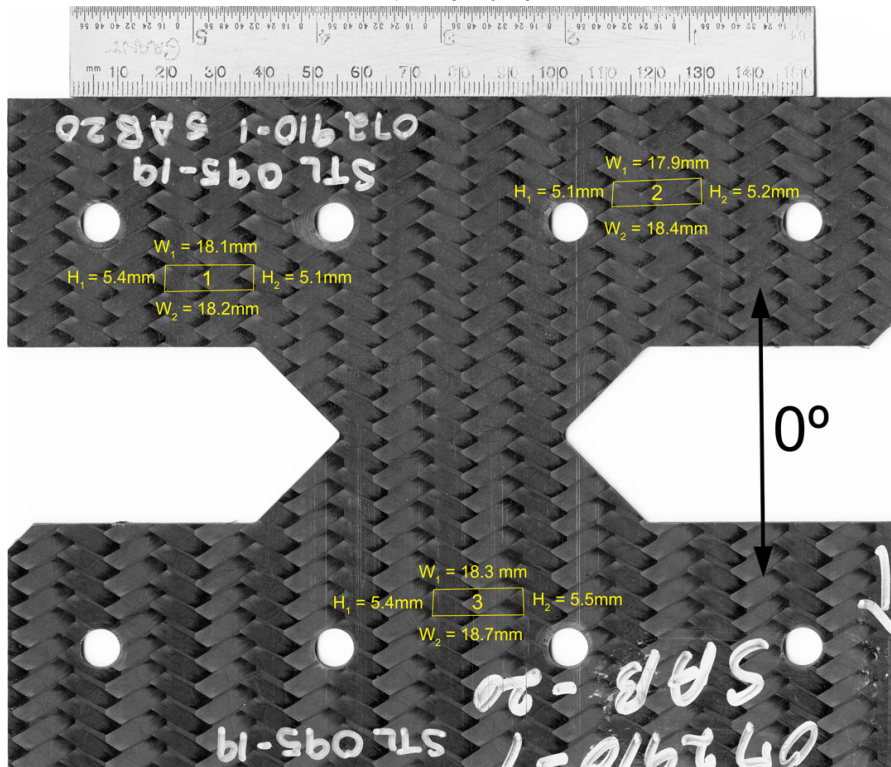
073010-6 Sub panel#

1				2			
H ₁	H ₂	W ₁	W ₂	H ₁	H ₂	W ₁	W ₂
5.1	5.3	17.7	17.6	5.4	5.3	17.2	17.3

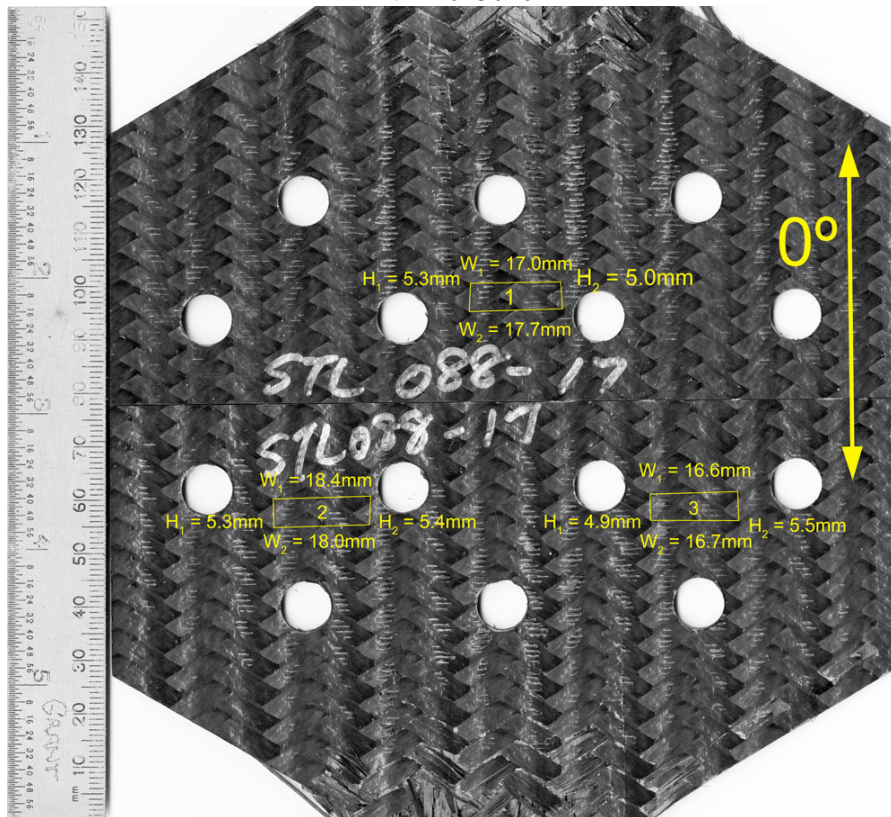
080210-6 Sub panel#

1				2				3			
H ₁	H ₂	W ₁	W ₂	H ₁	H ₂	W ₁	W ₂	H ₁	H ₂	W ₁	W ₂
4.9	5.0	17.5	18.4	4.8	5.0	18.2	18.2	5.4	5.3	18.0	18.3

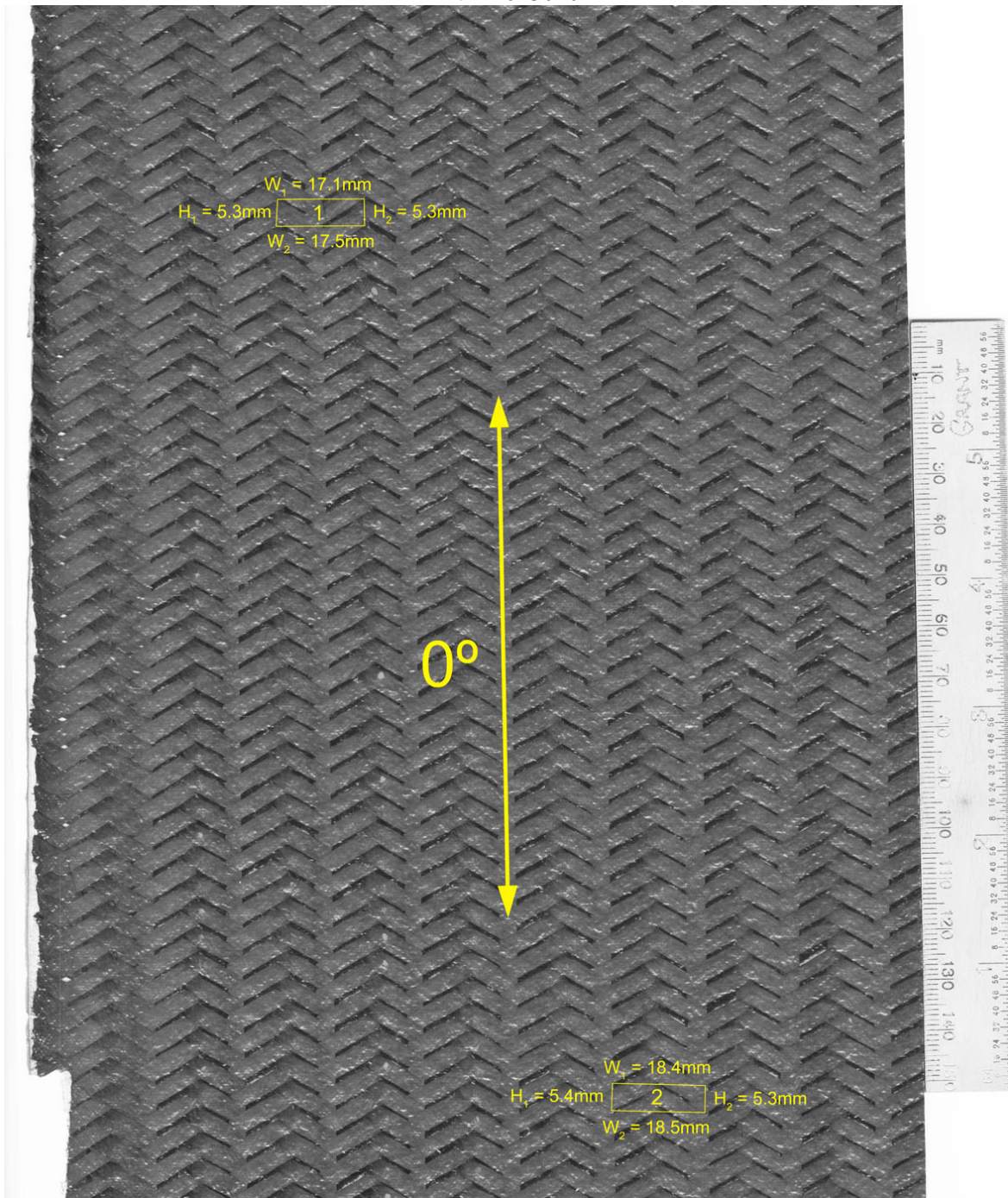
PANEL 072910-1

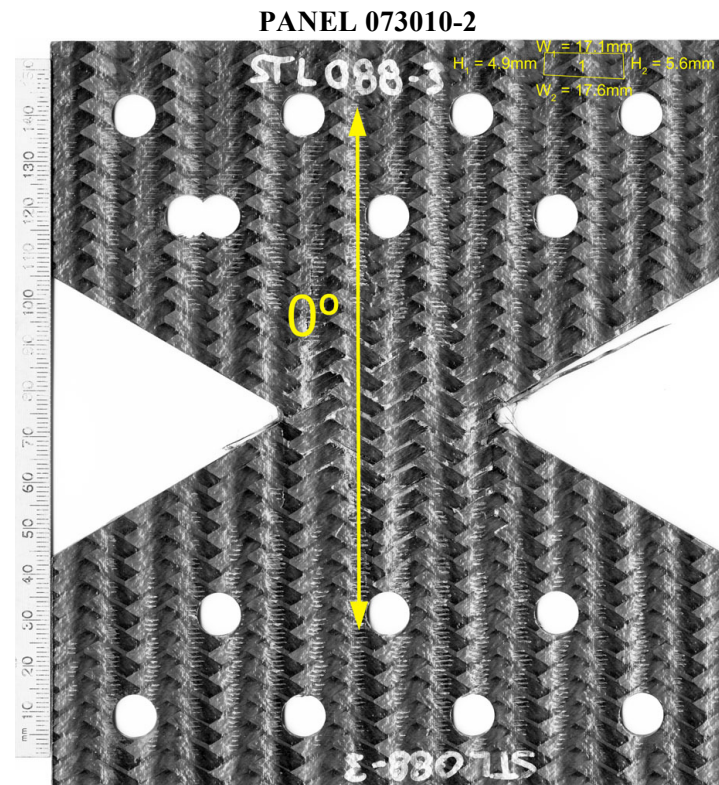
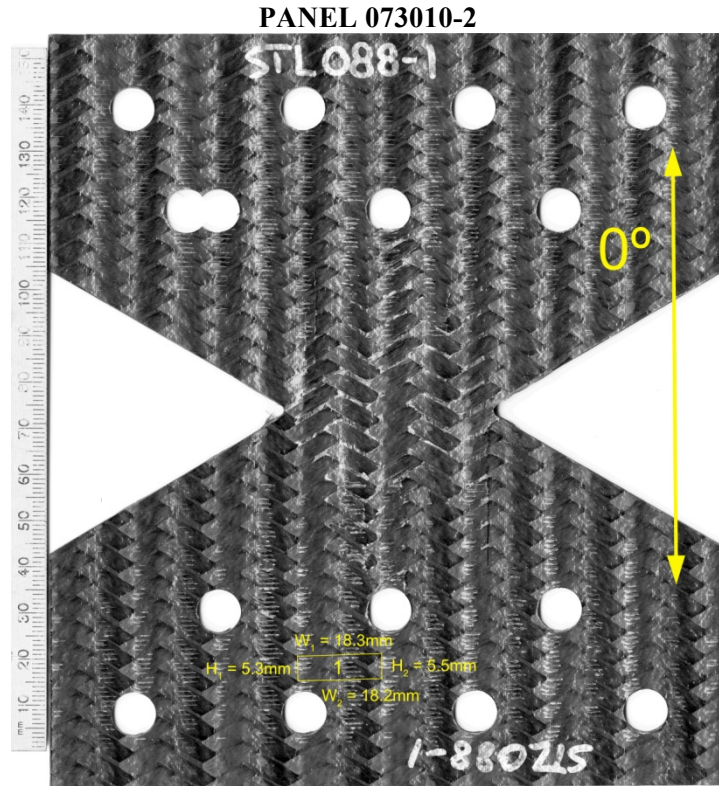


PANEL 073010-1

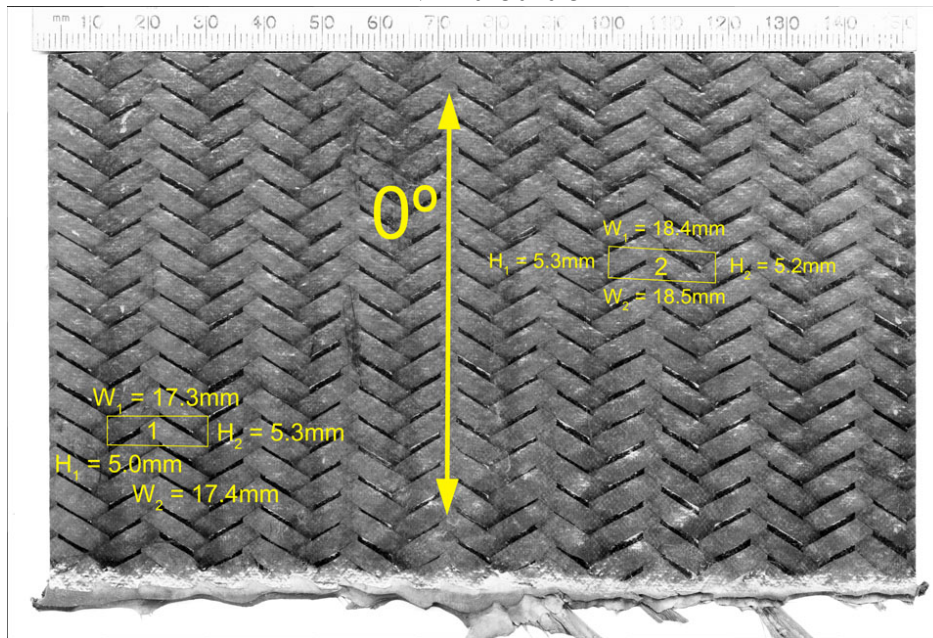


PANEL 073010-1

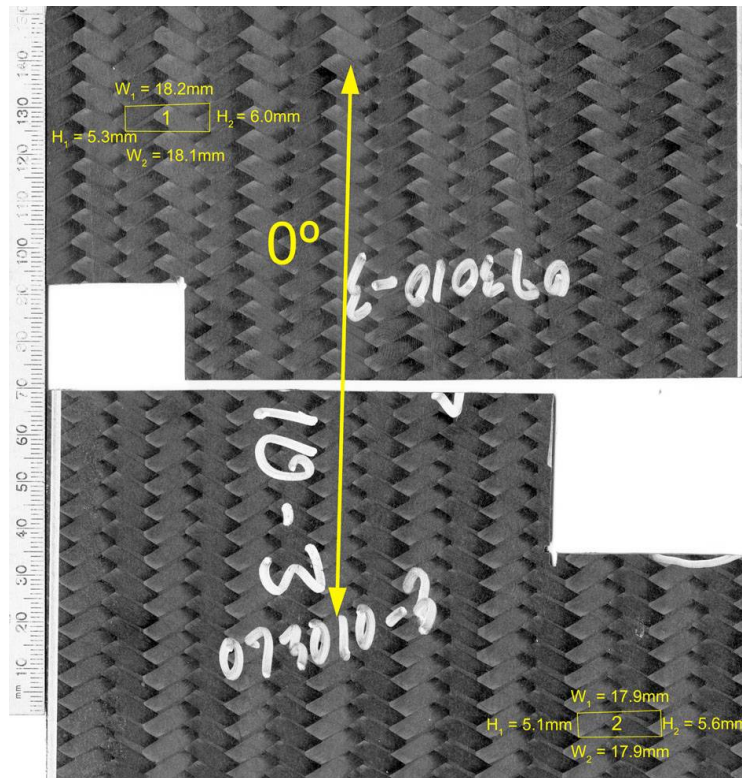




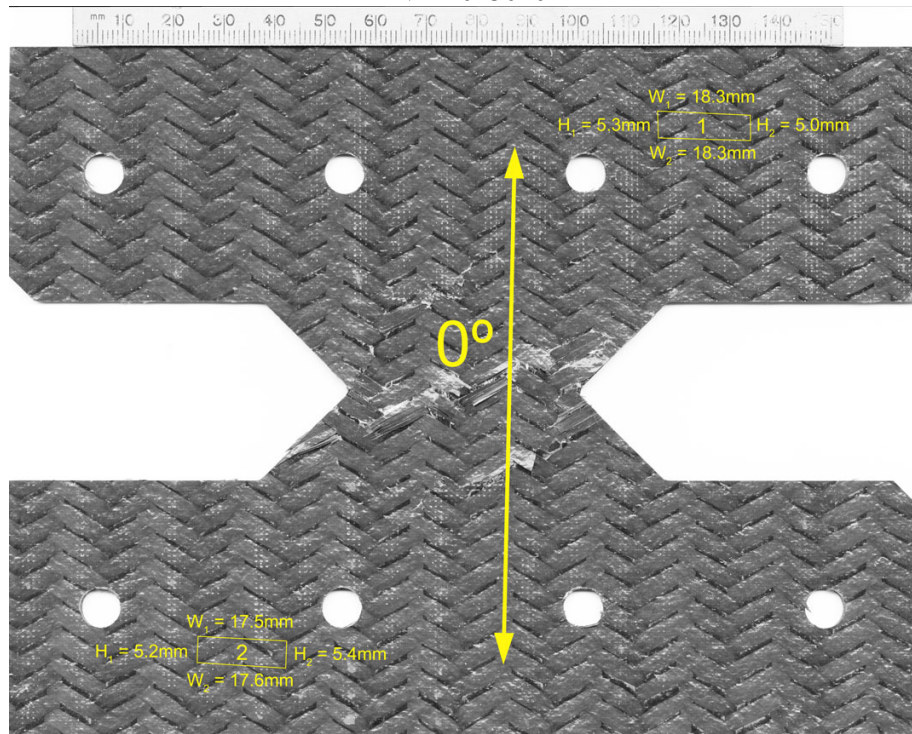
PANEL 073010-3



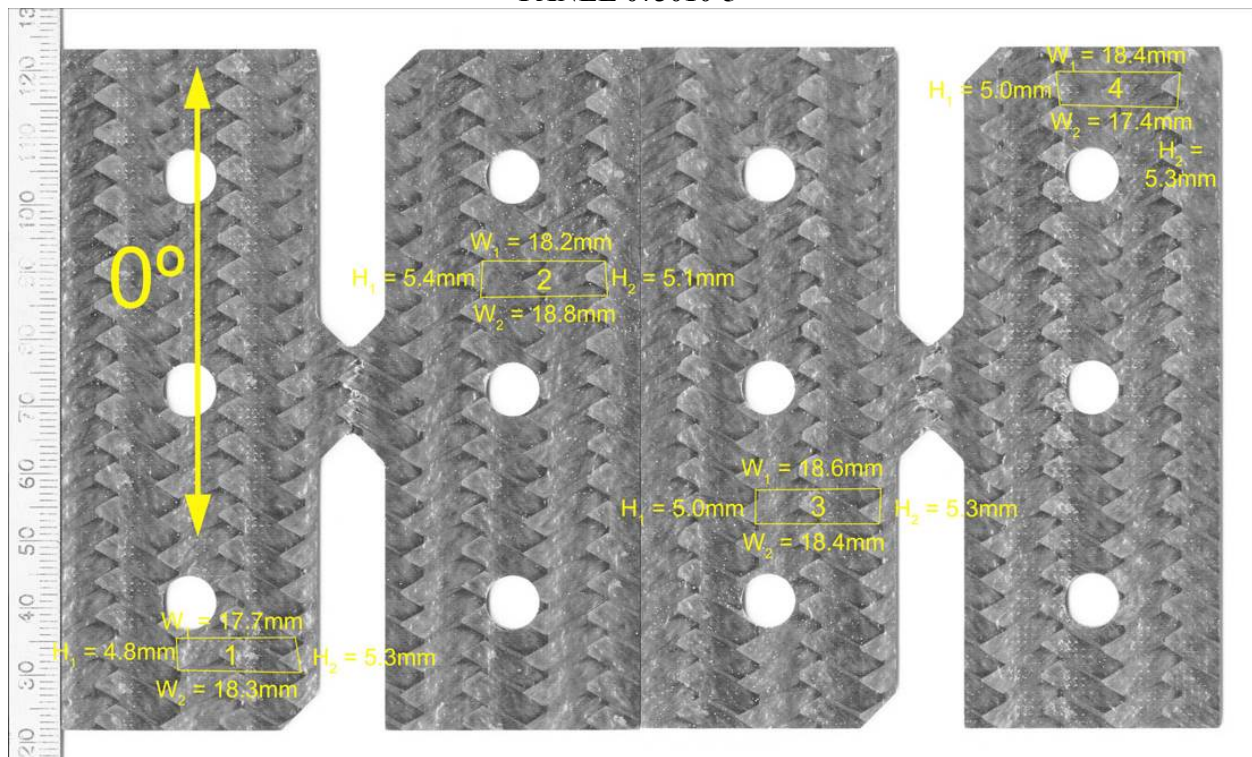
PANEL 073010-3



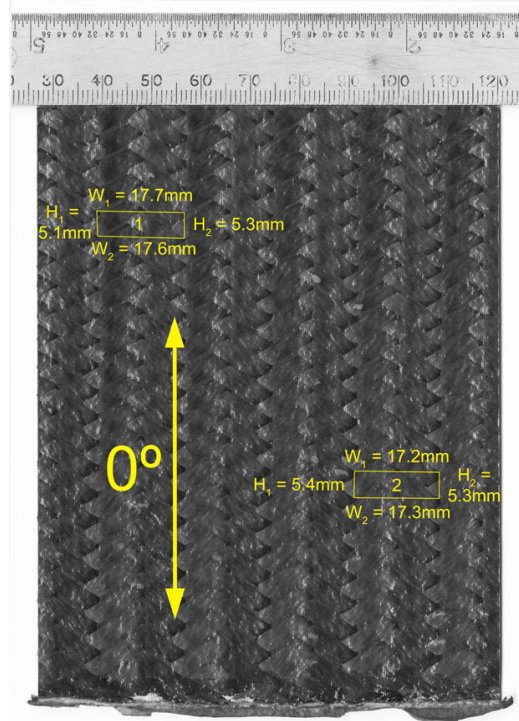
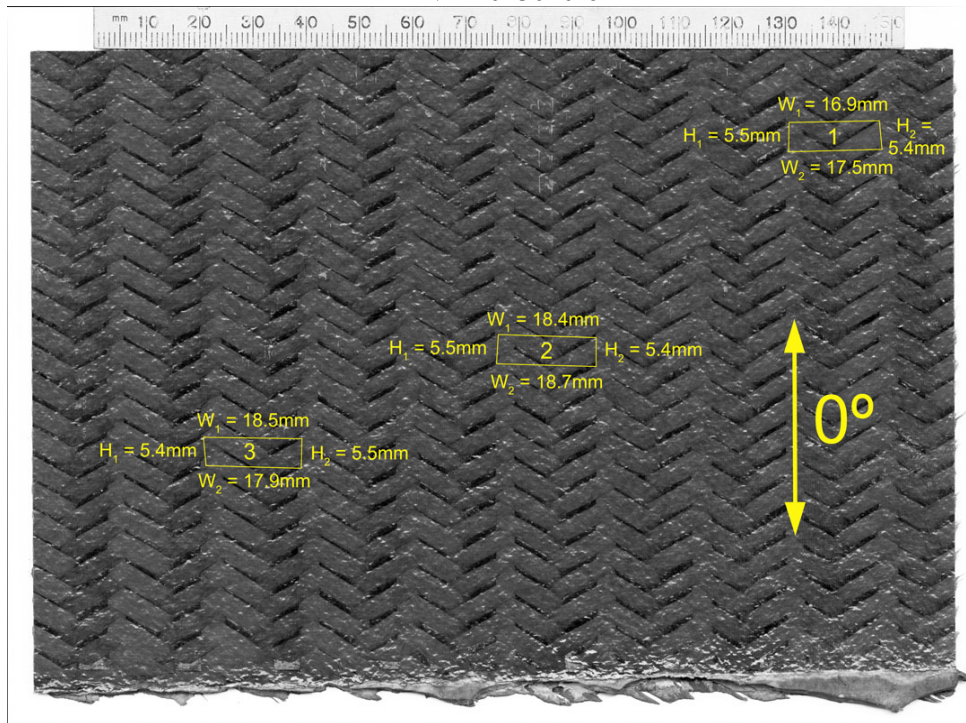
PANEL 073010-4



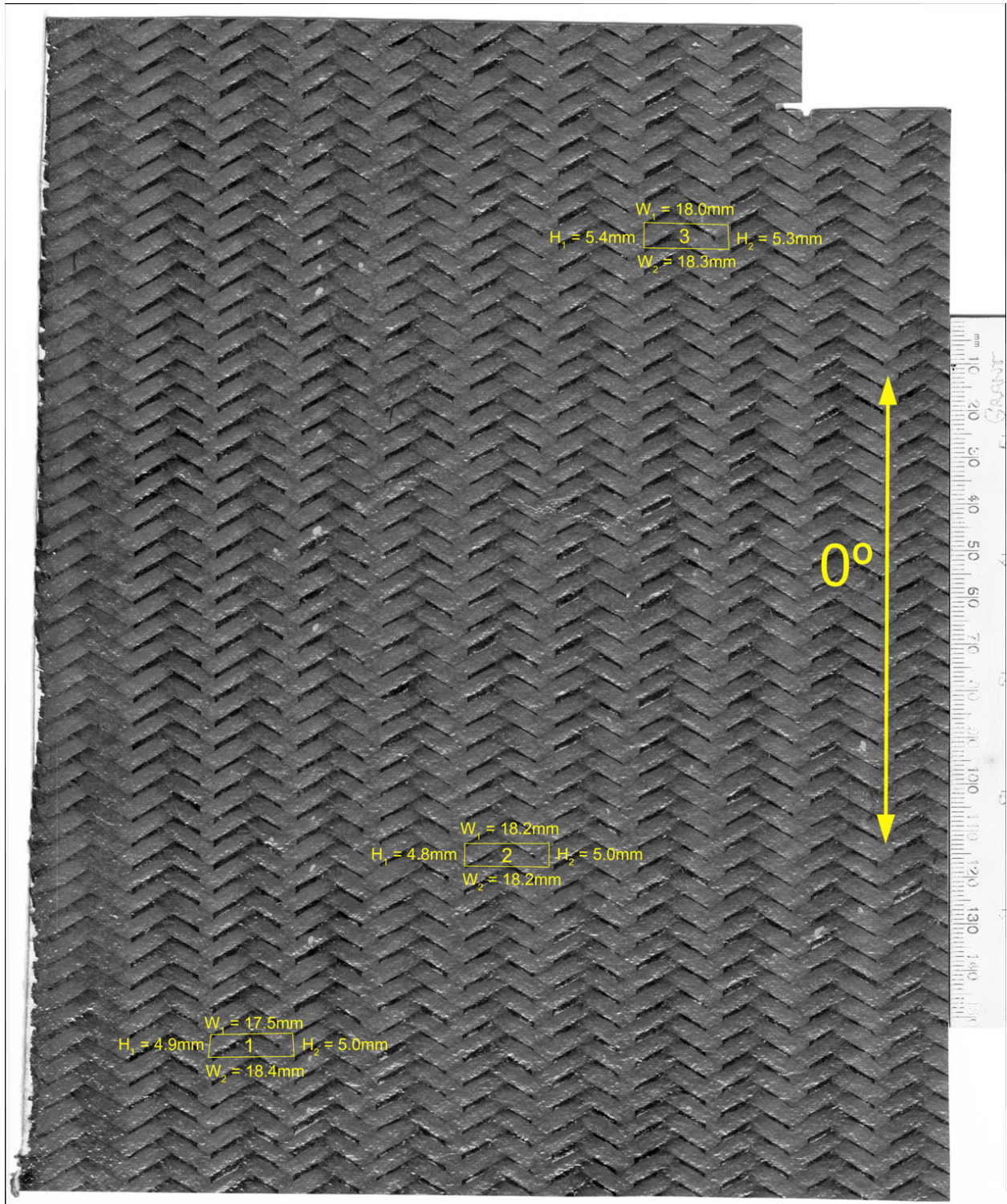
PANEL 073010-5



PANEL 073010-6

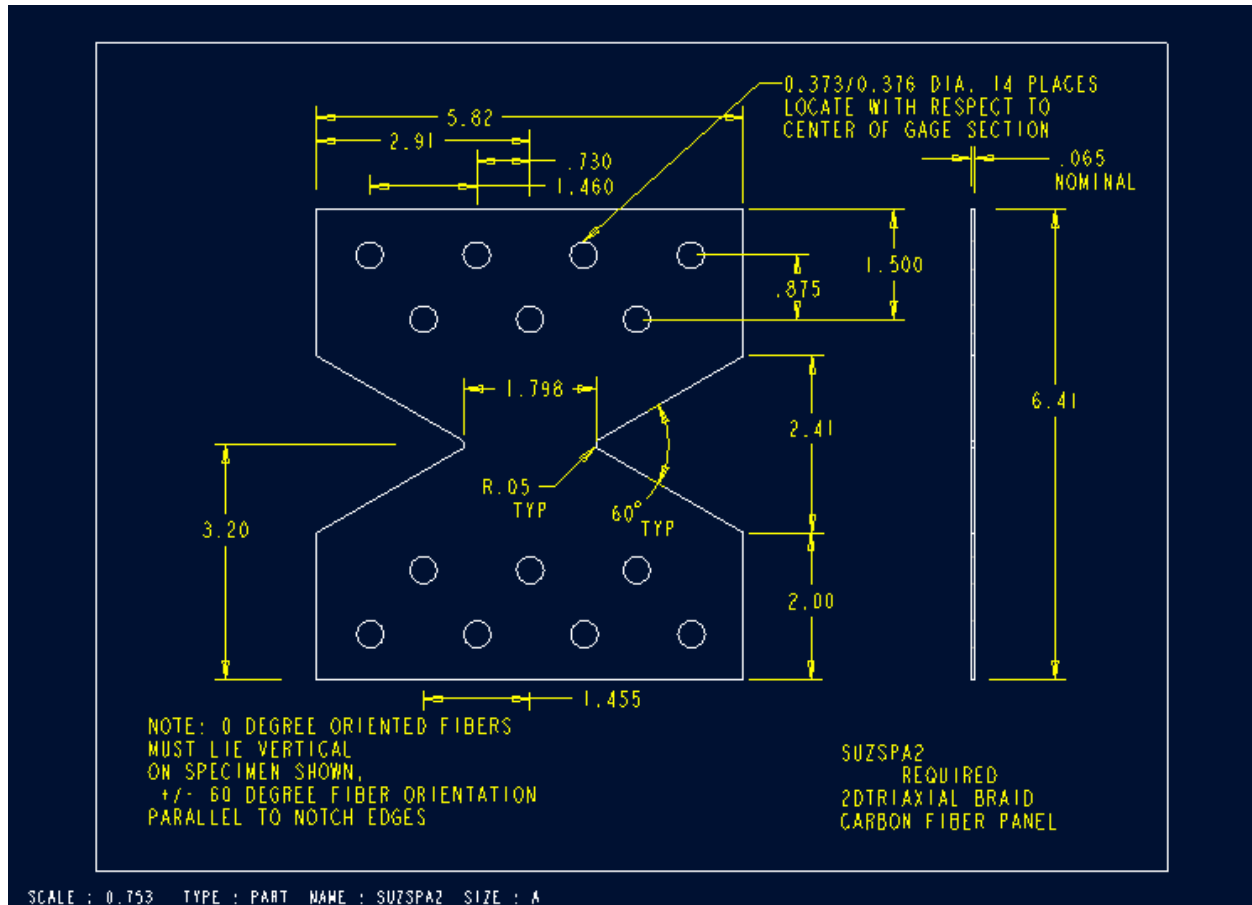


PANEL 080210-6

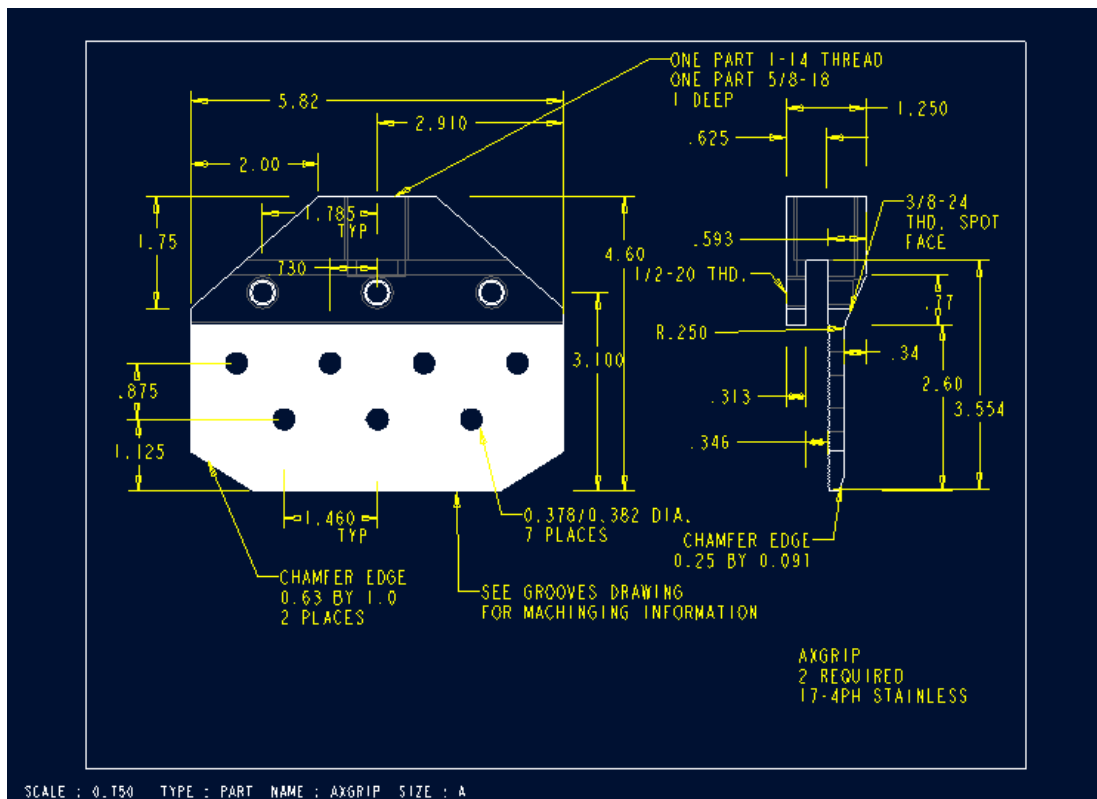
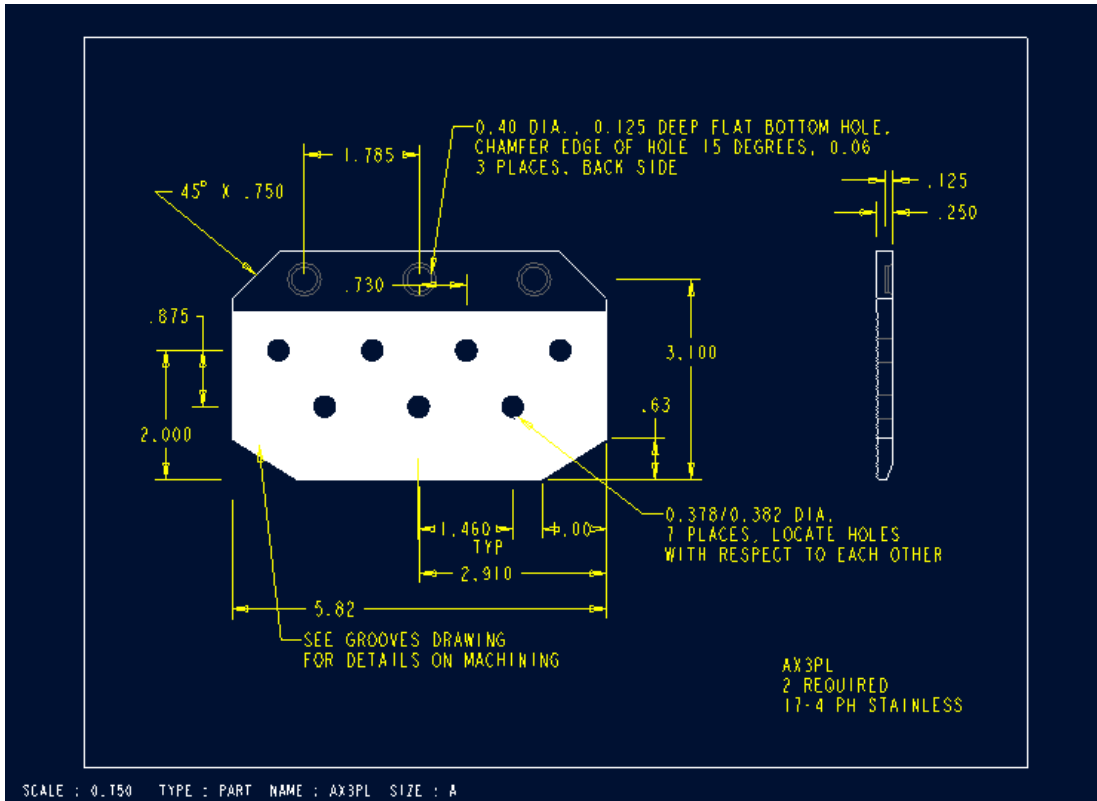


APPENDIX F.
BOWTIE TENSILE SPECIMENS AND FIXTURE DRAWINGS

BOWTIE AXIAL TENSION SPECIMEN
British units

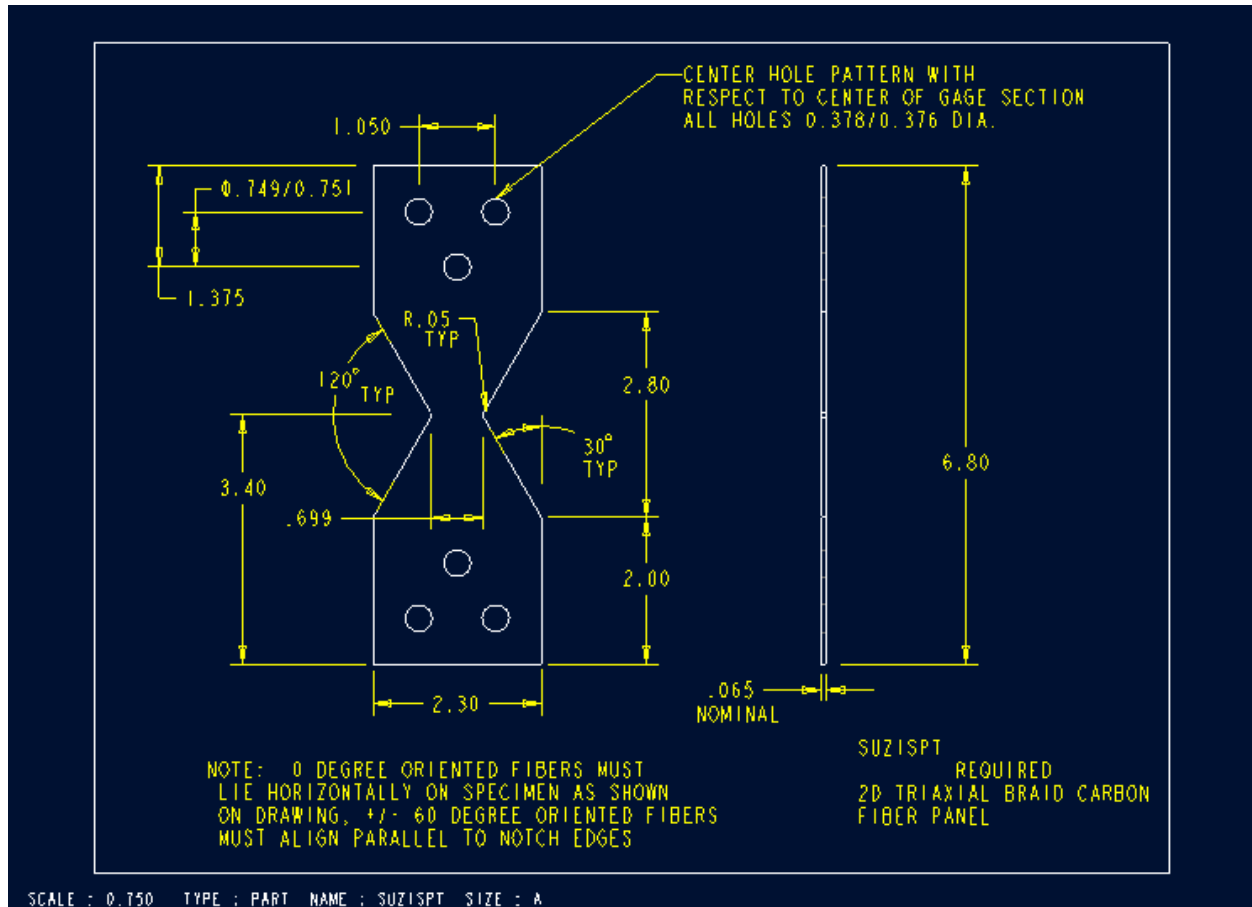


BOWTIE AXIAL TENSILE FIXTURE
British units

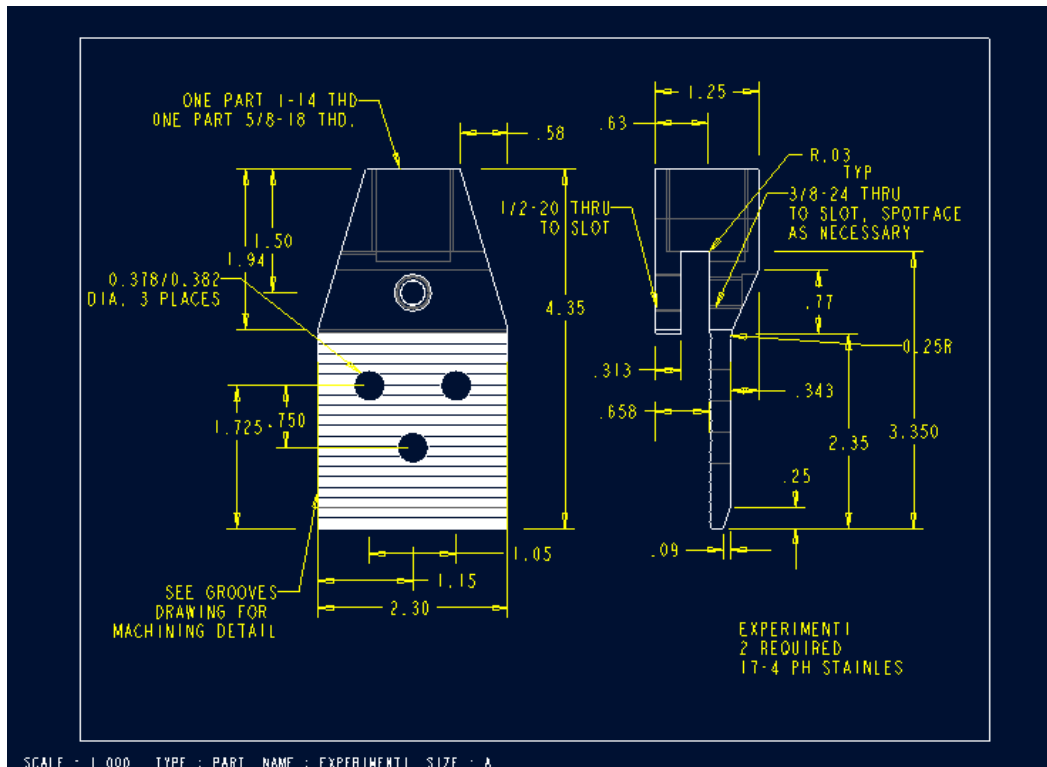
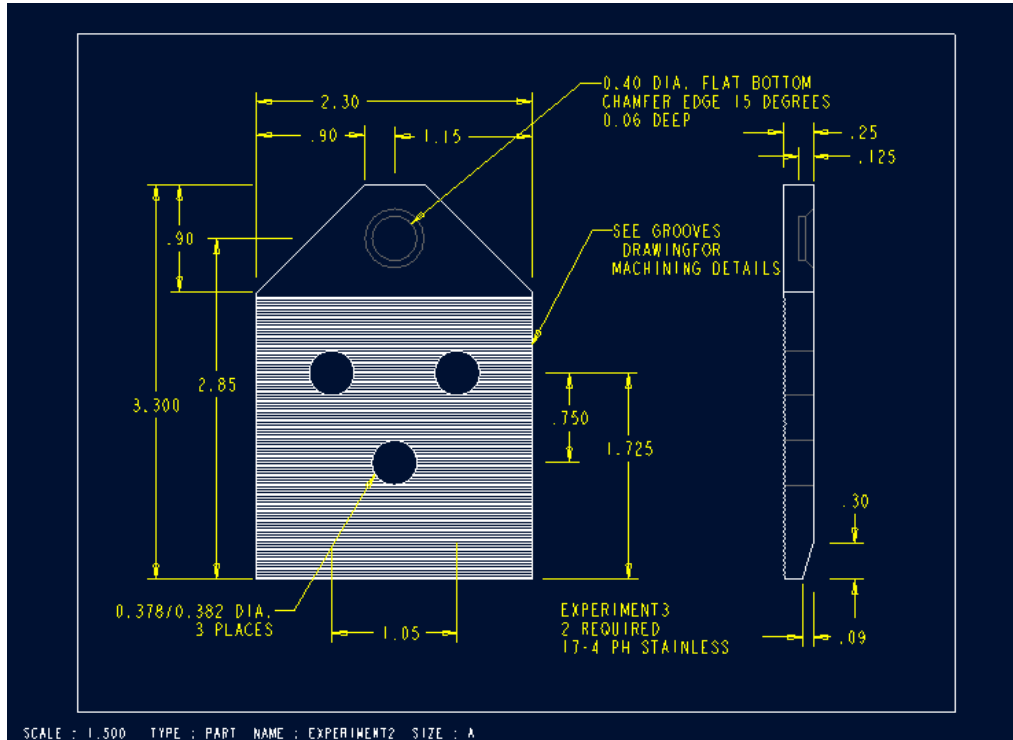


TRANSVERSE TENSILE BOWTIE SPECIMEN

British units

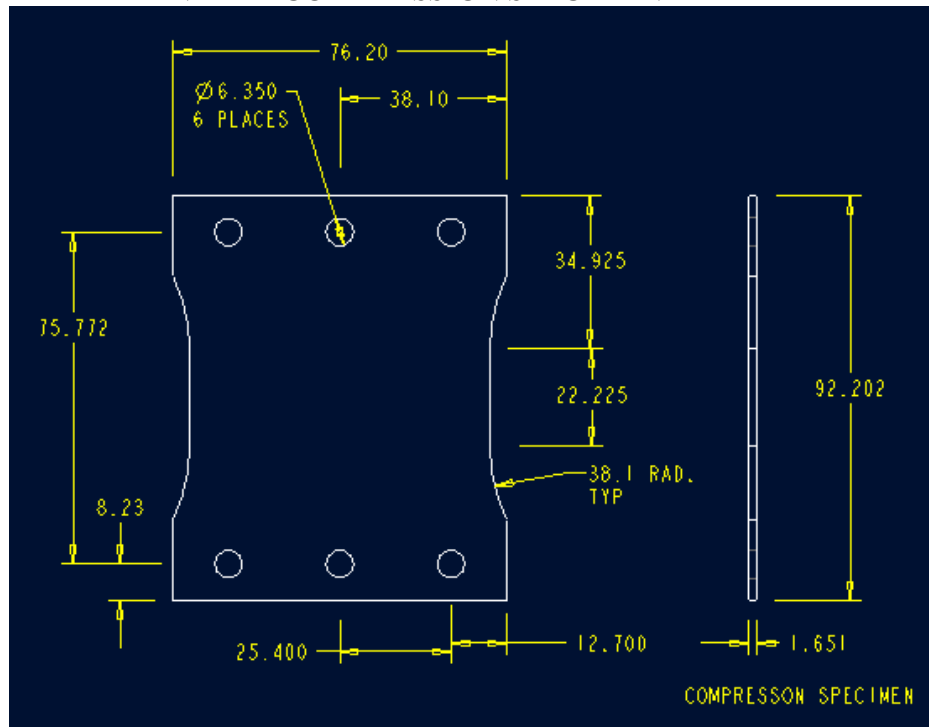


BOWTIE TRANSVERSE TENSILE FIXTURE
British units

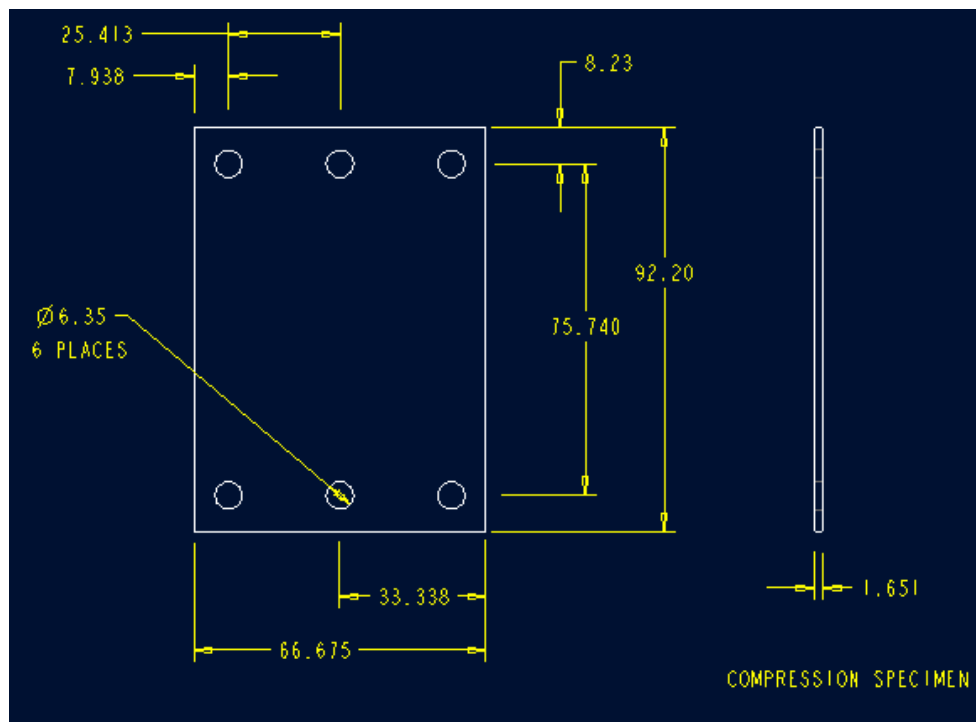


APPENDIX G.
COMPRESSION SPECIMEN AND FIXTURE DRAWINGS

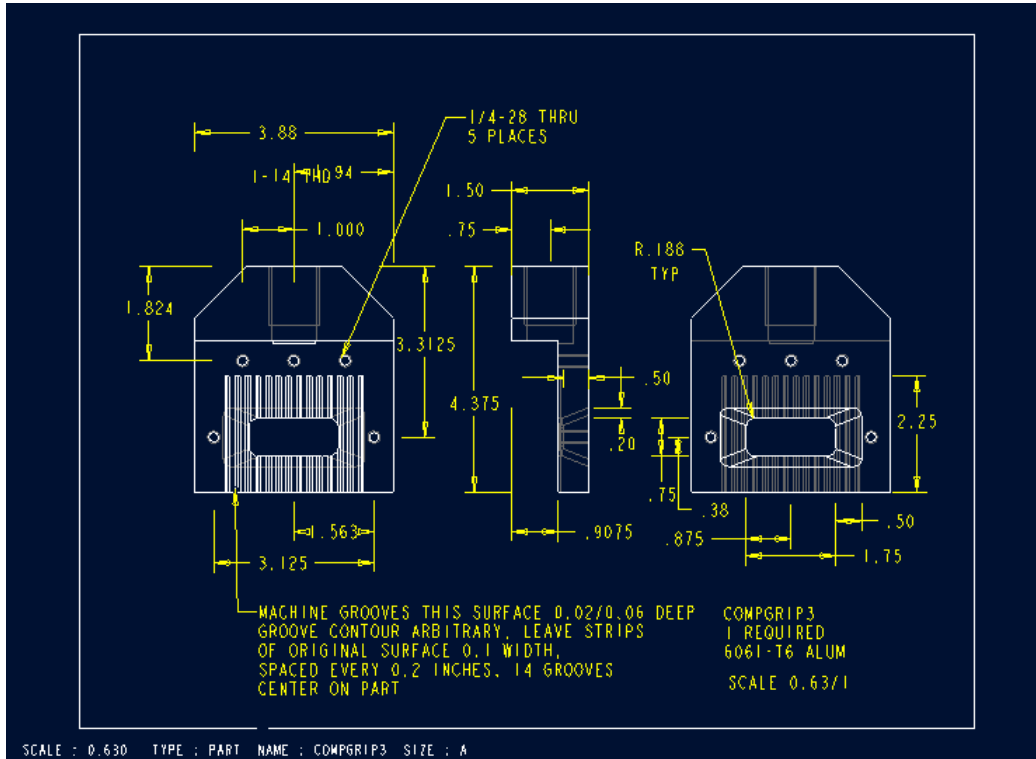
INITIAL COMPRESSION SPECIMEN – AXIAL

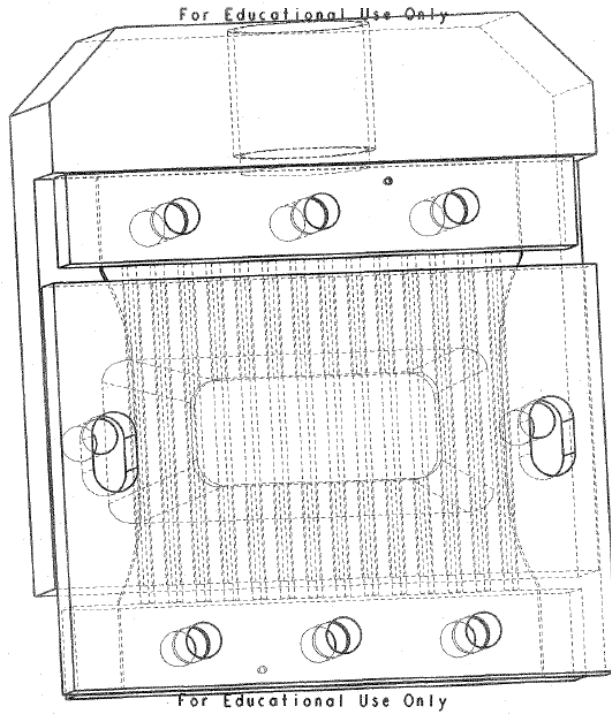


FINAL COMPRESSION SPECIMEN – BOTH ORIENTATIONS



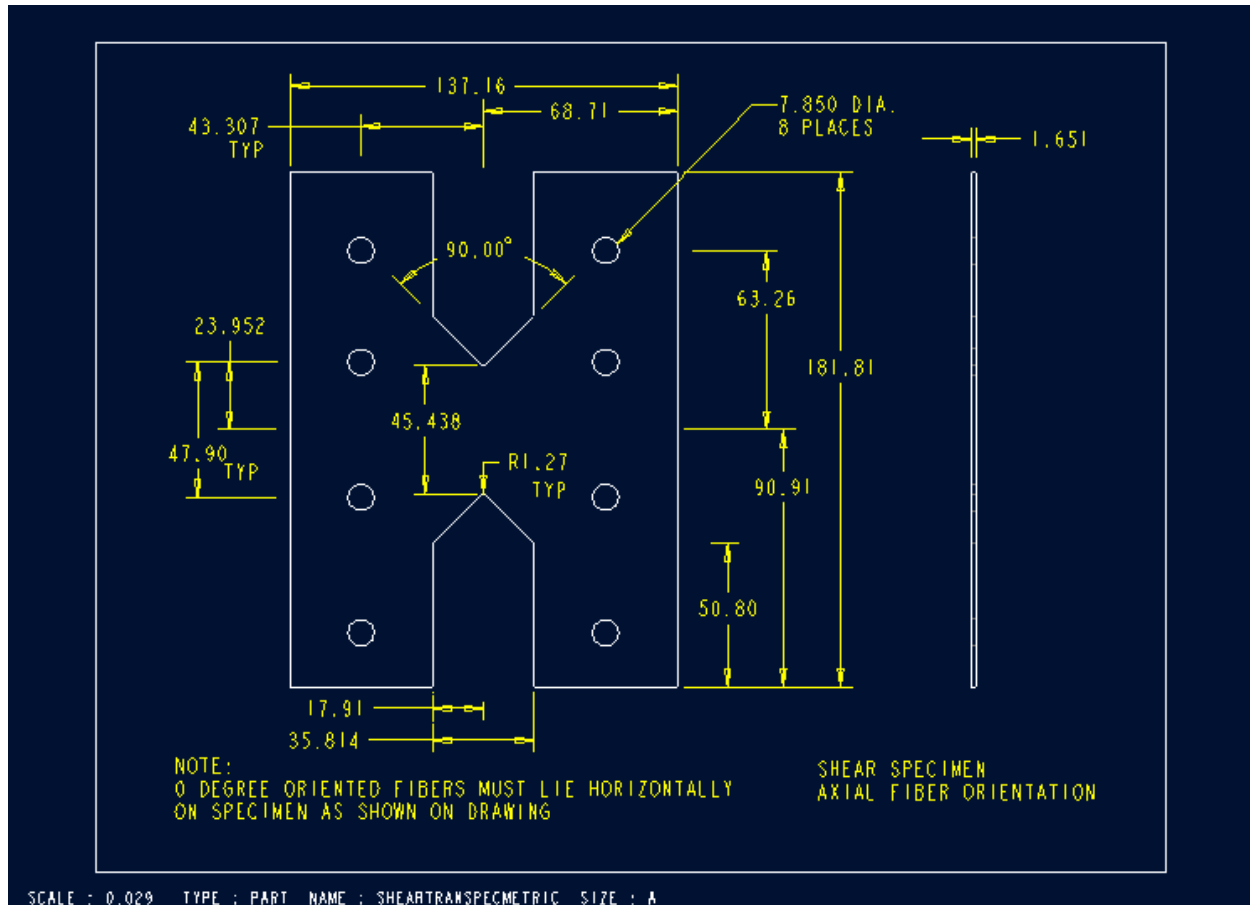
COMPRESSION FIXTURE – AXIAL ORIENTATION
British units



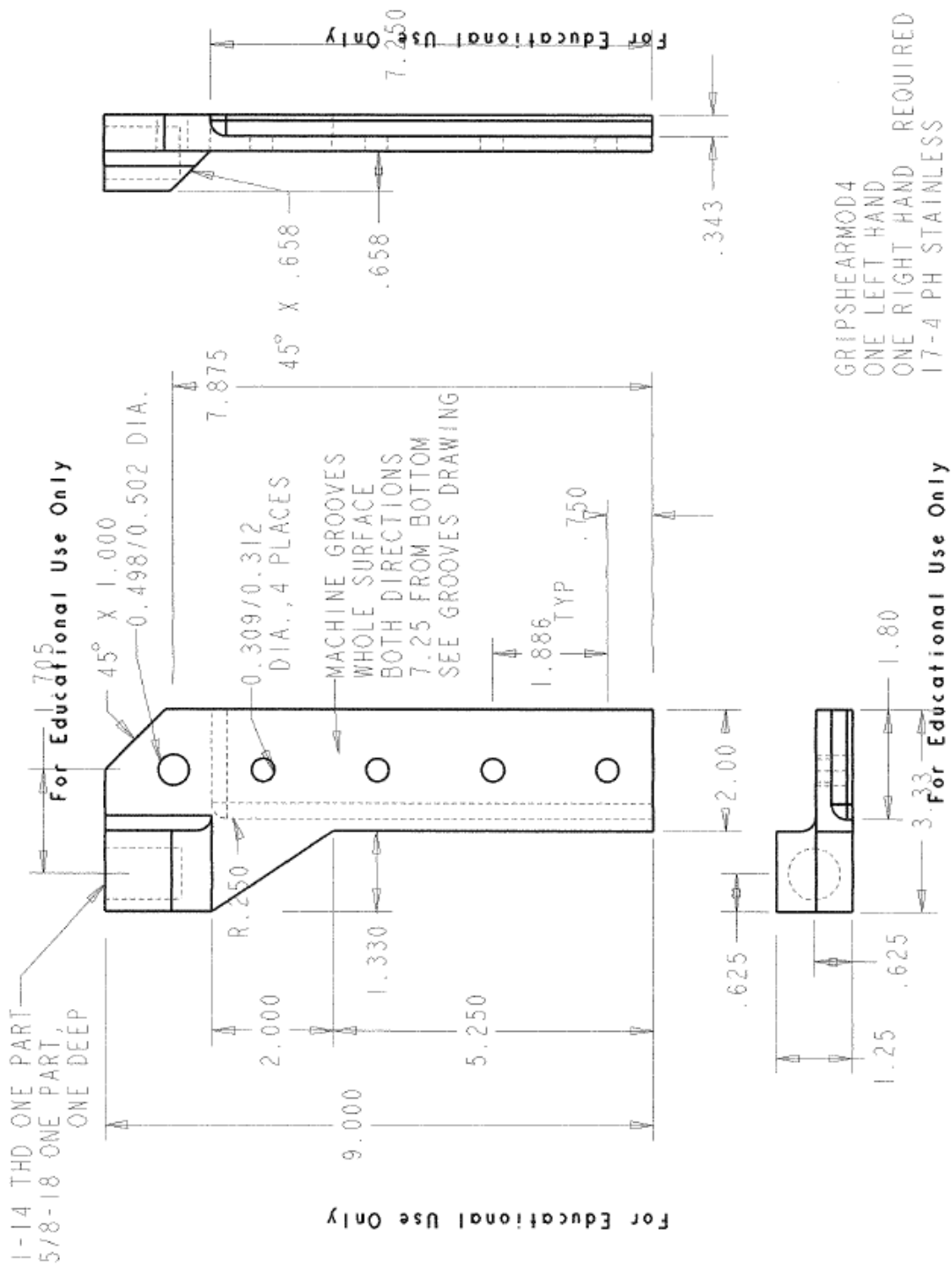


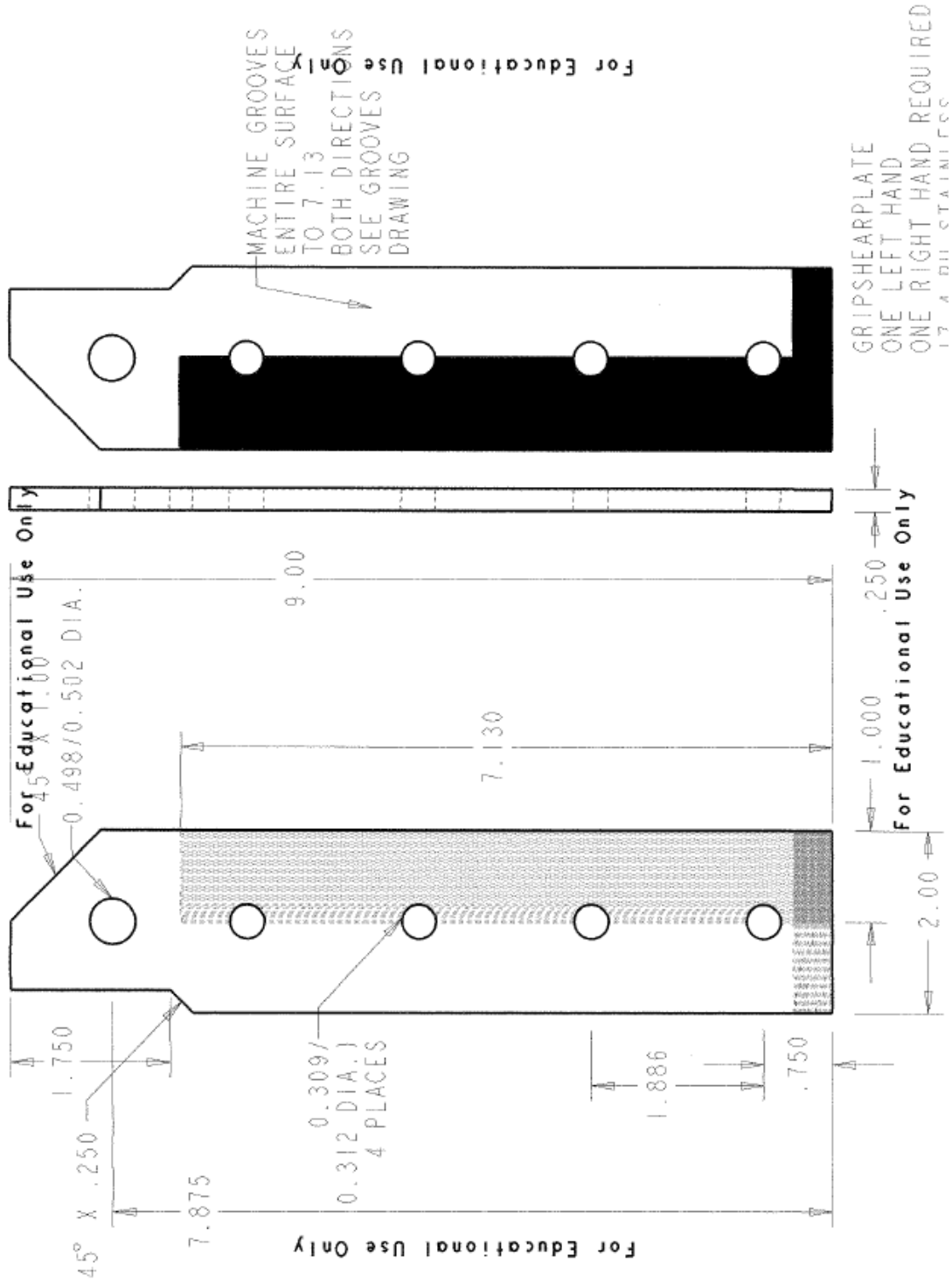
APPENDIX H.
SHEAR SPECIMEN AND FIXTURE DRAWINGS

SHEAR SPECIMEN – AXIAL
Shearing across 0° fibers
Metric units



SHEAR FIXTURE – AXIAL ORIENTATION
British units

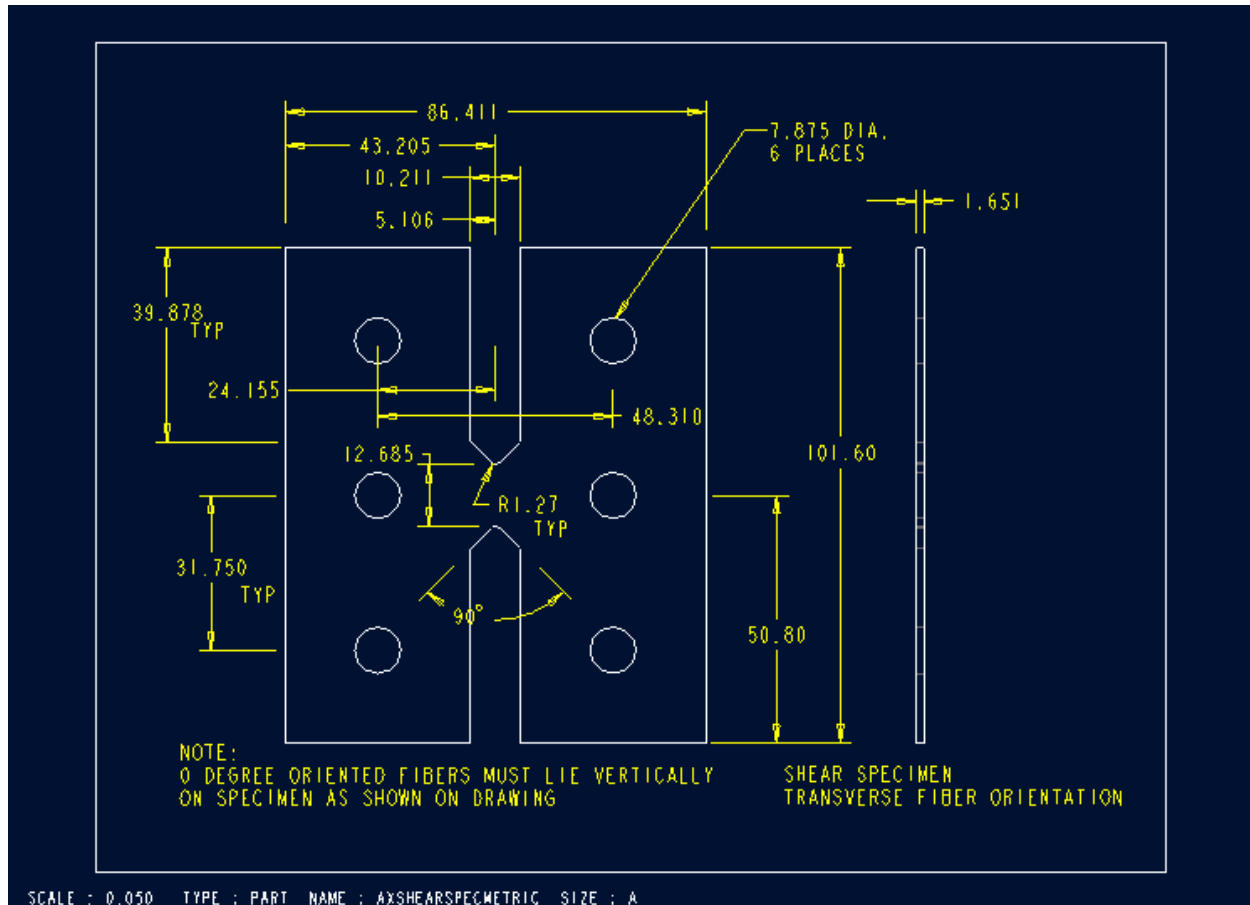




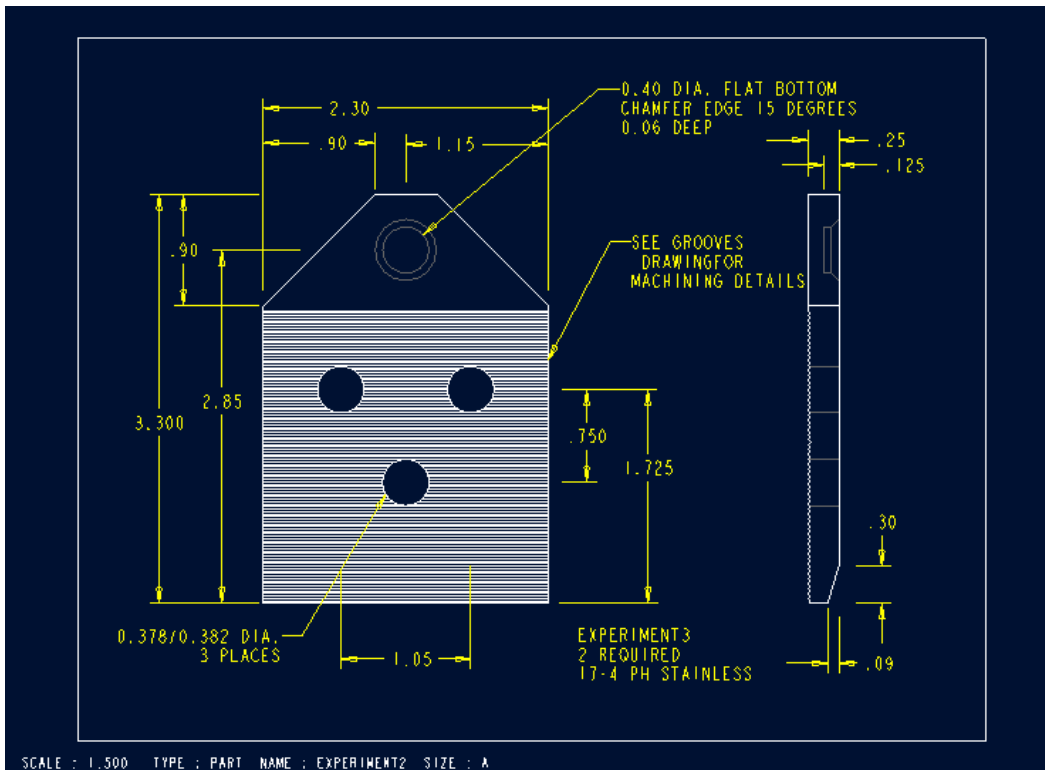
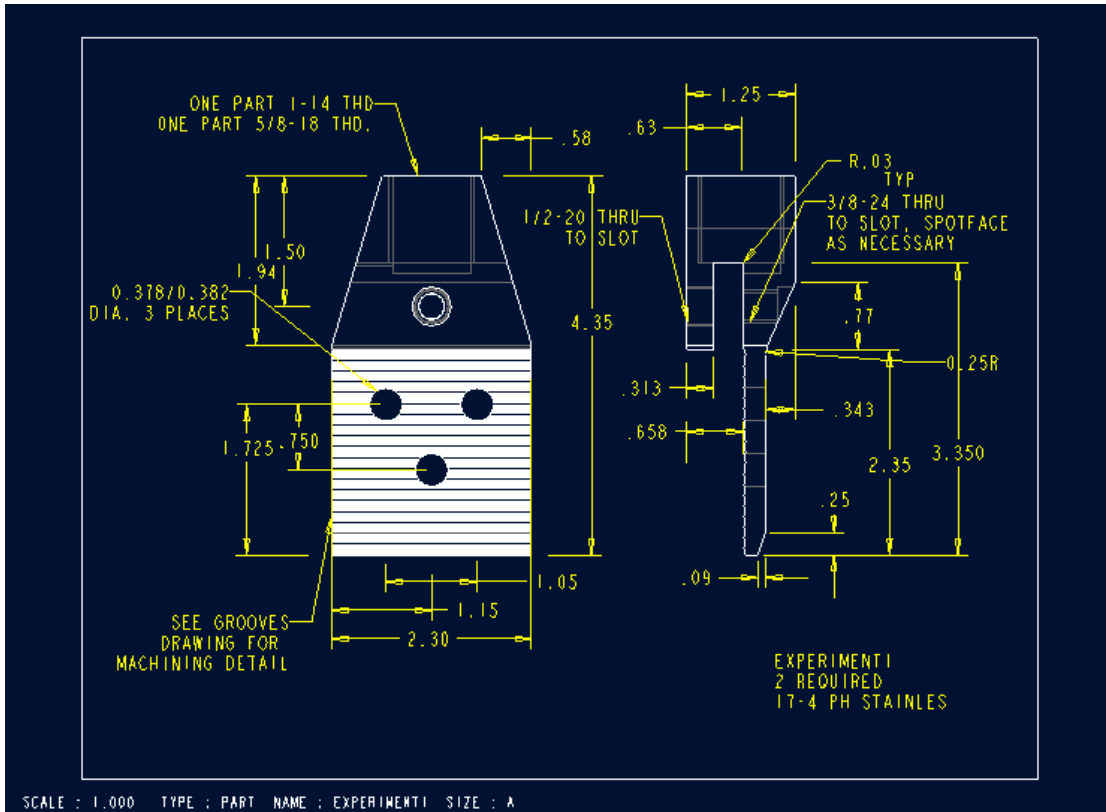
SHEAR SPECIMEN- TRANSVERSE ORIENTATION

Shear across bias fibers

Metric Units



SHEAR FIXTURE- TRANSVERSE ORIENTATION
British Units



APPENDIX I.
SME EQUIPMENT LIST AND CALIBRATIONS

**LOW SPEED SYSTEM
LVDT CALIBRATION**
UDRI Structural Test Laboratory

443

Displacement Transducer Calibration Sheet

Cat. Item Number 02/59

Machine Number	37	Calibration Date	12-Jan-10	Temp /Humidity	74F/39%	Performed by	R.Glett				
Transducer Type/Capacity	LVDT/+-2.5"		Transducer Conditioner	MTS 494.26 DUC 52-J1B AC		Readout	Station Manager				
Manufacturer	G.L.Collins		Serial Number	02050005		Mfgr	MTS				
Model Number	A5453	p/h 390751-03L	Gage Factor	See range Mode:Gain/Delta K		Model #	494.04 Flextest 40				
Serial Number	548262		Excitation Voltage	10		Serial #	02041419B				
Allowable tolerance:	1.0% of Standard value		Condition Rec'd.Ret'd:	Good/Good		Cal.Spec.#:	MTS 494.26CalProc.				
Comments:	From CSC 140C		Console Computer	Dell		4FDZ2B1 RC10861					
Standard Data	lvdt.scf		Range 1 :	5 in. =V. full scale		10 Cal Value:					
	% of Full Scale	Transducer Readings	Standard Readings	% Error							
		Pre-Cal	Post-Cal	Applied	Reading	Pre-Cal	Post-Cal				
Standard Used for This Range	17/24	Dial Indicator Std.		-66%	-3.2960	-3.2960	-3.285	-3.285	0.33	0.33	
Standard Type	Starett 25-5041		-60%	-3.0017	-3.0017	-3.000	-3.000	0.06	0.06		
Standard Capacity	0 - 5.000"		-50%	-2.4951	-2.4951	-2.500	-2.500	-0.20	-0.20		
Standard Serial Number 25-5041J			-40%	-1.9905	-1.9905	-2.000	-2.000	-0.48	-0.48		
Standard Calibration Data	23-Mar-09 w/B&S Gage Blocks		-30%	-1.4918	-1.4918	-1.500	-1.500	-0.55	-0.55		
Standard Readout Meter	Set F 39		-20%	-.9944	-.9944	-1.000	-1.000	-0.56	-0.56		
Standard Readout Meter S/N			-10%	-.4982	-.4982	-.500	-.500	-0.36	-0.36		
Comments	Gain=	.9025 x 1.27043 =	1.14656	0%	.0000	.0000	.000	.000	#DIV/0!	#DIV/0!	
	DK=	1.0000	Phase=	60	10%	.4982	.4982	.500	.500	-0.36	-0.36
	Exc. AHz=	10.00V0kHz		20%	.9972	.9972	1.000	1.000	-0.28	-0.28	
	Polarity=	normal	ValvePol=	invert.	30%	1.4964	1.4964	1.500	1.500	-0.24	-0.24
	Zf=	0.613		40%	1.9965	1.9965	2.000	2.000	-0.18	-0.18	
				50%	2.4992	2.4992	2.500	2.500	-0.03	-0.03	
				60%	2.9979	2.9979	3.000	3.000	-0.07	-0.07	
					3.3140	3.3140	3.310	3.310	0.12	0.12	
Standard Data	lvdt2.scf		Range 2 :	2.5 in. =V. full scale		10 Cal Value:					
	% of Full Scale	Transducer Readings	Standard Readings	% Error							
		Pre-Cal	Post-Cal	Applied	Reading	Pre-Cal	Post-Cal				
Standard Used for This Range	17/24	-100%	-2.50730	-2.50730	-2.50000	-2.50000	0.29	0.29			
Standard Type	Starett 25-5041		-80%	-2.00090	-2.00090	-2.00000	-2.00000	0.05	0.05		
Standard Capacity	0 - 5.000"		-60%	-1.49960	-1.49960	-1.50000	-1.50000	-0.03	-0.03		
Standard Serial Number 25-5041J			-40%	-.99990	-.99990	-1.00000	-1.00000	-0.01	-0.01		
Standard Calibration Data	23-Mar-09 w/B&S Gage Blocks		-20%	-.50090	-.50090	-.50000	-.50000	0.18	0.18		
Standard Readout Meter	Set F 39		0%	.00000	.00000	.00000	.00000	#DIV/0!	#DIV/0!		
Standard Readout Meter S/N			20%	.50010	.50010	.50000	.50000	0.02	0.02		
Comments	Gain=	1.7195 x 1.33114 =	2.28889	40%	.99990	.99990	1.00000	1.00000	-0.01	-0.01	
	DK=	0.9966	Phase=	49	60%	1.49970	1.49970	1.50000	1.50000	-0.02	-0.02
	Exc. AHz=	10.00V0kHz	Zf=	0	80%	2.00020	2.00020	2.00000	2.00000	0.01	0.01
	Polarity=	normal	ValvePol=	invert.	100%	2.50330	2.50330	2.50000	2.50000	0.13	0.13
Standard Data	lvdt3.scf		Range 3 :	1 in. =V. full scale		10 Cal Value:					
	% of Full Scale	Transducer Readings	Standard Readings	% Error							
		Pre-Cal	Post-Cal	Applied	Reading	Pre-Cal	Post-Cal				
Standard Used for This Range	17/24	-100%	-1.0010	-1.0010	-1.000	-1.000	0.10	0.10			
Standard Type	Starett 25-5041		-80%	-.8012	-.8012	-.800	-.800	0.15	0.15		
Standard Capacity	0 - 5.000"		-60%	-.6017	-.6017	-.600	-.600	0.28	0.28		
Standard Serial Number 25-5041J			-40%	-.4016	-.4016	-.400	-.400	0.40	0.40		
Standard Calibration Data	23-Mar-09 w/B&S Gage Blocks		-20%	-.2017	-.2017	-.200	-.200	0.85	0.85		
Standard Readout Meter	Set F 39		0%	.0000	.0000	.000	.000	#DIV/0!	#DIV/0!		
Standard Readout Meter S/N			20%	.2003	.2003	.200	.200	0.15	0.15		
Comments	Gain=	3.249 x 1.76449 =	5.73281	40%	.4002	.4002	.400	.400	0.05	0.05	
	DK=	0.9959	Phase=	49	60%	.6004	.6004	.600	.600	0.07	0.07
	Exc. AHz=	10.00V0kHz	Zf=	0	80%	.8001	.8001	.800	.800	0.01	0.01
	Polarity=	normal	ValvePol=	invert.	100%	1.0000	1.0000	1.000	1.000	0.00	0.00
Standard Data	lvdt4.scf		Range 4 :	0.5 in. =V. full scale		10 Cal Value: NA					
	% of Full Scale	Transducer Readings	Standard Readings	% Error							
		Pre-Cal	Post-Cal	Applied	Reading	Pre-Cal	Post-Cal				
Standard Used for This Range	17/24	-100%	-.49913	-.49913	-.5000	-.5000	-0.17	-0.17			
Standard Type	Starett25-5041		-80%	-.39974	-.39974	-.4000	-.4000	-0.07	-0.07		
Standard Capacity	.000 - 5.000		-60%	-.30046	-.30046	-.3000	-.3000	0.15	0.15		
Standard Serial Number 25-5041J			-40%	-.20055	-.20055	-.2000	-.2000	0.28	0.28		
Standard Calibration Data	23-Mar-09 w/B&S Gage Blocks		-20%	-.10016	-.10016	-.1000	-.1000	0.16	0.16		
Standard Readout Meter	Set F 39		0%	.00000	.00000	.0000	.0000	#DIV/0!	#DIV/0!		
Standard Readout Meter S/N			20%	.09978	.09978	.1000	.1000	-0.22	-0.22		
Comments	Gain=	6.2320 x 1.83981 =	11.4675	40%	.20023	.20023	.2000	.2000	0.11	0.11	
	DK=	0.9992	Phase=	49	60%	.30025	.30025	.3000	.3000	0.08	0.08
	Exc. AHz=	10.00V0kHz	Zf=	0	80%	.40015	.40015	.4000	.4000	0.04	0.04
	Polarity=	normal	ValvePol=	invert.	100%	.49987	.49987	.5000	.5000	-0.03	-0.03

Notes: Only range 1 was previously calibrated by MTS.

Restrictions: For UDRI use only.

Analysis: Range was within 1% required tolerance.

**LOW SPEED SYSTEM
LOAD CELL CALIBRATION
UDRI Structural Test Laboratory**

444	Load Transducer Calibration Sheet			Cat. Item Number _____ 03/53				
Machine Number	37	Calibration Date	12-Jan-10	Temp /Humidity	74F /39%	Performed by	R. Glett	
Transducer Type/Capacity	Load cell/4-22000#		Transducer Conditioner	MTS 494.26 DUC DC FlexTest 40		Readout	Flextest 40	
Manufacturer	MTS		Serial Number	02050005		Mfgr	MTS	
Model Number	661.20E - 03		Gage Factor	See range		Gain/Delta K Mode	Model # 494.04	
Serial Number	V90922		Excitation Voltage	10.000 Vdc.		Serial #	02041419B	
Allowable tolerance:	1% of Standard value		Condition Rec'd./Ret'd:	good		Cal.Spec. #:	MTS 494.26 dc cond.	
Comments	FromCSC 140C	Console	Computer	Dell 4FDZ2B1	RC10861	Cal. Procedure		
Standard Data	Range: 20000 lbs. (1) =V. full scale 10 Cal Value:							
Std. Shunt 60kOhms	-60570			%		%Error		
	60270			Full Scale				
Standard Used for This Range	Load cell std. 17/06							
Standard Type	Eaton Lebow 3156-100k							
Standard Capacity	+100000#							
Standard Serial Number	2905							
Standard Calibration Data	12-Jan-09 Morehouse Inst.							
Standard Readout Meter	Eaton Lebow 7530							
Standard Readout Meter S/N	1924							
Comments Gain=	285.98 x	1.75579 =	502.12205					
ValvePol=	Invert	Polarity=	normal					
Delta K=	0.9991	Zc=	-0.0061					
Excit.=	10.000	Zf=	0.000					
Standard Data	Range: 10000 lbs. (2) =V. full scale 10 Cal Value:							
Standard Used for This Range	Load cell std. 17/01							
Standard Type	Lebow 3157							
Standard Capacity	+ 10000 Lb.							
Standard Serial Number	696							
Standard Calibration Data	21-Nov-07 Morehouse Inst.							
Standard Readout Meter	Doric DS 300-T2-07-08-21							
Standard Readout Meter S/N	60407							
Comments Gain=	540.36 x	1.85918 =	1004.6267					
ValvePol=	Invert	Polarity=	normal					
Delta K=	1.0010							
Excit.=	10	Zf=	0					
Standard Data	Range: 5000 lbs. (3) =V. full scale 10 Cal Value:							
Standard Used for This Range	Load cell std. 17/01							
Standard Type	Lebow 3157							
Standard Capacity	+ 10000 Lb.							
Standard Serial Number	696							
Standard Calibration Data	21-Nov-07 Morehouse Inst.							
Standard Readout Meter	Doric DS 300-T2-07-08-21							
Standard Readout Meter S/N	60407							
Comments Gain=	1036.48 x	1.93694 =	2007.6022					
ValvePol=	Invert	Polarity=	normal					
Delta K=	1.0027							
Excit.=	10	Zf=	0					
Standard Data	Range: 2500 lbs. (4) =V. full scale 10 Cal Value:							
Standard Used for This Range	Load cell std. 17/26							
Standard Type	Sensotec 47,8587-07 -01							
Standard Capacity	3000 #							
Standard Serial Number	747474							
Standard Calibration Data	11-Sep-08 Moehouse Inst.							
Standard Readout Meter	HP 34401A							
Standard Readout Meter S/N	3146A33095							
Comments Gain=	1805.95 x	2.22901 =	4025.4896					
ValvePol=	Invert	Polarity=	normal	Filter				
Delta K=	1.0024	Zc=						
Excit.=	10	Zf=	0					

Notes: First Cal in our lab
Restrictions: Reproduceable for UDRI use only.
Analysis: Within the 1% required tolerance.

LOW SPEED SYSTEM ALIGNMENT

Alignment for George Washington University

Gages Used : CEA-06-125UW-120

Gage Factor : 2.095

Load	Orientation 1 Front			Orientation 2 Back			Orientation 3 BFF			Orientation 4 BFF		
	G1	G2	G3	G1	G2	G3	G1	G2	G3	G1	G2	G3
0	0	0	0	0	0	0	0	0	0	0	0	0
500	425	420	473	409	429	470	415	399	466	432	401	465
1000	880	855	927	863	869	946	869	841	935	871	835	927
1500	1312	1301	1385	1328	1315	1401	1320	1290	1399	1337	1296	1409
2000	1755	1745	1805	1767	1750	1860	1770	1739	1853	1775	1750	1857
2500	2219	2166	2290	2210	2192	2309	2207	2176	2305	2227	2148	2297
3000	2670	2610	2728	2667	2626	2740	2647	2621	2750	2669	2607	2738
3500	3125	3015	3183	3119	3075	3196	3093	3063	3198	3106	3070	3190
4000	3566	3473	3638	3554	3508	3655	3540	3502	3635	3563	3506	3630
Sum	15952	15585	16429	15917	15764	16577	15861	15631	16541	15980	15613	16513
E _{ave}	16099			16209			16144			16155		
B _{y%}	-2.05			-2.27			-2.46			-2.22		
B _{z%}	-3.04			-1.26			-1.9			-3.03		

LOW SPEED SYSTEM EQUIPMENT LIST- SETUP 1

Testing Equipment Information	
GeorgeWashingtonUniv _ DIC	4238020003
Testing laboratory: KL-22	Point of contact: John Chumack
Telephone/Fax: 937-229-4426	Address:
Test machine information	
Manufacturer: MTS 810 2 Poster Frame #37	Manufacturer's reference number: Flex Test Station # 37
Maximum capacity (test machine): 20 Kip	Machine type (servo-hydraulic / servo-electric): S-H
Maximum capacity (load cell): 20K range	Method of data acquisition: Flex Test Peak Detectors _DIC
Range load cell used: LC #90922 = 22kip Range,	Filtering (if applicable):
Comments: Load Cell Sn#90922, Calibration date 14Jan10 - shunt cal check 03Sept10	
Flex Test Program Controller Software	
20kip 6" stroke LVDT sn#548262 Calibrated flex test Displacement .5 inch range	
Gripping information	
Type of grip: MTS Hydraulic Grip	Type of loading (tab, shoulder): Tab grip
Manufacturer: MTS 647	Method of specimen alignment in grip: MTS 609 Align cell
Manufacturer's reference number: 661.20E.03	Visual & Dial Indicator
Surface type/finish: Silver Anodized	Self aligning load train or grip (if applicable):
Wedge angle (if applicable):	Self aligning cell
Comments: 1500 PSI gripping force	
Instrumentation information	
Calibration/verification dates: 03Sept2010	Data disk/filename: see Cal sheet 03/09
Method of calibration: Static Standard Cell and Ga	Data sampling rate: see Cal sheet 03/53
Shunt Cal Check of Load Cell SN#90922 for use on 03Sept2010	
Comments: LVDT Cal date =12Jan10 6" stroke Actuator, see Cal sheet 02/59	
Frequency response	
Component 1: Dantec DIC 3D Imaging system	Frequency response:
Component 2: DVM Kiethely 175 SN#409294	Frequency response:
Component 3: Vishay 2311 Amplifiers SN#108523	Frequency response: DIC channel 3
Component 4: Vishay 2311 Amplifiers SN#108525	Frequency response: DIC channel 4
Component 5: Dantec TU-4XB Slow Speed Timing	Frequency response: 30HZ
Overall frequency response:	
Ancillary equipment (please list and describe usage)	
Dantec DIC 3D Imaging system with Dantec Low Speed 5 Megapixel Cameras	
#3 Airbrush Spray Pattern 12 inches from subject	
Xenoplan 50mm lenses	
DIC 3D system with 2 Deedacool lights	
Vishay Strain Gages CEA-06-500UW-350 with cal resistor 3.921K ohm	
Dantec TU-4XB Slow Speed Timing Box	

LOW SPEED SYSTEM – SETUP 2

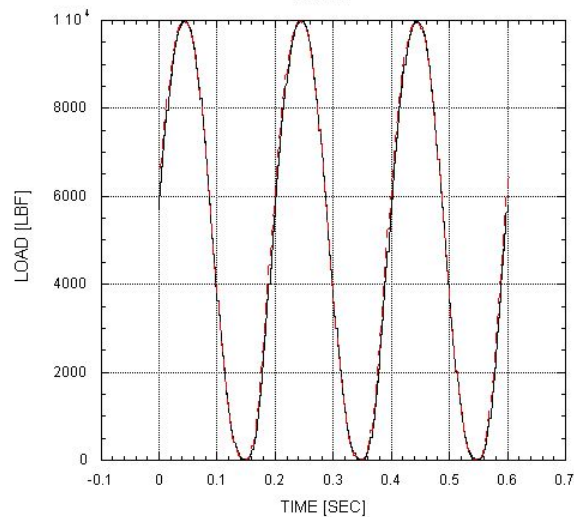
Testing Equipment Information	
GeorgeWashingtonUniv_ DIC_phase2	4238030003
Testing laboratory: KL-22	Point of contact: John Chumack
Telephone/Fax: 937-229-4426	Address:
Test machine information	
Manufacturer: MTS 810 2 Poster Frame #37	Manufacturer's reference number: Flex Test Station # 37
Maximum capacity (test machine): 20 Kip	Machine type (servo-hydraulic / servo-electric): S-H
Maximum capacity (load cell): 20K range	Method of data acquisition: Flex Test Peak Detectors_DIC
Range load cell used: LC #90922 = 22kip Range,	Filtering (if applicable):
Comments: Load Cell Sn#90922, Calibration date 14Jan10 - shunt cal check 03Sept10	
Flex Test Program Controller Software	
20kip 6" stroke LVDT sn#548262 Calibrated flex test Displacement .5 inch range	
Gripping information	
Type of grip: UDRI Grips, Shear, Tensile, and Com	Type of loading (tab, shoulder): Tab grip
Manufacturer: MTS 647	Method of specimen alignment in grip: MTS 609 Align cell
Manufacturer's reference number: 661.20E.03	Visual & Dial Indicator
Surface type/finish: Black Painted	Self aligning load train or grip (if applicable):
Wedge angle (if applicable):	Self aligning cell
Comments:	
Instrumentation information	
Calibration/verification dates: 03Sept2010	Data disk/filename: see Cal sheet 03/09
Method of calibration: Static Standard Cell and Ga	Data sampling rate: see Cal sheet 03/53
Shunt Cal Check of Load Cell SN#90922 for use on 03Sept2010	
Comments: LVDT Cal date =12Jan10 6" stroke Actuator, see Cal sheet 02/59	
Frequency response	
Component 1: Dantec DIC 3D Imaging system	Frequency response: DIC Stroke channel 1
Component 2: DVM Kiethely 175 SN#409294	Frequency response: DIC Load channel 2
Component 3: Dantec TU-4XB Slow Speed Timing	Frequency response: 30HZ
Component 4: Dantec TU-4XF High Speed Timing	Frequency response: 200KHZ
Component 5:	
Component 6:	
Overall frequency response:	
Ancillary equipment (please list and describe usage)	
Dantec DIC 3D Imaging system with Dantec Low Speed 5 Megapixel Cameras	
#3 Airbrush Spray Pattern 12 inches from subject @ 15psi	
Slow Cam Xenoplan 50mm lenses or HS Cam 100mm High speed Lenses	
DIC 3D system with 2 Deedacool lights	
Dantec TU-4XB Slow Speed Timing Box	
Dantec TU-4XF High Speed Timing Box	

HIGH RATE SYSTEM LOAD WASHER CALIBRATION

Customer: GWU for High Rate		Date: 26 + 27 January 2011		Tech: John Chumack	
MTS #37 LC =SN#A90922		FW= Sn# 1416810		Kistler 9061A 45KIP - 1"-14	
PC = RC10096 card and BNC2110		FW Cal software V0_02b			
20k Range					
Dynamic Tension	5hz	Gain sensitivity	Load Cell readin	FW reading lbf	
0% -	volts	0.777	0	0	
20% -	2		4000	4000	
40% -	4		8000	8000	
60% -	6		12000	12000	
80% -	8		16000	16000	
100% -	10		20000	20000	
0% -			0	0	
10k Range					
Dynamic Tension	5hz	Gain sensitivity	Load Cell readin	FW reading lbf	
0% -	volts	0.858	0	0	
20% -	2		2000	2000	
40% -	4		4000	4000	
60% -	6		6000	6000	
80% -	8		8000	8000	
100% -	10		10000	10000	
0% -			0	0	
5k Range					
Dynamic Tension	5hz	Gain sensitivity	Load Cell readin	FW reading lbf	
0% -	volts	0.897	0	0	
20% -	2		1000	1000	
40% -	4		2000	2000	
60% -	6		3000	3000	
80% -	8		4000	4000	
100% -	10		5000	5000	
0% -			0	0	

— Load Cell
 - - Force Washer

EXAMPLE OF FORCE WASHER CALIBRATION
 1-26-11



HIGH RATE SYSTEM LVDT CALIBRATION

UDRI Structural Test Laboratory								
Displacement Transducer Calibration Sheet						Cat. Item Number 02/35		
Machine Number	6	Calibration Date	26-Jan-11	Temp /Humidity	79F /7%	Performed by	R.Glett	
Transducer Type/Capacity	LVDT/+-2.5'		Transducer Conditioner	MTS458.13 ac		Readout	Console	
Manufacturer	G.L.Collins		Serial Number	410		Mfgr	MTS	
Model Number	LMT711-P 34		Gage Factor	see range below		Model #	458.10	
Serial Number	219172		Excitation Voltage	20.005 vp-p		Serial #	0125177-	
Allowable tolerance:	1.0% of Standard value		Condition Rec'd.Ret'd:	Fair/Fair used		Cal.Spec. #:	MTS407.14 LVDT	
Comments: in 22Kip actuator SN 466R								
Standard Data	Setup 1			Range 1 :	5 in.	=V. full scale	10 Cal Value: NA	
				% of	Transducer Readings		Standard Readings	
				Full Scale	Pre-Cal	Post-Cal	Applied Reading	
							%Error	
Standard Used for This Range	17/24 Dial Indicator			-65%	-3.2740	-3.2740	-3.237 -3.237	1.14 1.14
Standard Type	Starett	25-5041J		-60%	-3.0215	-3.0215	-3.000 -3.000	0.72 0.72
Standard Capacity	0-5.000"			-50%	-2.5050	-2.5050	-2.500 -2.500	0.20 0.20
Standard Serial Number	25-5041			-40%	-2.0015	-2.0015	-2.000 -2.000	0.08 0.08
Standard Calibration Data	1-Jun-10 B&S Gage blks.F39			-30%	-1.5010	-1.5010	-1.500 -1.500	0.07 0.07
Standard Readout Meter				-20%	-1.0000	-1.0000	-1.000 -1.000	0.00 0.00
Standard Readout Meter S/N				-10%	-.4990	-.4990	-.500 -.500	-0.20 -0.20
Comments				0%	.0000	.0000	.000 .000	0.00 0.00
				10%	.5025	.5025	.500 .500	0.50 0.50
				20%	1.0000	1.0000	1.000 1.000	0.00 0.00
				30%	1.4990	1.4990	1.500 1.500	-0.07 -0.07
				40%	1.9975	1.9975	2.000 2.000	-0.12 -0.12
				50%	2.5000	2.5000	2.500 2.500	0.00 0.00
				60%	3.0040	3.0040	3.000 3.000	0.13 0.13
				67%	3.3555	3.3555	3.355 3.355	0.01 0.01

HIGH RATE SYSTEM EQUIPMENT LIST

Testing Equipment Information	
GeorgeWashingtonUniv_ DIC_phase2	423803003
Testing laboratory: KL-22	Point of contact: John Chumack
Telephone/Fax: 937-229-4426	Address:
Test machine information	
Manufacturer: MTS 4 Poster Frame #6	Manufacturer's reference number: MTS 458.10 on #6
Maximum capacity (test machine): 50 Kip	Machine type (servo-hydraulic / servo-electric): S-H
Maximum capacity (load cell): FW 45K range	Method of data acquisition: HSDAQ & GPTC v03b
FW range used: FW #1416810= 20kip , calibrated 5k, 10k,19k range	Filtering (if applicable):
Comments:Force washer Sn#1416810, Calibration date 01Mar11 - shunt cal check 01Mar11	
HSDAQ 10 MHZ Pci card #6115	
22kip 6" stroke LVDT sn#219172 Calibrated Displacement 5 inch range	
MTS Micro Profiler 458.91	
Gripping information	
Type of grip:UDRI Grips, Shear, Tensile, and Compression	Type of loading (tab, shoulder): Tab grip
Manufacturer: UDRI Fixturing	Method of specimen alignment in grip: Dial indicator
Manufacturer's reference number: Compression, Axial, Transverse	Visual & Dial Indicator
Surface type/finish: Black Painted & white speckled	Self aligning load train or grip (if applicable):
Wedge angle (if applicable):	
Comments:	
Instrumentation information	
Calibration/verification dates: 01Mar2011	Data disk/filename: see Cal sheet 02/35
Method of calibration: Static Standard Cell and Gaged Blocks/dial indicat	Data sampling rate: see data run sheets
Shunt Cal Check of Load Cell #37 SN#90922 for use on 03Sept2010	
Comments: LVDT Cal date =26Jan11 6" stroke Actuator, see Cal sheet 02/35	
Frequency response	
Component 1: Dantec DIC 3D Imaging system	Frequency response: DIC Stroke channel 1
Component 2: DVM Kiethely 175 SN#409294	Frequency response: DIC Load channel 2
Component 3:Dantec TU-4XF High Speed Timing Box	Frequency response: 200KHZ
Component 4:	Frequency response:
Component 5:	
Component 6:	
Overall frequency response:	
Ancillary equipment (please list and describe usage)	
Dantec DIC 3D Imaging system with Dantec High Speed Cameras	
#3 Airbrush Spray Pattern & Spray can 12 inches from subject @ 15psi	
HS Cam 100mm High speed Lenses @ F11	
DIC 3D system with 2 Deedacool lights	
BNC-2110 NI A-D box	
Dantec TU-4XF High Speed Timing Box	
1 Jennings Fiber optics Bundle	

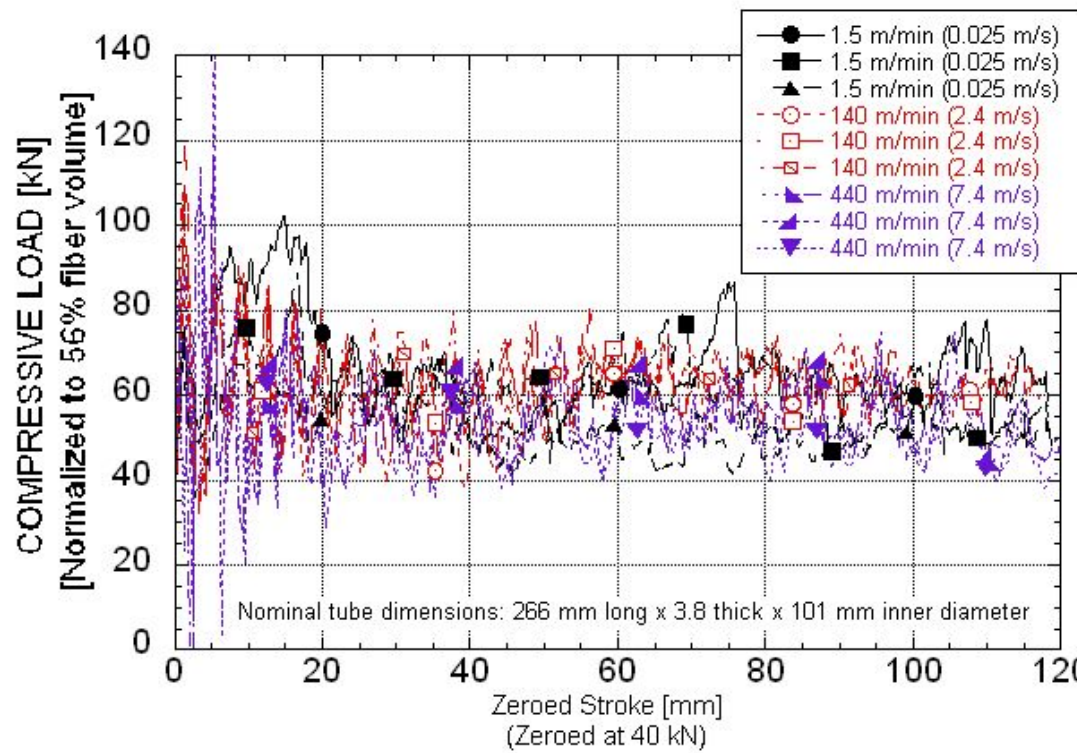
APPENDIX J.

MODIFIED ASTM D3039 TENSILE DATA PACKAGE

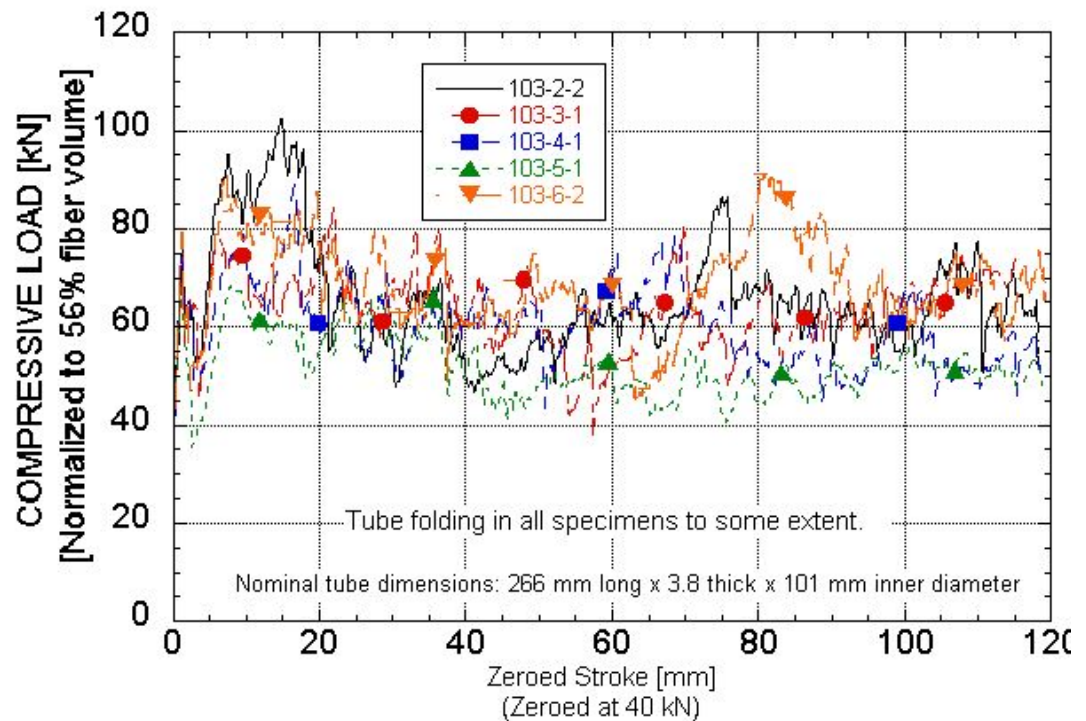
Summary Tables

Summary Plots

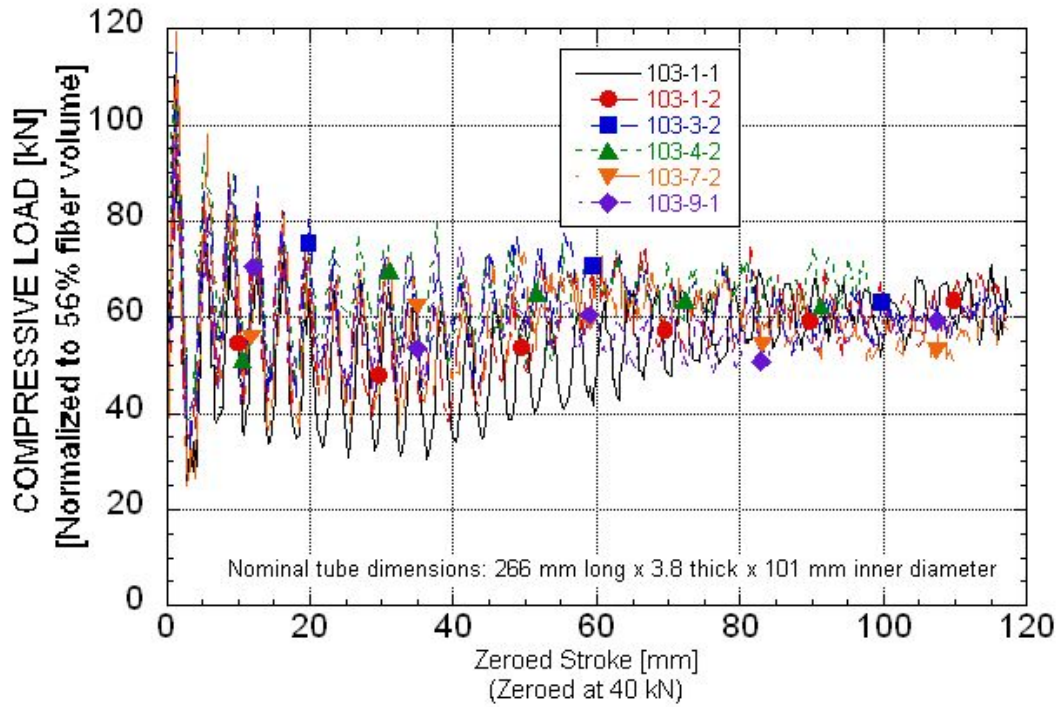
NORMALIZED LOAD vs. ACTUATOR DISPLACEMENT



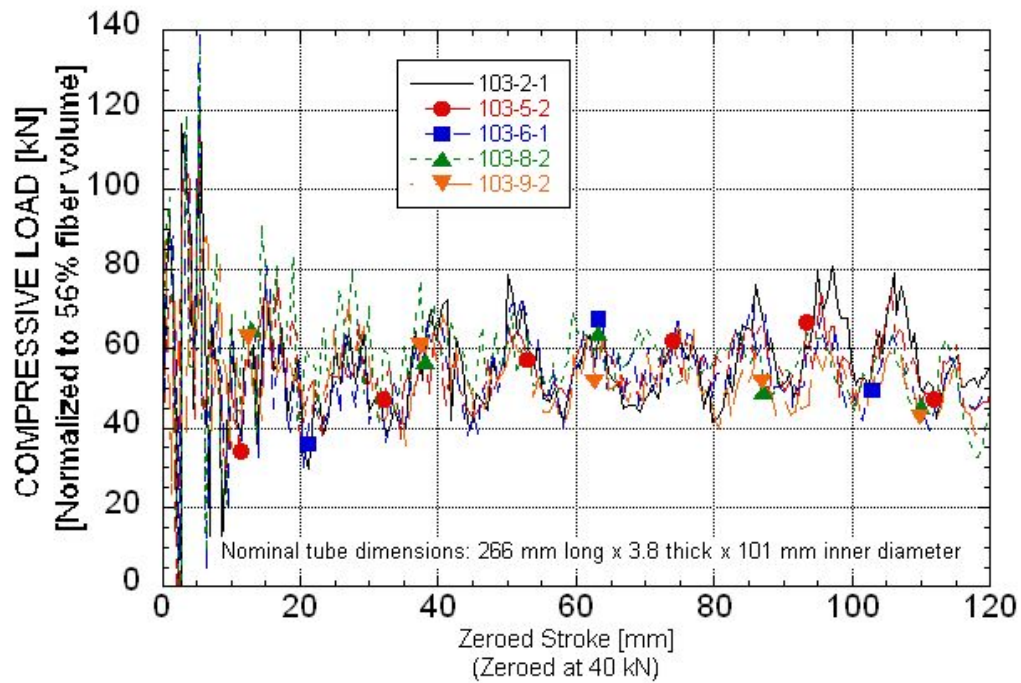
NORMALIZED LOAD vs. ACTUATOR DISPLACEMENT
1.52 m/min



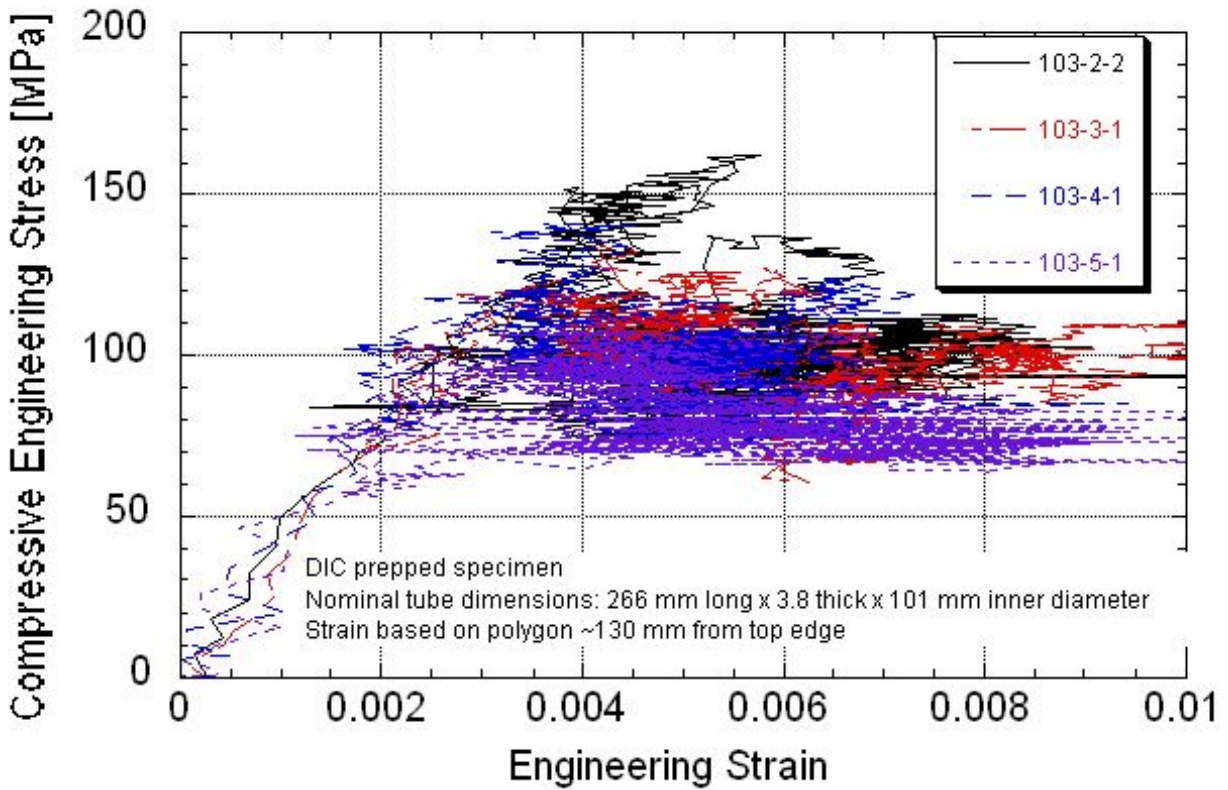
NORMALIZED LOAD vs. ACTUATOR DISPLACEMENT
140 m/min



NORMALIZED LOAD vs. ACTUATOR DISPLACEMENT
440 m/min



2D triaxial (-60/0/+60) carbon braid T700/Epon 682W resin Three plies
Tube Axial Compression - 0° fibers parallel to loading direction
Compressive stress-strain
1.5 m/min



Investigation of Opportunities For Light-Weighting Vehicles Using Advanced Plastics And Composites

Tube Compression Data Summary
2D Triaxial Carbon T700/ Epon862W Epoxy Braid
Average fiber content of 44.44 vol%. Nominal inner diameter of 101 mm and a wall thickness of 3.8 mm.

Speed on top edge a	Starting Tube Serial ID	UDRI STL number	Tube Weight [gm]	Cross-sectional Area [sq. mm]	Density [gm/cc]	Work up to $\phi=115$ mm [kJ]	Median Crush Load* [kN]	Median Crush Stress* [MPa]	Median Stress Normalized to 56% Fiber Volume [MPa]	Specific Sustained Crushing Stress [SSCS]	Crush Compression Ratio**	Specific Energy Absorption ⁽¹⁾ with folding mode failure [SEA-FM] [kJ/kg]	Specific Energy Absorption ⁽²⁾ [SEA] [kJ/kg]	Specific Energy Absorption ⁽³⁾ [SEA] [kJ/kg ²]	Average Peak ⁽⁴⁾ Temperature During Crush [°C]	Machine Rate [m/s]	Machine Rate [m/min]	Comments
1.5 m/min	1050	103-2-2	256	627	1.45	5.83	47.8	76.2	98.8	52.7	0.36	44.3	55.9	20.5	-	0.02548	1.53	
	1051	103-3-1	256	629	1.47	5.57	48.0	76.4	100	51.9	0.37	44.1	52.4	21.4	-	0.02546	1.53	
		103-4-1	258	629	1.45	5.34	45.1	71.7	93.6	49.6	0.35	41.0	51.0	18.5	-	0.02541	1.52	
	1053	103-5-1	253	626	1.47	5.04	42.2	67.3	80.4	45.8	0.30	39.9	47.6	17.9	-	0.02546	1.53	
	1054	103-6-2 Run 2	255	628	1.44	6.19	52.0	82.8	106	57.5	0.39	47.4	59.5	21.8	-	0.02542	1.53	Set-up initial run with a flat end. Exceed actuator capacity. Rerun with angle cut
		Average Standard Deviation COV [%]				5.60 0.44 7.89	47.0 3.66 7.78	74.9 5.79 7.74	95.8 9.61 10.0	51.5 4.29 8.32	0.35 0.04 10.0	43.3 2.96 6.84	53.3 4.56 8.56	20.0 1.75 8.7				
140 m/min	1049	103-1-1	253	619	1.47	5.19	47.6	76.9	92.5	52.3	0.34	-	49.6	20.3	296	2.38	143	
	1049	103-1-2	253	623	1.47	5.70	50.6	81.2	97.7	55.3	0.36	-	54.1	22.3	252	2.36	142	
	1051	103-3-2	253	629	1.45	5.43	47.2	75.1	98.7	51.9	0.36	-	51.9	21.2	233	2.36	142	
		103-4-2	235	619	1.45	4.89#	50.1	80.9	106	55.9	0.39	-	55.7	20.6	-	2.38	143	Setup run. Length shorter by 25 mm
	1055	103-7-2	253	621	1.43	5.14	44.9	72.4	95.3	50.8	0.35	-	50.5	20.1	173	2.37	142	
	103-9-1	255	614	1.44	5.43	46.7	75.9	95.0	52.7	0.35	-	53.3	21.0	362	2.36	141		
		Average Standard Deviation COV [%]				5.37 0.22 4.15	47.8 2.14 4.5	77.1 3.44 4.5	97.4 4.55 4.67	53.2 2.01 3.77	0.36 0.02 4.67		52.5 2.30 4.37	20.9 0.81 3.89	263 71 27			
440 m/min	1050	103-2-1	255	631	1.45	4.97	43.0	68.1	84.2	47.1	0.31	-	47.3	18.6	254	7.35	441	
	1053	103-5-2	255	625	1.47	5.36	45.9	73.5	90.9	50.0	0.34	-	50.7	20.0	404 [excluded from avg]	7.36	441	
	1054	103-6-1	253	622	1.44	4.89	42.0	67.5	83.6	46.9	0.31	-	47.4	18.4	254	7.34	440	
	1057	103-8-2	256	633	1.44	5.39	45.3	71.5	88.5	49.6	0.33	-	51.3	20.0	308	7.34	440	
		103-9-2	254	615	1.44	4.85	40.2	65.4	81.8	45.4	0.30	-	47.7	18.1	289	7.35	441	
		Average Standard Deviation COV [%]					43.3 2.35 5.43	69.2 3.24 4.69	85.8 3.77 4.39	47.8 1.95 4.08	0.32 0.01 4.39		48.9 1.95 3.98	19.0 0.94 4.96	276 27 10			
150 m/min Flat end	1055	103-7-1	255	622	1.43	5.10	43.4	69.7	91.7	48.9	0.34	-	50.0	19.6	311	2.37	142	No crack initiator

*Load/Stress measured over a region from 25 mm net zeroed displacement up to stroke limit. #Out to 98mm. Not included in average. ** Normalized to 56% fiber volume. Ultimate strength of 271 MPa.

The displacement was zeroed at a value of 40 kN normalized load. All failures at 1.5 m/min were a combination of folding and tearing, with the exception of 103-6-2. Failure for 103-6-2 was all by folding.

The specimen thickness varied due to the braid structure. The measured thickness was an average of "peaks" and "valleys" from three locations along the length of the original tube.

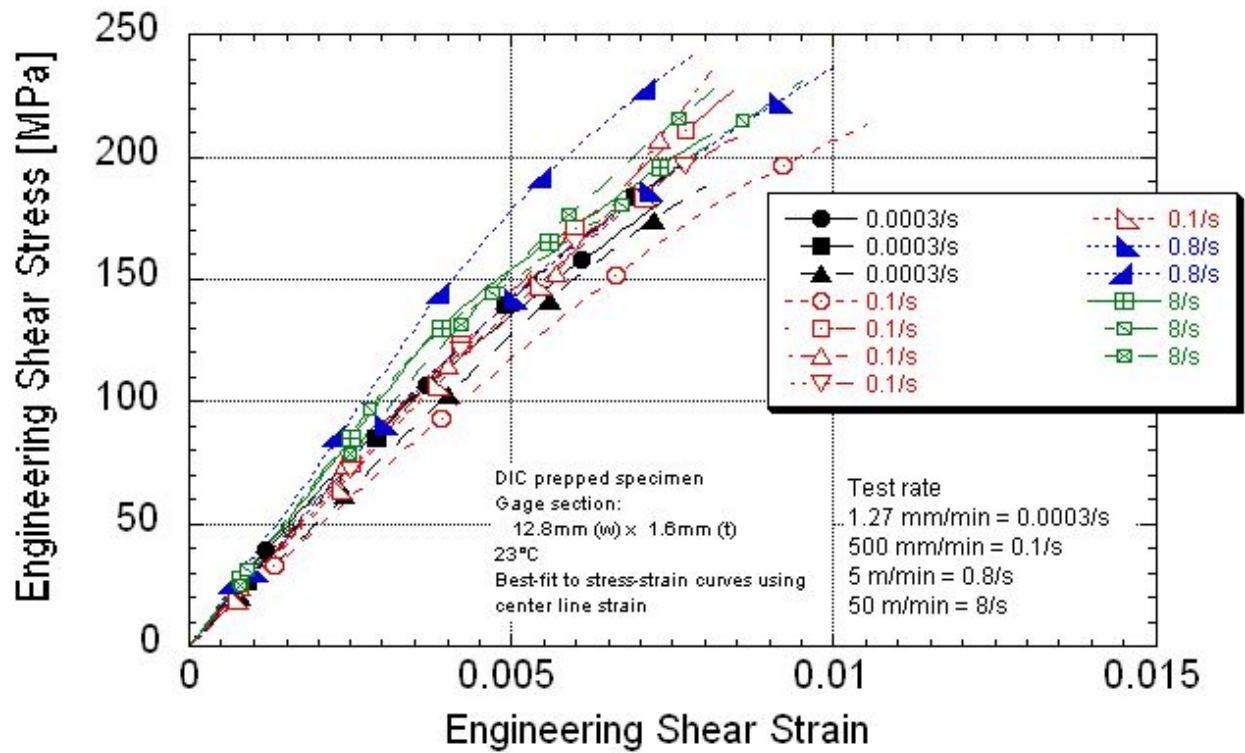
1) SEA calculated using $E_s = \text{Work}/(\text{area} \times \text{density}) \times (\text{actuator displacement} + \text{displacement of folded length})$

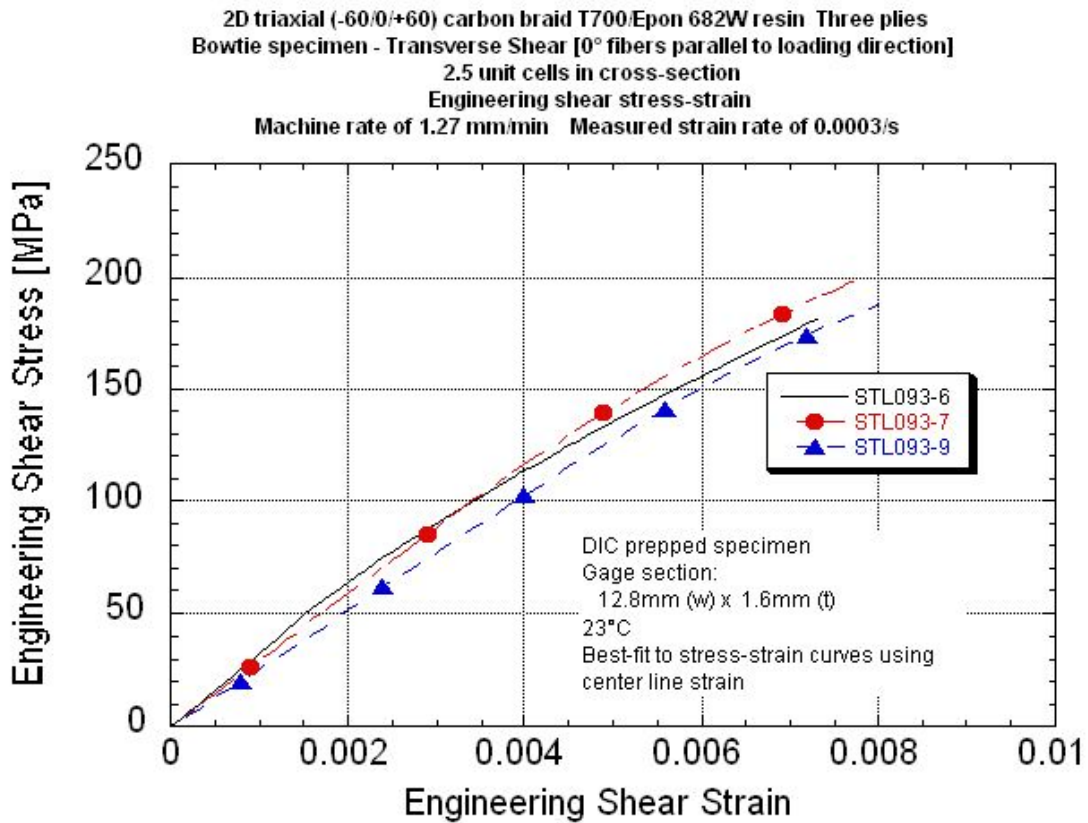
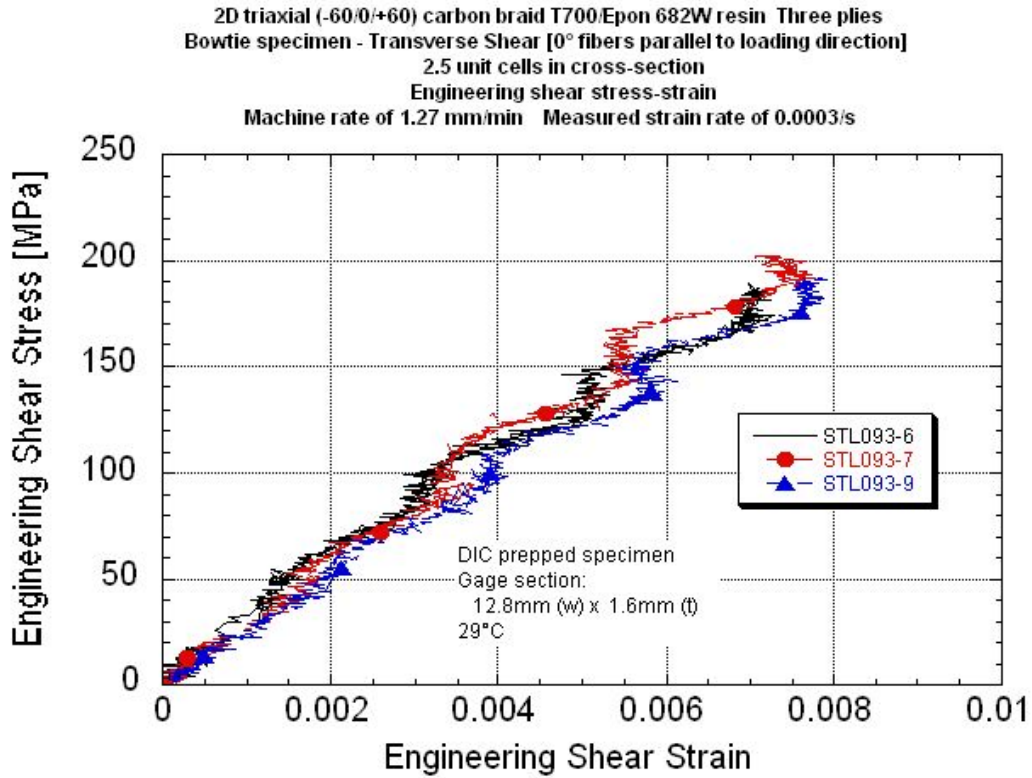
2) SEA calculated using $E_s = \text{Work}/(\text{area} \times \text{density}) \times \text{total actuator displacement}$

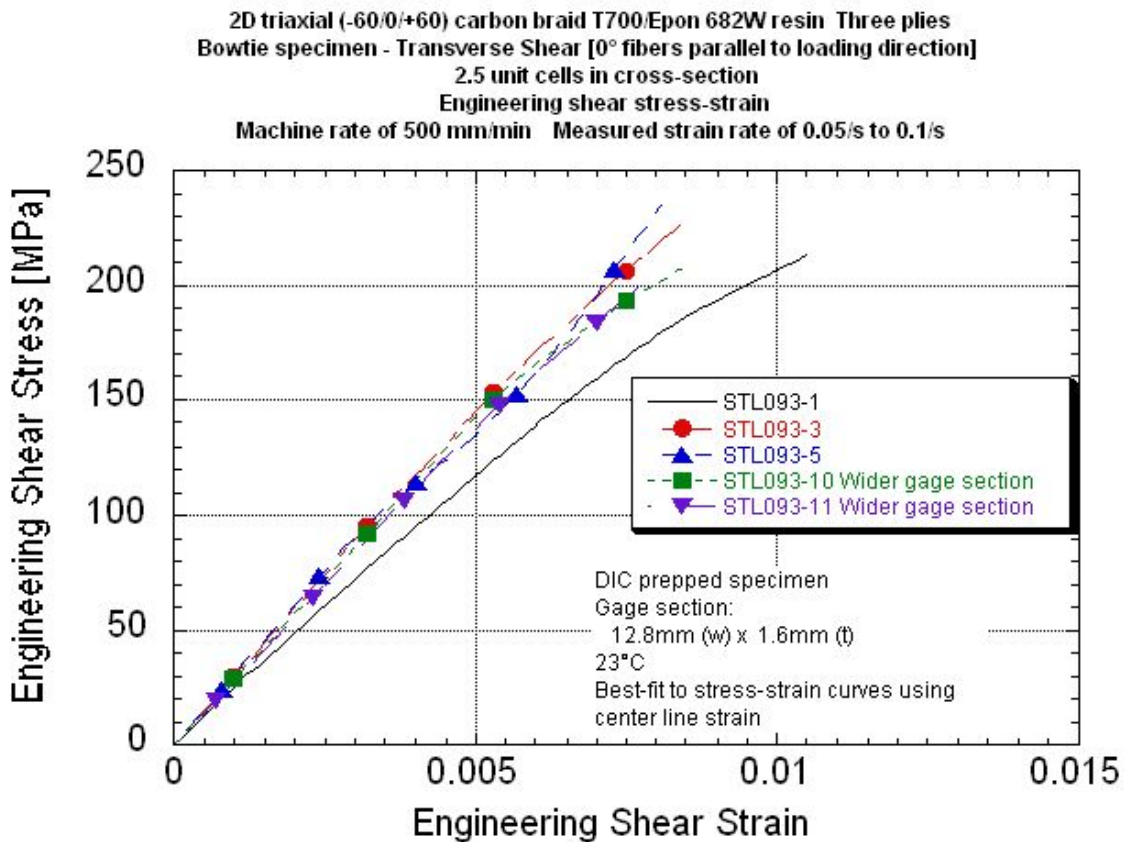
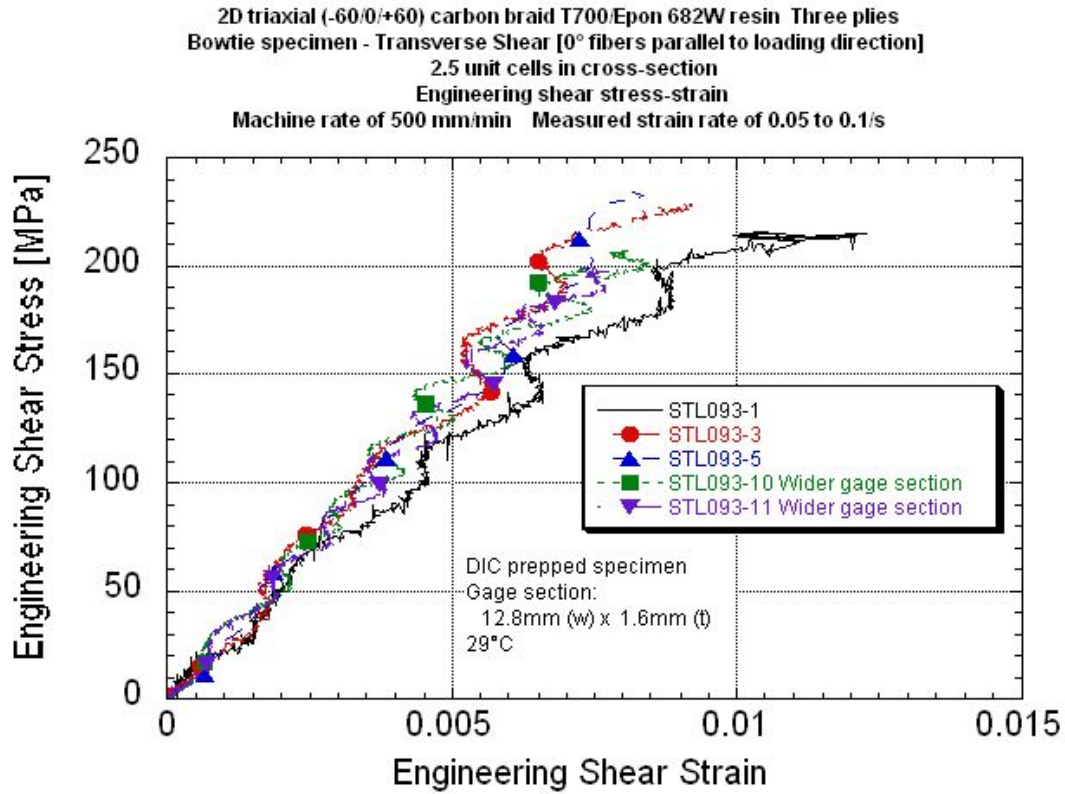
3) SEA for design purposes $E_s = \text{Work}(\text{displacement at peak} - \text{displacement at end})/(\text{mass of tube} \times \text{displacement at end})$ Adjusted for fan-fold length at 1.5 m/min.

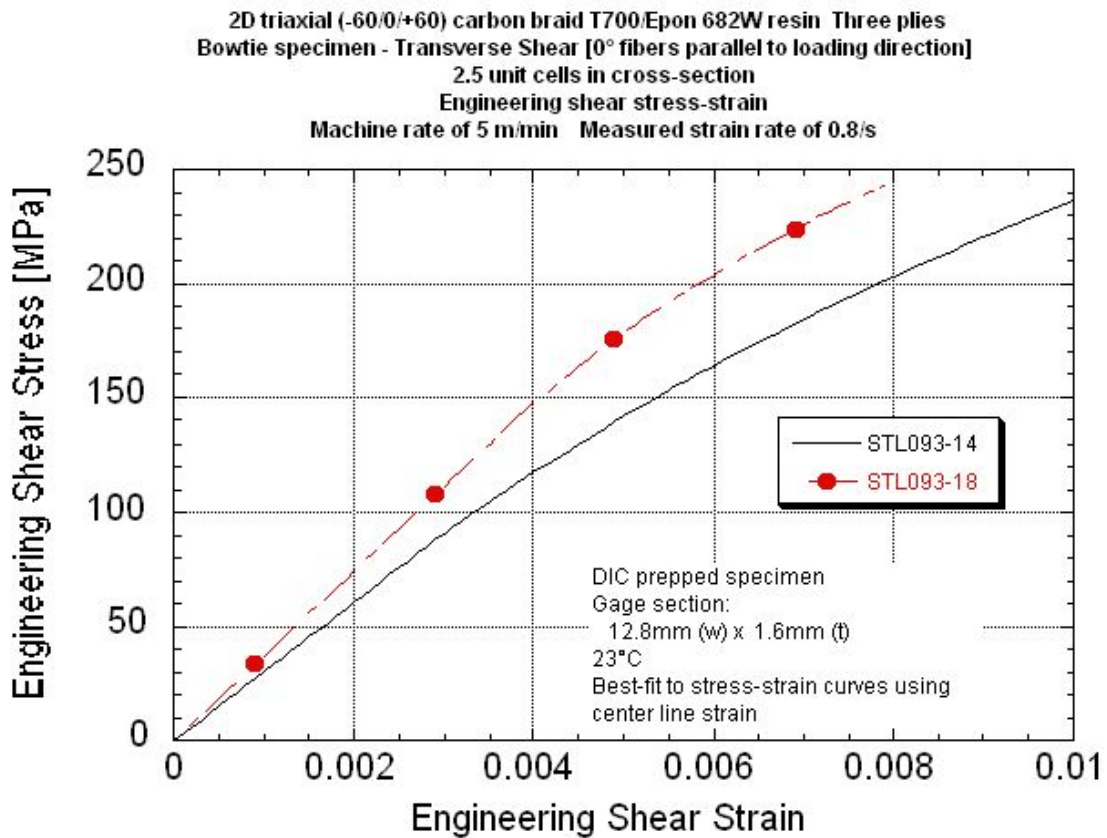
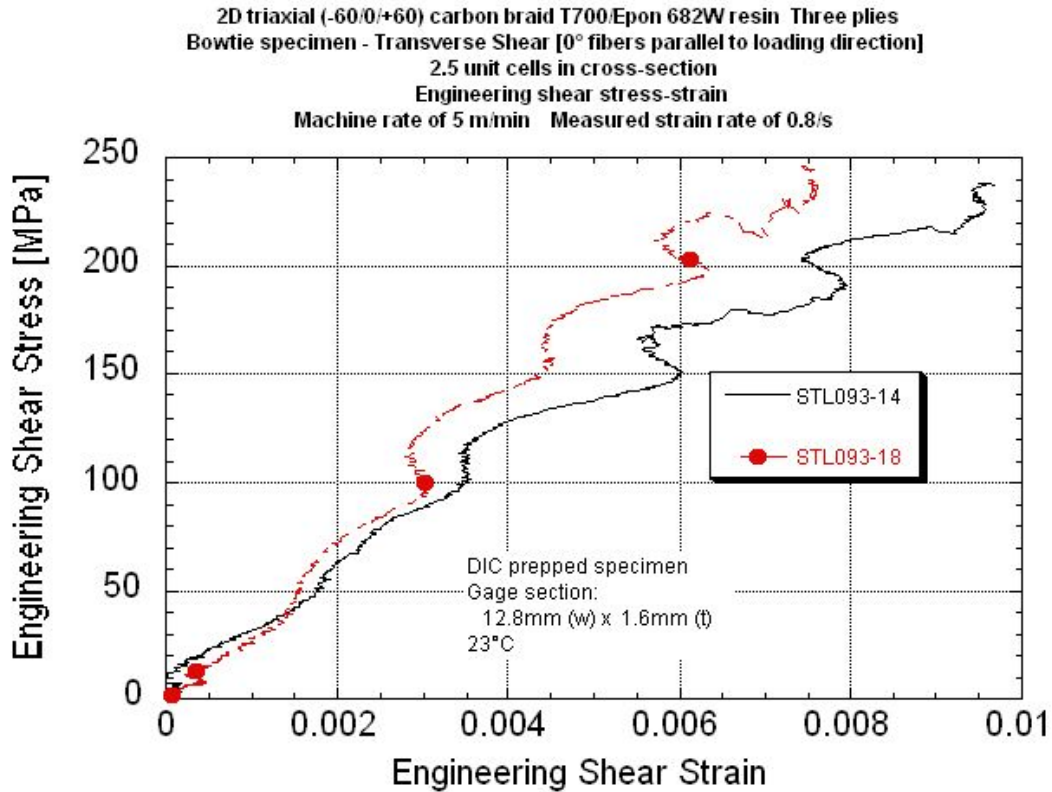
4) All but one of the specimens had the peak temperature exceed the calibration curve limit of 200°C. Peak data are estimated using the calibration correlation equation.

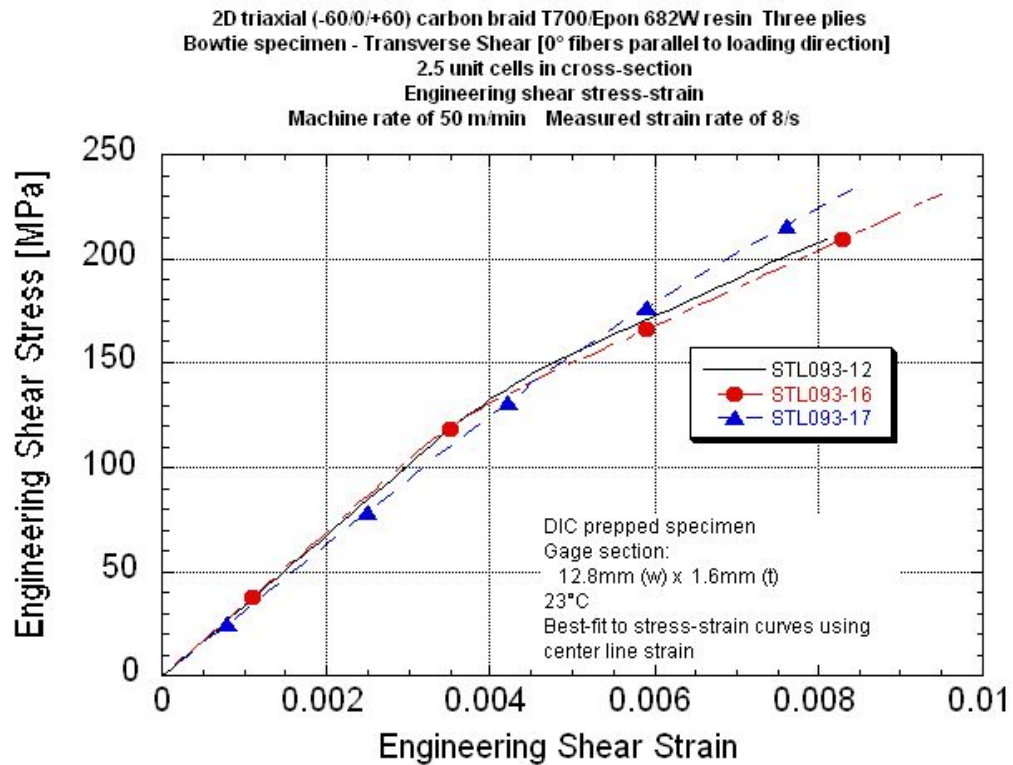
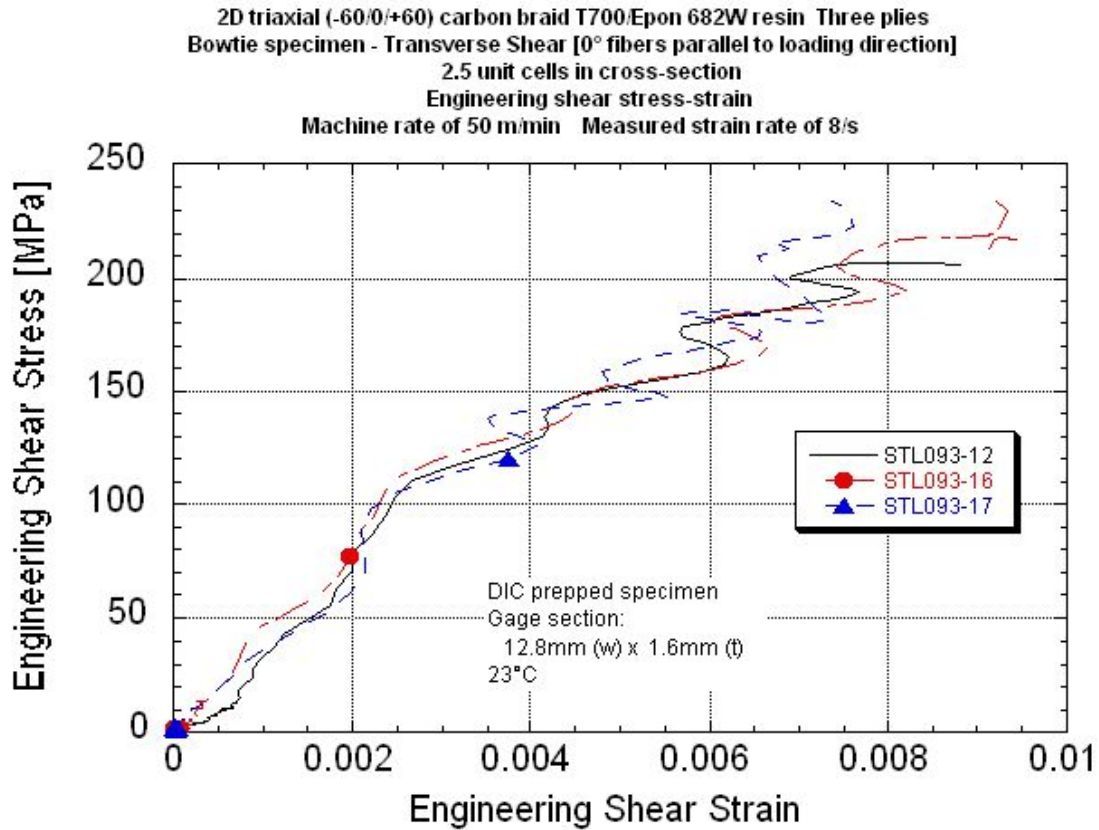
2D triaxial (-60/0/+60) carbon braid T700:Epon 682W resin Three plies
 Bowtie specimen - Transverse Shear [0° fibers parallel to loading direction]
 2.5 unit cells in cross-section
 Engineering shear stress-strain at all rates

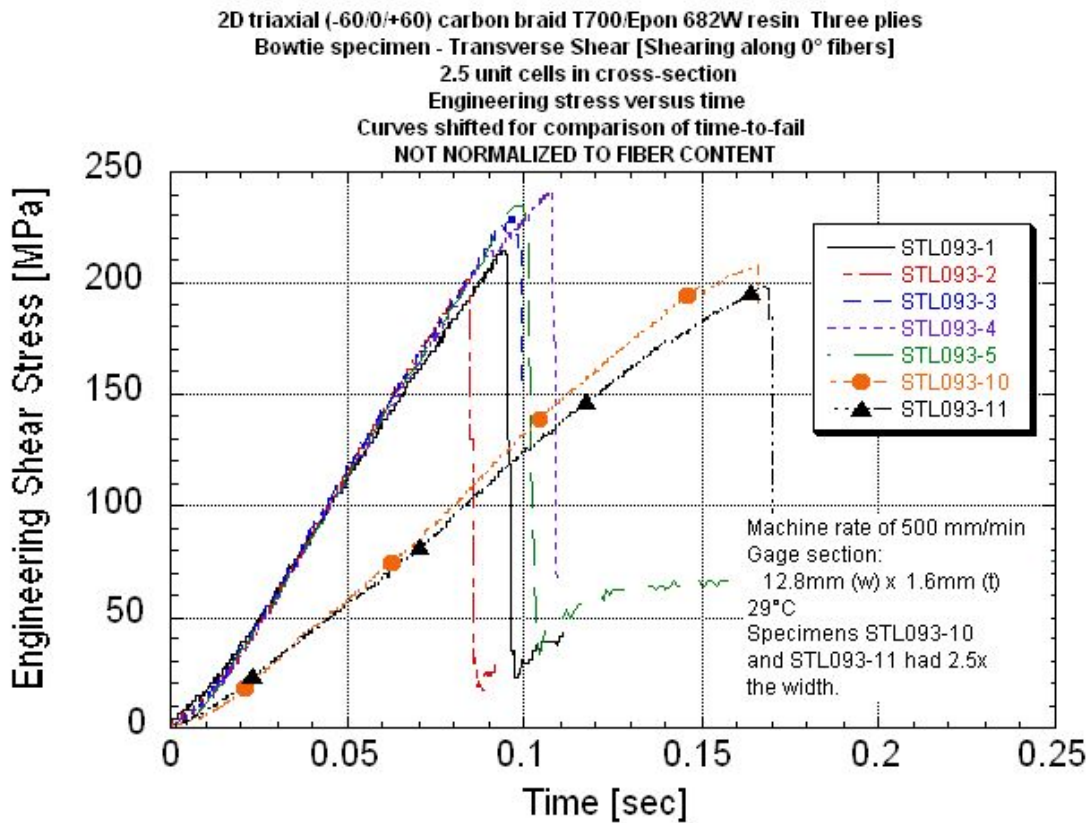
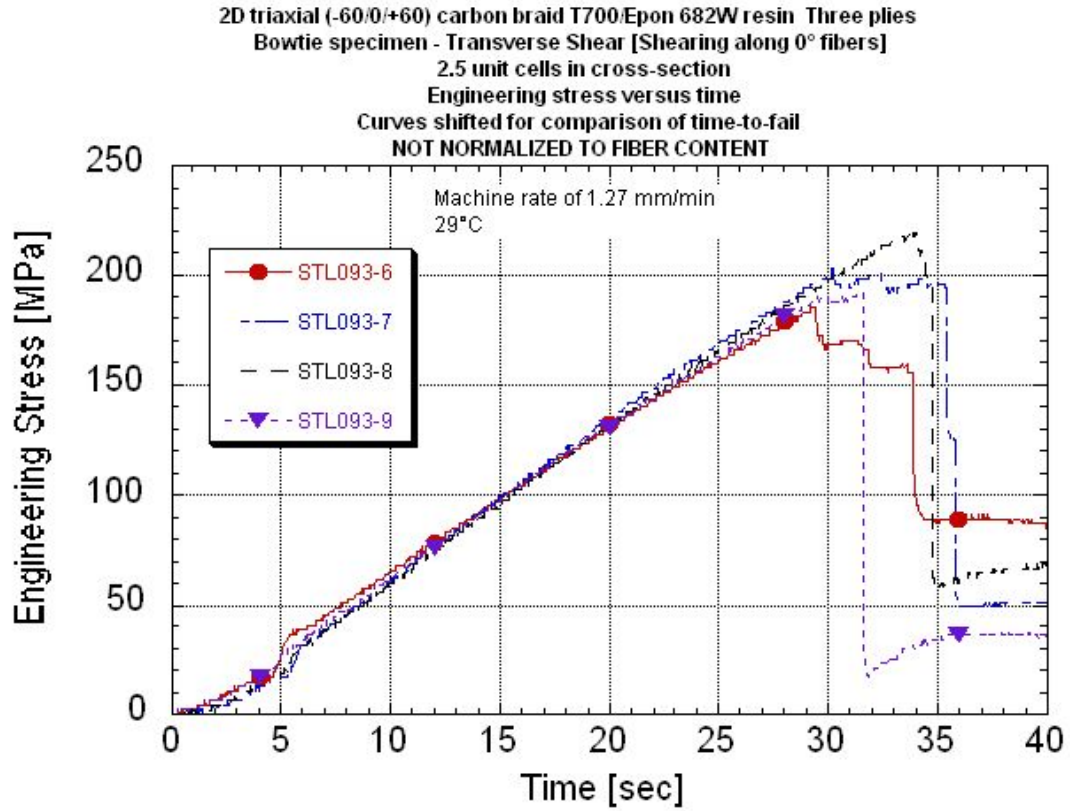


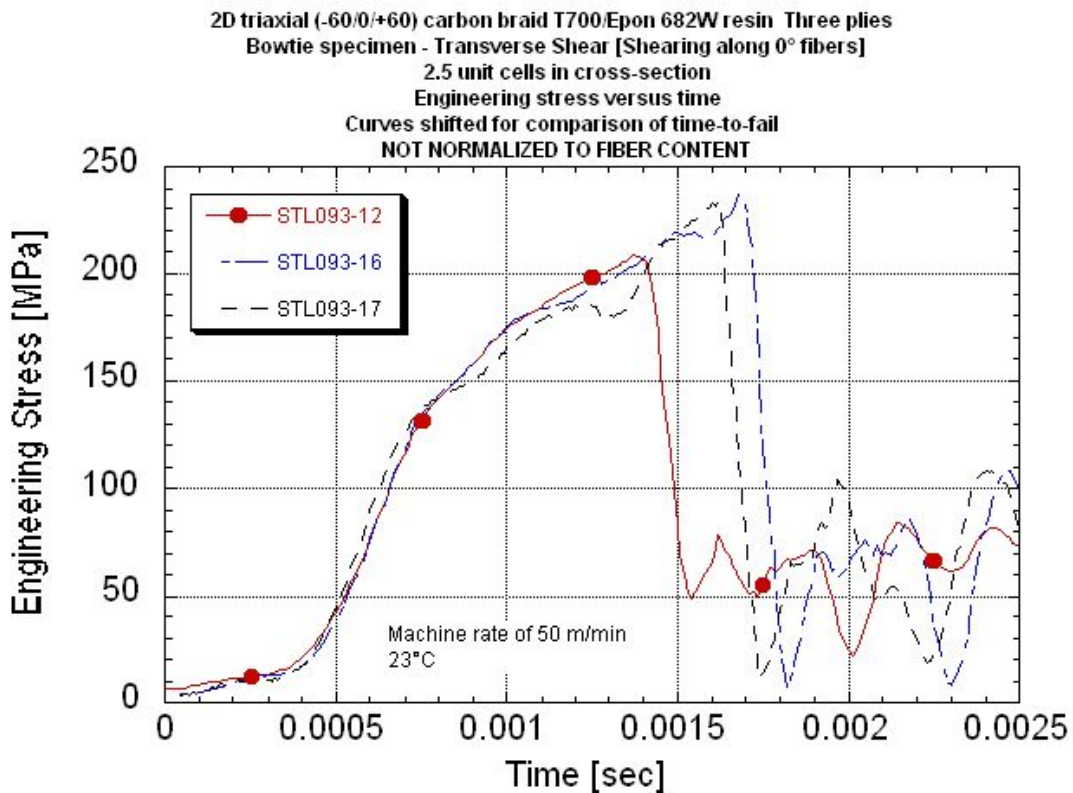
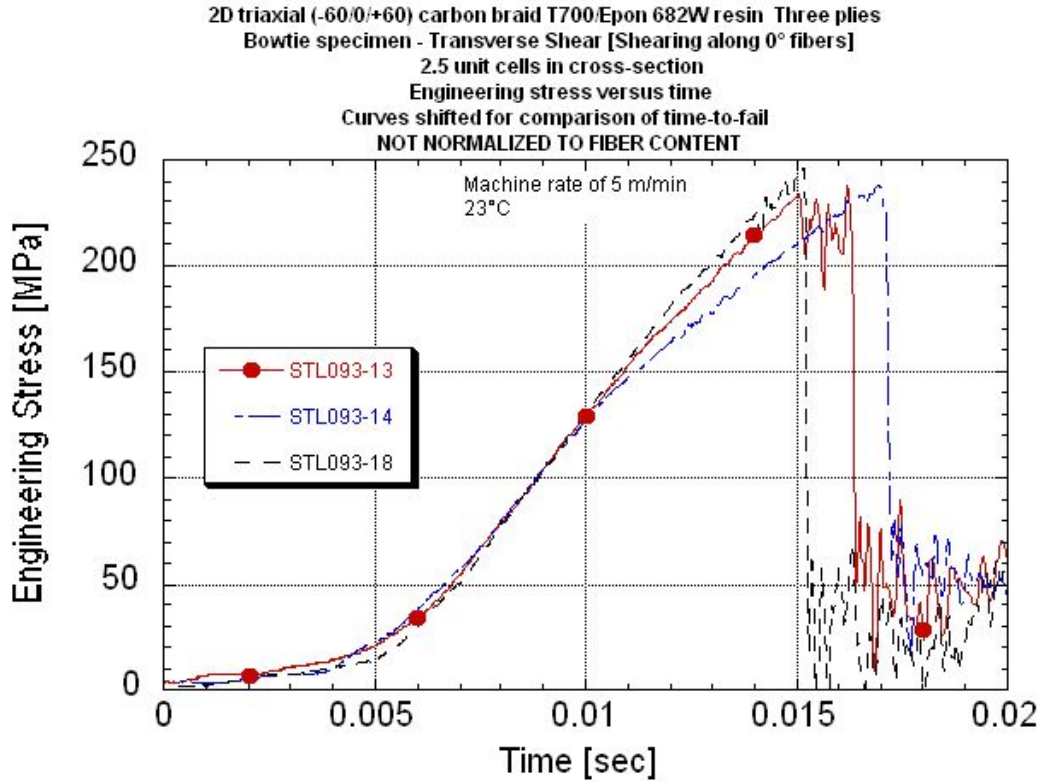












APPENDIX Q.

TUBE COMPRESSION DATA PACKAGE

Summary Table

Summary Plots

Investigation of Opportunities For Light-Weighting Vehicles Using Advanced Plastics And Composites

Transverse Shear⁽¹⁾Data Summary 2D Triaxial Carbon T700/ Epon862W Epoxy Braid Bowtie Specimen Configuration - 2.5 unit cells in reduced cross section Nominal center cross-section of 12.7mm wide x 1.65mm thick

	Panel ID	UDRI STL number	Center line length [mm]	Peak Stress [MPa]	Normalized Peak Stress to 56% Fiber Volume [MPa]	Engineering Breaking Strain [%]	Localized## Engineering Max Strain [%]	Localized## Engineering Min Strain [%]	Shear# Modulus [GPa]	Measured Strain Rate Before Failure [1/s]	Machine Rate [in/s]	Machine Rate [m/min]			
0.0003/s	073010-3 STB-5	093-6	9.32	186	175	0.711	-	-	32.6	0.000282	0.00084	0.00128			
	073010-4 STB-4	093-7	10.9	202	197	0.752	-	-	29.4	0.000276	0.00083	0.00127			
	073010-5 STB-4	093-8	-	218	216	-	-	-	-	-	0.00083	0.00127	No DIC data		
	073010-5 STB-5	093-9	9.39	193	191	0.783	-	-	25.7	0.000283	0.00083	0.00127			
		Average		200	195	0.749			29.2						
		Standard Deviation		14	17	0.036			3.5						
		COV [%]		7.02	8.76	4.82			11.9						
0.05 to 0.1/s	073010-5 STB-6	093-1	8.51	214	212	1.05	-	-	25.3	0.118	0.320	0.487			
	073010-5 STB-3	093-2	-	201	199	-	-	-	-	-	0.335	0.510	No DIC data		
	073010-5 STB-2	093-3	7.88	228	226	0.901	-	-	30.0	0.095	0.335	0.510			
	073010-4 STB-3	093-4	-	242	236	-	-	-	-	-	0.335	0.510	No DIC data		
	073010-4 STB-1	093-5	7.37	235	229	0.824	-	-	30.6	0.102	0.335	0.510			
	073010-3 STB-4	093-10	21.0	208	196	0.814	-	-	28.8	0.0559	0.341	0.520	Wider center section		
			073010-3 STB-3	093-11	24.5	198	187	0.737	1.05	0.52	28.0	0.0496	0.336	0.511	Wider center section
		Average		218	212	0.864			28.5						
		Standard Deviation		17	19	0.117			2.1						
		COV [%]		7.86	8.87	13.5			7.28						
0.8/s	073010-6 STB-Y-1	093-13	7.34	233	228	-	-	-	-	-	3.26	4.96	Issues with DIC		
	073010-6 STB-Y-2	093-14	7.31	238	232	0.958	1.33	0.93	28.7	0.812	3.26	4.96			
	073010-4 STB-2	093-18	7.62	246	240	0.759	0.80	0.63	37.2	0.753	3.26	4.97			
		Average		239	233	0.858			32.9						
		Standard Deviation		6	6										
		COV [%]		2.66	2.61										
8/s	073010-6 STB-Y-3	093-12	7.67	208	203	0.883	-	-	33.9	7.49	31.8	48.4	Note 1		
	073010-3 STB-3	093-16	8.20	237	224	0.937	0.96	-	34.6	7.73	31.9	48.6	Note 1		
	073010-3 STB-1	093-17	7.62	233	220	0.755	-	-	31.6	7.97	32.4	49.3	Note 1		
		Average		226	216	0.858			33.4						
		Standard Deviation		16	11	0.093			1.6						
		COV [%]		7.02	5.1	10.9			4.8						

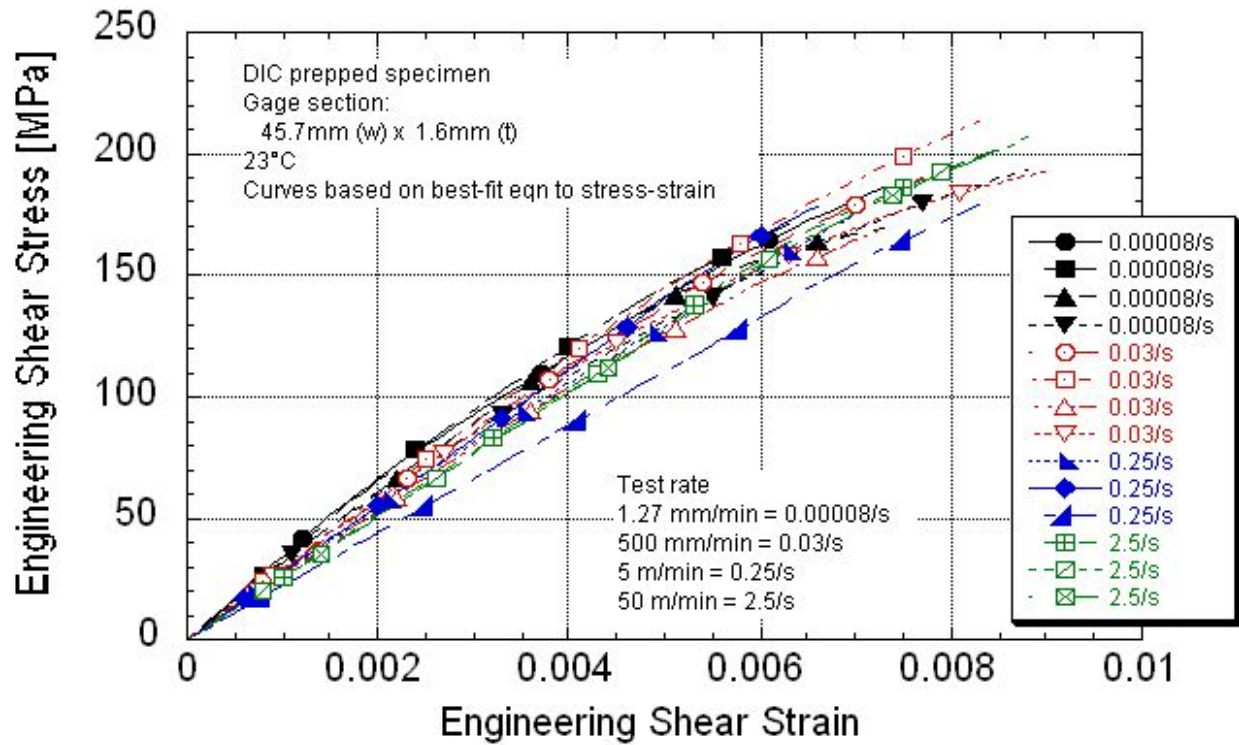
(1) Shear through the short side (5mm) of the unit cell. 0° fibers parallel to loading direction.

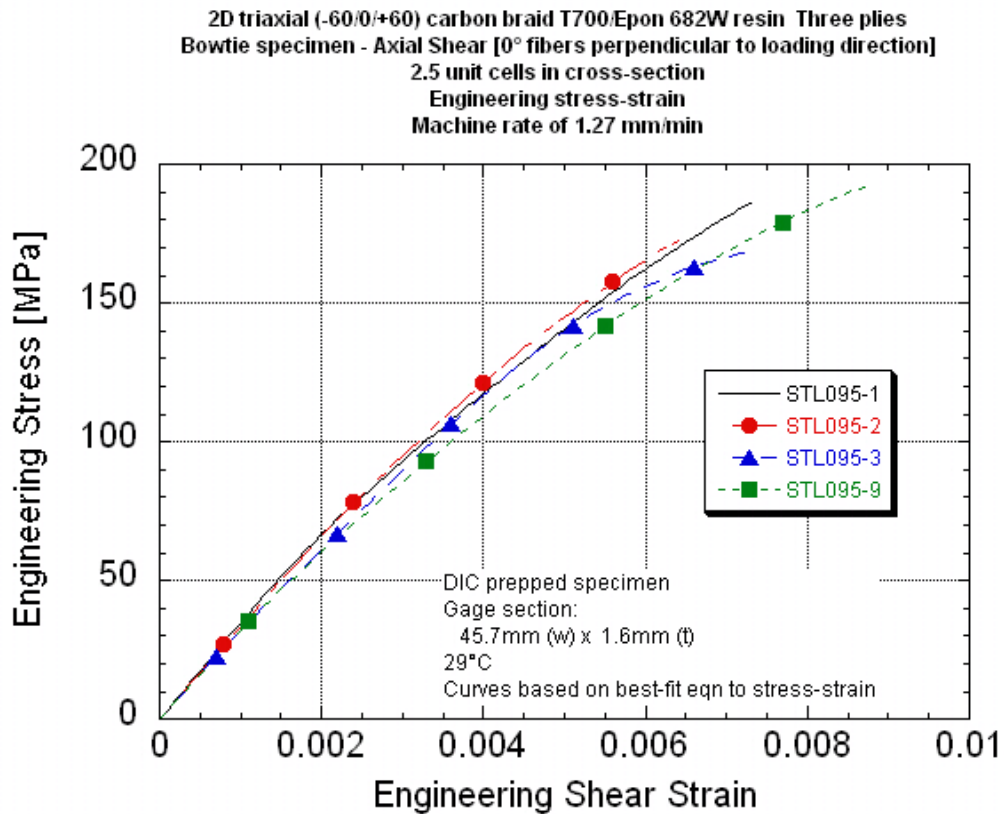
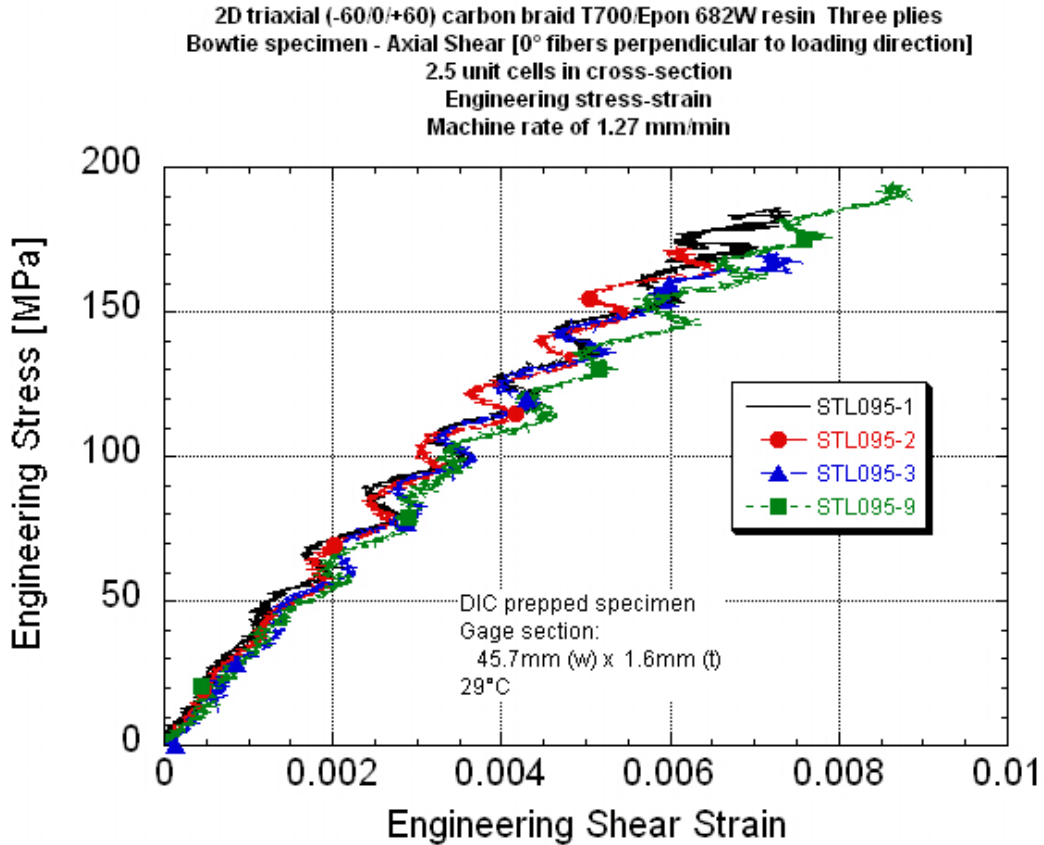
#Based on center line strain. ## Strain as measured at a region of high strain on a fiber braid and low strain in center. Strain data from the onset of cracking and final break.

Specimen thickness varied due to the braid structure. Thickness was measured at two "peak" and two "valley" locations and averaged.

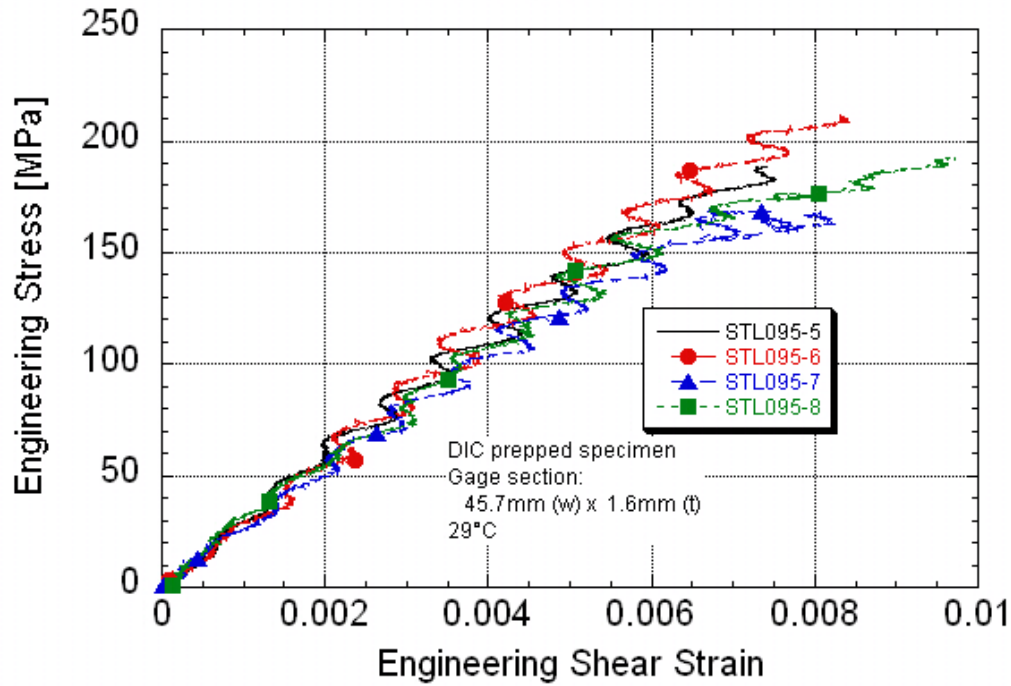
Note 1 Three to four low amplitude system resonant waves in stress response before failure. Failure stress at break depended on when failure occurred, i.e., in the peak or valley of a stress wave.

2D triaxial (-60/0/+60) carbon braid T700/Epon 682W resin Three plies
 Bowtie specimen - Axial Shear [0° fibers perpendicular to loading direction]
 2.5 unit cells in cross-section
 Engineering shear stress-strain at all rates

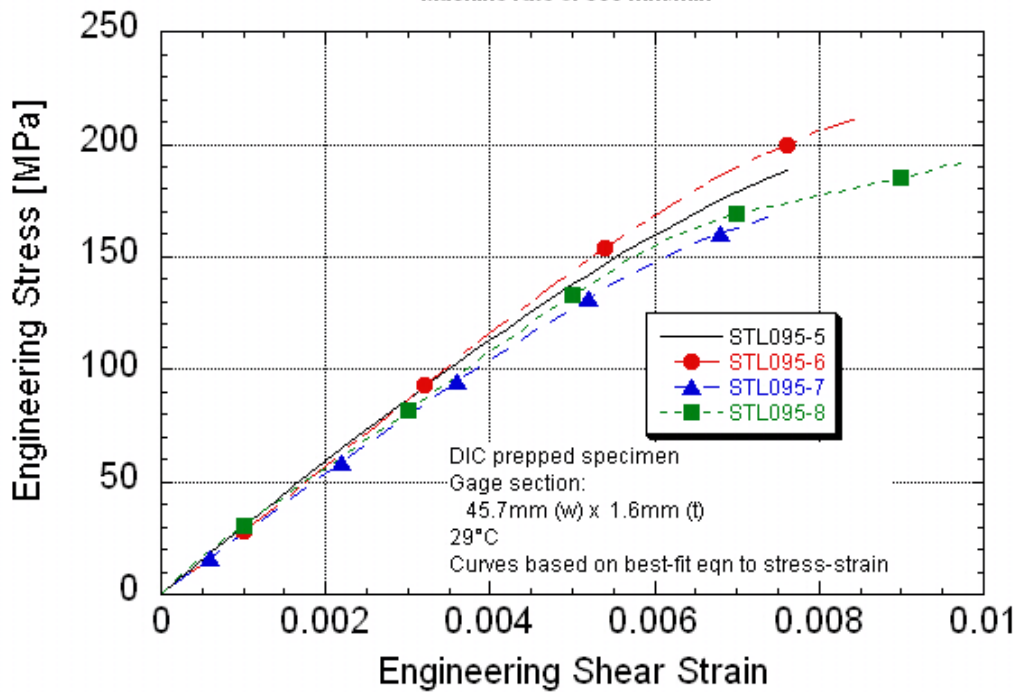




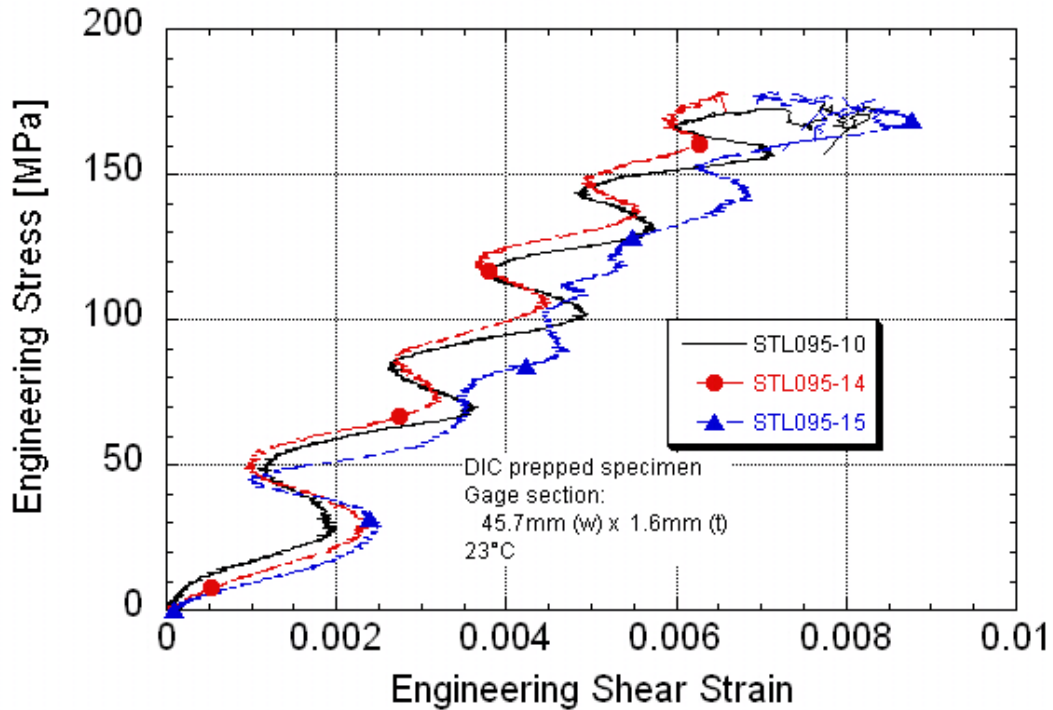
2D triaxial (-60/0/+60) carbon braid T700/Epon 682W resin Three plies
 Bowtie specimen - Axial Shear [0° fibers perpendicular to loading direction]
 2.5 unit cells in cross-section
 Engineering stress-strain
 Machine rate of 500 mm/min



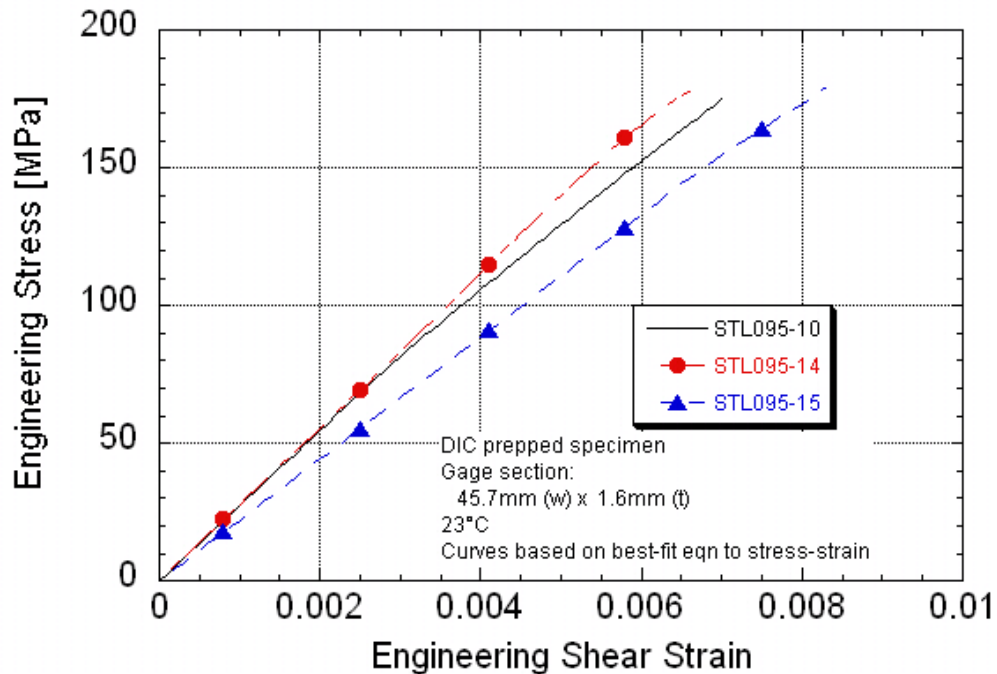
2D triaxial (-60/0/+60) carbon braid T700/Epon 682W resin Three plies
 Bowtie specimen - Axial Shear [0° fibers perpendicular to loading direction]
 2.5 unit cells in cross-section
 Engineering stress-strain
 Machine rate of 500 mm/min



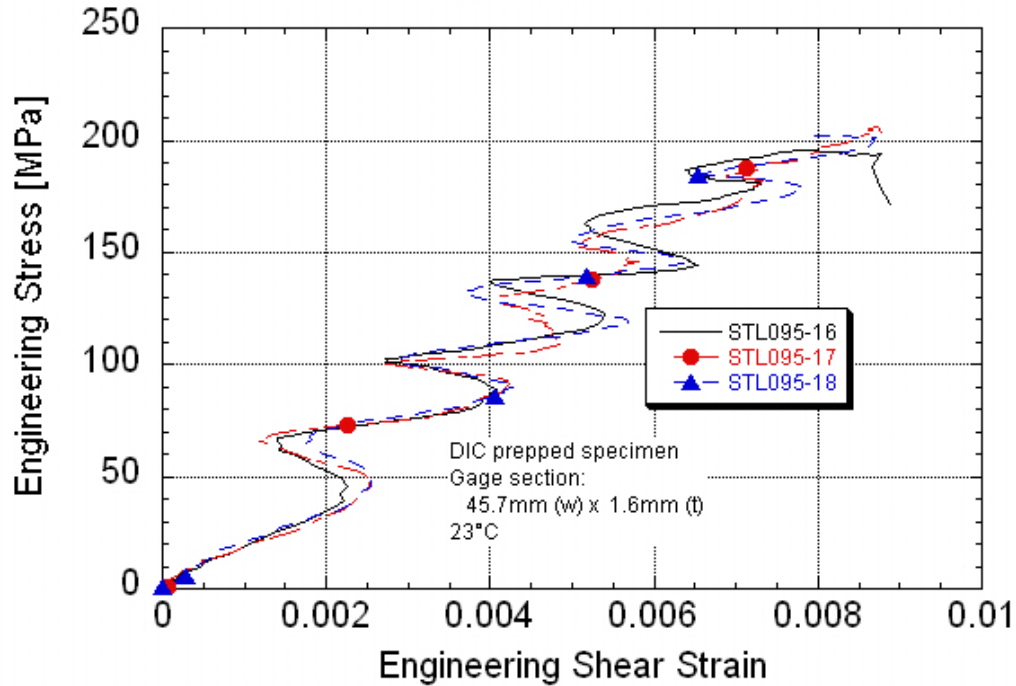
2D triaxial (-60/0/+60) carbon braid T700/Epon 682W resin Three plies
 Bowtie specimen - Axial Shear [0° fibers perpendicular to loading direction]
 2.5 unit cells in cross-section
 Engineering stress-strain
 Machine rate of 5 m/min



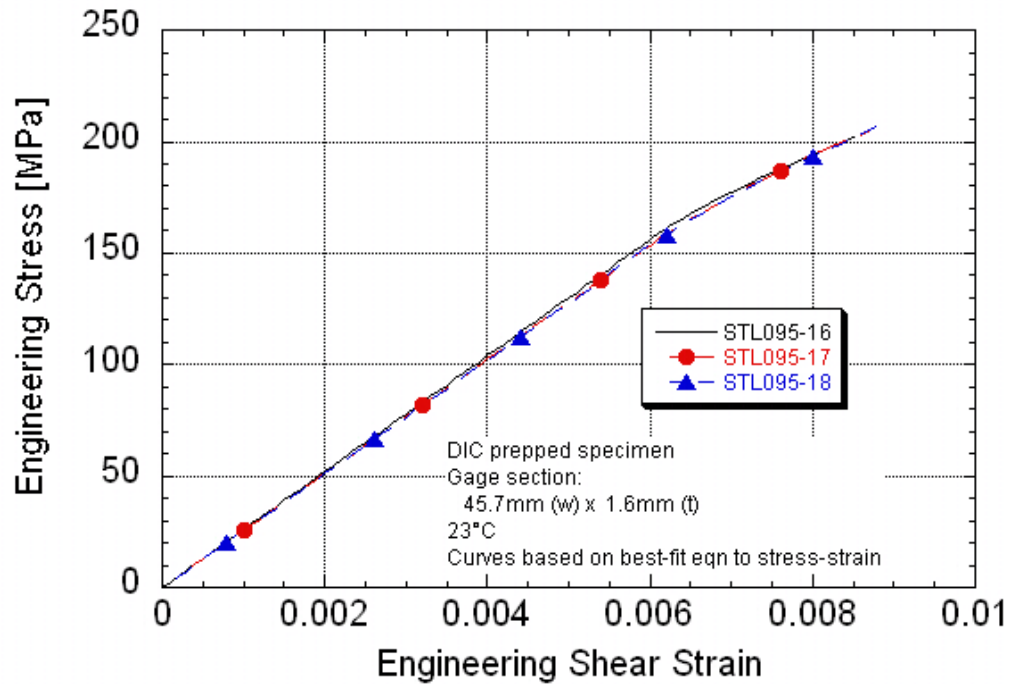
2D triaxial (-60/0/+60) carbon braid T700/Epon 682W resin Three plies
 Bowtie specimen - Axial Shear [0° fibers perpendicular to loading direction]
 2.5 unit cells in cross-section
 Engineering stress-strain
 Machine rate of 5 m/min

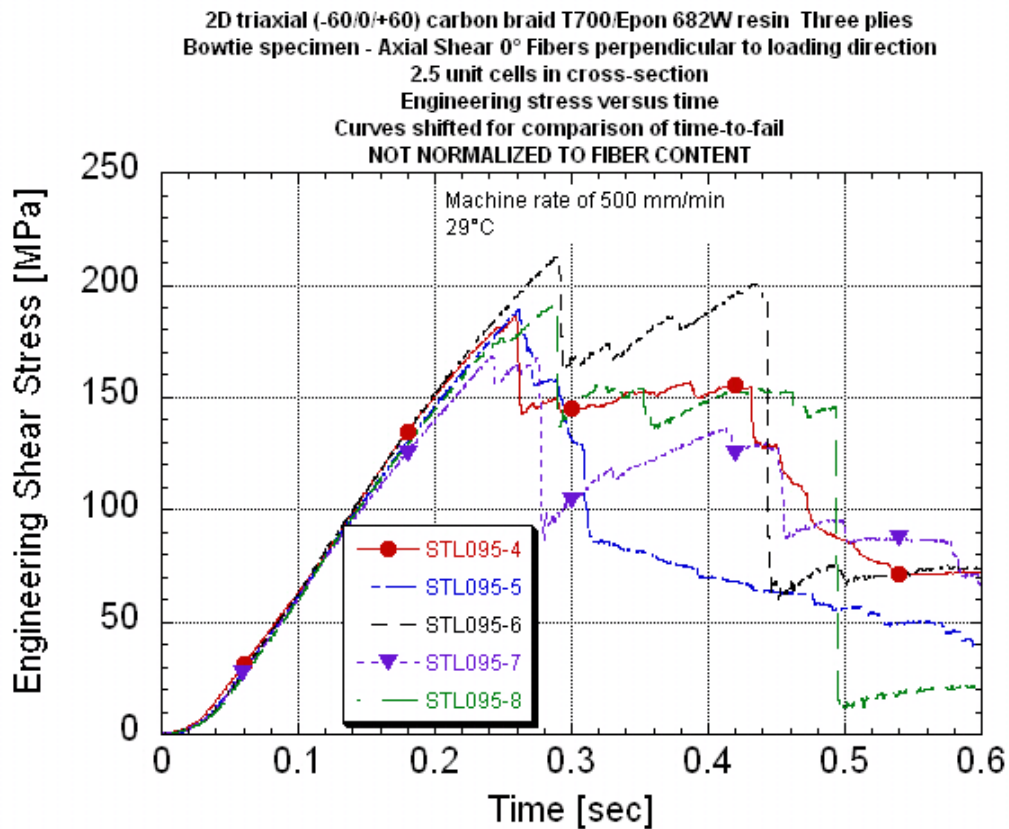
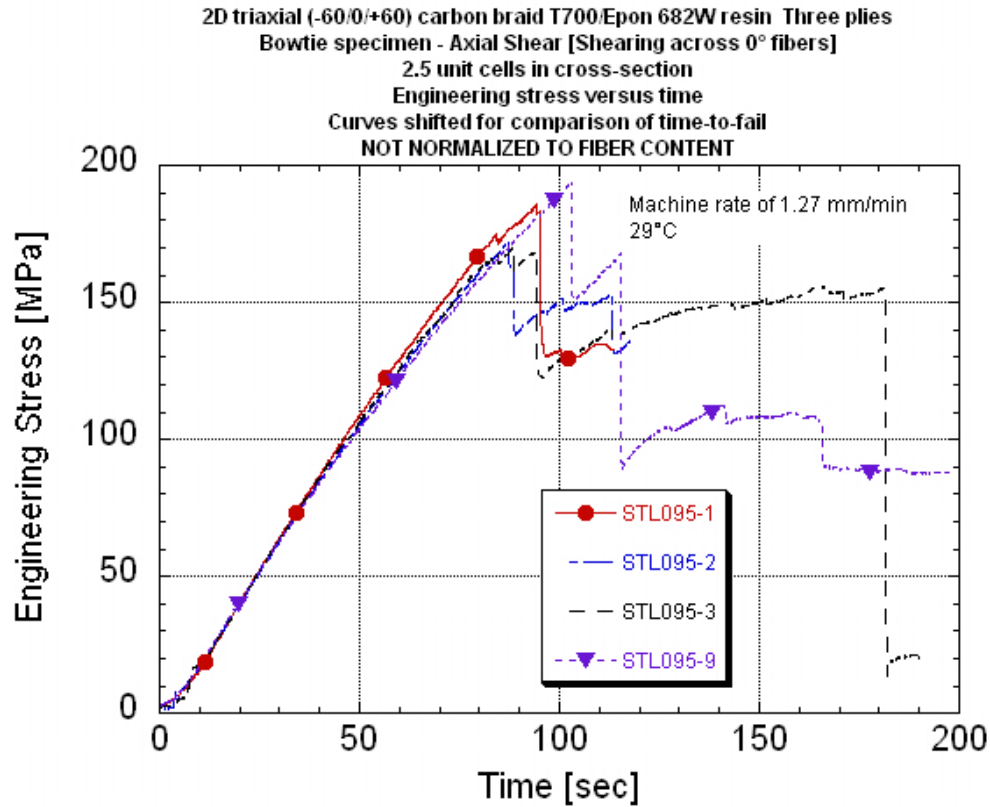


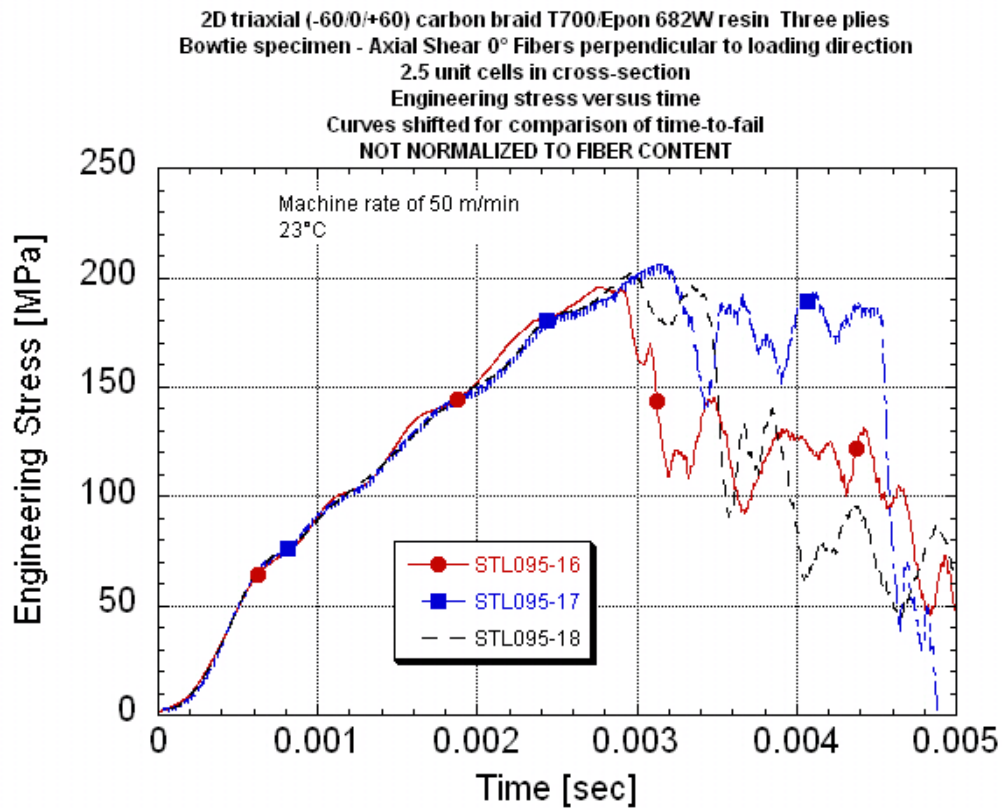
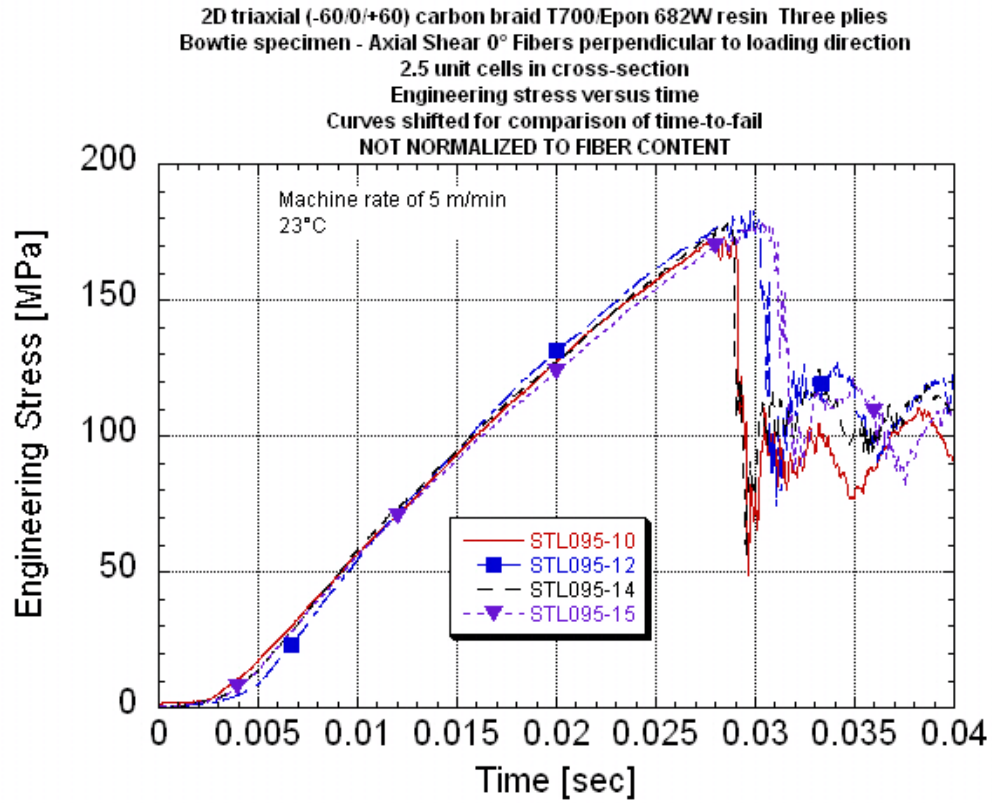
2D triaxial (-60/0/+60) carbon braid T700/Epon 682W resin Three plies
 Bowtie specimen - Axial Shear [0° fibers perpendicular to loading direction]
 2.5 unit cells in cross-section
 Engineering stress-strain
 Machine rate of 50 m/min



2D triaxial (-60/0/+60) carbon braid T700/Epon 682W resin Three plies
 Bowtie specimen - Axial Shear [0° fibers perpendicular to loading direction]
 2.5 unit cells in cross-section
 Engineering stress-strain
 Machine rate of 50 m/min







APPENDIX P.

TRANSVERSE SHEAR DATA PACKAGE

Shearing along 0° Fibers

Summary Table

Summary Stress-strain Plots With Rate

Summary Stress-time Plots With Rate

Investigation of Opportunities For Light-Weighting Vehicles Using Advanced Plastics And Composites

**Axial Shear⁽¹⁾ Data Summary
 2D Triaxial Carbon T700/ Epon862W Epoxy Braid
 Bowtie Specimen Configuration - 2.5 unit cells in reduced cross section
 Nominal center cross-section of 46mm wide x 1.65mm thick**

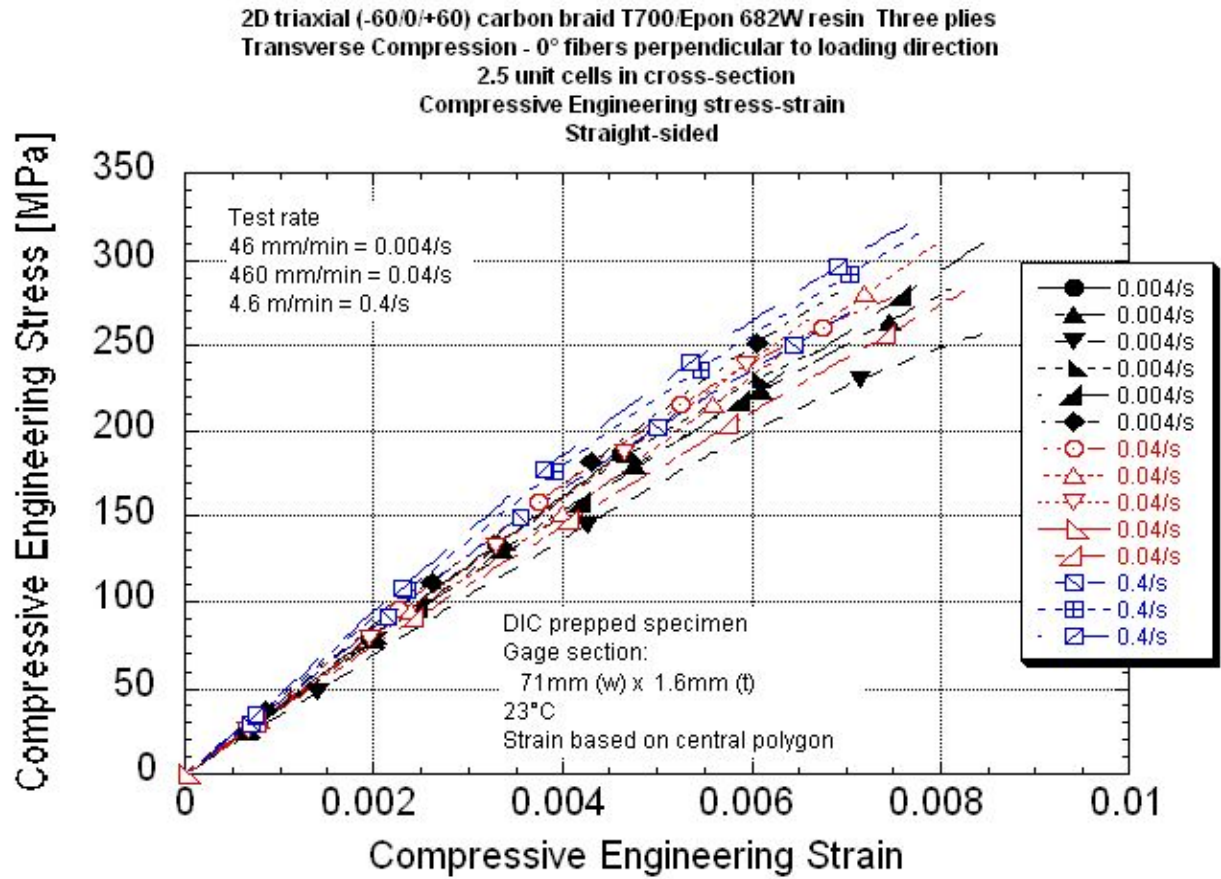
	Panel ID	UDRI STL number	Center line/polygon length [mm]	Peak Stress [MPa]	Normalized Peak Stress to 56% Fiber Volume [MPa]	Engineering Breaking Strain # [%]	Localized## Engineering Max Strain [%]	Localized## Engineering Min Strain [%]	Shear Modulus Based on Center Line [GPa]	Measured Strain Rate	Machine Rate [in/s]	Machine Rate [m/min]	
0.00008/s	073010-4 SAB-4	095-1	37.4	186	181	0.724	0.963	0.700	34.7	0.000089	0.00083	0.00127	
	073010-4 SAB-6	095-2	27.8	172	167	0.638	0.947	0.400	33.4	0.000077	0.00083	0.00127	
	073010-4 SAB-3	095-3	26.7x5.71	170	166	0.780	1.07	0.491	31.4	0.000076	0.00083	0.00127	Final failure at 1.22%
	073010-5 SAB-4	095-9	28.9	193	192	0.876	1.29	0.742	32.2	0.000085	0.00083	0.00127	
		Average		180	177	0.755	1.07	0.583	32.9				
		Standard Deviation		11	12	0.100	0.16	0.164	1.45				
		COV [%]		6.30	7.01	13.2	14.6	28.2	4.40				
0.03/s	073010-4 SAB-5	095-4	-	186	182	-	-	-	-	-	0.334	0.509	No DIC data
	073010-5 SAB-9	095-5	23.1	189	188	0.786	-	-	28.9	0.0339	0.334	0.509	
	073010-5 SAB-1	095-6	29.6	213	211	0.846	1.02	0.726	28.5	0.0318	0.335	0.510	
	073010-5 SAB-2	095-7	30.4	168	167	0.723	0.934	0.608	26.8	0.0339	0.326	0.497	
	073010-5 SAB-3	095-8	30.7	192	190	0.980	1.11	-	29.8	0.0330	0.333	0.508	Final failure at 1.63%
		Average		190	188	0.834	1.02	0.667	28.5				
		Standard Deviation		16	16	0.109	0.088		1.24				
		COV [%]		8.40	8.54	13.1	8.6		4.35				
0.25/s	073010-5 SAB-5	095-10	27.4	173	171	0.682	-	-	27.1	0.279	3.26	4.96	
	073010-5 SAB-7	095-12	-	177	176	-	-	-	-	-	3.26	4.96	No DIC data
	073010-4 SAB-1	095-14	27.0	179	174	0.642	0.960	-	27.3	0.240	3.26	4.97	
	073010-5 SAB-8	095-15	27.4	178	176	0.842	-	-	22.2	0.260	3.27	4.98	
		Average		177	174	0.722			25.5				
		Standard Deviation		3	2	0.106			2.91				
		COV [%]		1.48	1.29	14.7			11.4				
2.5/s	072910-01 SAB-21	095-16	27.8	196	193	0.811	-	-	27.0	2.60	32.3	49.3	Note 1
	072910-01 SAB-24	095-17	28.0	202	199	0.871	-	-	25.6	2.50	32.2	49.1	No DIC data. Note 1
	072910-01 SAB-22	095-18	28.2	206	203	0.842	-	-	25.5	2.47	32.4	49.4	Note 1
		Average		201	199	0.841			26.0				
		Standard Deviation		5	5	0.03			0.84				
		COV [%]		2.58	2.58	3.57			3.24				

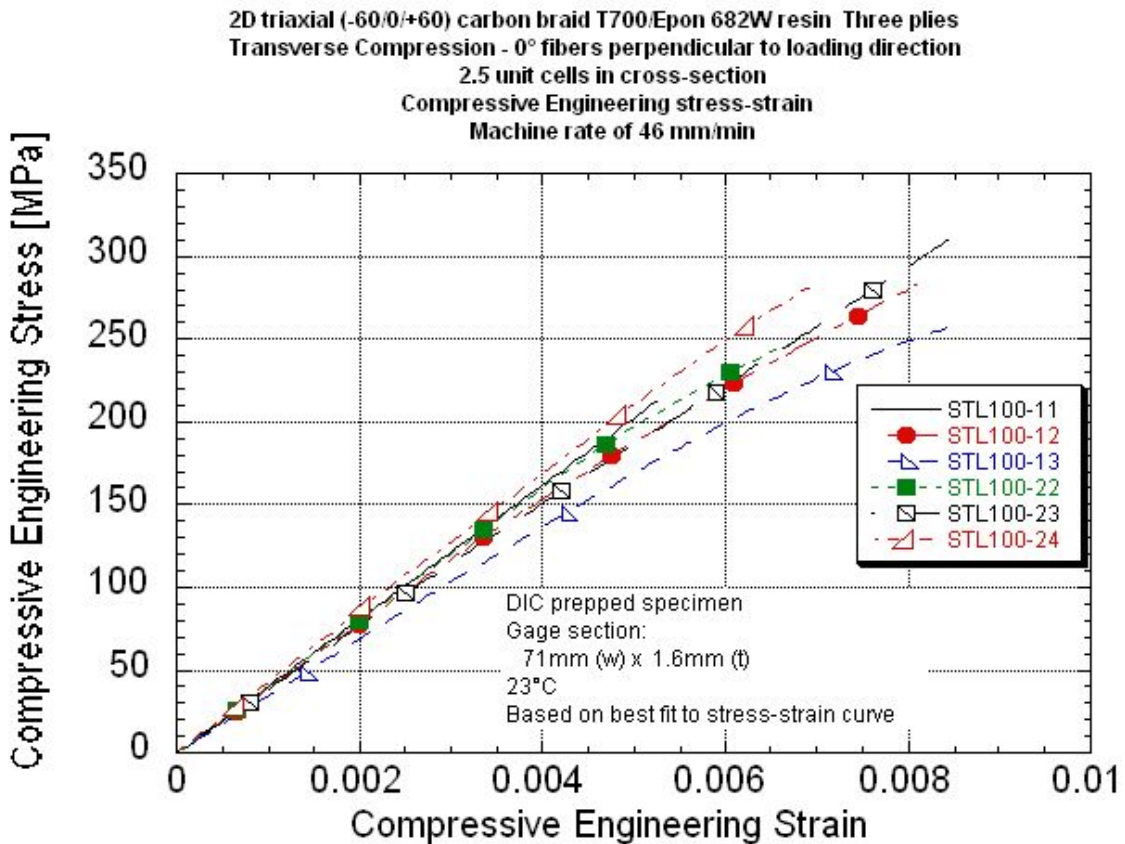
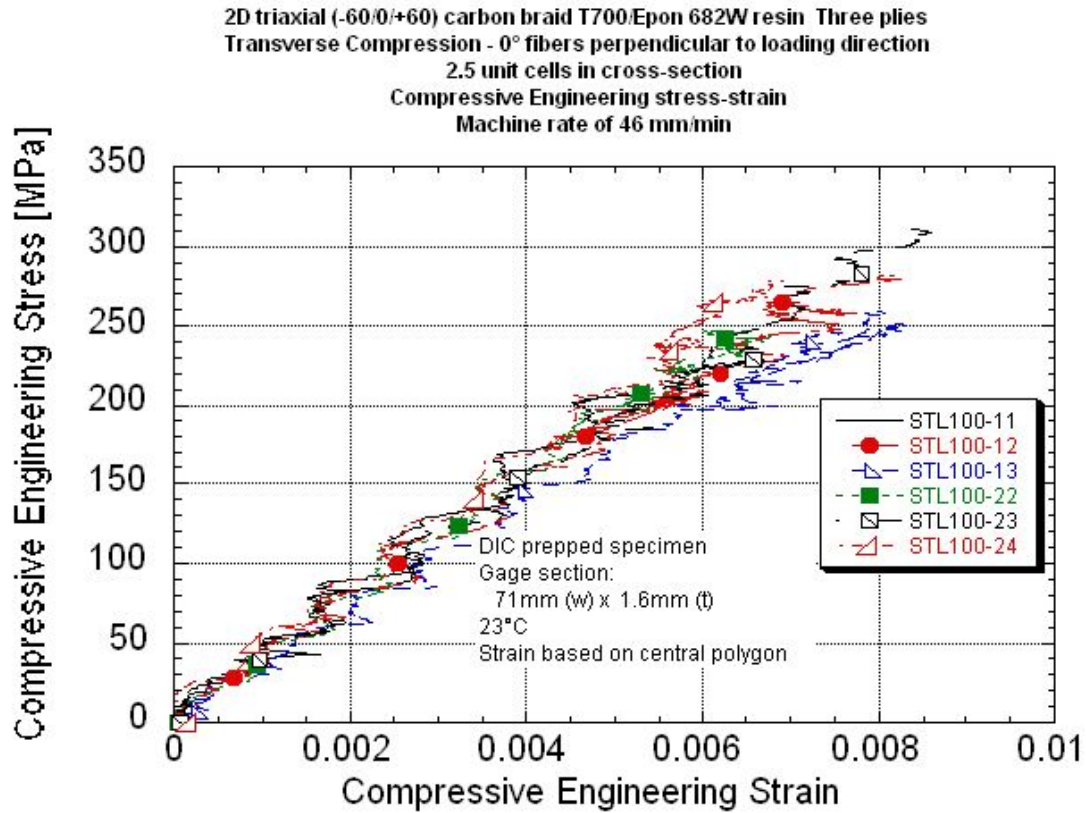
(1) Shear through the long side (18mm) of the unit cell. 0° fibers perpendicular to loading direction.

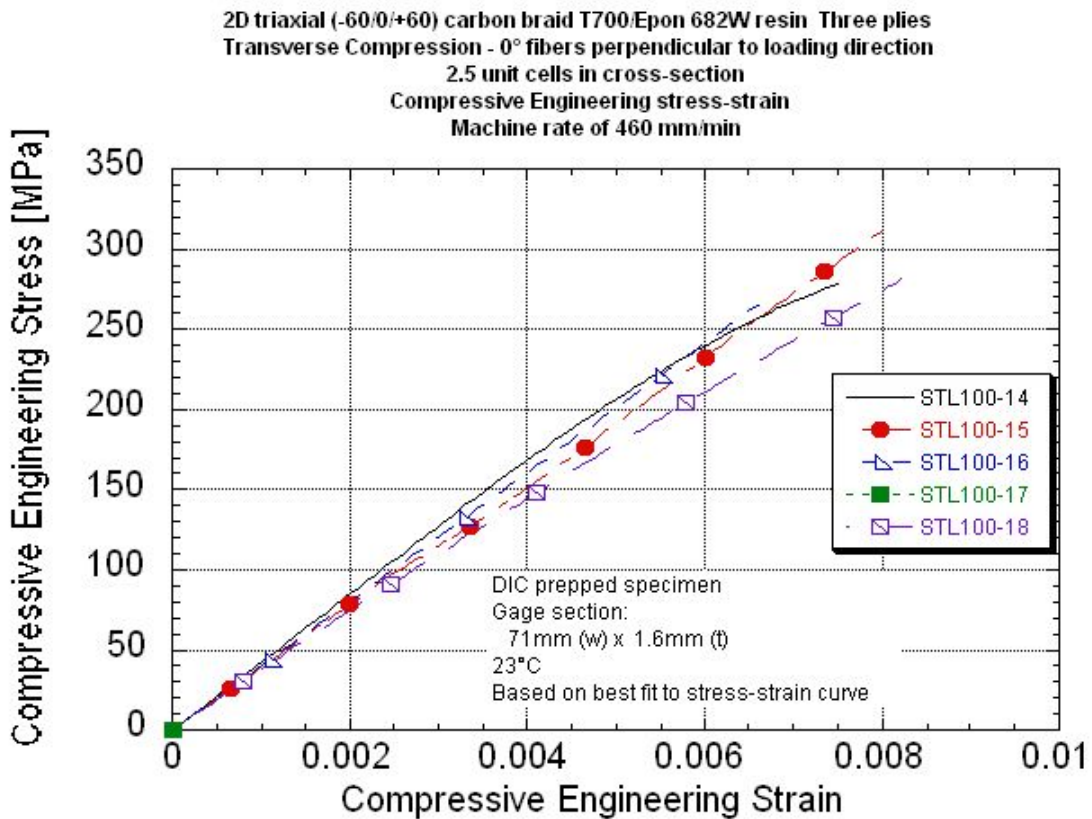
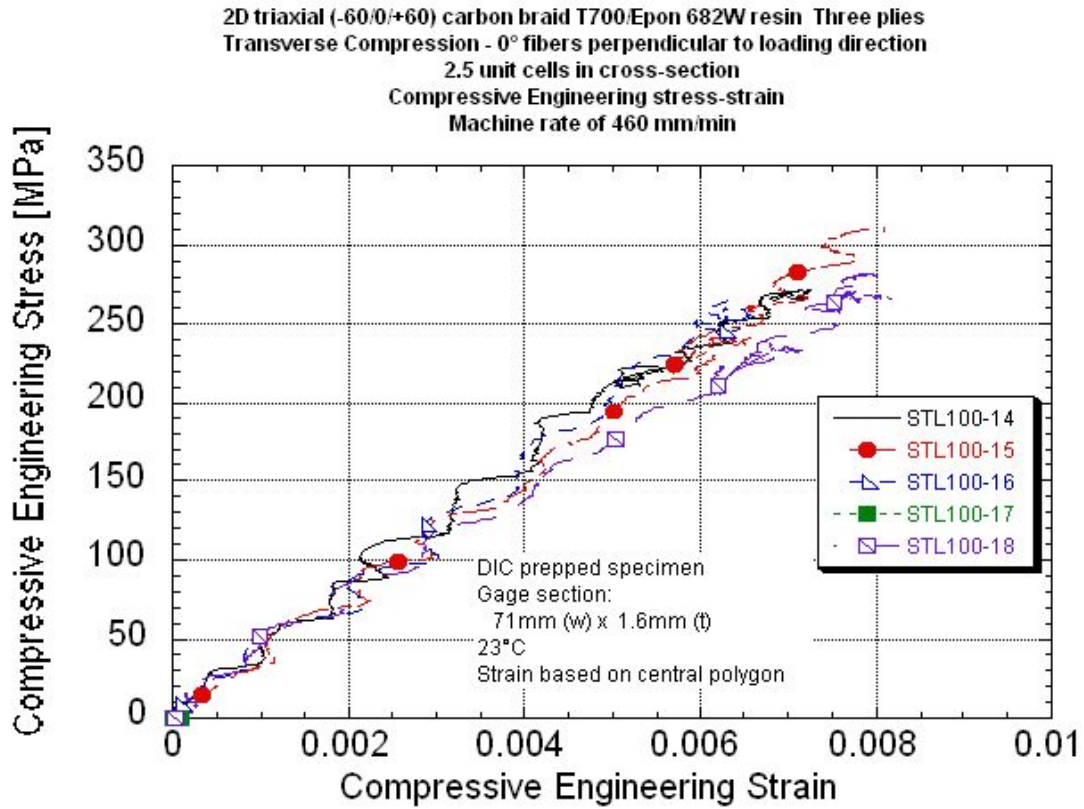
#Based on center line ## Strain as measured at a region of high strain on a fiber braid and low strain in center. Breaking strain taken at first large drop in stress.

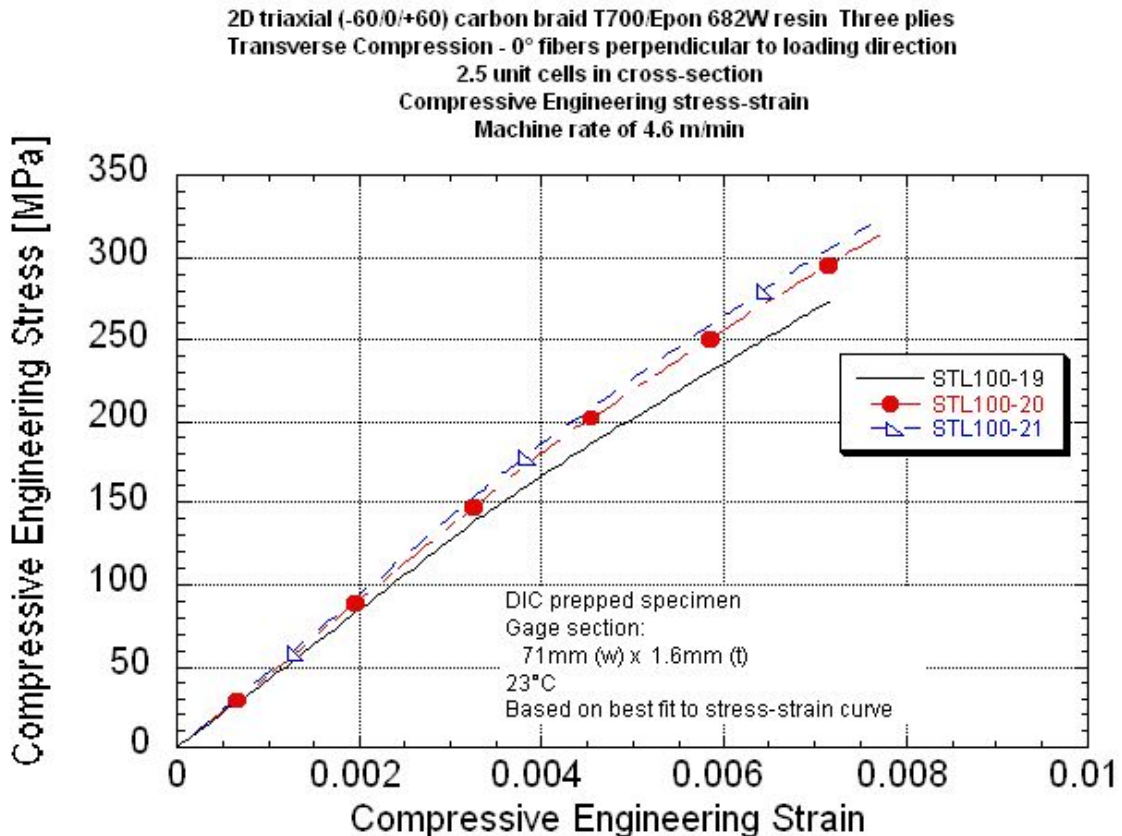
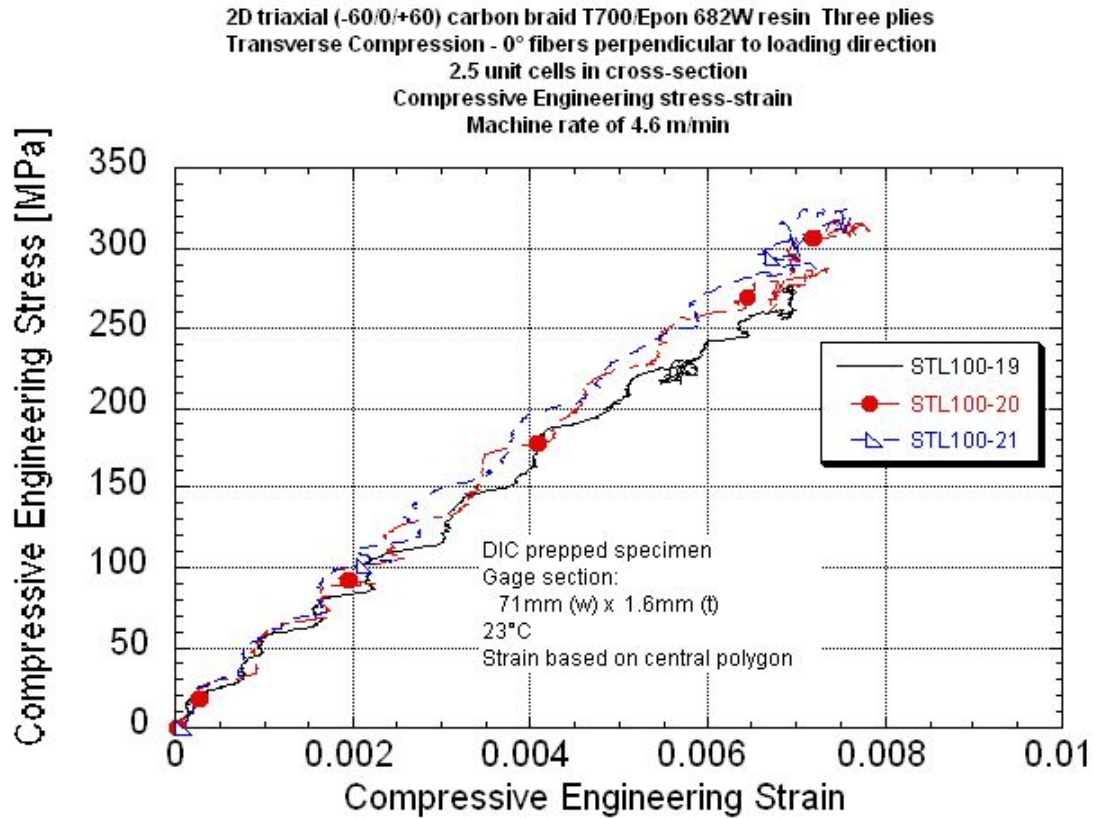
Specimen thickness varied due to the braid structure. Thickness was measured at two "peak" and two "valley" locations and averaged.

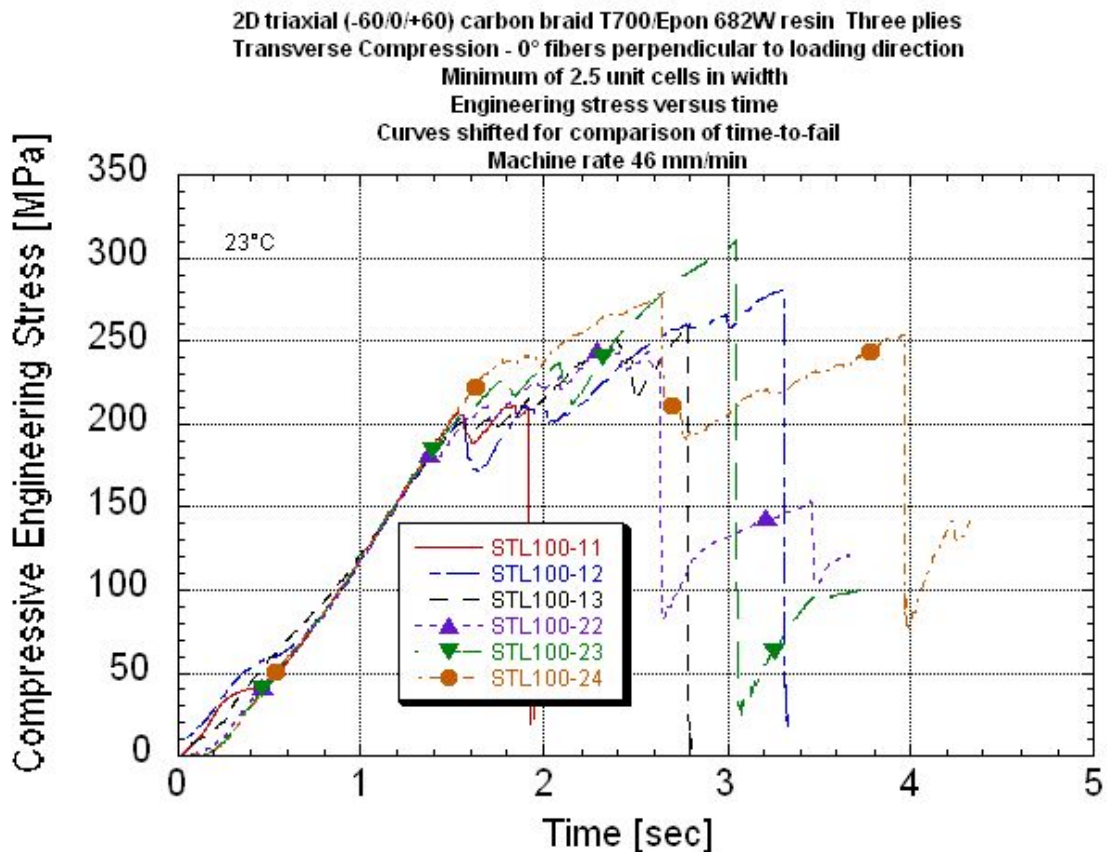
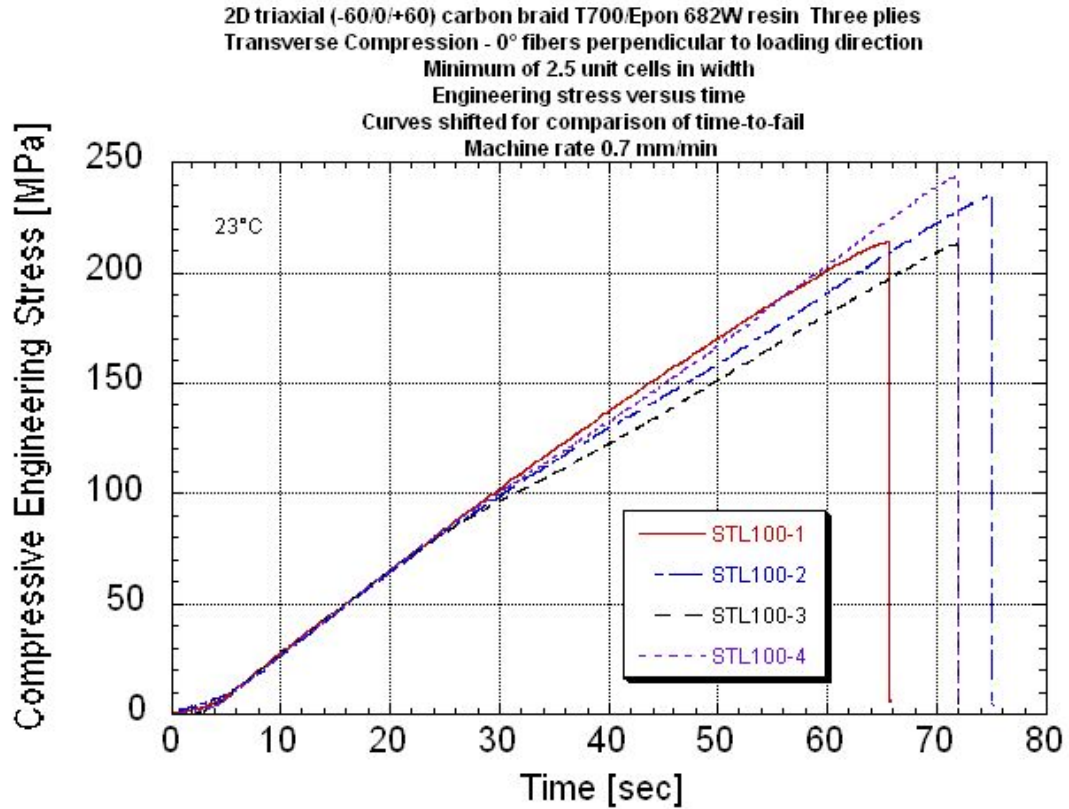
Note 1 Five to six low amplitude system resonant waves in stress response before failure.

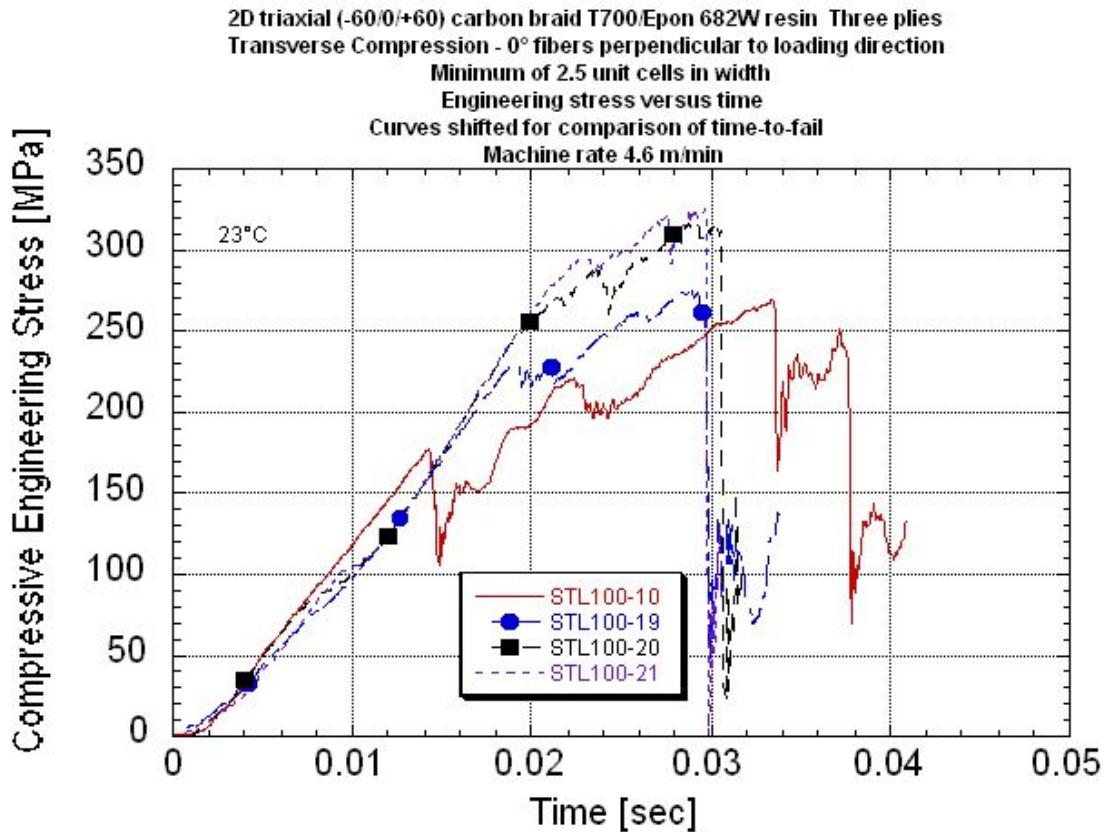
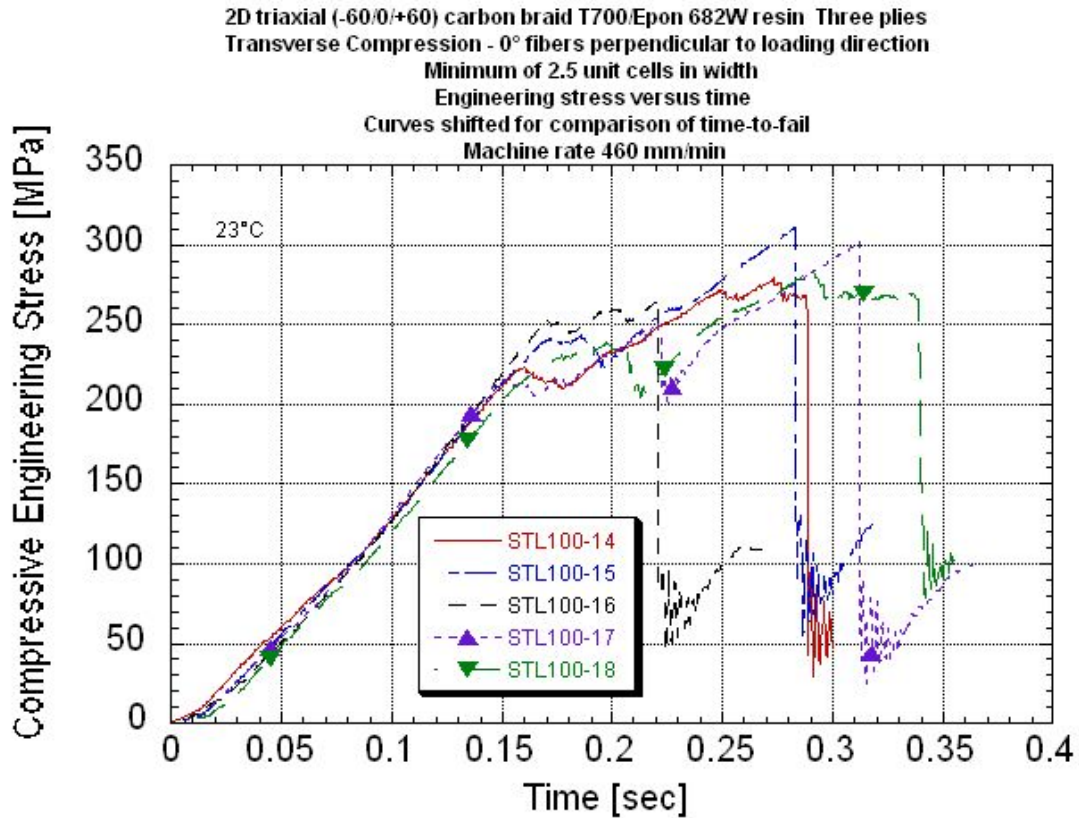












APPENDIX O.

AXIAL SHEAR DATA PACKAGE

Shearing across 0° Fibers

Summary Table

Summary Stress-strain Plots With Rate

Summary Stress-time Plots With Rate

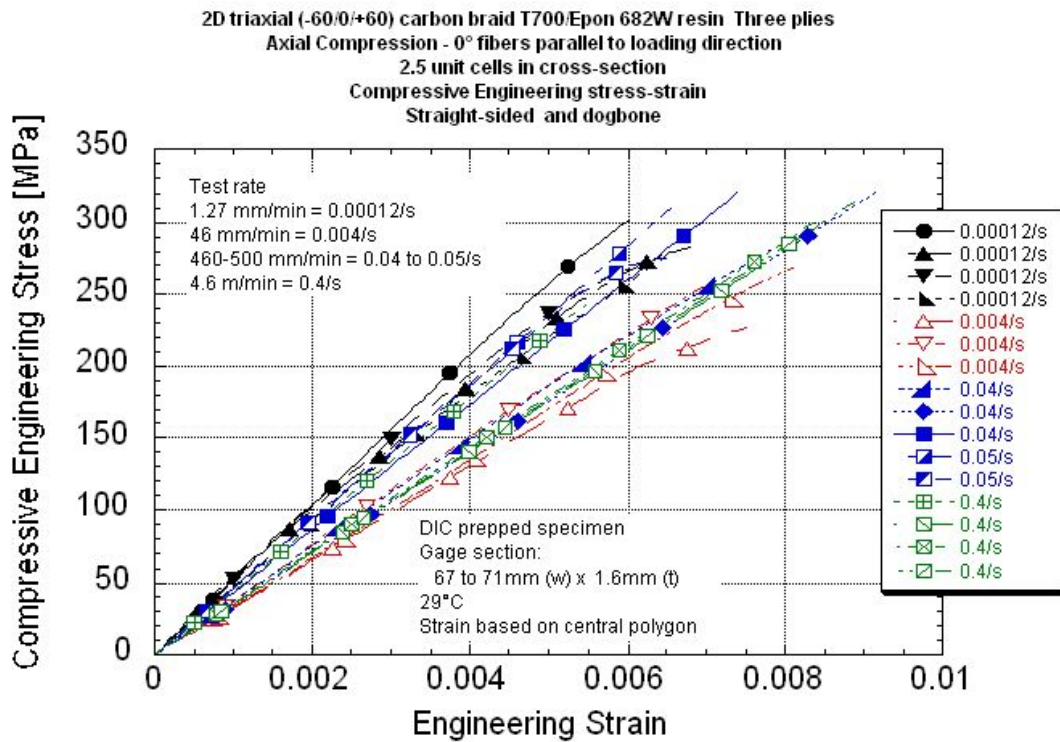
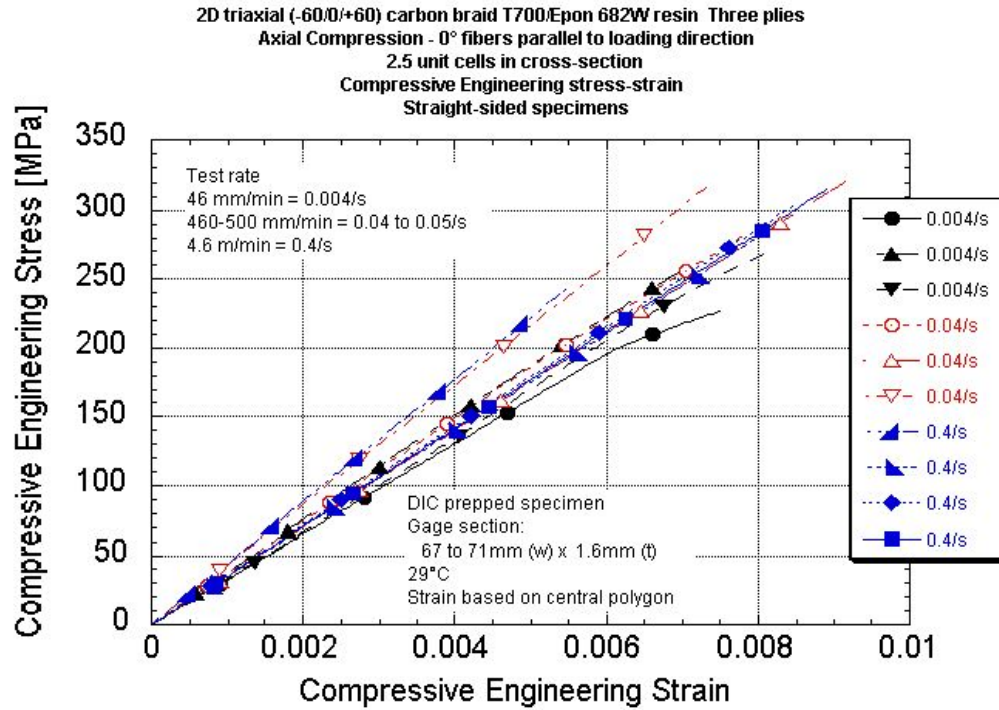
Investigation of Opportunities For Light-Weighting Vehicles Using Advanced Plastics And Composites

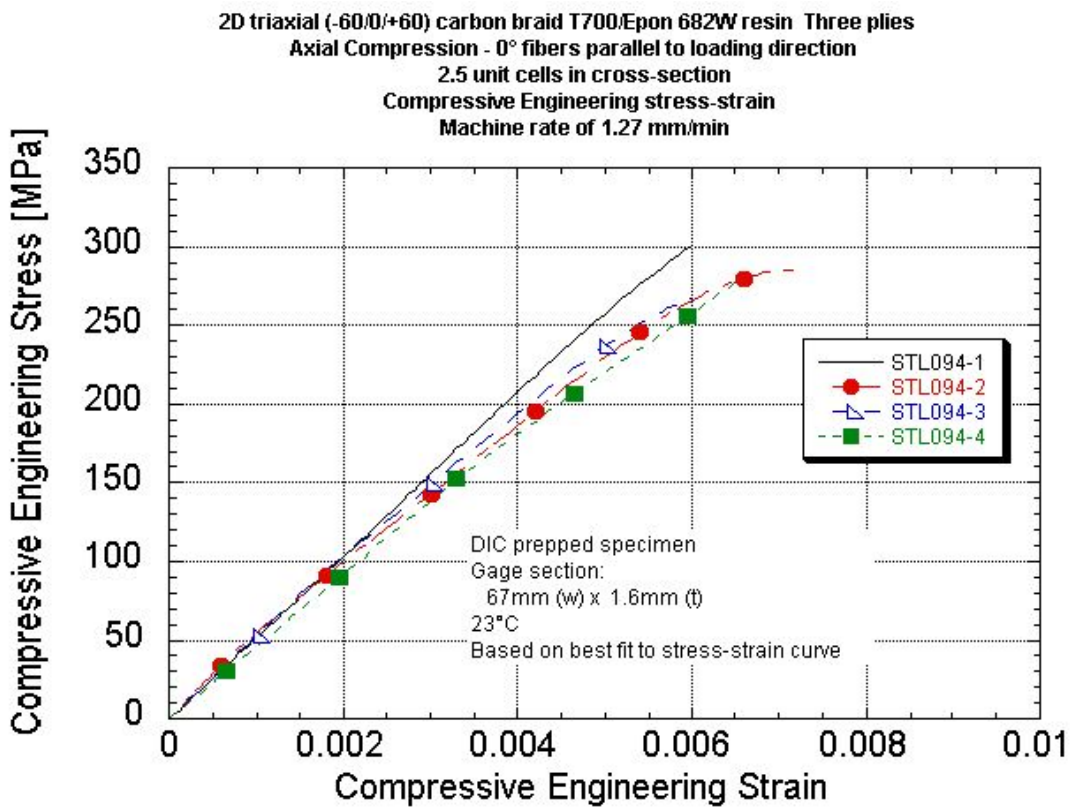
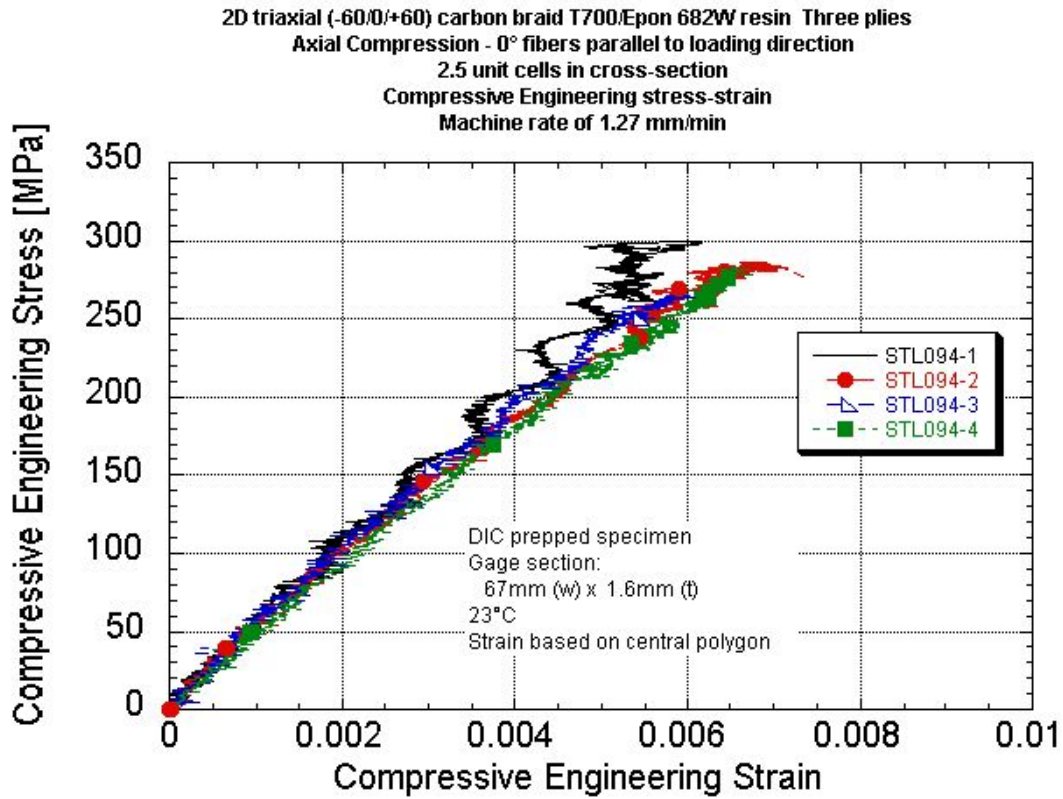
Transverse Compression Data Summary - 0° Fibers perpendicular to loading direction
2D Triaxial Carbon T700/ Epon862W Epoxy Braid
Minimum of 2.5 unit cells in cross section
Nominal center cross-section of 71mm wide x 1.65mm thick

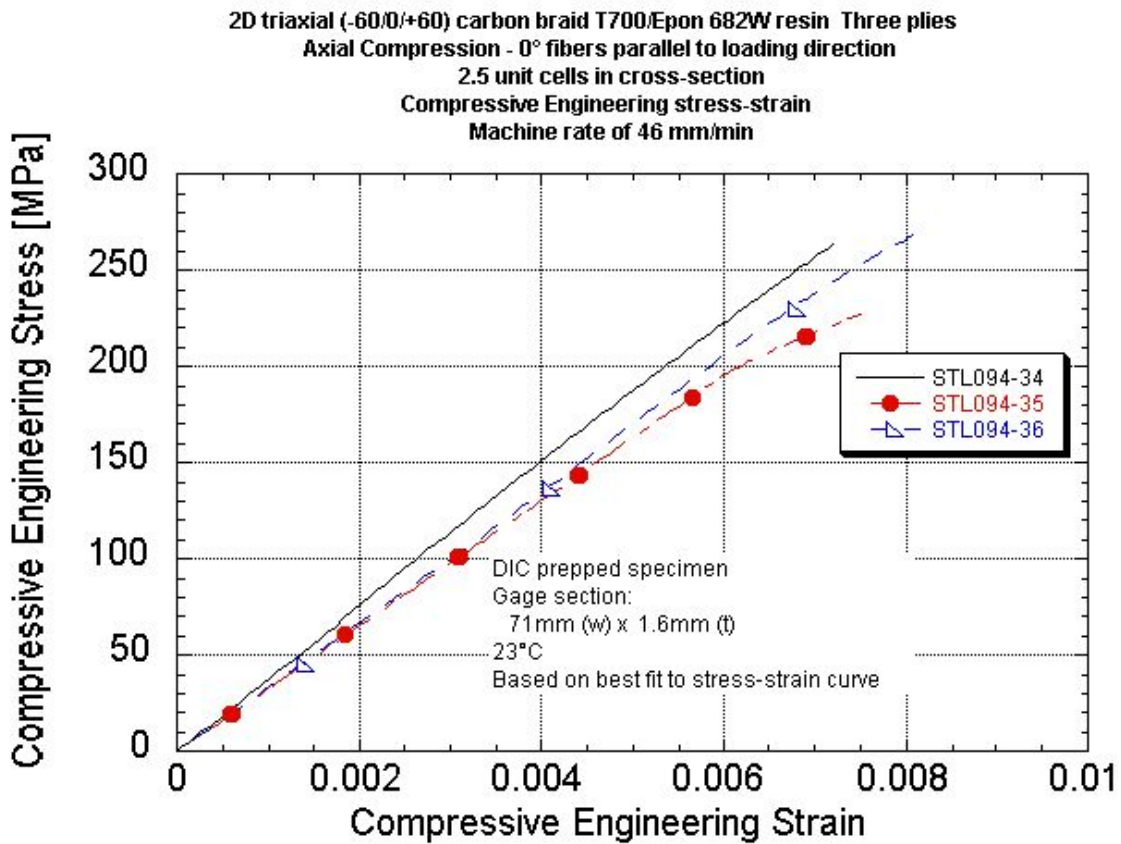
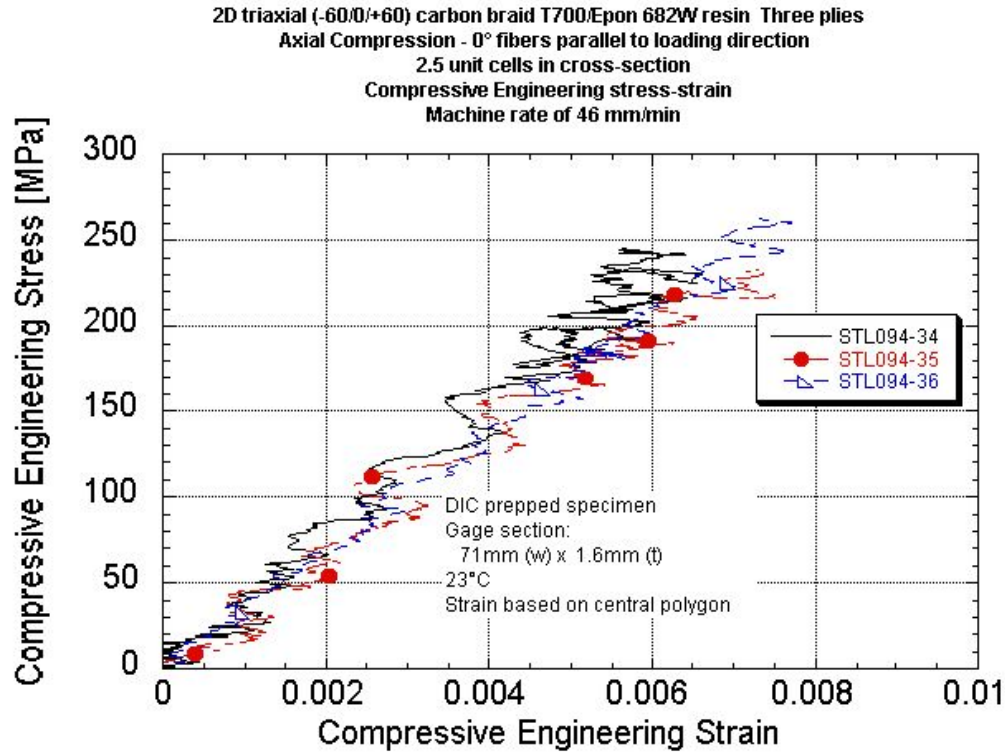
	Panel ID	UDRI STL number	Center polygon size length x width [mm]	Stress at Onset of Crush [MPa]	Normalized Stress at Onset of Crush to 56% Fiber Volume [MPa]	Peak Stress [MPa]	Normalized Peak Stress to 56% Fiber Volume [MPa]	Engineering Breaking Strain [%]	Elastic Modulus Based on Center [GPa]	Measured Strain Rate * [1/s]	Machine Rate [in/s]	Machine Rate [m/min]	Comments
~0.00005/s	073010-6 CTB-1	100-1	-	214	209	214	209	-	-	-	0.00041	0.00062	No DIC
	073010-6 CTB-2	100-2	-	235	229	235	229	-	-	-	0.00041	0.00063	No DIC
	073010-6 CTB-3	100-3	-	213	208	213	208	-	-	-	0.00041	0.00063	No DIC
	073010-6 CTB-4	100-4	-	244	238	244	238	-	-	-	0.00041	0.00063	No DIC
		Average		226	221	226	221						
		Standard Deviation		15	15	15	15						
		COV [%]		6.73	6.73	6.73	6.73						
0.004/s	072910-2 CTB-11	100-11	7.89x27.16	207	195	212	199	0.52	40.5	0.00410	0.031	0.047	
	072910-2 CTB-12	100-12	7.42x25.44	206	194	282	265	0.81	39.0	0.00422	0.032	0.048	
	072910-2 CTB-13	100-13	7.79x26.38	202	190	259	244	0.82	34.5	0.00407	0.032	0.048	
	072910-2 CTB-22	100-22	7.61x26.17	211	199	247	233	0.67	40.1	0.00385	0.032	0.049	bottom fixture paired
	072910-2 CTB-23	100-23	7.83x26.34	230	216	310	292	0.85	38.5	0.00427	0.032	0.049	bottom fixture paired
	072910-2 CTB-24	100-24	7.70x26.43	238	225	280	264	0.69	43.2	0.00414	0.032	0.049	bottom fixture paired
		Average		216	203	265	249	0.72	39.3				
		Standard Deviation		15	14	34	32	0.12	2.8				
		COV [%]		6.90	6.90	12.85	12.85	17.17	7.25				
0.04/s	072910-2 CTB-14	100-14	7.67x26.52	223	210	279	263	0.71	42.4	0.0356	0.32	0.48	
	072910-2 CTB-15	100-15	7.85x25.75	241	227	311	293	0.80	39.3	0.0421	0.31	0.48	
	072910-2 CTB-16	100-16	7.78x27.54	253	238	266	250	0.64	40.2	0.0410	0.31	0.47	
	072910-2 CTB-17	100-17	7.88x27.46	216	203	302	284	0.81	40.5	0.0392	0.32	0.48	
	072910-2 CTB-18	100-18	7.66x27.49	238	225	282	266	0.80	37.9	0.0486	0.32	0.48	
			Average		234	221	288	271	0.75	40.1			
		Standard Deviation		15	14	18	17	0.08	1.7				
		COV [%]		6.27	6.27	6.33	6.33	10.0	4.12				
0.4/s	072910-2 CTB-10	100-10	25.54x8.09	177	167	269	253	>.483	35.5	0.366	3.24	4.9	DIC window horizontal
	072910-2 CTB-19	100-19	7.84x26.04	230	217	274	258	0.69	42.5	0.361	3.09	4.7	
	072910-2 CTB-20	100-20	7.54x26.42	288	272	317	299	0.77	45.3	0.372	3.11	4.7	
	072910-2 CTB-21	100-21	7.79x27.72	295	277	325	307	0.76	47.1	0.406	3.00	4.6	
		Average [EXCLUDING 100-10]		271	255	305	288	0.74	45.0				
		Standard Deviation		35	33	28	26	0.04	2.3				
		COV [%]		13.0	13.0	9.11	9.11	5.8	5.17				

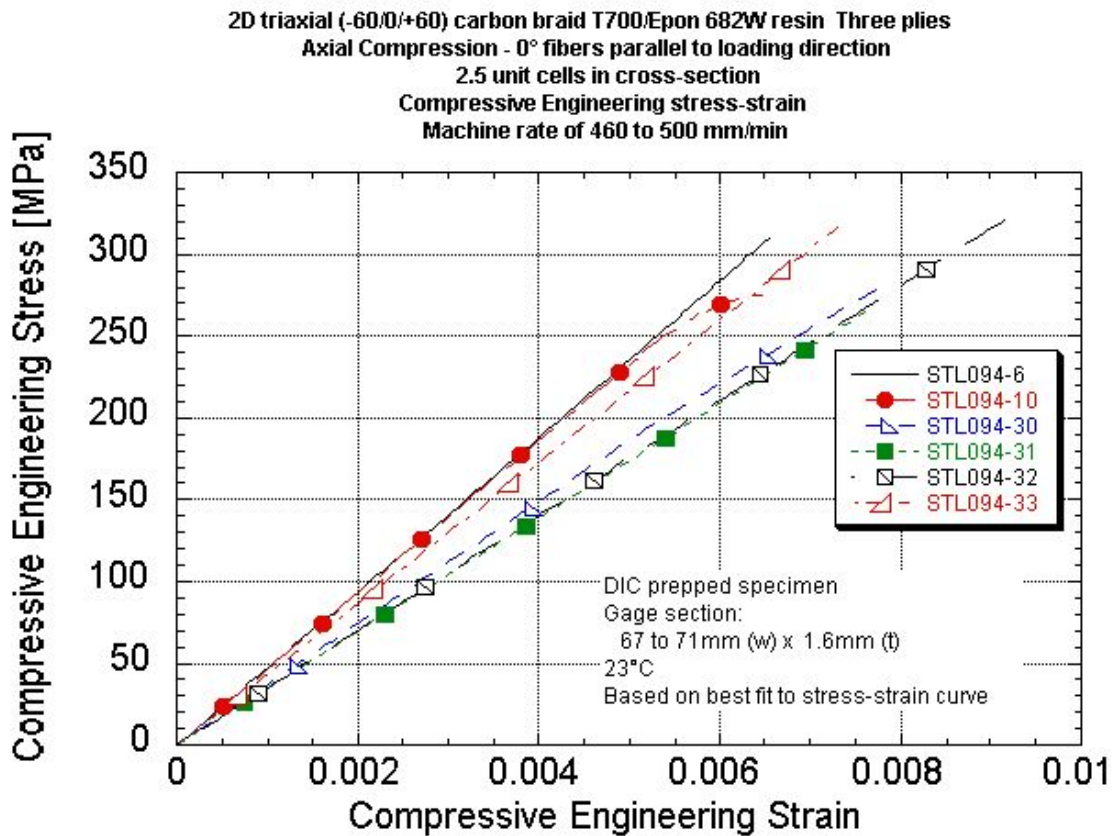
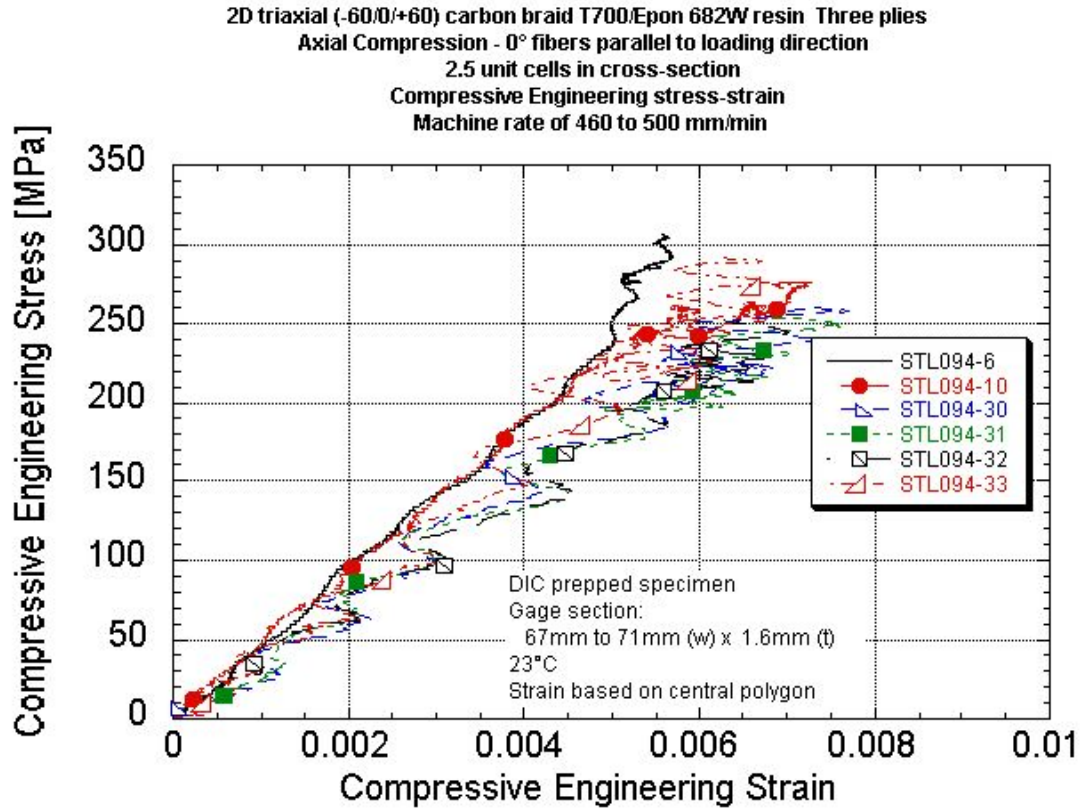
* Strain rate of central region

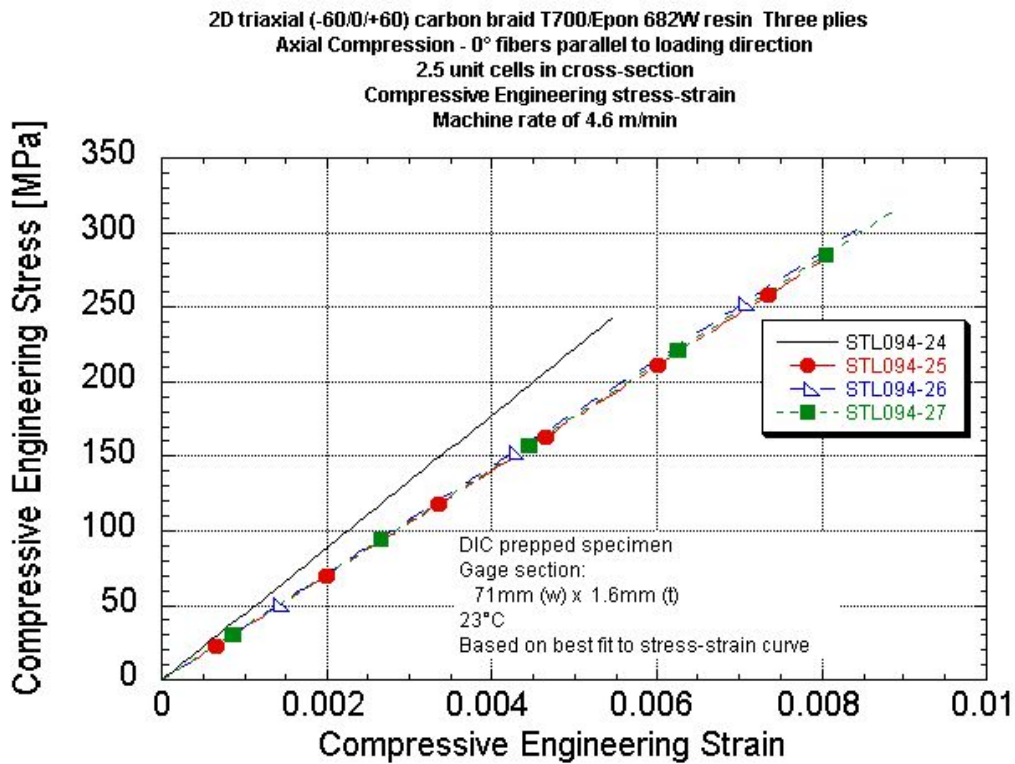
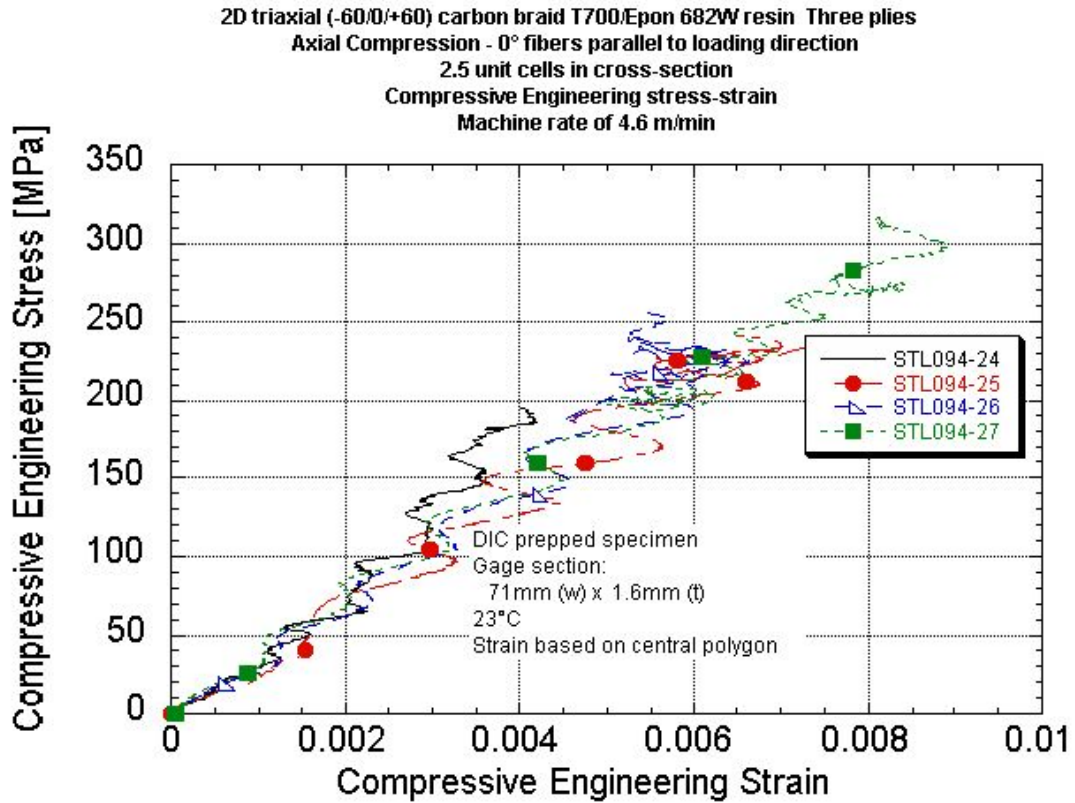
Specimen thickness varied due to the braid structure. Thickness was measured at two "peak" and two "valley" locations and averaged.

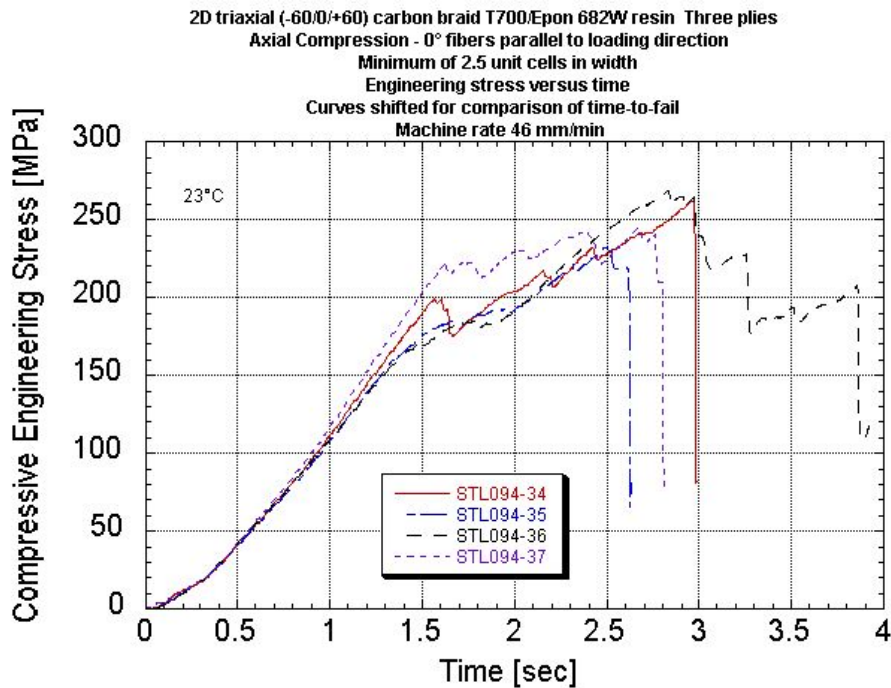
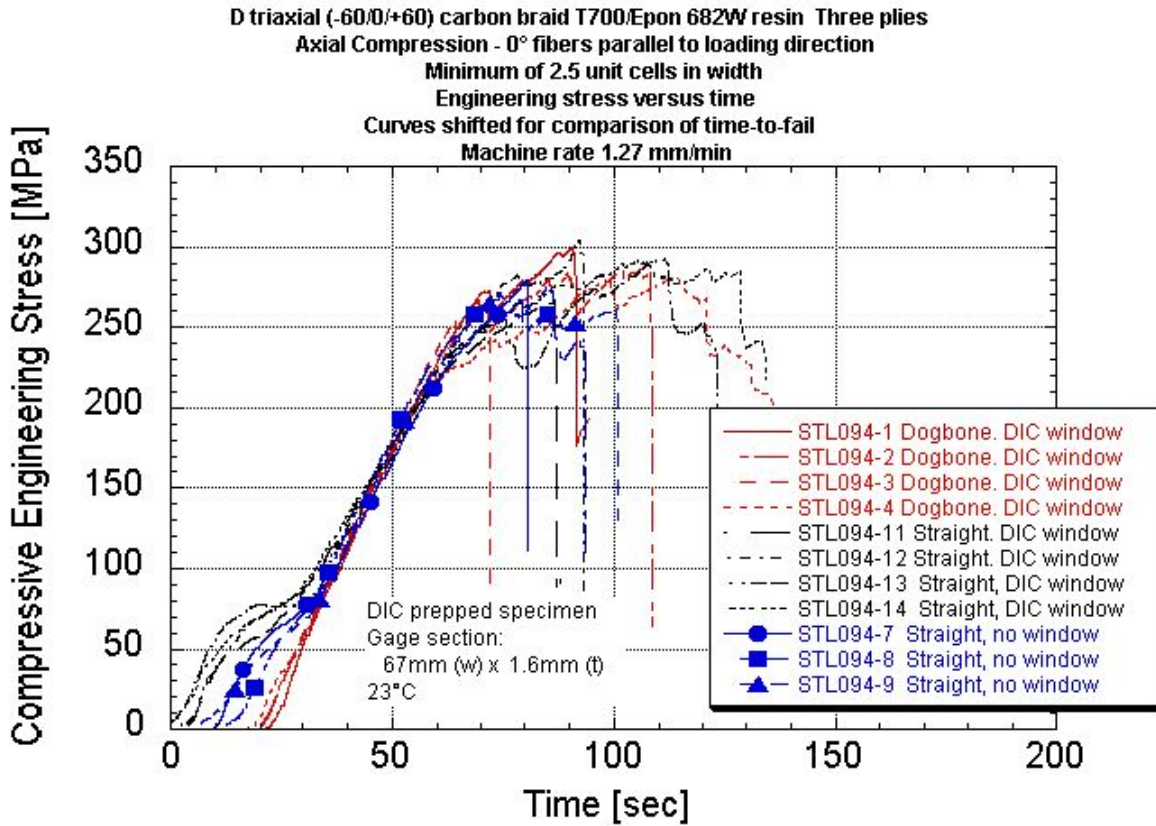


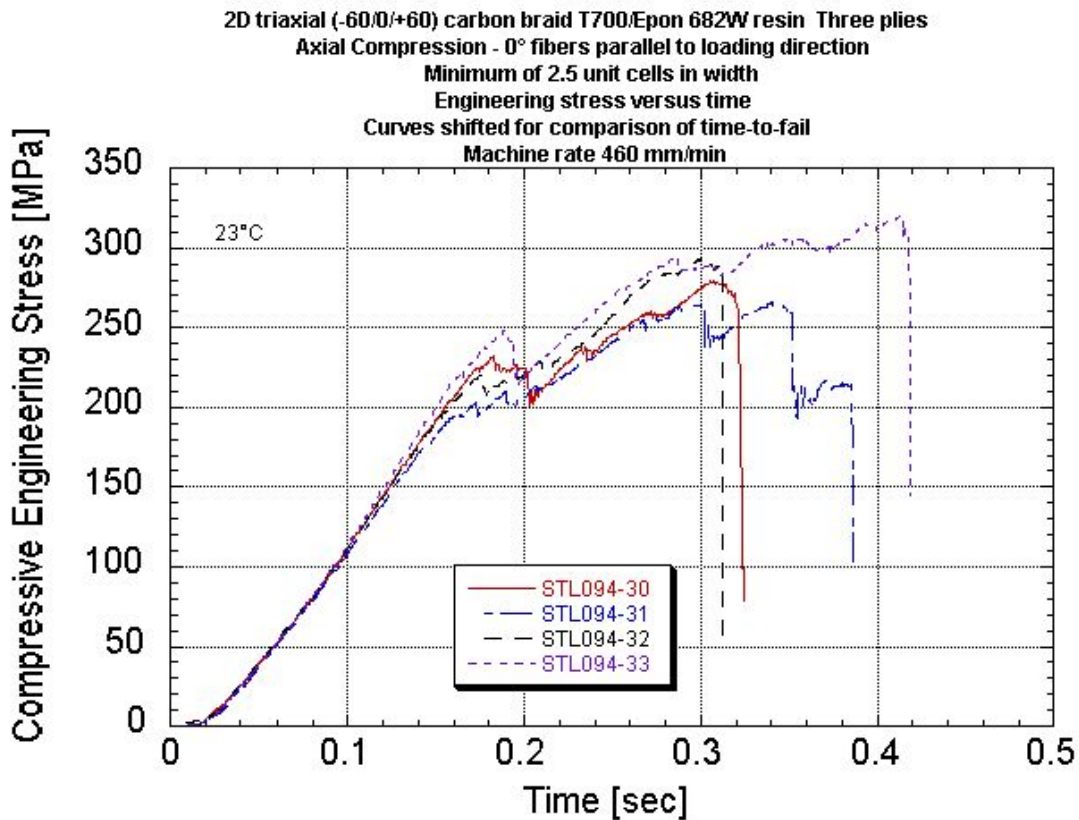
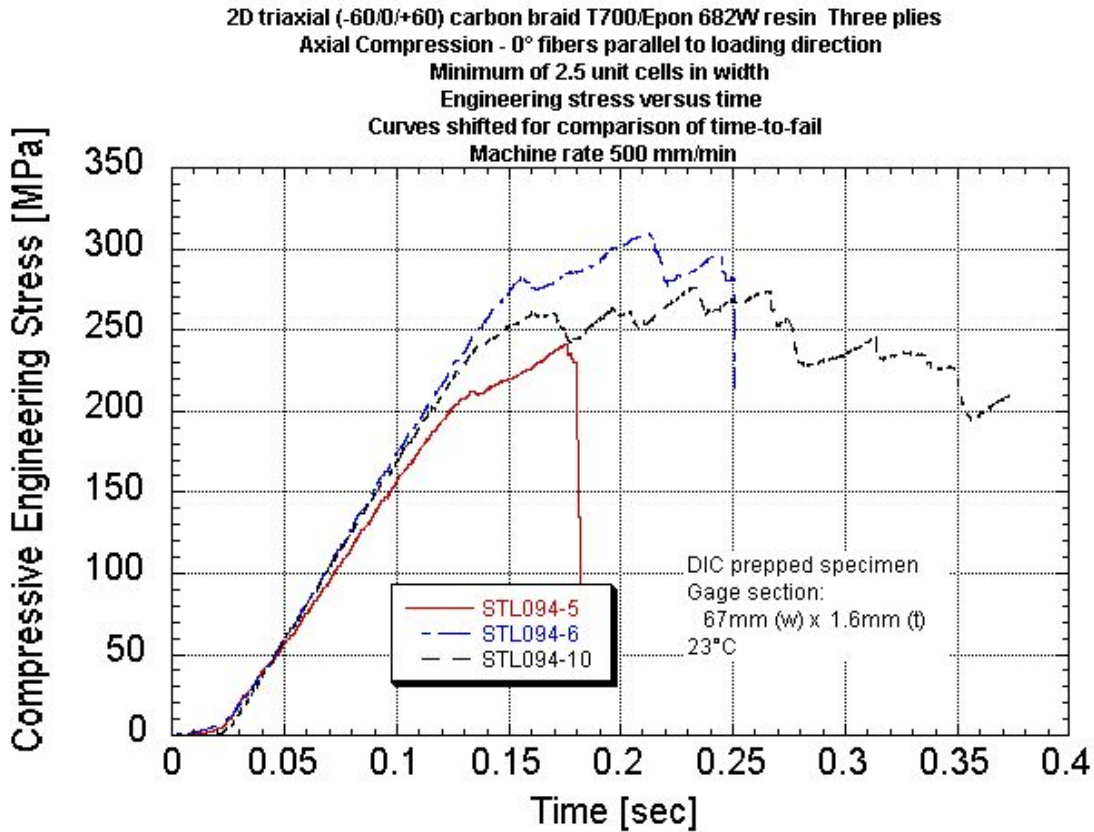


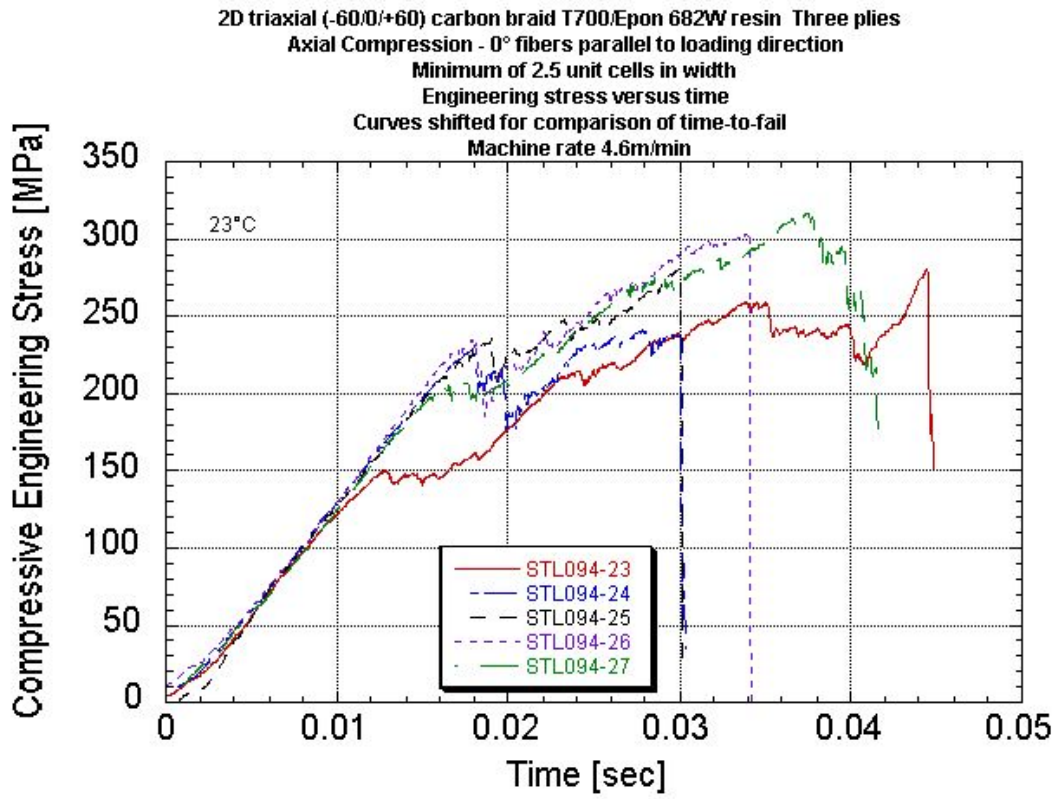












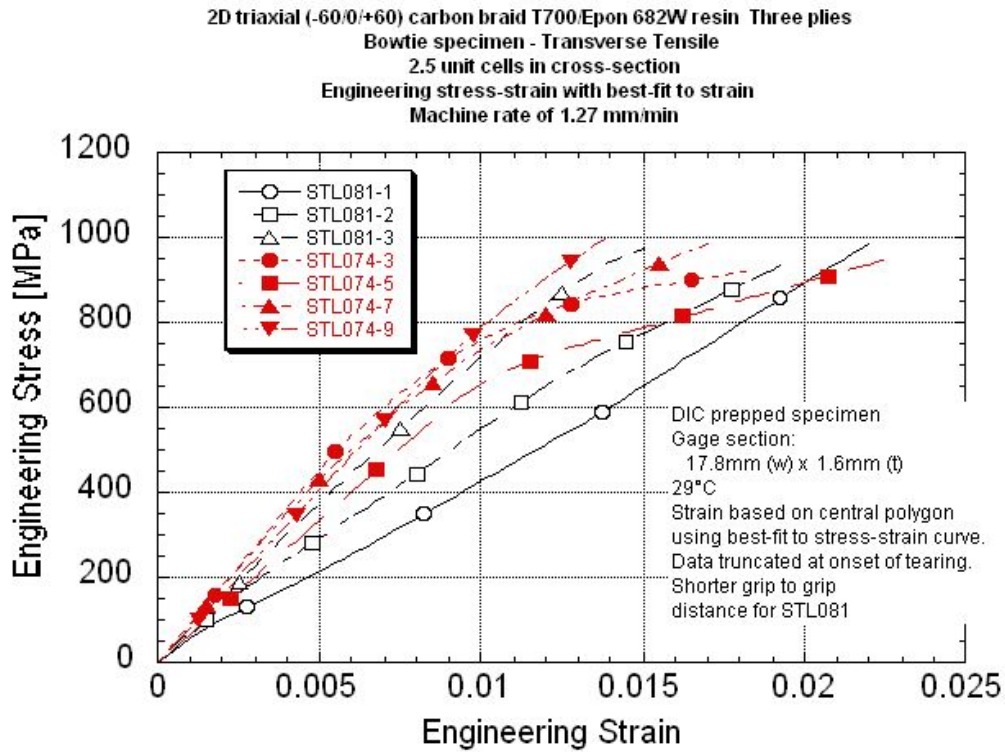
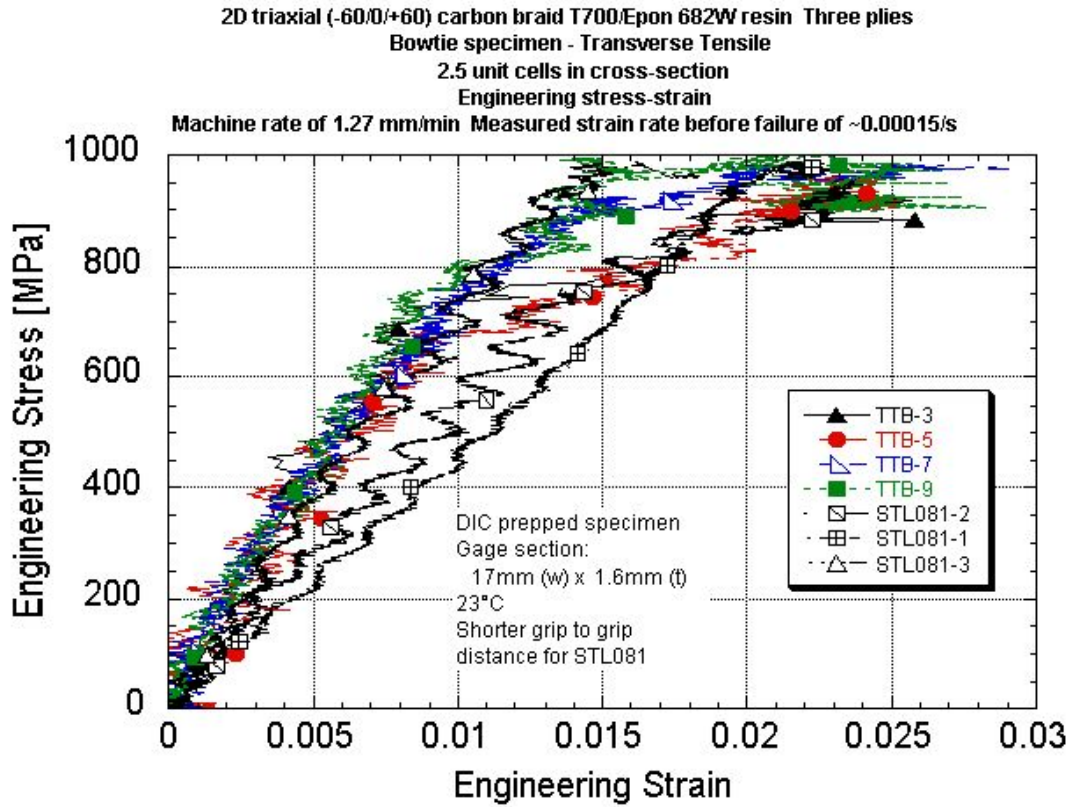
APPENDIX N.
TRANSVERSE COMPRESSION DATA PACKAGE
Summary Table
Summary Stress-strain Plots With Rate
Summary Stress-time Plots With Rate

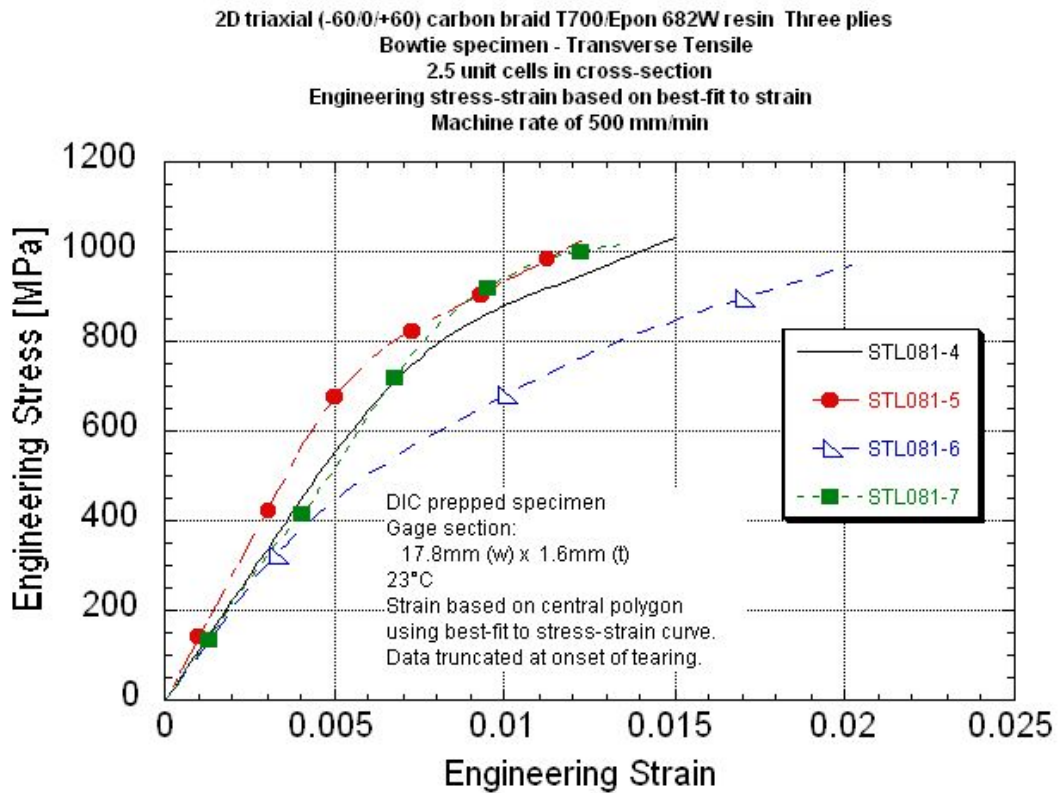
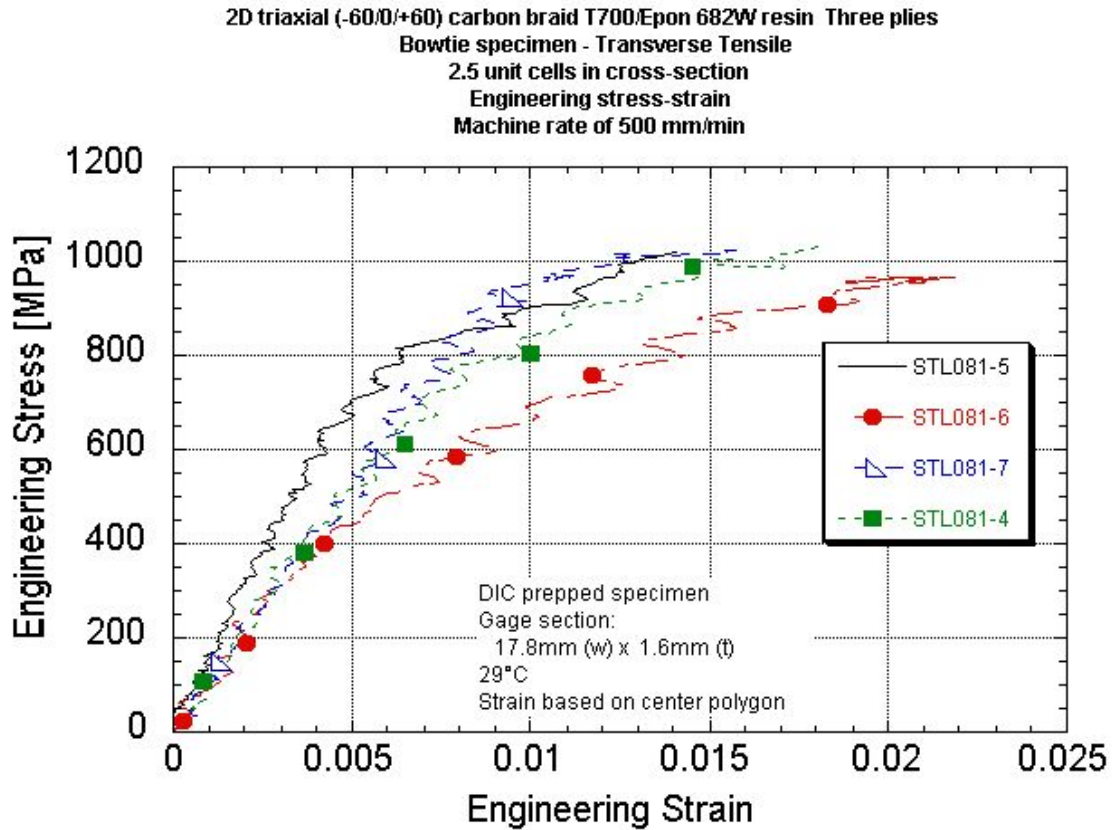
Investigation of Opportunities For Light-Weighting Vehicles Using Advanced Plastics And Composites

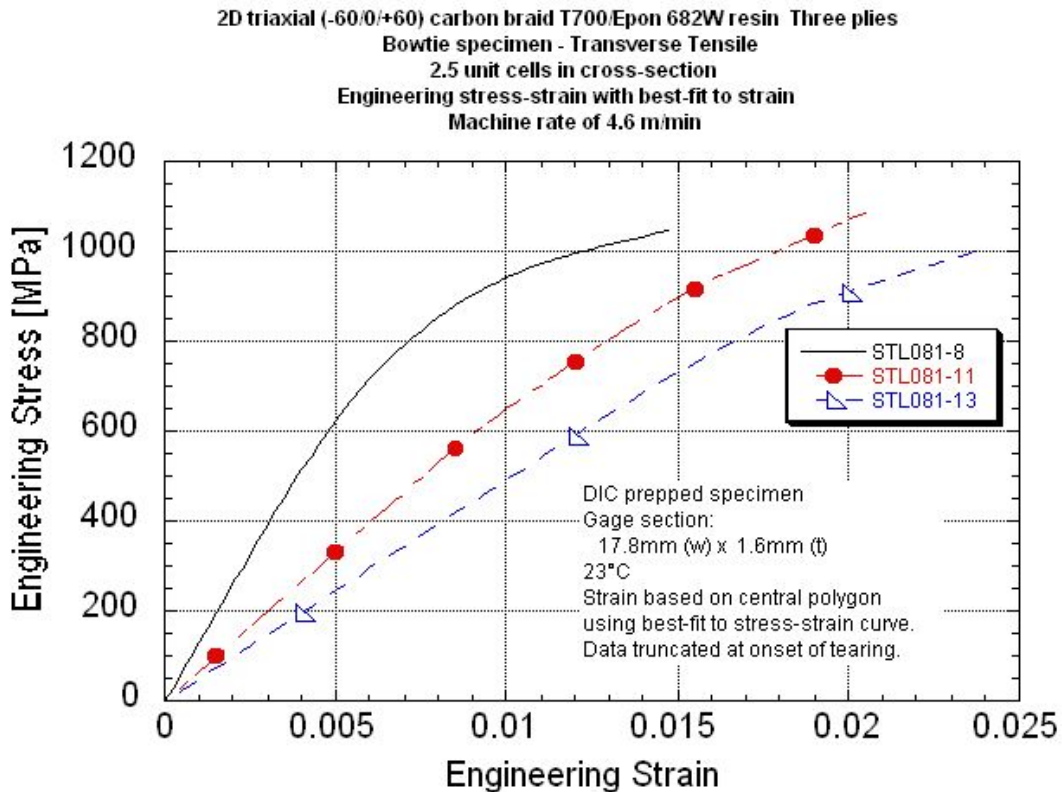
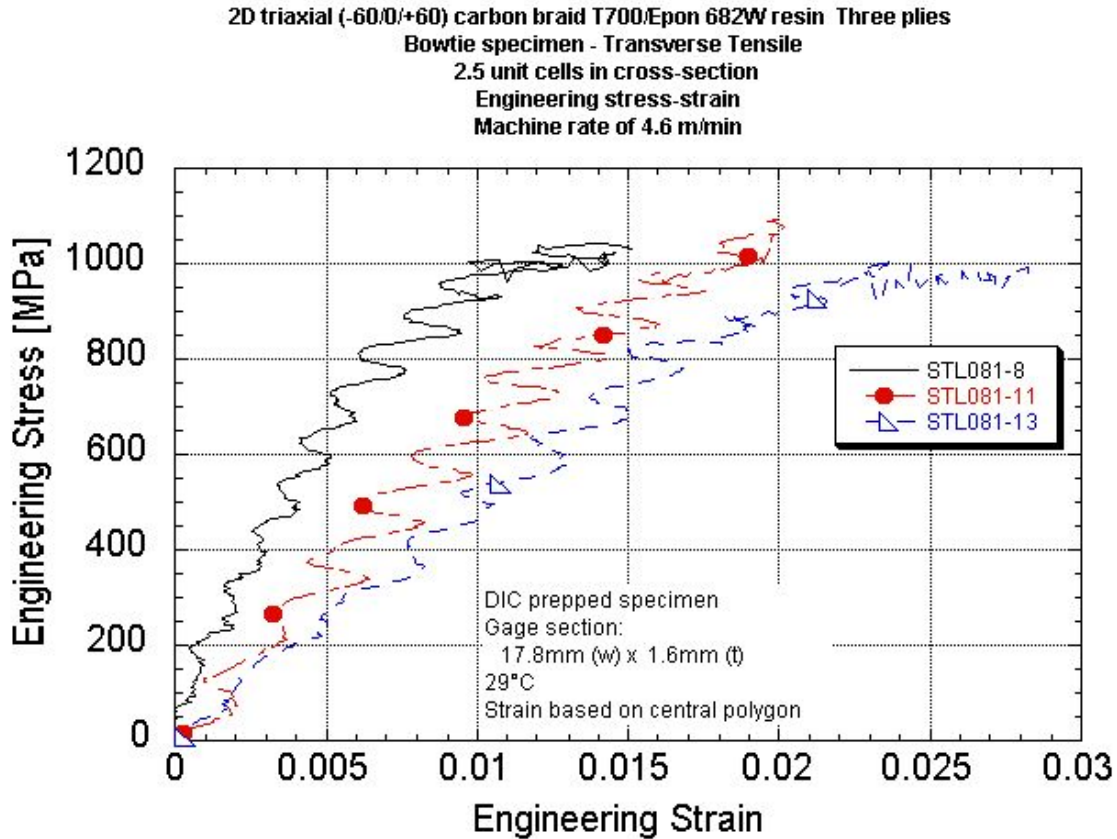
Axial Compression Data Summary - 0° fibers parallel to loading direction
2D Triaxial Carbon T700/ Epon862W Epoxy Braid
Minimum of 2.5 unit cells in cross section - Unit cell size (length x width) = 17.8mm x 5.5mm
Nominal center cross-section of 71mm wide x 1.65mm thick

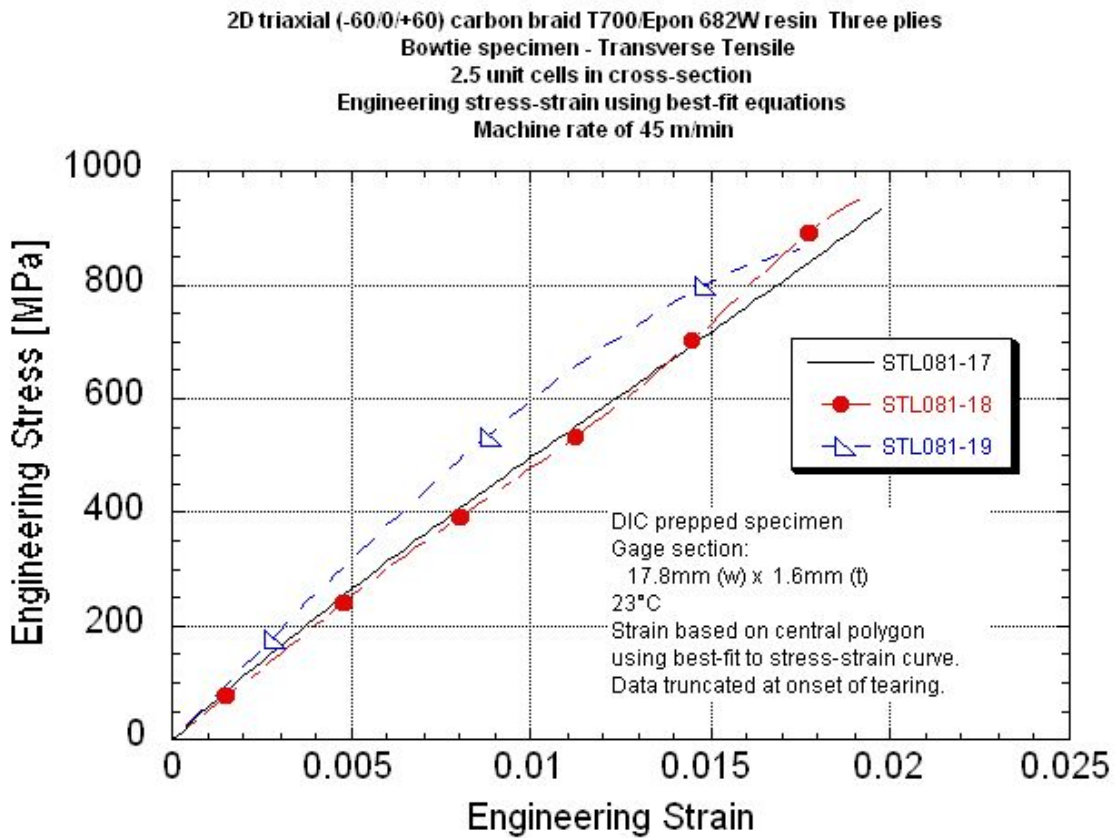
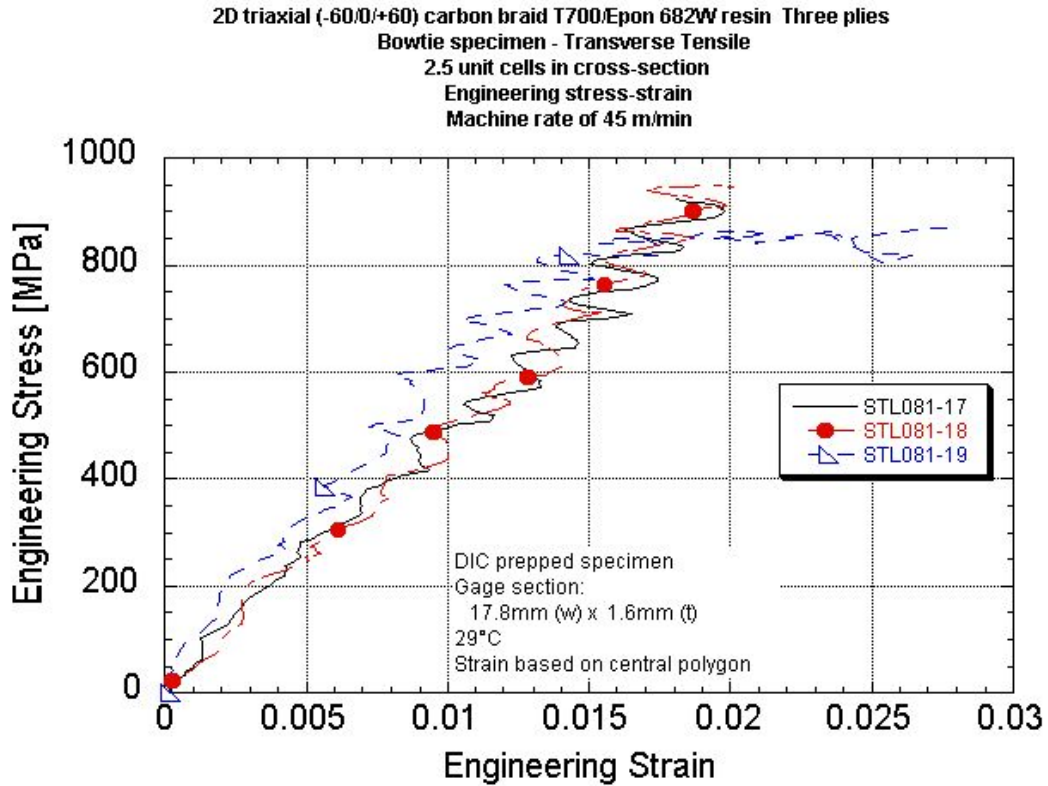
	Panel ID	UDRI STL number	Center polygon size length x width [mm]	Stress at Onset of Crush [MPa]	Onset of Crush Stress Normalized to 50% Fiber Volume [MPa]	Peak Stress [MPa]	Peak Stress Normalized to 50% Fiber Volume [MPa]	Engineering Breaking Strain # [%]	Localized## Engineering Max Strain [%]	Localized## Engineering Min Strain [%]	Elastic Modulus Based on Center [GPa]	Elastic Modulus Based on High Strain Point [GPa]	Measured Strain Rate* [1/s]	Machine Rate [m/s]	Machine Rate [mm/min]	Comments
0.00012/s	073010-6 CAB-1	094-1	25.7x6.55	272	266	299	292	0.62	0.92	0.35	51.5	68.3	0.000121	0.00083	0.00127	Dogbone
	073010-6 CAB-2	094-2	-	259	253	286	279	0.70	-	-	56.0	-	0.000131	0.00083	0.00127	Dogbone
	073010-6 CAB-3	094-3	28.4x6.41	268	261	267	261	0.60	0.71	-	53.0	-	0.000124	0.00083	0.00127	Dogbone
	073010-6 CAB-4	094-4	27.0x8.28	221	215	282	275	0.65	-	-	46.2	-	0.000125	0.00083	0.00127	Dogbone
	073010-6 CAB-8	094-7	-	279	272	279	273	-	-	-	-	-	-	0.00083	0.00127	Straight. No DIC window
	073010-6 CAB-9	094-8	-	267	261	267	261	-	-	-	-	-	-	0.00084	0.00127	Straight. No DIC window
	073010-6 CAB-10	094-9	-	271	264	275	268	-	-	-	-	-	-	0.00084	0.00127	Straight. No DIC window
	073010-1 CAB-18	094-11	-	267	277	267	277	-	-	-	-	-	-	0.00083	0.00127	Straight. DIC window
	073010-1 CAB-21	094-12	-	282	292	304	315	-	-	-	-	-	-	0.00083	0.00127	Straight. DIC window
	073010-1 CAB-22	094-13	-	259	268	292	303	-	-	-	-	-	-	0.00083	0.00127	Straight. DIC window
073010-1 CAB-25	094-14	-	249	257	291	301	-	-	-	-	-	-	0.00083	0.00127	Straight. DIC window	
		Average		263	262	283	282	0.64	0.81		51.7					
		Standard Deviation		17	19	13	18	0.04	0.15		4.1					
		COV [%]		6.41	7.15	4.63	6.37	6.84	18.3		7.97					
0.004/s	072910-2 CAB-34	094-34	26.57x7.39	199	187	262	246	0.66	-	-	37.4	-	0.003942	0.0312	0.0475	
	072910-2 CAB-35	094-35	26.16x7.94	186	175	233	220	0.74	-	-	32.6	-	0.003932	0.0313	0.0476	
	072910-2 CAB-36	094-36	26.83x8.57	186	175	269	253	0.78	-	-	33.4	-	0.004134	0.0318	0.0485	
	072910-2 CAB-37	094-37	-	223	210	245	231	-	-	-	-	-	-	0.0311	0.0474	No Dic data
			Average		198	187	252	237	0.73			34.5				
		Standard Deviation		17	16	16	15	0.06			2.6					
		COV [%]		8.82	8.82	6.37	6.37	8.8			7.46					
0.04-0.05/s	073010-6 CAB-5	094-5	-	213	207	242	236	-	-	-	-	-	-	0.341	0.520	Dogbone. No DIC data
	073010-6 CAB-6	094-6	25.66x6.55	282	276	310	303	0.66	0.73	-	47.2	-	0.0477	0.335	0.510	Dogbone
	073010-6 CAB-13	094-10	30.05x9.07	261	255	276	269	0.65	-	-	46.5	-	0.0474	-	-	Dogbone. Issues with stroke data capture
	072910-2 CAB-30	094-30	26.99x7.62	233	219	279	263	0.76	-	-	37.3	-	0.0401	0.312	0.476	Straight
	072910-2 CAB-31	094-31	26.03x7.54	203	191	266	251	0.77	-	-	34.8	-	0.0406	0.318	0.485	Straight
	072910-2 CAB-32	094-32	26.60x7.04	220	207	293	276	0.71	-	-	35.1	-	0.0426	0.320	0.487	Straight
	072910-2 CAB-33	094-33	25.94x7.43	248	234	320	301	0.74	-	-	43.3	-	0.0366	0.315	0.480	Straight
			Average		237	227	284	271	0.71			40.7				
		Standard Deviation		28	30	27	25	0.05			5.7					
		COV [%]		12.0	13.1	9.39	9.12	7.2			14.0					
0.4/s	073010-6 CAB-11	094-23	-	150	146	259	252	-	-	-	-	-	-	3.15	4.80	Straight. No DIC
	073010-6 CAB-16	094-24	25.37x7.87	229	224	242	236	0.55	-	-	44.4	-	0.245	3.01	4.58	Straight
	073010-6 CAB-17	094-25	26.52x8.44	234	229	280	273	0.80	-	-	35.1	-	0.363	2.98	4.54	Straight
	072910-2 CAB-26	094-26	25.81x7.74	234	220	303	285	0.84	-	-	35.9	-	0.371	3.01	4.59	Straight
	072910-2 CAB-27	094-27	27.79x7.30	206	194	316	298	0.87	-	-	35.4	-	0.364	3.08	4.69	Straight
			Average		211	203	280	269	0.76			37.7				
		Standard Deviation		36	34	31	25	0.15			4.5					
		COV [%]		17.0	16.9	11.0	9.32	19.4			11.9					

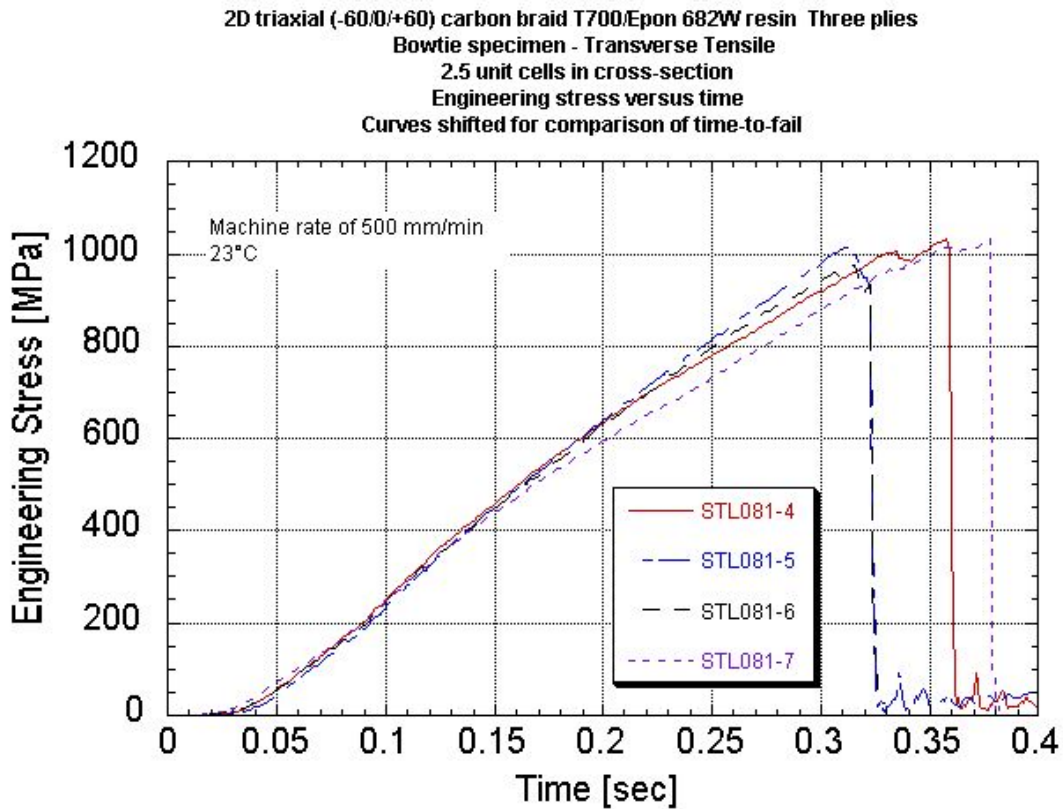
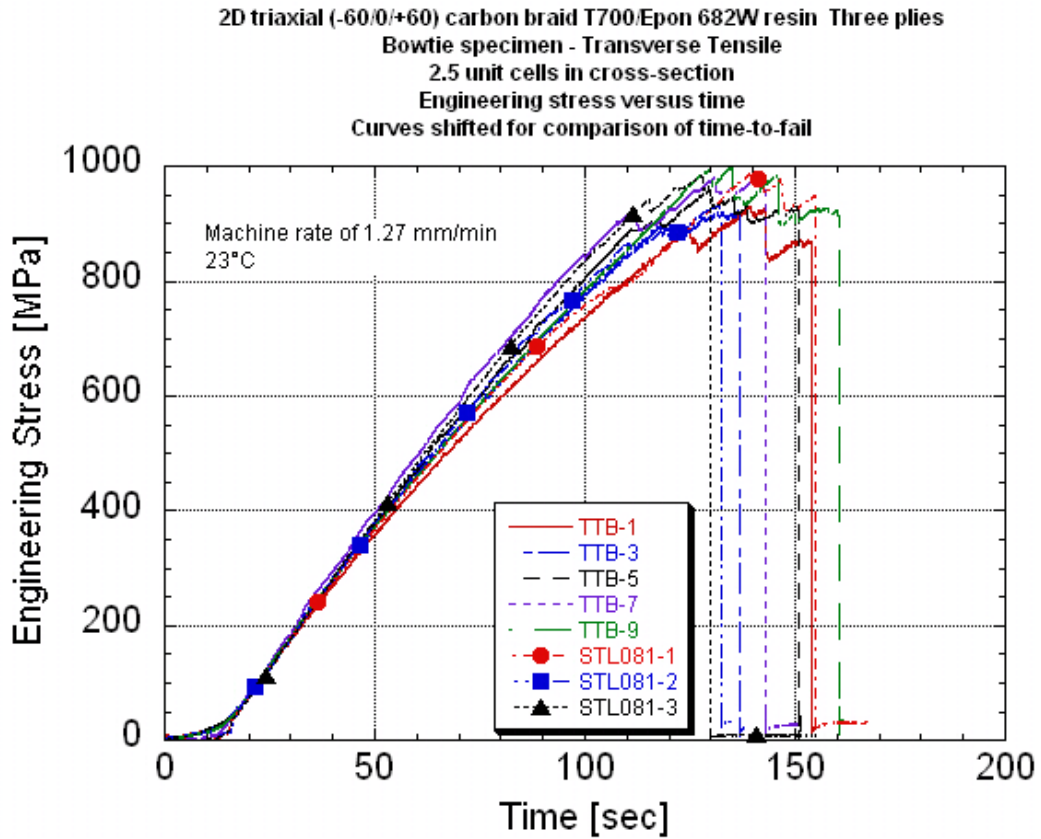
* Strain rate of central region ## Strain as measured at a region of high strain on a fiber braid and a low strain region.
 Specimen thickness varied due to the braid structure. Thickness was measured at two "peak" and two "valley" locations and averaged.

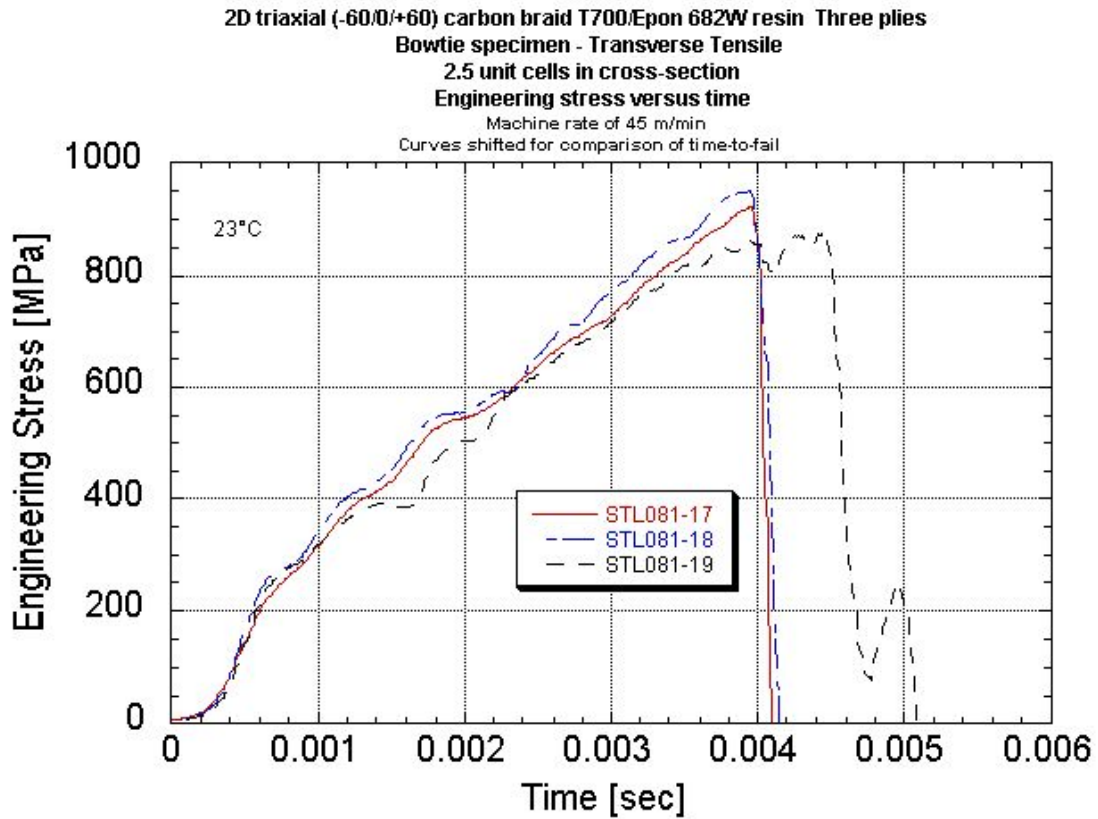
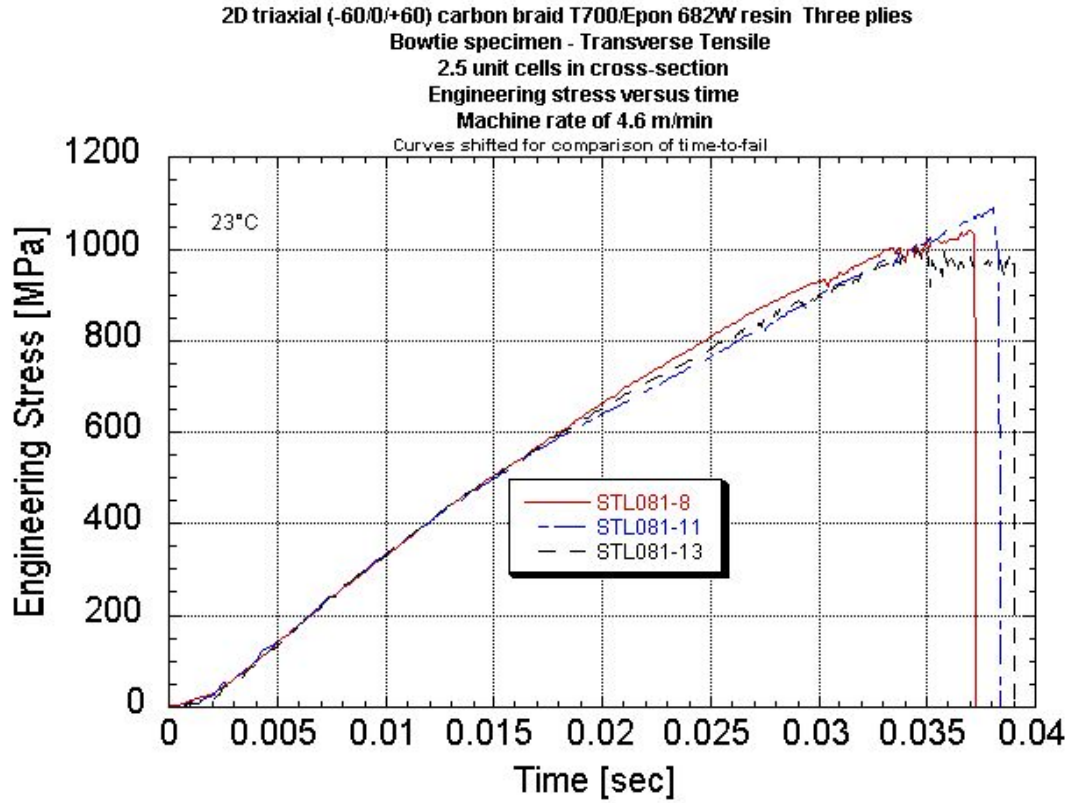












APPENDIX M.

AXIAL COMPRESSION DATA PACKAGE

Summary Table

Summary Stress-strain Plots With Rate

Summary Stress-time Plots With Rate

Investigation of Opportunities For Light-Weighting Vehicles Using Advanced Plastics And Composites

Transverse Tensile Data Summary
2D Triaxial Carbon T700/ Epon862W Epoxy Braid
Bowtie Specimen Configuration - Minimum of 2.5 unit cells in reduced cross-section
Nominal center cross-section of 17mm wide x 1.6mm thick

	Panel ID	UDRI STL number	Center polygon/line Gage Width [mm]	Peak Stress* [MPa]	Normalized Peak Stress to 56% Fiber Volume [MPa]	Engineering Breaking Strain #	Localized## Engineering Max Strain [%]	Localized## Engineering Min Strain [%]	Elastic Modulus Based on Center [GPa]	Elastic Modulus Based on High Strain Point	Elastic Modulus Based on Low Strain Point	Poisson's Ratio Center line	Poisson's Ratio Center polygon	Measured Strain Rate*	Machine Rate [in/s]	Machine Rate [m/min]	Comments
0.00015/s Longer grip to grip distance	073010-2	074-1	-	931	914	-	-	-	-	-	-	-	-	-	0.00083	0.00126	No DIC data
	073010-2	074-3	6.88	923	907	2.05	3.76/4.99	0.93/1.55	91.1	-	-	-	0.47	0.00013	0.00083	0.00127	
	073010-2	074-5	12.69	960	944	2.47	3.80/3.84	1.59/1.82	67.0	-	-	-	0.51	0.00023	0.00083	0.00127	
	073010-2	074-7	7.49	982	964	1.52/2.60	2.02/4.01	1.32/1.70	89.4	-	-	-	0.22	0.00015	0.00083	0.00126	
	073010-2	074-9	9.59	1000	983	1.44/2.38	3.13/3.64	1.43/1.73	81.3	-	-	-	0.19	0.00010	0.00083	0.00127	
		Average		959	943	1.84/2.48	3.18/4.12	1.30/1.70	82.2				0.35				
		Standard Deviation		33	32	0.47/0.09	0.83/0.60	0.28/0.11	11.0				0.17				
		COV [%]		3.42	3.42	25.6/3.64	26.1/14.6	21.3/6.60	13.4				48.3				
0.00015/s Shorter grip to grip distance	073010-6	081-1	7.75	989	965	2.35	2.63	1.49	57.0	35.0	49.6	0.01	0.02	0.00020	0.00083	0.00127	
	073010-6	081-2	7.34	931	909	2.38	3.71	1.59	65.8	36.0	50.5	0.20	0.24	0.00017	0.00083	0.00127	
	073010-6	081-3	7.75	976	952	1.49	2.57	1.05	76.3	44.1	-	0.36	0.31	0.00014	0.00083	0.00127	
		Average		965	942	2.07	2.97	1.37	66.4	38.3	50.1		0.19				
		Standard Deviation		30	29	0.50	0.64	0.29	9.65	5.00	0.67		0.15				
		COV [%]		3.12	3.12	24.3	21.6	21.0	14.5	13.0	1.34		81.3				
0.045/s Shorter grip to grip distance	073010-6	081-4	7.49	1034	1009	1.82	2.87	0.68	112	48.9	-	0.60	0.54	0.0446	0.333	0.508	
	073010-6	081-5	7.82	1022	997	1.41	2.35	0.82	141	-	-	0.63	0.63	0.0298	0.334	0.509	
	073010-6	081-6	7.79	977	954	2.11	-	-	102	-	-	0.44	-	0.0706	0.334	0.509	center line strain only
	073010-6	081-7	7.87	1033	1008	1.54	-	-	109	-	-	0.238/0.408	0.238/0.408	0.0344	0.336	0.513	
		Average		1017	992	1.72	2.61	0.75	116				0.47/0.52				
		Standard Deviation		27	26	0.31	0.37	0.10	17.2				0.2-0.11				
		COV [%]		2.65	2.65	18.1	14.1	13.2	14.8				43.5/20.9				
0.45/s Shorter grip to grip distance	073010-6	081-8	7.87	1044	1019	1.62	-	-	130	-	-	0.47	0.50	0.412	3.08	4.70	
	073010-2	081-11	7.32	1093	1074	2.07	-	-	66.2	-	-	0.14	0.14	0.465	3.18	4.84	
	073010-2	081-13	8.05	1002	985	2.37	3.60	2.29	49.2	49.4	-	0.03	0.03	0.698	3.10	4.73	
		Average		1046	1026	2.02			81.9				0.22				
		Standard Deviation		46	45	0.38			42.8				0.24				
		COV [%]		4.35	4.40	18.6			52.2				109				
5/s Shorter grip to grip distance	073010-1	081-17	7.83	924	957	1.96	-	-	58.3	-	-	0.03	0.03	5.09	28.3	43.2	
	073010-1	081-18	7.75	949	982	1.87	2.28	-	50.6	45.1	-	0.06	0.09	5.05	29.7	45.3	
	073010-1	081-19	7.92	881	911	3.20	-	-	64.7	-	-	0.03	0.05	3.50	29.1	44.4	
		Average		918	950	2.34			57.9				0.06				
		Standard Deviation		35	36	0.74			7.1				0.03				
		COV [%]		3.77	3.77	31.7			12.2				50.2				

#Extended failure as cracking initiated along sides and traveled into center. Strain for central polygon at onset of cracking and final break.

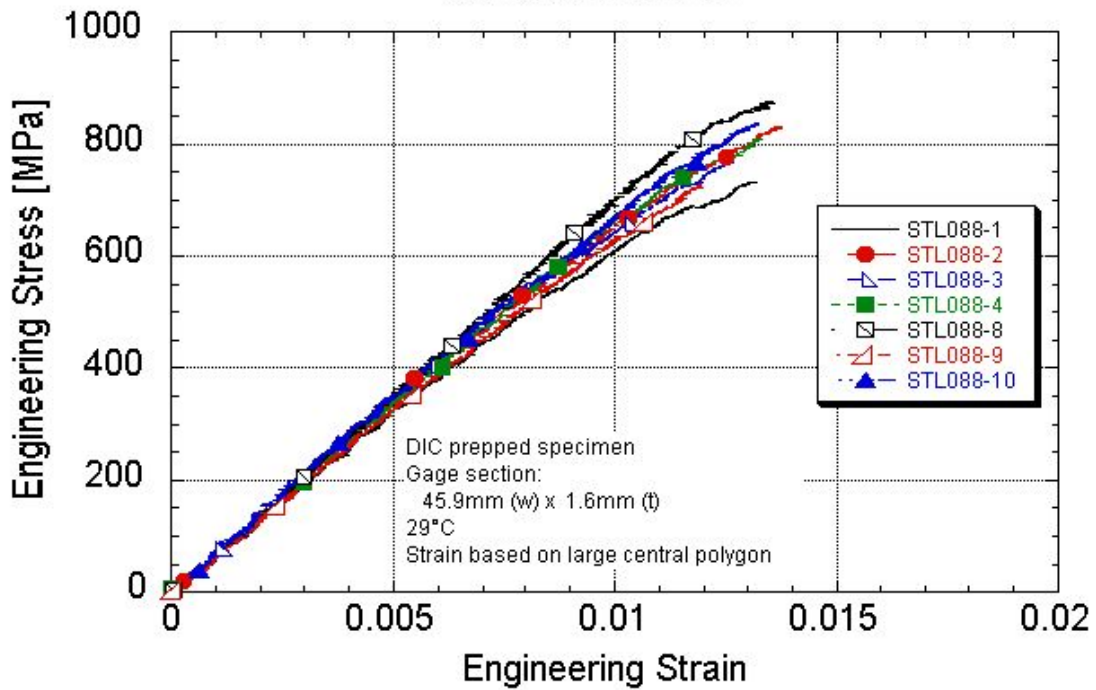
Strain as measured at a region of high strain on a fiber braid and low strain in center. Strain data from the onset of cracking and final break.

Specimen thickness varied due to the braid structure. Thickness was measured at two "peak" and two "valley" locations and averaged.

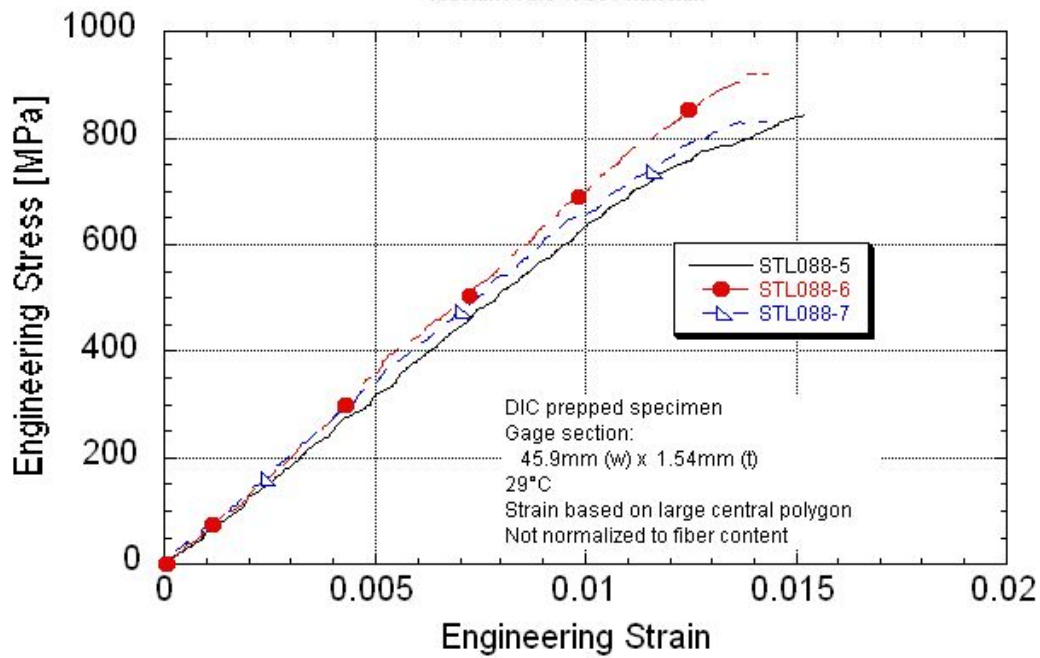
* The strain rate was measured over the strain experience over a stress range of 300 to 600 MPa.

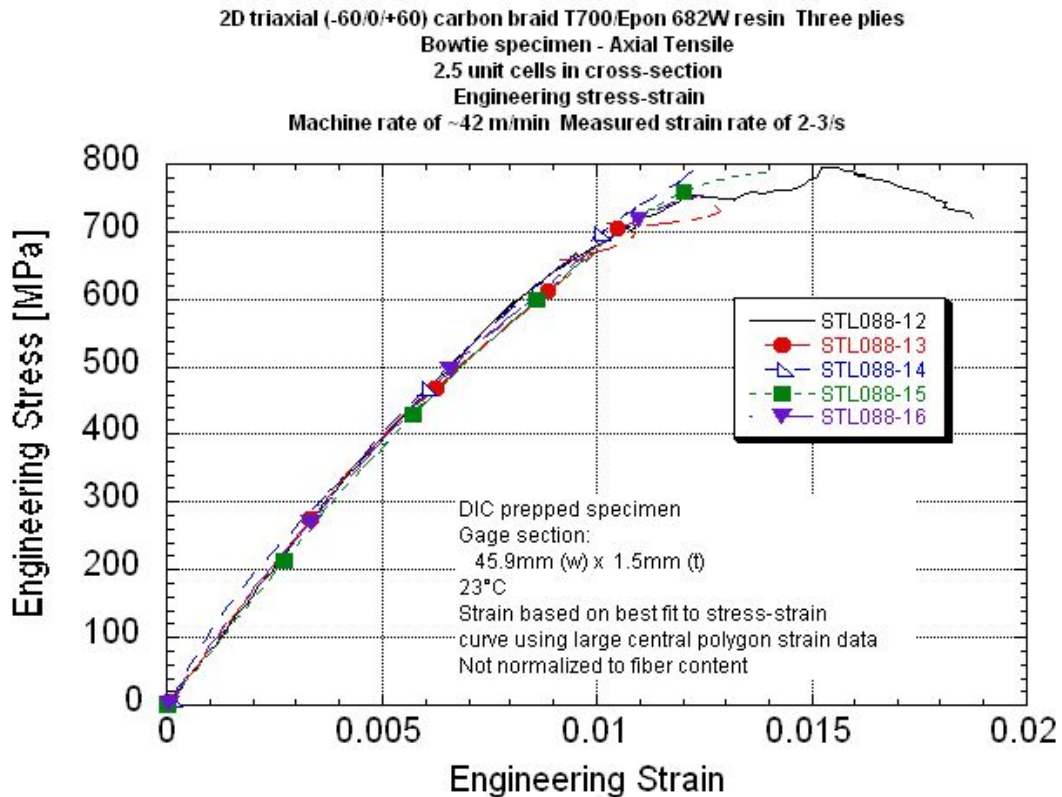
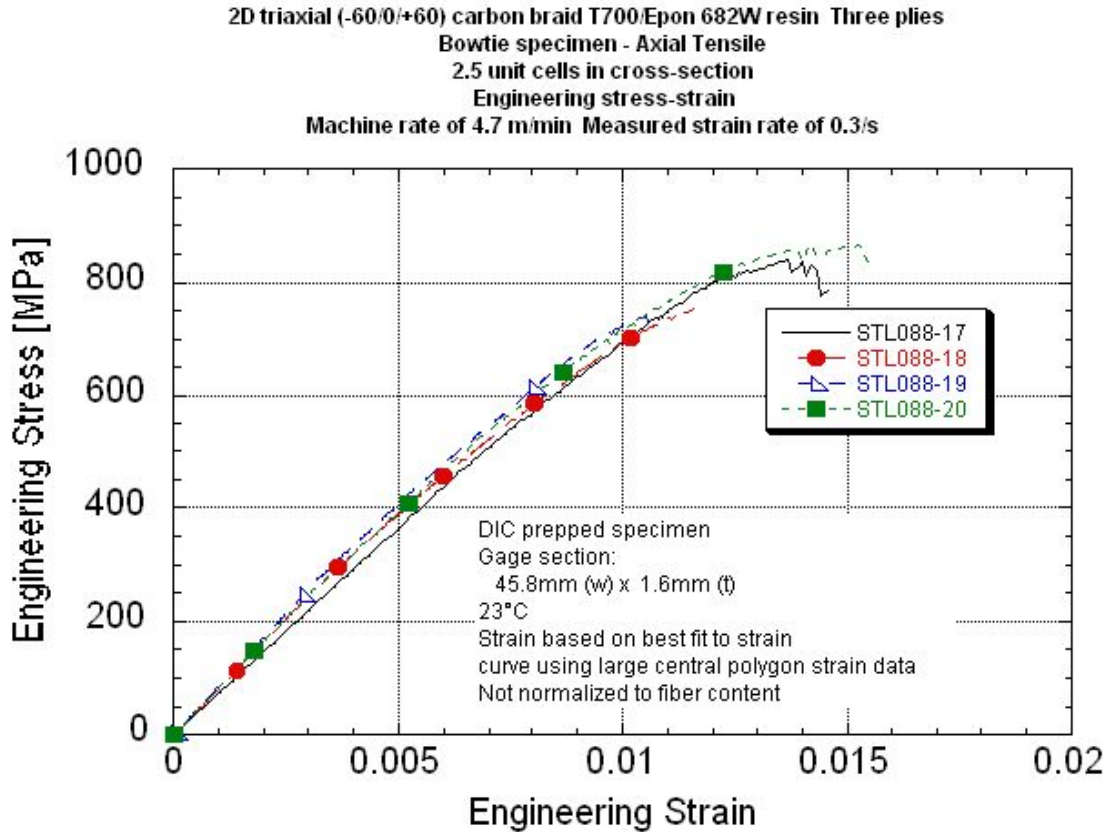
**The center line/polygon width traversed at least one unit cell (short side).

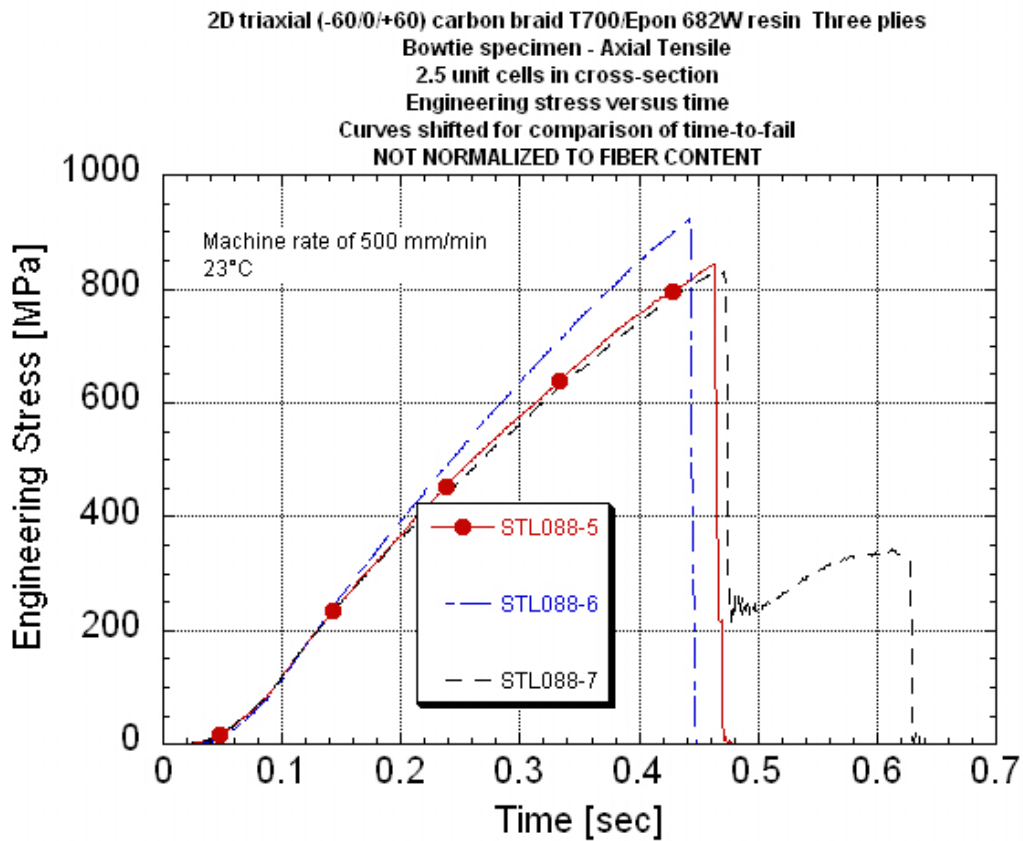
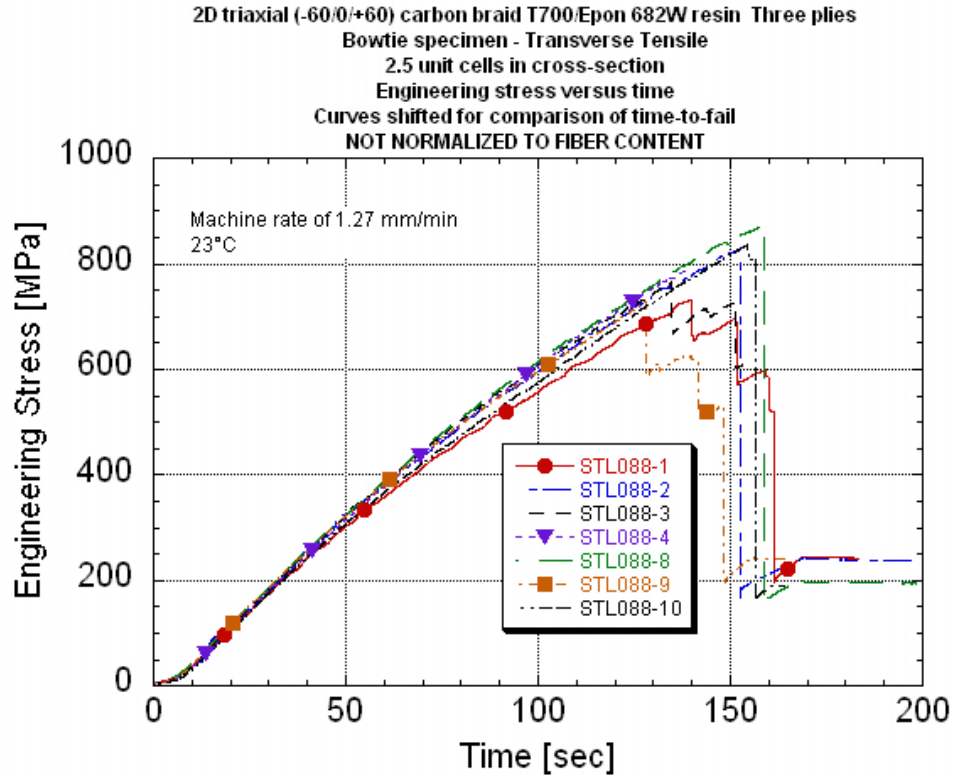
2D triaxial (-60/0/+60) carbon braid T700/Epon 682W resin Three plies
 Bowtie specimen - Axial Tensile
 2.5 unit cells in cross-section
 Engineering stress-strain
 Machine rate of 1.27 mm/min

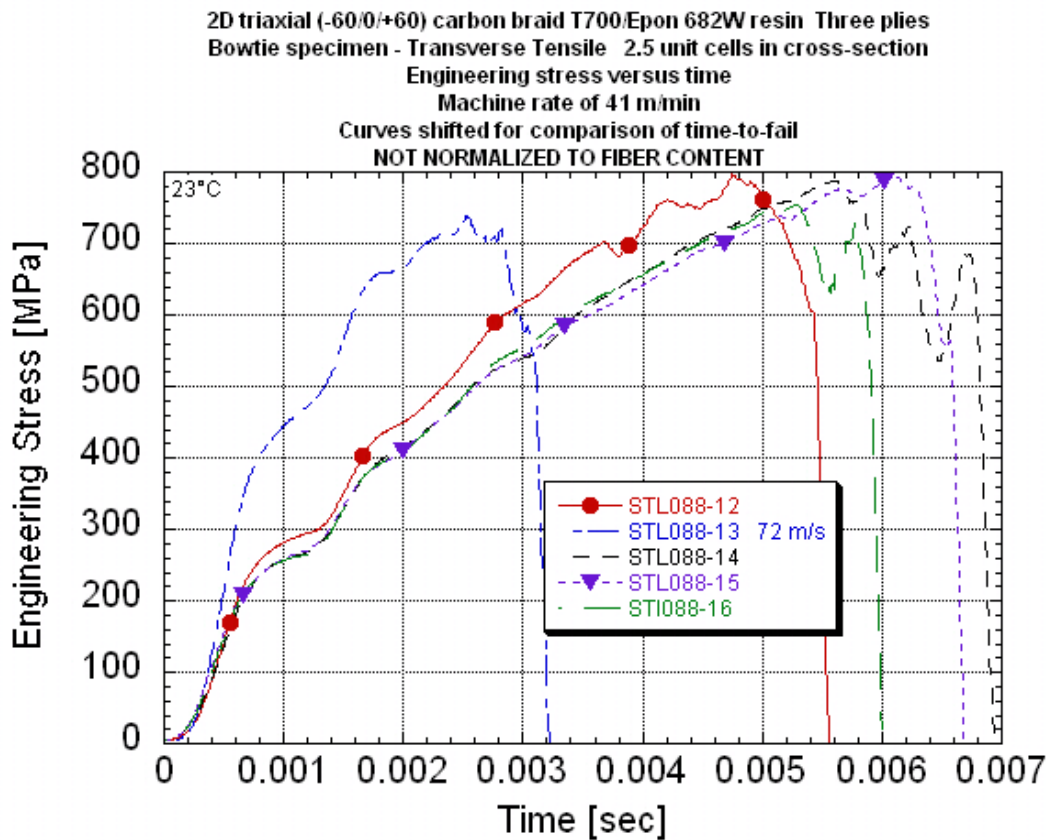
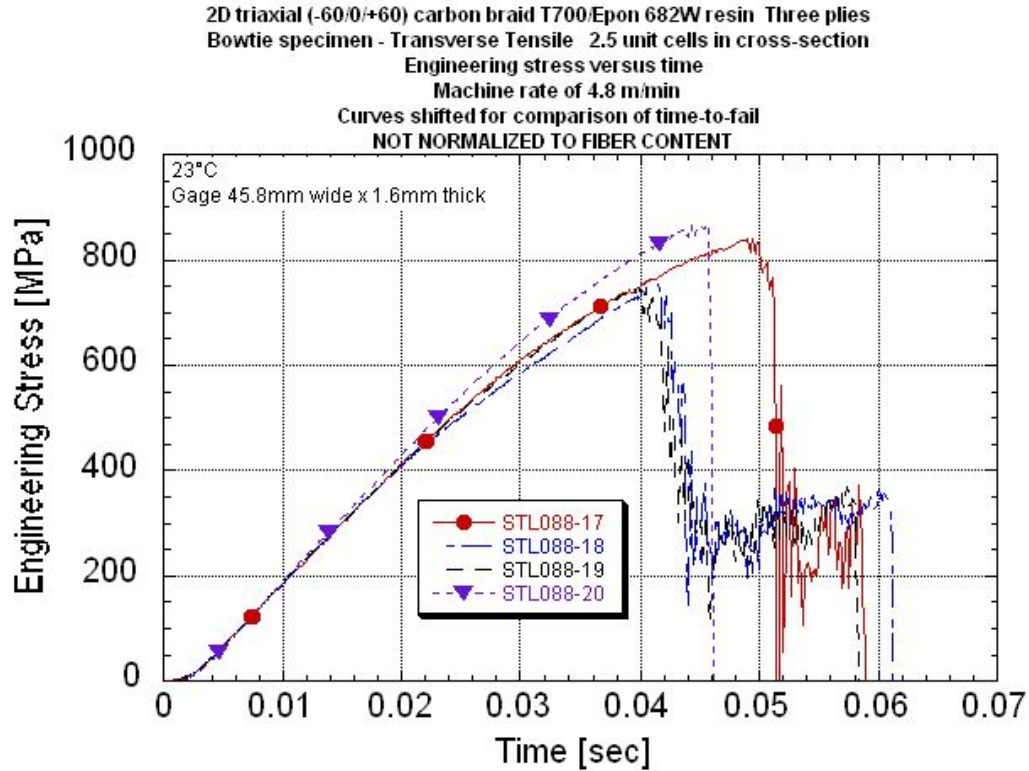


2D triaxial (-60/0/+60) carbon braid T700/Epon 682W resin Three plies
 Bowtie specimen - Axial Tensile
 2.5 unit cells in cross-section
 Engineering stress-strain
 Machine rate of 500 mm/min









APPENDIX L.

BOWTIE TRANSVERSE TENSILE DATA PACKAGE

Summary Table

Summary Stress-strain Plots With Rate

Summary Stress-time Plots With Rate

Investigation of Opportunities For Light-Weighting Vehicles Using Advanced Plastics And Composites

Axial Tensile Data Summary
2D Triaxial Carbon T700/ Epon862W Epoxy Braid
Bowtie Specimen Configuration - 2.5 unit cells in reduced cross section
Nominal center cross-section of 45.5mm wide x 1.65mm thick

	UDRI STL number	Peak Stress [MPa]	Normalized Peak Stress to 56% Fiber Volume [MPa]	Engineering Breaking Strain # [%]	Localized## Engineering Max Strain [%]	Localized## Engineering Min Strain [%]	Elastic Modulus Based on Center [GPa]	Elastic Modulus Based on High Strain Point [GPa]	Elastic Modulus Based on Low Strain Point [GPa]	Poisson's Ratio**	Measured Strain Rate Before Failure* [1/s]	Machine Rate [in/s]	Machine Rate [m/min]	Comments
0.00009/s	088-1	731	718	1.31	2.22	0.62	62.9	46.6	71.3	0.26	0.000109	0.00083	0.00126	Note 1
	088-2	829	815	1.37	2.06	0.88	67.3	43.2	77.8	-	0.000085	0.00083	0.00127	Note 1
	088-3	767	754	1.26	1.55	0.71	66.9	56.7	91.7	0.25	0.000083	0.00083	0.00127	
	088-4	822	808	1.35	1.88	0.60	66.5	-	94.5	-	0.000092	0.00083	0.00127	Note 1
	088-8	875	860	1.36	1.88	0.69	70.5	59.9	100	-	0.000077	0.00083	0.00127	Note 1
	088-9	728	686	1.20	2.00	0.44	65.8	41.5	92.7	-	0.000089	0.00083	0.00126	Note 1
	088-10	836	787	1.33	1.60	0.63	69.4	-	-	-	0.000083	0.00083	0.00127	Final failure at 1.72%. Note 1
	Average	798	775	1.31	1.88	0.65	67.0	49.6	88.0	0.25				
	Standard Deviation	57	60	0.06	0.24	0.13	2.5	8.3	11.0					
	COV [%]	7.11	7.76	4.81	12.7	20.5	3.69	16.7	12.5					
Excluding Specimens 088-1, 088-3, and 088-9 which had cracking into the grip before failure	Average	841	817	1.35	1.85	0.70	68.4	51.6	90.8					
	Standard Deviation	24	31	0.02	0.19	0.13	1.84	11.8	11.6					
	COV [%]	2.82	3.75	1.38	10.2	18.4	2.69	22.9	12.8					
0.03/s	088-5	844	795	1.51	2.44	0.94	62.5	46.1	62.7	-	0.0319	0.331	0.504	Final failure at 2.78%. Note 1
	088-6	921	868	1.43	1.50	0.48	70.8	52.7	101	-	0.0344	0.330	0.503	Note 1.
	088-7	831	782	1.37	1.83	0.55	65.9	50.7	94.5	0.36	0.0312	0.331	0.505	
	Average	865	815	1.44	1.92	0.65	66.4	49.8	85.9					
	Standard Deviation	49	46	0.07	0.48	0.25	4.2	3.4	20.4					
	COV [%]	5.65	5.65	5.13	24.8	37.8	6.30	6.75	23.74					
0.3/s	088-17	841	829	1.37	1.54	1.08	72.9	52.0	84.8	-	0.310	3.01	4.59	Note 1
	088-18	754	744	1.16	1.83	0.85	81.7	67.3	89.9	0.38	0.295	2.95	4.50	
	088-19	749	739	1.05	1.12	0.80	85.4	85.4	85.3	0.39	0.295	3.18	4.84	
	088-20	868	817	1.51	1.74	0.99	82.3	66.3	83.6	0.37	0.323	3.01	4.59	
	Average	803	782	1.27	1.56	0.93	80.6	67.7	85.9	0.38				
	Standard Deviation	60	48	0.21	0.32	0.13	5.4	13.7	2.8	0.01				
	COV [%]	7.53	6.09	16.2	20.3	14.0	6.66	20.2	3.23	2.33				
	2/s Low amplitude resonant ringing ~5 to 10 waves before failure	088-12	797	777	1.53	2.06	0.83	81.5	67.3	97.8	0.33	2.61	27.2	41.4
088-13		738	719	1.27	1.77	0.62	83.2	65.1	124	0.42	4.95	48.1	73.2	Notes 2 and 3
088-14		789	769	1.22	1.49	0.55	95.0	85.1	118	0.47	2.19	23.7	36.0	Note 2
088-15		790	744	1.39	1.59	0.86	78.2	58.9	79.2	-	1.97	24.8	37.8	Note 2
088-16		754	711	1.22	1.99	0.88	88.9	70.6	97.8	0.38	2.23	25.0	38.0	Note 2
	Average [EXCLUDING 088-13]	783	744	1.33	1.78	0.75	85.4	69.4	103	0.40				
	Standard Deviation	19	29	0.13	0.25	0.15	6.6	9.7	18	0.06				
	COV [%]	2.46	3.96	10.0	13.8	20.5	7.76	14.0	17.4	15.2				

* Strain rate of central region ** Poisson's ratio taken at the first region of zero slope from the E11 vs Ratio curve.

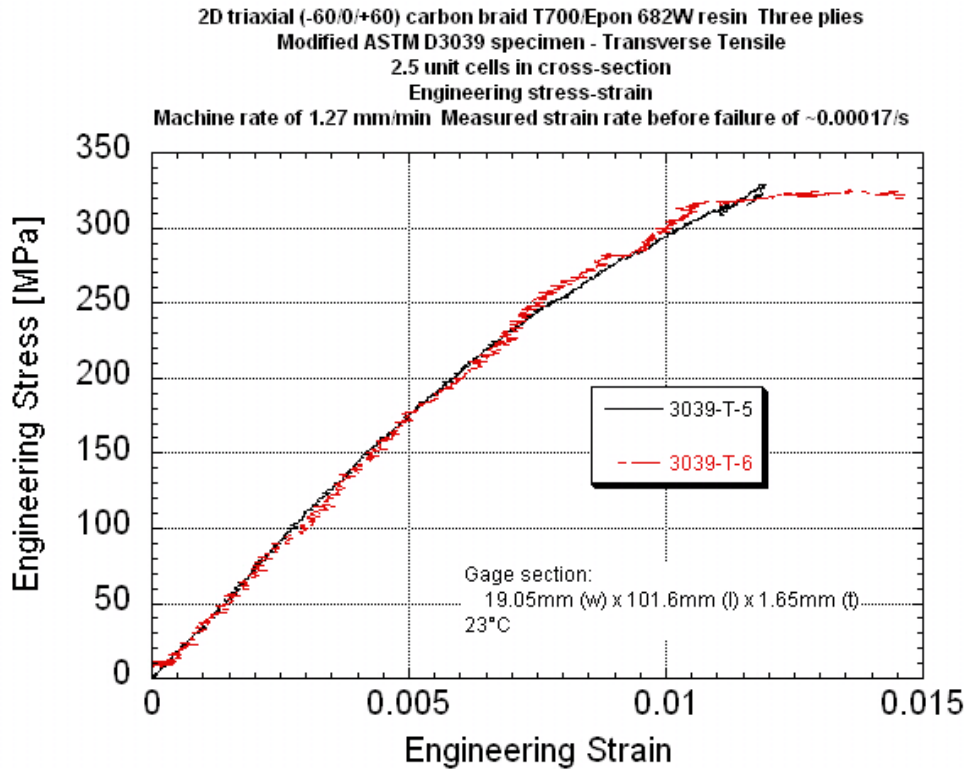
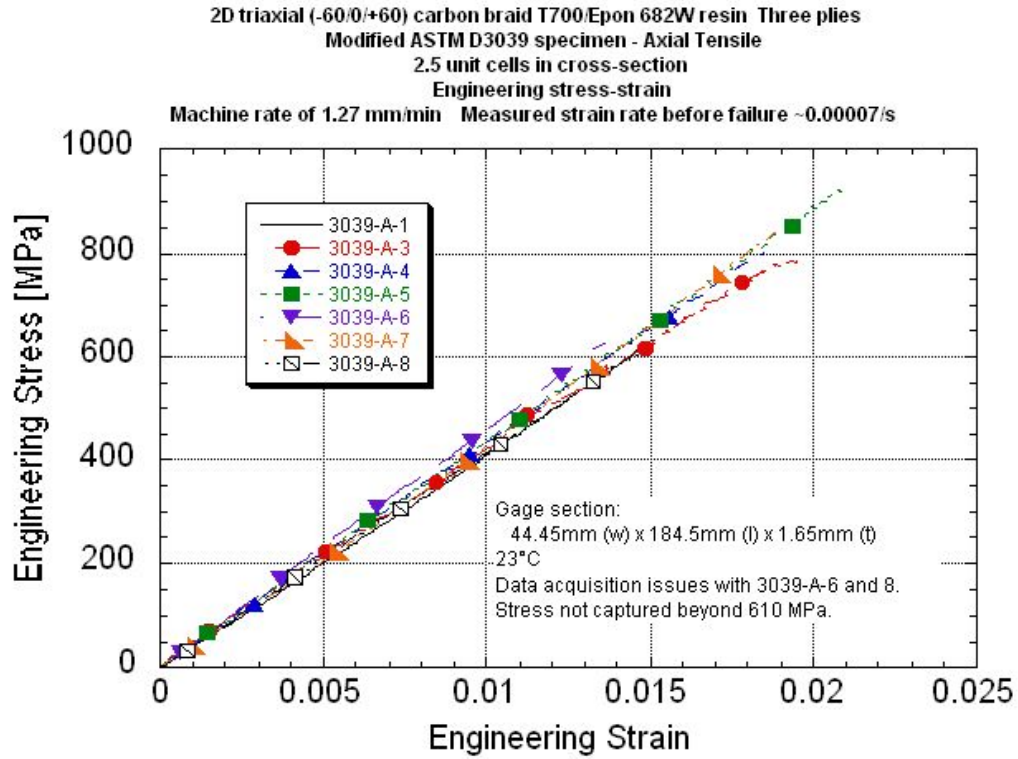
Strain as measured at a region of high strain on a fiber braid and a low strain region.

Specimen thickness varied due to the braid structure. Thickness was measured at two "peak" and two "valley" locations and averaged.

Note 1 Nonlinear increase of Poisson's ratio to end of test.

Note 2 Nonlinear stroke rate throughout loading cycle. Initial rate was 45.7 m/min through ~half of the loading. Had decreased to ~35 m/min by the end of the test. Reported machine rate is the average rate throughout the loading time.

Note 3 Resonant ringing superimpose onto material response. Limited number of stress waves before failure (~3 waves). Not included in average.



APPENDIX K.

BOWTIE AXIAL TENSILE DATA PACKAGE

Summary Table

Summary Stress-strain Plots With Rate

Summary Stress-time Plots With Rate

Investigation of Opportunities For Light-Weighting Vehicles Using Advanced Plastics And Composites

Table J-1 Triaxial Braid T700 Carbon/ Epon 862W Quasi-static Summary Table Using Modified ASTM D3039 Specimens - Axial Orientation

Digital Image Correlation (DIC) and Back-to-Back Gaged
 Nominal gage dimensions of 44.45 mm (w) X 1.65 mm (t) x 184.5 mm (l)
 Test speed of 1.275 mm/min (0.05 in/min) Minimum test system resonant frequency of 1 kHz
 Test conditions: 23°C RH: 50 +/-10%

	Test Date	UDRI Specimen ID	Panel ID	Engineering Peak* (Breaking) Stress [ksi]	Engineering Peak* (Breaking) Stress [MPa]	Engineering Breaking Strain [%]	Elastic Modulus [GPa]	Poisson's Ratio	Machine Rate [m/s]	Machine Rate [in/s]	Nominal Strain Rate [1/s]	Measured Strain Rate# [1/s]	Strain Range for Strain Rate Calc. [%]	Failure Location	Comments
Axial	9/20/2010	064-1	080210-6	117	808	1.91	42.2	0.289	0.000021	0.000834	0.000115	0.0000729	1.0-1.8	gage	Re-run. Increased grip pressure after slippage at 12786 lbf. Note 1
	9/20/2010	064-2	080210-6	131	903	-	-	-	0.000021	0.000834	0.000115	-	-	-	Note 1
	9/22/2010	064-3	080210-6	114	787	1.82 gaged 1.95 DIC	44.9 gaged 41.3 DIC	0.300 DIC	0.000021	0.000834	0.000115	0.0000720 gaged 0.0000708 DIC	1.0-1.8	gage	Gaged and DIC
	9/21/2010	064-4	080210-6	117	807	1.85	43.4	0.314	0.000021	0.000833	0.000115	0.0000737	1.0-1.8	gage	Broke both ends
	9/21/2010	064-5	080210-6	134	924	2.08	44.2	0.304	0.000021	0.000833	0.000115	0.0000715	1.0-1.8	gage	Broke both ends
	9/21/2010	064-6	080210-6	125	860	1.86	45.8	0.333	0.000021	0.000824	0.000113	0.0000722	1.0-1.8	gage	Note 1
	9/21/2010	064-7	080210-6	122	841	1.91	44.6	0.310	0.000021	0.000834	0.000115	0.0000753	0.8-1.9	gage	Re-run. Increased grip pressure after slippage
	9/21/2010	064-8	080210-6	122	842	2.07	41.3	0.307	0.000021	0.000833	0.000115	0.0000715	1.0-2.0	gage	Note 1
Average [DIC data]				123	846	1.95	43.3	0.308							
Std.Dev.				6.94	47.8	0.09	1.72	0.01							
Coeff. of Var. [%]				5.65	5.65	4.81	3.98	4.38							

Strain gage full scale was 2%. Strain data from back-to-back gages averaged to adjust for potential bending.

Note 1: Issues with DIC-recorded load. Full scale reached at 10,000 lbf [-620-640 Mpa]. Peak stress recorded by Test data acquisition.

Nominal rate based on gage length of 184.5mm.

1. Thickness was measured at two "peak" and two "valley" locations and averaged.

*DIC system 1-2 Hz sampling frequency was not always sufficient to capture peak. The sampling frequency was low in order to view most of the specimen within the region of interest for most tests. The peak stress was taken from the test machine output.

Investigation of Opportunities For Light-Weighting Vehicles Using Advanced Plastics And Composites

Table J-2 Triaxial Braid T700 Carbon/ Epon 862W Quasi-static Summary Table Using Modified ASTM D3039 Specimens - Transverse Orientation

Digital Image Correlation (DIC) and Back-to-Back Gaged
 Nominal gage dimensions of 19.05 mm (w) X 1.65 mm (t) x 101.6 mm (l) for transverse
 Test speed of 1.275 mm/min (0.05 in/min) Minimum test system resonant frequency of 1 kHz
 Test conditions: 23°C RH: 50 +/-10%

	Test Date	UDRI Specimen ID	Panel ID	Engineering Peak* (Breaking) Stress [ksi]	Engineering Peak* (Breaking) Stress [MPa]	Onset of Engineering Failure Strain ** [%]	Final Engineering Breaking Strain ** [%]	Elastic Modulus [GPa]	Poisson's Ratio	Machine Rate [m/s]	Machine Rate [in/s]	Nominal Strain Rate [1/s]	Measured Strain Rate# [1/s]	Strain Range for Strain Rate Calc. [%]	Failure Location	Comments
Transverse	9/16/2010	063-1	080210-6	49.0	338	-	-	-	-	0.000021	0.00083	0.000208	-	-	gage	No DIC data
	9/16/2010	063-2	080210-6	47.1	325	-	-	-	-	0.000021	0.00083	0.000208	-	-	gage	No DIC data
	9/16/2010	063-3	080210-6	49.7	343	-	-	-	-	0.000021	0.00083	0.000208	-	-	gage	No DIC data
	9/16/2010	063-4	080210-6	49.3	340	-	-	-	-	0.000021	0.00083	0.000208	-	-	gage	No DIC data
	9/27/2010	063-5	080210-6	47.7	329	1.36	1.44	34.7	0.32	0.000172	0.000832	0.000208	0.000172	0.6-1.1	gage	
	9/27/2010	063-6	080210-6	47.2	325	1.10 gaged 1.06 DIC	1.41 gaged 1.45 DIC	36.9 gaged 34.4 DIC	-	0.000157	0.000833	0.000208	0.000157	0.2-1.0	gage	Gaged and DIC. DIC modulus measured over a larger region.
Average of DIC specimens			48.3	333	1.36	1.44	34.70									
Std.Dev.			1.16	7.98												
Coeff. of Var. [%]			2.40	2.40												

Strain gage full scale was 5%. Strain data from back-to-back gages averaged to adjust for potential bending.

Note 1: Issues with DIC-recorded load. Full scale reached at 10,000 lbf [-620-640 Mpa]. Peak stress recorded by Test data acquisition.

Nominal rate based on gage length of 101.6mm.

1. Thickness was measured at two "peak" and two "valley" locations and averaged.

*DIC system 1-2 Hz sampling frequency was not always sufficient to capture peak. The sampling frequency was low in order to view most of the specimen within the region of interest for most tests. The peak stress was taken from the test machine output.

**Transverse specimens - failure was taken at the point of maximum stress and strain before tearing.